

**Molecular and Functional Characterization of  
Polychlorinated Biphenyl (PCB) Degrading Bacteria**

**THESIS**

Submitted in partial fulfilment  
of the requirements for the degree of  
**DOCTOR OF PHILOSOPHY**

by

**MONIKA SANDHU**

**ID. No. 2016PHXF0401P**

Under the Supervision of  
**Prof. Prabhat Nath Jha**



**BITS Pilani**  
Pilani | Dubai | Goa | Hyderabad

**BIRLA INSTITUTE OF TECHNOLOGY & SCIENCE, PILANI**

**2023**

**BIRLA INSTITUTE OF TECHNOLOGY AND SCIENCE, PILANI**

**CERTIFICATE**

This is to certify that the thesis titled, “Molecular and Functional Characterization of Polychlorinated Biphenyl (PCB) Degrading Bacteria” submitted by Monika Sandhu ID No 2016PHXF0401P for award of Ph.D. of the Institute embodies original work done by her under my supervision.



Signature of the Supervisor:

Name in capital letters: DR. PRABHAT NATH JHA

Designation: Professor, Department of Biological Science

Date: 30.05.2023

## Table of Contents

Content	Title	Page No.
	<i>Certificate</i>	<i>i</i>
	<i>Acknowledgements</i>	<i>ii</i>
	<i>Abstract</i>	<i>iv</i>
	<i>List of Tables</i>	<i>x</i>
	<i>List of Figures</i>	<i>xii</i>
	<i>List of Abbreviations</i>	<i>xxii</i>
Chapter I	General Introduction	1
Chapter II	Analysis of metabolic potential and bacterial diversity of PCB degrading bacteria using a metagenomic approach	27
Chapter III	Enrichment, isolation, and characterization of PCB-degrading bacteria	66
Chapter IV	Metabolite profiling of selected bacterial isolates grown in biphenyl-supplemented Minimal Media	108
Chapter V	Optimization of consortia-based bacterial formulation and evaluation of bioformulation for enhanced PCB degradation	123
Chapter VI	Whole genome sequencing of <i>Brucella anthropi</i> MAPB -9	149
Chapter VII	Summary, Conclusions and Future Perspectives	178
	Bibliography	182
<i>Appendix</i>	<i>List of Publications</i>	<i>A1</i>
	<i>Brief Biography</i>	<i>A3</i>

## ACKNOWLEDGEMENTS

It is my privilege to have **Prof. Prabhat Nath Jha** from the Department of Biological Sciences as my research guide and I wish to express my deepest sense of gratitude and courteous regards to him. His adept guidance infused the spirit of committed hard work in me. In addition to being a great scientist, he is a benevolent personality. I am grateful to **Prof. V Ramgopal Rao** (Vice-Chancellor, BITS, Pilani), **Prof. Souvik Bhattacharyya** (Ex-Vice-Chancellor, BITS, Pilani), **Prof. Sudhir Kumar Barai** (Director, BITS Pilani, Pilani Campus), **Prof. Ashoke K. Sarkar** (Ex-Director, BITS Pilani, Pilani Campus), **Prof. S. K. Verma** (Dean, Administration), **Prof. M B Srinivas** (Dean, AGSRD) and **Prof. Srinivas Krishnaswamy** (Ex-Dean, AGSRD) for their support in this research work.

Thoughtful suggestions and critical review of research work from the doctoral advisory committee (DAC) members **Prof. Jitendra Panwar** (Ex-Associate Dean, AGSRD) and **Prof. Sandhya Marathe** are sincerely acknowledged.

I express my sincere thanks to **Prof. Rajdeep Choudhary** (HoD, Biological Sciences) and **Prof. P R Deepa** (Ex. Head, Biological Sciences) for their motivation, constant support, and encouragement. My sincere thanks to **Prof. Ashis K. Das**, **Prof. Shibasis Chowdhary**, **Prof. Shilpi Garg**, **Prof. Vishal Saxena**, **Prof. B. Vani**, **Prof. Sudeshna Mukerhjee**, **Prof. Syamantak Majumdar**, **Prof. Rita Sharma**, **Prof. Pankaj Sharma**, **Prof. Uma Dubey**, **Prof. Meghana Tare**, **Dr. Mukul Joshi**, and **Dr. Balakumaran Chandrasekar** for their encouragement throughout my association with Department of Biological Sciences, BITS, Pilani.

I wish to express my sincere thanks to the **Department of Science and Technology, New Delhi** for the **Women Scientist award** (both the 1-year internship grant and 3-year research grant) without which I would have not been able to complete my doctorate. The generous financial support is duly acknowledged.

All the staff and students from the Department of Biological Sciences at BITS, Pilani have been very friendly and helpful. I would like particularly to acknowledge **Shahid, Sandeep, Vikram, Vikas, Shraddha, Poonam, Monika, Tripti, Saumya, Vishalakshi, Shobham, Simran, Ginson, and Pracheta** for their support and friendly gesture. Thanks to all the members of the Bio and Pharma group that have helped me along the way (there are too many to mention you all!).



Thanks, are also due to **Mr. Mandeep Phogat** [Ex-Technical Assistant, SIF] and **Mr. Sandeep Ruhidas** [Technical Assistant, SIF] for their initial help in GC-MS/MS instrument operation.

I thank the Almighty for giving me such a caring and loving family. Words cannot express my gratitude and reverence for all the sacrifices that they have made to make this possible. I want to mention special thanks to my husband, **Prof. Atish T. Paul**, as it would not be possible to count his endless support to me, morally, scientifically, and personally. I am grateful for my darling daughters, **Avni** and **Anika** who are as lovely as they could get, and for placing immense faith in me and my work. Finally, my **parents and parents-in-law** are remembered with love and gratitude for their guidance and blessings throughout my life.

I would like to express my gratitude to all those golden beings who helped me directly or indirectly to complete this chapter of my life.

**Monika Sandhu**

## Abstract

Increased industrialization has elevated the level of anthropogenic chemicals in the environment. Among the various pollutants, PCBs belong to a wide family of anthropogenic chlorinated hydrocarbons one of the most recalcitrant pollutants that are difficult to remediate. According to Stockholm Convention on Persistent Organic Pollutants (POPs), under the United Nations Environment Programme (UNEP-2004), PCB is 5<sup>th</sup> among the 12 listed POPs. PCBs are omnipresent and are mainly found in transformer oil, shipyard waste, industrial waste, paints, ink, municipal incinerators, etc. Various human diseases such as cancer, diabetes, cardiovascular disease, hypertension, parkinson and thyroid dysfunction are caused by them. Remediation of PCBs has been attempted using various strategies including chemical/physical methods, however, these strategies suffer from various disadvantages. Bioremediation is the most promising approach for the removal of PCB from contaminated soil. The combination of bacteria and plant bioremediation can further enhance the process of PCB removal. However, to date, there has been no successful bioremediation formulation in the market, especially for contaminants from the Steel industry. There are several gaps in existing research including skewed studies on biodegradation and metagenomics of Steel Industry contaminants, lack of mechanistic/interaction studies for consortia and bio- formulation development.

Considering the above potential gaps in the existing research, the present thesis aims at "Molecular and Functional Characterization of Polychlorinated Biphenyl (PCB) Degrading Bacteria" from contaminated soil from nearby areas of the Bhilai steel plant. It includes a wide array of studies that include metagenomics, molecular biology techniques, and formulation preparation.

In order to investigate the microbial diversity using a metagenomics study initially three soil samples (MGB-1, MGB-2, and MGB-3) were collected. Using GC-MS/MS analysis, MGB-2 and MGB-3 the soil samples were found to be contaminated with PCBs e.g., PCB-15 in MGB-2 and PCB-95 & PCB-136 in MGB-3. In addition, physicochemical profiling of the soil samples provided valuable information regarding the presence of organic (C/N/P), inorganic nutrients (Ca, K, Mg, Na, Mn), and metal (Fe, Mn, Cu, Zn) present, that can be an essential parameter for designing biodegradation strategies. To date, no reports on metagenomics studies have been undertaken for contaminated soil of the Bhilai steel plant region. Whole-genome metagenomics analyses were conducted for taxonomic diversity and to elucidate the

the metabolic pathways in the two soil samples. The standard alpha diversity indices namely Chao, Simpson, and Shannon, indices depicted equivalent overall diversity in both samples. Beta diversity between MGB-2 and MGB-3 based on Bray-Curtis dissimilarity depicted similar distribution patterns of bacterial communities in these samples. Oxford Nanopore Technology and MG-RAST database search provided detailed microbial taxonomy of MGB-2 and MGB-3. The differences were noticeable at the domain level, where MG- RAST derived reads accounted majorly for bacteria (97.4%; 97.5%) followed by eukaryote (1.4%; 1.5%), archaea (1.2%; 0.9%), and virus (0.02%; 0.04%) in MGB-2 and MGB-3, respectively. Among bacteria, phylum *Proteobacteria* (45.0%; 50.0%) was the most predominant, followed by *Actinobacteria* (22.1%; 19.5%) and *Firmicutes* (6.3%; 5.4%) in both MGB-2 and MGB-3 samples. RefSeq annotations at the genus level, possessed a significant abundance level with  $p < 1 e^{-5}$  for *Streptomyces*, *Candidatus Koribacter*, *Gemmata*, *Conexibacter*, *Anaeromyxobacter*, and *Nocardioides* in MGB-2, while *Hypomicrobium*, *Pseudomonas*, *Mycobacterium*, *Roseomonas*, and *Methylobacterium* with  $p < 1e^{-5}$  in MGB-3.

Higher proportions of *Proteobacteria* and *Actinobacteria* indicated the two samples possess good biodegradation potential. Overall, 708 (MGB-2) and 760 (MGB-3) annotated genes corresponding to 17 pathways linked with xenobiotic biodegradation and metabolism were identified, although with varying levels of abundance in both samples. The presence of reads for biphenyl degradation, dioxin degradation, and PAH degradation pathways correlates with the presence of PCBs and PAHs detected in the MGB-2 and MGB-3 samples. The coordination among different biodegraders and the presence of functional genes involved in biodegradation pathways and energy metabolism has provided an in-depth understanding of their survival under stress conditions of persistent organic pollutants. Moreover, these potential indigenous biodegraders such as *Bradyrhizobium*, *Burkholderia*, *Mycobacterium*, *Rhodopseudomonas*, and *Pseudomonas* identified in the present study can be further enriched and isolated for PCB degradation studies. Therefore, it can be concluded that investigating microbial communities and exploring their potential for biodegradation is a critical factor in maximizing the efficacy of the bioremediation process, and the metagenomic approach can help in a big way.

Repetitive enrichment and subsequent subculturing in MM with biphenyl at 30°C for 7 days resulted in the isolation of 33 morphologically distinct bacteria. Based on the prominent

growth on the biphenyl as the sole carbon source in MM, four bacterial isolates were selected for further studies. The selected strains MAPB-2, MAPB-6, MAPB-9, and MAPB-27 were identified based on 16S rDNA sequencing as *Pseudomonas aeruginosa*, *Pseudomonas plecoglossicida*, *Brucella anthrophi*, and *Priestia megaterium*, respectively. qPCR results indicated that available inducer biphenyl, as well as physical environmental conditions i.e., concentration and time of incubation affects aromatic ring hydroxylating dioxygenase gene expression in the selected bacteria isolates. In addition to the characterization of PCB- degradation potential, plant growth-promoting and biosurfactant-producing properties of the selected isolates were also evaluated. The detailed characterization done with different analytical techniques such as HPTLC, ATR-FTIR, and GC-MS/MS have highlighted the presence and nature of the biosurfactant produced by the selected isolates. The biosurfactant- producing property of these isolates can be attributed to good PCB degradation. MAPB-2, MAPB-6, MAPB-9, and MAPB-27 showed chemotaxis toward biphenyl intermediates such as, dihydroxy biphenyl, benzoate, and catechol. Isolates MAPB-2, MAPB-6, MAPB-9, and MAPB-27 could tolerate up to 500 mgL<sup>-1</sup> biphenyl. Optimized growth conditions with the addition of 0.2% glucose in biphenyl (200 mgL<sup>-1</sup>) supplemented MM led to enhanced biodegradation i.e., 66.1 to 100% by MAPB-9, 57.02 to 97.1 by MAPB-6 and 62.1 to 67.5 MAPB-2 within 48h. Also, this study is the first report of effective PCB-77 degradation with 59.89%, 30.49%, 27.19%, and 4.43% degradation by MAPB-6, MAPB-9, MAPB-2, and MAPB-27 respectively, using biphenyl as inducer. Metabolites produced during the biphenyl and PCB-77 degradation were also identified using GC-MS/MS. Thus, the four selected isolates possessed high biphenyl tolerances and PCB-77 degradation efficiency.

Further metabolomics of the isolates was studied in the MM-supplemented biphenyl. Benzoic acid (m/z=194) was identified as one of the major metabolites during the biphenyl degradation by MAPB-2, MABP-6, MAPB-9, and MAPB-27 at R<sub>t</sub> 17.5, 17.3, 17.6, and 17.3 min, respectively. However, 3-hydroxybenzoic acid was identified in MAPB-2 eluting at R<sub>t</sub> 23.1 min, while 2,3 dihydroxybenzoic acid was identified in MAPB-9 (25.5 min) and MAPB- 27 (25.4 min). Benzoic acid is considered a dead-end metabolite product during biphenyl degradation. Identifying benzoic acid in the extract confirms that biphenyl degradation occurs in all the selected bacterial isolates. In addition, identifying the hydroxylated benzoic acid (hydroxybenzoic in MAPB-2 and 2,3-hydroxybenzoic acid in MAPB-9 and MAPB-27) in the extracts reveals benzoic acid degradation *via* protocatechuate pathway followed by upper

biphenyl degradation pathway and channeled into central metabolism. Benzoic acid catabolic pathways, such as the  $\beta$ -keto adipate pathway, are widespread in the soil environment.

In general, larger numbers of different metabolites were observed in biphenyl-grown bacterial isolates MAPB-2, MAPB-6, MAPB-9, and MAPB-27 than in their respective control. Different organic acid, fatty acid, sugar, and amino acid metabolites were identified by the mass spectral NIST14 library. Different fermentative products, such as lactic acid, malonic acid (propanedioic acid), 2,3-butanediol, acetoin, and butanedioic acid (succinic acid), were found in the extract of MAPB-2, MAPB-6, MAPB-9 and MAPB-27 grown in biphenyl-supplemented medium. Metabolites such as glycine, 2-oxobutanoate, L-asparagine, citrate, and L-isoleucine identified in the extract are reported to be involved in amino acid biosynthesis metabolism. Acetyl derivative amino acids such as aceturic acid (N-acetyl lysine), N-acetyl L-alanine, and L-asparagine were present in MAPB-2. At the same time, N-acetyl tyrosine was identified in the MAPB-27 extract. 3-Hydroxyisovaleric acid is a byproduct of leucine metabolism that was identified in all the isolates. Glutamate, another amino acid, was present in all the selected isolates except MAPB-9. A relatively higher abundance of saturated fatty acids was observed in the presence of biphenyl as compared to the control in all experimental sets. The TMS derivative stearic acid, palmitic, 11,14-eicosadienoic acid, and 5-dodecenoic acid (Z) were found in the extract of MAPB-2, MAPB-6, MAPB-9, and MAPB-27 showing a high percentage of fatty acid in the total lipid than in control. Overall, the metabolomic profiling results and the metabolism enrichment analysis indicated that the selected bacteria showed an adaptative mechanism to survive under biphenyl-induced stress conditions.

In order to explore the PCB degradation potential of the isolates their consortia were developed. The isolates and their consortia were tested for PCB congener mix (containing tri, tetra, penta, hexa, and hepta homologs). The individual isolates namely MAPB-2, MAPB-6, and MAPB-9 completely degraded tri chlorobiphenyl, whereas MAPB-27 degraded the same to 92%. Consortia (1-11) developed were able to hydrolyze the lower chlorinated PCBs ( $Cl_{1-4}$ ) compared to the higher chlorinated PCBs ( $Cl_{\geq 5}$ ). Consortium #11 (containing 4 best isolates MAPB-2, MAPB-6, MAPB-9, and MAPB-27; 1:1:1:1) was found to possess the most potential biodegradation ability wherein it caused 100%, 60.5%, 6.9%, & 100% degradation of trichlorobiphenyl, tetrachlorobiphenyl, pentachlorobiphenyl, and hexachlorobiphenyl, respectively. The best consortium #11 was selected and encapsulated in sodium alginate

beads followed by pot study using *B. nigra* plant. Encapsulation of the selected consortium #11 and its isolates was done with Ca-alginate to get beads of uniform size with smooth surfaces. Two bioformulation subtypes (T1 and T2) were prepared to contain MAPB-2, MAPB-6, MAPB-9, and MAPB-27 in ratios (1:1:1:1 & 1:1:2:2). The bacterial isolates were found to be entrapped in their respective beads as understood from FESEM analysis. Bioformulations T1 and T2 showed 100 % degradation for tri and hexachlorobiphenyl, while the percentage degradation for tetra and penta chlorobiphenyl was more than 70% and 80% in T1 and T2, respectively. In bioformulations (T5-T8) trichlorobiphenyl was degraded 100%, while tetrachloro- and pentachloro- showed more than 50% degradation in all the encapsulated bacterium. Based on the metabolites identified by GC-MS/MS studies indicate the involvement of 2,3 dioxygenase and 3,4 dioxygenase pathways.

Finally, as MAPB-9 was the best degrader amongst all the isolates, its whole genome sequencing was carried out. The top BLASTX hit of each gene was studied, and the organism's name was extracted. The majority of the top BLASTX hits belong to *O. anthropi* ATCC 49188/ DSM 68882/ JCM 21032/ NBRC 15819/ NCTC 12168. The *Ochrobactrum* genus has been reclassified to *Brucella*. Therefore, the analyzed genome sequence belongs to *Brucella anthropi*. *B. anthropi* MAPB-9 consisted of a circular genome having a total size of 4,824,454 bp. The assembled genome was arranged in 57 contigs/scaffolds, comprised 4,749 CDSs and the total GC content was 55.87%. JGI genome online portal was used to identify genes accounting for the ability of the *B. anthropi* MAPB-9 for xenobiotic degradation, esp. dioxin, PCB, biphenyl, naphthalene, PAH, and benzoate. The genes in a subset of the KEGG xenobiotic biodegradation pathways belonging to benzoate, chloroalkane and chloroalkene, chlorocyclohexane and chlorobenzene, dioxin, naphthalene, and polycyclic aromatic hydrocarbons metabolism were identified in the *B. anthropi* MAPB-9 genome. Dehalogenase, aromatic ring hydroxylating dioxygenase, naphthalene dioxygenase, bleomycin resistance protein, glyoxalase I, and type I ring-cleaving dioxygenases were found to be present in *B. anthropi* MAPB-9. Whole genome sequencing of MAPB-9 revealed the presence of genes required for motility, chemotaxis, adhesion gene and biosurfactant production. Overall, the whole genome analysis confirmed *B. anthropi* MAPB-9 as a potent candidate for the biodegradation of PCB and other chlorinated organic compounds.

To conclude, the bacterial isolates growing in contaminated soil of areas near by Bhilai steel plant were found to possess biphenyl and PCB degrading ability. They were

further found to produce biosurfactants, possess PGPR, and antifungal activity. The consortium and bio-formulation developed using the 4 bacterial strains degraded the PCB congener mix in the pot study. Further, the genome analysis done for the selected best strain

*B. anthropi* MAPB-9 showed the presence of genes responsible for xenobiotics, plant growth promotion, chemotaxis, biosurfactant etc. The overall work resulted in the development of a prototype bio-formulation that can be tested in field conditions for PCB degradation.

### List of Tables

Table No.	Caption	Pg.no.
1.1	Details of the total number of PCB congener	1
1.2	Summary of bacteria and their consortia that degrade PCBs	10
1.3	Summary of bacteria/ fungi assisted phytoremediation of PCB	12
2.1	Barcodes used for sequencing	29
2.2	Physio-chemical parameters of the contaminated soil sample MGB-2 and MGB-3 from polluted near the Bhilai steel plant	33
2.3	Total number of unassembled and assembled reads used for downstream analyses	34
2.4	Alpha diversity for bacterial, archaea, and Eukaryota communities of collected soil from the polluted site near the Bhilai steel plant	36
2.5	Annotated gene and enzyme identified in metagenome MGB-2 and MGB-3 for methane metabolism	45
2.6	Annotated gene and enzyme identified in metagenome MGB-2 and MGB-3 for N and S metabolism	46
2.7	Annotated enzyme and the assigned genera in metagenome MGB-2 and MGB-3 for chlorocyclohexane and chlorobenzene degradation pathway	51-52
2.8	Annotated enzyme and the assigned genera in metagenome MGB-2 and MGB-3 for Biphenyl/ PAH degrading pathway.	54-55
2.9.	Annotated gene/enzyme and the bacterial genera involved in the benzoate degradation pathway via benzoyl CoA, protocatechuate, and catechol pathways identified in MGB-2 and MGB-3	56-59
3.1	Thirty-three bacterial strains isolated from PCB-contaminated soil and sequence deposited with provided accession no. in NCBI database	79
3.2	Morphological and biochemical properties of the screened PCB-degrading bacterial isolates	83
3.3	PGPR properties of the selected isolates	86
3.4	Details of ARHD gene in the selected bacterial isolate MAPN-2, MAPB-6, MAPB-9, and MAPB-27 designed using Primer3 software	87
3.5	GC-MS/MS analysis and characterization of the identified compound from biosurfactant	92
3.6	GC-MS/MS Mass spectral features of metabolites identified during PCB-77 degradation by the selected isolates	106
4.1	Mass spectral features of the TMS-derived metabolites generated from biphenyl	111
4.2	List of identified metabolites in MAPB-2, MAPB-6, MAPB-9, and MAPB-27 grown in biphenyl	114
5.1	List of bacterial isolates and their respective proportions used to prepare bacterial consortia for PCB congener degradation	124
5.2	Preparation of bioformulation of selected consortium for PCB congener mix degradation in pot experiment	127
5.3	List of metabolites identified during the degradation of PCB congeners by bioformulation of consortia in pot experiment	147
6.1	Taxonomy of <i>B. anthropi</i> MAPB-9	149



6.2	Raw read summary of <i>B. anthropi</i> MAPB-9	152
6.3	Details of the status of genome sequencing of <i>B. anthropi</i> species	155
6.4	Details of assembled genome of <i>B. anthropi</i> MAPB-9	156
6.5	Genome annotation of <i>B. anthropi</i> MAPB-9 providing protein features using UniProt	156
6.6	Details of Haloacid dehalogenases identified in <i>B. anthropi</i> MAPB-9	164
6.7	Distribution and location of genes encoding dioxygenase alpha- and beta-subunits in the genome of MAPB-9	171

### List of Figure

Fig No.	Caption	Pg.no.
1.1.	General structure of PCB congeners	1
1.2.	Structure of various coplanar PCBs with various chlorination patterns	3
1.3	Toxic effect of PCBs on the human body and the occurrence of different diseases (Carpenter et al., 2016). PCBs accumulate in adipose tissues and interact with several nuclear receptors and disrupt the endocrine system. Toxic effects on the target site include effects on neurodevelopmental, reproduction, hormone homeostasis, thyroid hormone disorder, liver hypertrophy, and cancer through nongenotoxic mechanisms	4
1.4.	The structure of planar PCBs consists of one or more chlorine atom at the ortho-position	5
1.5.	Phytoremediation of PCBs involving phytoextraction, phyto-transformation, bio-stimulation, and rhizoremediation. Plant-microbe beneficial interactions plays an important role in bioremediation of the contaminated soil. Many plant species have the ability to grow PCB contaminated soils. Plant Growth Promoting Rhizobacteria (PGPR) helps the plant by promoting plant growth. Plant in turn secretes plant secondary metabolites to enhance the growth of bacteria present in the contaminated soil. The phytoextraction process includes uptakes of PCB from soil to plant tissues, where they are transformed by plant enzyme via the phyto-transformation process. Rhizoremediation takes into account the capability of indigenous bacteria to uptake and degrade PCB.	7
1.6	Reductive dehalogenation of PCBs results in the release of chlorine from meta- and para-positions of biphenyl scaffold. Anaerobic degradation of PCB takes place in highly chlorinated PCB i.e with more than four chlorine atoms attached to biphenyl scaffold. Under anaerobic conditions 2,3,4,5,6-pentachlorinated PCB act as electron acceptors, resulting in release of one chlorine atoms in every step. Reductive dehalogenase (RDase) is the key enzyme catalyzing the PCB dechlorination process in <i>Dehalococcoides ethenogens</i>	14
1.7.	The aerobic degradative pathway of biphenyl involves an upper degradation pathway where biphenyl is converted to benzoic acid. The benzoic acid product so formed is channeled through a lower degradation pathway converting into pyruvate and Acetyl-CoA. Blue, biphenyl degradation; red, benzoate degradation via catechol; pink, benzoate degradation via protocatechuate; enter central pathway via protocatechuate intermediate	16
1.8.	Genetic organization of <i>bph</i> gene cluster of <i>Burkholderia</i> sp. LB400, <i>Pseudomonas putida</i> KF715, <i>Rhodococcus</i> sp. M5 and <i>Rhodococcus</i> sp. RHA1 (adapted from Furukawa et al., 2004)	21
1.9.	Transcriptional regulation of <i>bph</i> genes in <i>P. pseudoalcaligenes</i> KF707 (adapted from Watanabe et al., 2003). In <i>P. pseudoalcaligenes</i> KF707 <i>bph</i> genes are likely to be regulated by two regulatory systems: <i>bphR2</i> -dependent transcription for <i>bphA1A2-(orf3)-bphA3A4BC</i> and <i>bphR1</i> -dependent transcription for <i>bphR1</i> itself, <i>bphX0X1X2X3</i> , and <i>bphD</i> . The BphR1 protein,	22

	<p>belonging to the GntR-type family, is required to express <i>bphR1</i> itself and <i>bphX0X1X2X3D</i>, while BphR2 protein belongs to LysR-type family. In these systems, <i>BphR2</i> first activates the transcription of <i>bphA1A2-(orf3)- bphA3A4BC</i> to convert biphenyl to HOPD, which binds to <i>BphR1</i> to activate this protein. The activated <i>BphR1</i> then promotes the transcription of <i>bphX0X1X2X3</i> and <i>bphD</i></p>	
1.10.	<p>Transcriptional regulation of <i>bph</i> genes in <i>Burkholderia</i> sp. strain LB400 via activation of <i>bphA1</i> promoter in the presence of biphenyl. PCB degradation by strain LB400 is greatest when the cells are grown with biphenyl as the sole source of carbon and energy. It consists of glutathione transferase gene (<i>bphK</i>), two ORFs (<i>ORF0</i> and <i>ORF1</i>), and three promoters (p1, p2, and p3). Promoter p1 and p2 are located directly upstream of the gene <i>bphA1</i> and reported to have constitutive transcription, whereas p3, located upstream of <i>ORF1</i>, was described to be activated in the presence of biphenyl. The expression of <i>bphK</i> is coregulated with the expression of genes responsible for the catabolism of biphenyl</p>	23
2.1.	<p>Map illustrating the sampling location of two soil samples (Metagenomic Bhilai MGB-2 and MGB-3) collected from a polluted site near Bhilai steel plant, Chattisgarh (India)</p>	28
2.2	<p>Structure and relative abundance of the PCB identified in MGB-2 and MGB-3. Bph, PCB-15, PCB-95, and PCB-136 represent biphenyl, 1,1'-biphenyl, 4,4'-dichloro, biphenyl, 1,1'-biphenyl 2,2',3',5,6 pentachloro and 1,1'-biphenyl 2,2',3,3',6,6' hexachloro, respectively</p>	31
2.3	<p>GC-MS/MS-based identification of PCB in MAPB-2 and MGB-3 soil sample (A) Biphenyl and 1,1' Biphenyl 4,4'-dichloro- identified at Rt 5.9 and 8.4 min respectively, in MAPB-2 while (B) 1,1' Biphenyl 2,2',3',5,6-pentachloro- and 1,1' Biphenyl 2,2',3,3',6,6'-hexachloro- was identified at 7.4 and 9.7 min respectively, in MAPB-3</p>	31
2.4.	<p>Rarefaction curve represented species richness indicating the function of a number of reads (y-axis) per MGB-2 and MGB-3 (x-axis)</p>	35
2.5.	<p>Taxonomic analysis of beta diversity of MGB-2 and MGB-3 on Bary-Curtis dissimilarity indicating the abundances of microbes shared between MGB-2 and MGB-3 and the number of microbes found in each metagenome. The first PC (Principle component) accounts for most of the variance, and the first eigenvector (principal axis) has all positive coordinates. It probably means that the two metagenomes are positively correlated with each other, and the first PC represents a "common genus". All genera in MGB-2 and MGB-3 have positive values in the PC1 axis, while genera depicted in MGB-2 are positive in PC2 and MGB-3 are negative. Component 1 and component 2 represents the PC1 and PC2 axis</p>	36
2.6 (A)	<p>Krona plot demonstrating the relative abundance of taxa of bacteria across phylum to genus level hierarchy of MGB-2. Among bacteria, phylum <i>Proteobacteria</i> (45.0%), <i>Actinobacteria</i> (22.1%), and <i>Firmicutes</i> (6.3%), while <i>Streptomyces</i> (3.7%) and <i>Candidatus Solibacter</i> (2.7%) were the most predominant genera in MGB-2</p>	38

2.6 (B)	Krona plot demonstrating the relative abundance of taxa of bacteria across phylum to genus level hierarchy of MGB-3. Among bacteria, phylum <i>Proteobacteria</i> (50.0%) <i>Actinobacteria</i> (19.5%), and <i>Firmicutes</i> (5.4%), while <i>Mycobacterium</i> (3.1%) and <i>Streptomyces</i> (3.0%) were the most predominant genera in MGB-3	39
2.7	The scatter plot indicates the linear relationship between the dominance of genera between MGB-2 and MGB-3 metagenome. The difference between proportions (%) of <i>Mycobacterium</i> (1.8, 3.1, $p < 1e^{-5}$ ), <i>Streptomyces</i> (3.6, 3.0, $p < 1e^{-5}$ ), <i>Candidatus Solibacter</i> (2.6, 2.2, $p < 1e^{-5}$ ), <i>Burkholderia</i> (1.6, 1.8, $p = 3.32e^{-5}$ ), <i>Rhodopseudomonas</i> (1.3, 1.6, $p < 1e^{-5}$ ), <i>Pseudomonas</i> (1.0, 1.4, $p < 1e^{-5}$ ), and <i>Anaeromyxobacter</i> (1.6, 0.9, $p < 1e^{-5}$ ) in MGB-2 and MGB-3, respectively with significant p values. The genera towards the linear line indicate a similar proportion of reads in the metagenome	41
2.8.	SEED subsystem analysis in MG-RAST assigned reads in MGB-2 and MGB-3 based on various functions. MG-RAST assigned reads based on various functions consist of 60% of the total function metabolisms and the remaining 40% of functions include cellular processes, organismal systems, genetic, and environmental processing, and human diseases. Out of this 60%, 2% accounts for xenobiotic biodegradation and metabolism	43
2.9.	Comparative analysis of potential metabolic pathways in the metagenome of MGB-2 and MGB-3 at SEED level using online available STAMP software. The graph highlights the relative dominance of methane (1.246, 0.267, $p = 5.61e^{-4}$ ), citrate cycle (1.158, 0.329, $p = 1.62e^{-3}$ ), pyruvate (1.127, 0.309, $5.80e^{-3}$ ), benzoate degradation (1.232, 0.099, $p = 0.045$ ) in MGB-2 and lipoic acid (0.49, -0.85, $p = 7.58e^{-4}$ ), folate biosynthesis (0.751, -0.102, $p = 0.017$ ), fatty acid metabolism (0.662, -0.055, $p = 0.042$ ), and lysine degradation (0.870, -0.149, $p = 0.42$ ) in MGB-3	44
2.10.	Comparative analysis of metagenome MGB-2 and MGB-3 using STAMP SEED level based on genus level with RefSeq for metabolism. The data represents the ratio of proportion and the difference between the proportion (%) of <i>Mycobacterium</i> (0.65, -1.086, $p < 1e^{-5}$ ), <i>Pseudomonas</i> (0.784, -0.300, $p = 1.65e^{-4}$ ), <i>Norcardioides</i> (1.265, 0.306, $p = 1.77e^{-4}$ ), <i>Anaeromyxobacter</i> (1.230, 0.302, $p = 4.71e^{-4}$ ), and <i>Burkholderia</i> (0.861, -0.293, $p = 3.33e^{-3}$ ) between MGB-2 and MGB-3 with significant p values	47
2.11.	Comparison between MGB-2 and MGB-3 of functional gene annotation using STAMP using SEED subsystems including (A) Phosphate transporter (B) two-component system (C) membrane transport. The data represents the ratio of proportion and the difference between the proportion (%) of the reads with significant $p < 0.05$ under phosphate transport, two-component and membrane transport system in MGB-2 and MGB-3	49
2.12.	Annotated pathways for xenobiotic degradation and metabolism accounted for metagenome MGB-2 and MGB-3	50
2.13.	Analysis of various xenobiotic biodegradation pathways in (A) MGB-2 and (B) MGB-3 at SEED subsystem level using MG-RAST assigned reads	50
2.14.	Comparative analysis of metagenome MGB-2 and MGB-3 based on	60

	Peripheral aromatic degradation metabolism at SEED subsystem level by using STAMP. These enzymes depicted in the graph cleave the rings of aromatic compounds and represent groups in the peripheral aromatic degradation pathway and transformed the aromatic compounds into intermediary metabolites	
2.15.	Comparative analysis of metagenome MGB-2 and MGB-3 based on biphenyl degradation metabolism at SEED subsystem level by using STAMP	61
2.16.	Comparative analysis of metagenome MGB-2 and MGB-3 based on aromatic degradation metabolism at ReFSeq genus level by using STAMP	62
2.17.	Reconstruction of complete Biphenyl/PCB and PAH degradation pathways based on annotated genes identified., biphenyl degradation (Blue); benzoate degradation <i>via</i> catechol (red); benzoate degradation <i>via</i> protocatechuate (pink); benzoate degradation <i>via</i> benzoyl CoA degradation (orange); PAH degradation (Black) enters central pathway <i>via</i> protocatechuate intermediate. PAH, like pyrene and phenanthrene, produces a common degradation intermediate, i.e., 3,4 hydroxy phenanthrene, which gets converted into protocatechuate through a series of enzymes involved in the PAH degradation pathway. The upper biphenyl degradation pathway consists of the degradation of biphenyl to benzoic acid. The benzoic acid product so formed is channeled to a lower degradation pathway <i>via</i> protocatechuate converting into pyruvate and acetyl-CoA	63
2.18.	Cytoscape-based networking depicted the interrelationship of key biodegraders in PAH, biphenyl, dioxin, halogenated, catechol, and protocatechuate pathways. Key biodegraders in metagenome MGB-2	64
2.19.	Cytoscape-based networking depicted the interrelationship of key biodegraders in PAH, biphenyl, dioxin, halogenated, catechol, and protocatechuate pathways. Key biodegraders in metagenome	65
3.1	Phylogenetic tree by Maximum Likelihood method and Kimura 2-parameter model based on 16S rRNA gene sequences (A) MAPB-2, (B) MAPB-6, (C) MAPB-9, and (D) MAPB-27. Bootstrap values (expressed as percentages generated from 1000 replicates) are shown at branch points	81
3.2.	Growth and colony morphology of selected bacterial isolates on (A) LB and (B) MM supplemented with biphenyl.	82
3.3.	Sensitivity of selected isolates towards different antibiotics (A) MAPB-2, (B) MAPB-6, (C) MAPB-9, and (D) MAPB-27	84
3.4.	Antifungal properties of the selected isolates MAPB-2, MAPB-6, MAPB-9, and MAPB-27 against (A) <i>Aspergillus. niger</i> , (B) <i>A. favus</i> and (C) <i>Fusarium solani</i>	85
3.5	Biphenyl induced gene expression of ARHD by the selected isolates at different concentration 100-300 mgL <sup>-1</sup> supplemented in MM and incubated for 72 and 120 h. Increase in biphenyl concentrations from 100 to 300 mgL <sup>-1</sup> , highly upregulated the ARHD gene expression in MAPB-6, MAPB-9 and MAPB-27. (A) ARHD gene expression was 56.1-fold and 40.7-fold at 100 mgL <sup>-1</sup> for 72 and 120 h, respectively by MAPB-2 (B) ARHD gene expression was 76.6 at 300 mgL <sup>-1</sup> for 72 h while 50.6- fold change at 100 mgL <sup>-1</sup> for 120	88

	h by MAPB-6 (C) ARHD gene expression upregulated to 59.5-fold and 1.0- fold at 300 mgL <sup>-1</sup> for 72 and 120 h, respectively by MGB-9 (D) ARHD gene expression upregulated to 5.5- fold and 62.6- fold at 300 mgL <sup>-1</sup> for 72 and 120 h, respectively by MAPB-27	
3.6	Visualization of the biosurfactant produced by MAPB-2 (I), MAPB-9 (II), MAPB-6(III), and MAPB-27 (IV) by HPTLC. The TLC plates were visualized under (A) In short UV (254 nm), 0.72 (as black spots) observed indicates dirhamnolipid, and (B) In 366 nm wavelength, encircled component with fluorescence having R <sub>f</sub> values of 0.54, 0.72, and 0.91 indicates the ester present in the biosurfactant (C) shows TLC plates derivatized with anisaldehyde indicated the presence of carbohydrate moiety showing the pinkish-black band with an R <sub>f</sub> value of 0.91 in MAPB-2 and MAPB-6	90
3.7	ATR-FTIR-based structural characterization of the biosurfactant produced by (A) MAPB-2, (B) MAPB-6, (C) MAPB-9, and (D) MAPB-27	91
3.8.	Optimization of the growth parameter for potential PCB degrading bacterial isolates grown in minimal medium in 48 h (A) biphenyl concentration range (10-500 mgL <sup>-1</sup> ) (B) glucose conc. (0.1-3%) with 200 mgL <sup>-1</sup> biphenyl (C) pH (4-9) and (D) Temperature (20-40°C)	94
3.9.	Growth curve of selected isolates on (A) LB media (B) growth pattern of MAPB-2, MAPB-6, MAPB-9, and MAPB-27 graph depicting the exponential phase	96
3.10	Growth curve of selected isolates on (A) biphenyl supplemented MM media (B) growth pattern of MAPB-2, MAPB-6, MAPB-9, and MAPB-27 graph depicting the exponential phase	97
3.11	Chemotaxis of the selected isolates by drop assay in the presence of intermediates of upper (biphenyl, dihydroxybiphenyl) and lower (benzoic acid, catechol) biphenyl degrading pathway (A) <i>P. aeruginosa</i> MAPB-2 (B) <i>P. plecoglossicida</i> MAPB-6 (C) <i>B. anthropi</i> MAPB-9 (D) <i>P. megaterium</i> MAPB-27	98
3.12	SEM image of MAPB-2 grown in (A) LB medium, 10, 000X (B) LB media, 50 000X, arrow indicates EPS production (C) MM with biphenyl, 10, 000X (D) MM with biphenyl, 50,000X	100
3.13	SEM analysis of MAPB-6 grown in (A) LB media, 10,000X (B) LB media, 50 000X, arrow indicates tube-like appendages and (C) MM with biphenyl, 10,000X (D) MM with biphenyl, 50,000X, EPS secretion observed	101
3.14.	SEM analysis of MAPB-9 grown in (A) LB media, 10,000X (B) LB media, 50 000X, and (C) MM with biphenyl, 10,000X (D) MM with biphenyl, 50,000X, arrow indicates outer membrane vesicles	102
3.15.	SEM analysis of MAPB-27 grown in (A) LB media, 10,000X-(B) LB media, 50 000X and (C) MM with biphenyl, 10,000X arrow indicates membrane vesicle (D) MM with biphenyl, 50 000X, membrane vesicle observed	103
3.16	Quantitative estimation of biphenyl degradation by GC-MS/MS. The selected bacterial isolates were grown in MM supplemented with 200 mg L <sup>-1</sup> biphenyl at 30°C for 48 h, 150 rpm	104
3.17.	GC-MS/MS Chromatogram of biphenyl degradation under optimized	104



	conditions. (A) control without inoculum (B) <i>P. aeruginosa</i> MAPB-2 showing 67.5% (C) <i>P. Plecoglossicida</i> MAPB-6 showing 97.1% (D) <i>B. anthropi</i> MAPB-9 showing 100% (E) <i>P. megaterium</i> MAPB-27 showing 53.3% degradation. Biphenyl (200 mg L <sup>-1</sup> ) supplemented MM with the addition of 0.2% glucose was kept at 30°C for 48h, 150 rpm	
3.18	Percentage degradation of PCB 77 (50 mg L <sup>-1</sup> ) by MAPB-2, MAPB-6, MAPB-9, and MAPB-27 kept at 30°C for 7 d. The areas of specific peaks in the chromatogram of the samples were measured and compared to those of control samples supplemented with PCB-77 without inoculum	106
4.1.	GC-MS/MS analysis of the metabolites produced during biphenyl degradation by the selected bacteria grown on MM supplemented with 200 mg L <sup>-1</sup> biphenyl for 48 h. GC chromatograph represents the peaks of organic acids, fatty acids, and sugar, amino acids. (A) benzoic acid and 3-hydroxy benzoic acid intermediate produced by MAPB-2, (B) benzoic acid produced by MAPB-6, (C) benzoic acid and 2,3- dihydroxy benzoic acid intermediate produced by MAPB-9, and (D) benzoic acid and 2,3- hydroxybenzoic acid intermediate produced by MAPB-27. LA, GA, EDA, DDA, and HAD represent lactic acid, glycolic acid, 11,14-Eicosadienoic acid, dodecenoic acid, and heptadecanoic acid, respectively	116
4.2.	GC-MS/MS analysis of the metabolites produced by the selected bacteria grown on LB for 48 h. GC chromatograph represents the peaks of organic acids, fatty acids, and sugar, amino acids. (A) MAPB-2, (B) MAPB-6, (C) MAPB-9 and (D) MAPB-27. LA, GA, EDA, DDA, and HAD represent lactic acid, glycolic acid, 11,14-eicosadienoic acid, dodecenoic acid, and heptadecanoic acid, respectively	117
4.3.	Metabolite Set Enrichment Analysis to identify biologically meaningful patterns significantly enriched in metabolomic data. Metabolomic data analysis was done by using MetaboAnalyst 5.0 software. The metabolites detected by the GC-MS/MS analysis were used as input for the analysis to determine the metabolic pathway. The enrichment ratio is computed by Hits / Expected, where hits = observed hits; expected = expected hits. Fatty acid biosynthesis and biosynthesis of unsaturated fatty acid metabolism were identified as the most prominent metabolism in (A) MABP-2, (B) MAPB-6, and, (C) MAPB-9, while glyoxylate and dicarboxylate metabolism was found to be in (D) MAPB-27	120
4.4.	GC-MS/MS fatty acid composition profile of the selected bacterial isolates during biphenyl degradation in biphenyl supplemented MM. (A) <i>P. aeruginosa</i> MAPB-2 (B) <i>P. plecoglossicida</i> MAPB-6 (C) <i>B. anthropi</i> MAPB-9 (D) <i>P. megaterium</i> MAPB-27	121
5.1	Biodegradation of PCB congener mix by consortia and selected bacterial isolates. The number on X-axis refers to the isolate or consortia mentioned in Table 5.1. (A) Y-axis refers to the abundance of PCB congeners. (B) Y-axis refers to the percent degradation of PCB congener. #1-4 consist of individual isolates MAPB-2, MAPB-6, MAPB-9, and MAPB-27, #5-7 isolates present in combination of two, #8-10 consist of three combinations, while #11 consist of	130

	consortium of all the four bacteria	
5.2	FESEM analysis of encapsulated alginate bead surface of the selected bacterial isolates at a magnification of 50 000 X (A) MAPB-2 (B) MAPB-6 (C)MAPB-9 and (D) MAPB-27. Selected bacteria encapsulated in a criss- cross matrix of alginate with a smooth and uniform surface. No bacteria were present on the surface of the beads	133
5.3	FESEM analysis depicting encapsulated bacteria isolates(A) MAPB-2 at magnification 50 000X (B) MAPB-6 at magnification 40 000X (C) MAPB-9 at magnification 40 000X (D) MAPB-27 at magnification 31 156X	134
5.4	FESEM analysis depicting an arrangement of encapsulated bacteria isolates(A) MAPB-2 diplobacillus arrangement observed at magnification 60 000X (B) MAPB-6 diplobacillus arrangement observed at magnification 100 000X (C) MAPB-9 side-to-side arrangement observed at magnification 80 000X (D) MAPB-27 cell contact through tube-like structure at magnification 15 000X	135
5.5	Effect of encapsulated bacterial bioformulation on the growth of <i>B. nigra</i> and respective control. T1 and T2 represent plants in PCB congener spiked soil, bioformulation with consortium #11 in 1:1:1:1 and 1:1:2:2, respectively. T5 to T8 are bioformulation with individual entrapped isolates MAPB-2, MAPB-6, MAPB-9, and MAPB-27, respectively. C2 represents plants grown in sterile soil without bioformulation, while C3 represents the control group with plants grown in PCB congener spiked soil	136
5.6	Pot study of <i>B. nigra</i> growth in various bioformulation treatment and control groups. (A) T1: bioformulation with consortium #11 in ratio 1:1:1:1; (B) T2: bioformulation with consortium #11 in ratio 1:1:2:2; (C) C1 Control with PCB congener spiked soil; (D) C2 control having sterile soil with the plant (E) C3 control with PCB congener spiked soil and plant (F) T5 encapsulated MAPB-2 with spiked soil and plant; (G) T6 encapsulated MAPB-6 with spiked soil and plant; (H) T7 encapsulated MAPB-9 with spiked soil and plant (I) T8 encapsulated MAPB-27 with spiked soil and plant. The pot study was conducted for 45 days	137
5.7	FESEM analysis of the rhizospheric region of the spiked soil with encapsulated <i>P. aeruginosa</i> MAPB-2 isolates (A) MAPB-2 in the rhizospheric region and the remains of beads [20 000X] (B) MAPB-2 tube- like attachments with the <i>B. nigra</i> plant root observed [60 000X] (C) MAPB-2 attached to another and with the roots [100 000X]	139
5.8	FESEM analysis of the rhizospheric region of the spiked soil with encapsulated <i>P. plecoglossicida</i> MAPB-6 isolates (A) MAPB-6 in the rhizospheric region [20 000 X] (B) MAPB-6 attached with the <i>B. nigra</i> plant root [10 000 X]	140
5.9	FESEM analysis of the rhizospheric region of the spiked soil with encapsulated <i>B. anthropi</i> MAPB-9 isolates (A) MAPB-9 in the rhizospheric region and the remains of beads (B) MAPB-9 attached with the <i>B. nigra</i> plant root	141
5.10.	SEM analysis of the rhizospheric region of the spiked soil with encapsulated	142



	<i>Priestia megaterium</i> MAPB-27 isolates (A) MAPB-27 EPS secretion in the rhizospheric region observed (B) MAPB-27 attached with the <i>B. nigra</i> plant root is not clearly observed	
5.11.	FESEM analysis of the rhizospheric region of the spiked soil with encapsulated consortium #11. MAPB-2, MAPB-6, MAPB-9 and MAPB-27 isolates in the rhizospheric region are observed	143
5.12.	GC-MS/MS analysis of PCB congener mix degradation by different treatments. The number on the X-axis refers to the no. of treatments. (A) Y- axis refers to the abundance of PCB congener (B)Y-axis refers to the percent degradation of PCB congener. PCB congener consist of tri-, tetra-, penta-, hexa-, and hepta-chlorinated biphenyls. Treatment includes bioformulation, with consortium #11 having four bacteria (T1-T4) and single bacterial isolate (T5-T8)	144
5.13.	Mass fragmentation pattern of some of the identified metabolites in T2 during biodegradation of PCB congener mix in spiked soil. (A) 4-chloro 1,1'- Biphenyl with base peak $m/z$ 188 (B) 4-chloro benzoate; base peak and molecular ion peak at $m/z$ 139, 156 respectively (C) 4- hydroxyBenzoate base peak and molecular ion peak at 121,138 respectively (D) Benzoate base peak and molecular ion peak at $m/z$ 122, 105 respectively. (E) Dihydroxyacetophenone base peak and molecular ion peak at $m/z$ 105. X-axis represents $m/z$ ratio, while Y axis represents the abundance	148
6.1	Organism annotation based on the top BLASTX hits	153
6.2	Hierarchical Clustering of <i>B. anthropi</i> MAPB-9 based on the functional profiles with the 20 selected genomes belonging to <i>B. anthropi</i> and <i>O. spp.</i> The proximity of grouping indicates the relative degree of similarity of samples.	154
6.3	A circular graphical display of the distribution of the genome <i>B. anthropi</i> MAPB-9 annotations. This includes, from outer to inner rings, the contigs, CDS on the forward strand, CDS on the reverse strand, RNA genes, CDS with homology to known antimicrobial resistance genes, CDS with homology to known virulence factors, GC content, and GC skew. The circular genome map representation was constructed using PATRIC v3.6.9	157
6.4	Annotation of genes based on their (A) biological process, (B) molecular function, (C) cellular component	158
6.5	Subsystem distribution statistic of <i>B. anthropi</i> MAPB-9 based on genome annotation by PATRIC software. The pie chart denotes the abundance of subsystem categories, and each subsystem feature with protein coding genes is listed in parentheses separated by comma in the legend chart	159
6.6	RAST server based on genome annotation revealed the subsystem distribution of <i>B. anthropi</i> MAPB-9. The pie chart represents the abundance and the count of each subsystem category is listed in parenthesis in the chart legend	160
6.7	Region of Contig #1 consists of ferredoxin-NADP reductase COG 1018 and Rieske 2Fe-2S ARDH alpha large unit of COG4638 in (-) strand at locus 20663-21781 and 21815-23062, respectively.	165
6.8	Gene Neighborhoods of aromatic ring-hydroxylating dioxygenase, large	166

	terminal subunit in <i>B. anthropi</i> MAPB-9 (enclosed in red box) and 10 other isolates. Gene of the same color (except light yellow) is from the same orthologous group (top COG hit). Light yellow = no COG assignment, white = pseudo gene, Red = marker gene i.e. ARHD	
6.9	A phylogenetic tree of aromatic ring hydroxylating dioxygenase (ARHD) gene of <i>B. anthropi</i> MAPB-2 and other closely related bacteria. The evolutionary history was inferred by using the Maximum Likelihood method and the Kimura 2-parameter model. The bootstrap consensus tree inferred from 1000 replicates is taken to represent the evolutionary history of the taxa analyzed. Initial tree(s) for the heuristic search were obtained automatically by applying Neighbor-Join and BioNJ algorithms to a matrix of pairwise distances estimated using the Maximum Composite Likelihood (MCL). Evolutionary analyses were conducted in MEGA XI	167
6.10	Benzoate-degrading gene clusters of <i>B. anthropi</i> MAPB-9 with 14 COG in contig #2	168
6.11	Gene Neighborhoods of Protocatechuate 3,4 dioxygenase alpha subunit ( <i>pcaG</i> ) in <i>B. anthropi</i> MAPB-9 (enclosed in red box) and 20 other isolates. Gene of the same color (except light yellow) is from the same orthologous group (top COG hit). Light yellow = no COG assignment, white = pseudo gene, Red = marker gene i.e. <i>pcaG</i>	169
6.12	Region of Contig #9 consists of naphthalene 1,2-dioxygenase ferredoxin reductase component COG 0633 in (+) strand at locus 57102-58130	170
6.13	Region of Contig #11 consists of salicylate hydroxylase COG 0654 in (+) strand at locus 162476-163702	170
6.14	Gene Neighborhoods of naphthalene 1,2-dioxygenase ferredoxin reductase ( <i>nahAa</i> , <i>nagAa</i> , <i>ndoR</i> , <i>nbzAa</i> , <i>dntAa</i> ) in <i>B. anthropi</i> MAPB-9 (enclosed in red box) and other isolates. Gene of the same color (except light yellow) is from the same orthologous group (top COG hit). Light yellow = no COG assignment, white = pseudo gene, Red = marker gene, i.e. ( <i>nahAa</i> , <i>nagAa</i> , <i>ndoR</i> , <i>nbzAa</i> , <i>dntAa</i> )	172
6.15	Region of Contig #3 consists of vicinal oxygen chelate (VOC) superfamily, including the bleomycin resistance protein, glyoxalase I, and type I ring-cleaving dioxygenases in <i>B. anthropi</i> MAPB-9 shown in red	173
6.16	Contig #4 consists of exopolysaccharide, flagella, chemotaxis, and zinc transport genes present in <i>B. anthropi</i> MAPB-9. #1-2 EPS biosynthesis <i>WecE</i> , <i>TagA</i> , <i>CpsF</i> ; #3-4 Multidrug efflux system <i>DHA2</i> ; #5-6 <i>AcrR</i> Family transcriptional regulator; #7-8 Flagellar <i>FlhB</i> , <i>FlhG</i> , <i>FlhN/FlhY</i> #9 peptidoglycan hydrolase <i>CwlO</i> ; #10 Flagellar motor switch protein <i>FlhM</i> ; #11 Chemotaxis motor protein <i>MotA</i> , #12-19 Flagellar basal protein <i>FlhF</i> , <i>FliC</i> , <i>FlhB</i> , <i>FlhC</i> , <i>FlhE</i> , <i>FlhG</i> , <i>FlhA</i> , <i>FlhI</i> ; #20 Chemotaxis protein <i>MotC</i> ; #21-25 Flagellar basal protein <i>FlhE</i> , <i>FlhH</i> , <i>FliL</i> , <i>FliP</i> , <i>Flagellin</i> , <i>FliF</i> ; #26-28 Chemotaxis protein <i>MotB</i> , <i>MotC</i> , <i>MotD</i> ; #29 DNA response regulator <i>OmpR</i> ; #30-39 Flagellar protein <i>FlgE</i> , <i>FlgK</i> , <i>FlgL</i> , <i>FlgF</i> , <i>FliT</i> , <i>FlgD</i> , <i>FliQ</i> , <i>FliA</i> , <i>FliR</i> , <i>FlgJ</i> ; #42-43 Zinc protein <i>Zur</i> , <i>ZnuB</i> , <i>ZnuC</i> , <i>ZnuA</i>	174
6.17	Contig #12 consists of rhamnolipid synthesis genes in <i>B. anthropi</i> MAPB-9;	175

	#1 <i>rfbA</i> , <i>rmlA</i> , <i>rffH</i> ; #2 <i>rfbC</i> , <i>rmlC</i> ; #3 <i>rfbB</i> , <i>rmlB</i> , <i>rffG</i> ; #4 <i>rfbD</i> , <i>rmlD</i> in (+) strand	
6.18	Contig #4 consists of a siderophore and peptide/nickel transport system and genes in <i>B. anthropi</i> MAPB-9. #1 peptide/nickel transport system <i>ddpF</i> , #2 ABC.PE.P1, #3 ABC.PE.P, #4 ABC.PE.S, #5 LysR family transcriptional regulator; siderophore and ferric hydroxamate transport system #6 <i>fhuB</i> , #7 <i>fhuD</i> , #8 TC.FEV.OM, #9 <i>fecR</i> , #10 RNA polymerase sigma factor; #11 peptide/nickel transport system <i>ddpF</i> , #12 <i>ddpD</i> , #13 ABC.PE.P1, #14 ABC.PE.P, #15 ABC.PE.Sin (-) strand	177

### List of Abbreviations

ACC	aminocyclopropane-1-carboxylate
Ah	Aryl hydrocarbon
ANOVA	Analysis of variance
ARHD	Aromatic ring hydroxylating dioxygenase
ATR-FTIR	Attenuated total reflectance - Fourier transform infrared spectroscopy
BSTFA	Bis-(trimethylsilyl) trifluoroacetamide
BLAST	Basic local alignment search tool
BSA	Bovine serum albumin
CAS	Chrome-azurol-S
CAT	Catalase
CB	Chlorinated biphenyl
CBA	Chlorobenzoic acid
CFU	Colony forming unit
COG	Clusters of Orthologous Genes
CTAB	N-cetyl trimethyl ammonium bromide
DF	Dworkin-Foster
DHB	Dihydroxy biphenyl
DNA	Deoxyribonucleic acid
dNTPs	Deoxynucleotide triphosphate
EPS	Exopolysaccharide
FESEM	Field emission scanning electron microscopy
FTIR	Fourier-transform infrared spectroscopy
GA	Gibberellic acid
GC-MS/MS	Gas chromatography-mass spectroscopy
HCN	Hydrogen cyanide
HOPDA	2-hydroxy-6-oxo-6-phenylhexa-2,4-dienoic acid
HPTLC	High-performance thin layer chromatography
IAA	Indole-3-acetic acid
IMViC	Indole, methyl red test, Voges-Proskauer test
LB	Luria-Bertani
MEGA	Molecular Evolutionary Genetics Analysis

MG-RAST	Metagenomic Rapid Annotations using Subsystems Technology
<i>m/z</i>	mass/charge
NA	Nutrient-agar
NCBI	National Centre for Biotechnology Information
OD	Optical density
ONT	Oxford Nanopore Technology
OTU	Operational taxonomic unit
PAH	Polyaromatic hydrocarbons
PBS	Phosphate-buffered saline
PCA	Principal component analysis
PCB	Polychlorinated biphenyl
PCR	Polymerase chain reaction
PDA	Potato dextrose agar
PGPR	Plant growth promoting rhizobacteria
POP	Persistent organic pollutant
PTFE	Polytetrafluoroethylene
$R_f$	Retention factor
RNA	Ribonucleic acid
ROS	Reactive oxygen species
$R_t$	Retention time
TCA	Trichloroacetic acid
TMCS	Trimethylchlorosilane
TMS	Trimethyl silane
TSCA	Toxic Substances Control Act
rpm	Revolutions per minute
SE	Standard error
SIM	Selected ion monitoring
SPE	Solid phase extraction
STAMP	Statistical Analysis of Metagenomic Profiles
UNEP	United Nations Environment Programme
US EPA	United States Environmental Protection Agency
UV	Ultraviolet

WGS	Whole-genome sequencing
w/v	weight/volume
ZOI	Zone of inhibition

# **Chapter I**

## **General Introduction**

## 1. General Introduction

### 1.1. General Information, importance, distribution, impact on Environment and Health

Increased industrialization has elevated the level of anthropogenic chemicals in the environment. Organic chemicals such as pesticides, herbicides, polychlorinated biphenyls (PCBs), and polycyclic aromatic hydrocarbons (PAHs) are widely distributed in environments across the globe. Among the pollutants mentioned above, PCBs are one of the most recalcitrant pollutants that are difficult to remediate. Stockholm Convention on Persistent Organic Pollutants (POPs), under the United Nations Environment Programme (UNEP-2004), has listed twelve organic compounds, including PCBs, as POPs (Pieper and Seeger, 2008). PCBs belong to a wide family of anthropogenic chlorinated hydrocarbons (Abraham et al., 2002). The general structure of PCB is depicted in Fig 1.1.

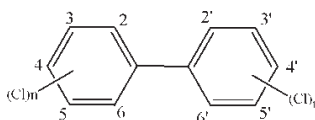


**Fig. 1.1.** General structure of PCB congeners.

PCBs were commercially available from 1929 until their manufacturing was banned in 1979 by the Toxic Substances Control Act (TSCA). PCBs are ranked fifth on the priority list of hazardous substances. They contain a biphenyl scaffold substituted with chlorine functionality, giving rise to 209 congeners, as depicted in Table 1.1 (Abramowicz, 1990). The congener represents the total number and the position of the chlorine substituents.

**Table 1.1** Details of the total number of PCB congener

PCB number	Cl substitution	Homolog group	Molecular wt.	Chlorine (%)	No. of possible congener
1-3	Mono	C <sub>12</sub> H <sub>9</sub> Cl	154.1	19	3
4-15	Di	C <sub>12</sub> H <sub>8</sub> Cl <sub>2</sub>	188	32	12
16-39	Tri	C <sub>12</sub> H <sub>7</sub> Cl <sub>3</sub>	222	41	24
40-81	Tetra	C <sub>12</sub> H <sub>6</sub> Cl <sub>4</sub>	256	49	42
82-127	Penta	C <sub>12</sub> H <sub>5</sub> Cl <sub>5</sub>	289.9	54	46
128-169	Hexa	C <sub>12</sub> H <sub>4</sub> Cl <sub>6</sub>	323.9	59	42
170-193	Hepta	C <sub>12</sub> H <sub>3</sub> Cl <sub>7</sub>	357.8	63	24
194-205	Octa	C <sub>12</sub> H <sub>2</sub> Cl <sub>8</sub>	391.8	66	12
206-208	Nona	C <sub>12</sub> HCl <sub>9</sub>	425.8	69	3
209	Deca	C <sub>12</sub> Cl <sub>10</sub>	459.7	71	1
<b>Total number of PCB congener</b>					<b>209</b>



PCBs have commercial importance with chemical and physical properties like non-flammability, stability, high electrical insulation, and high boiling point. PCBs have wide applications in industries and are used in commercial products. However, PCBs have adverse effects on the environment. After so many years of its ban, PCBs are still being released from the improperly preserved polluted area, old transformer oils, PCB blended products into landfill sites outside cities and towns, and industrial/municipal incinerators. PCBs enter the environment by accidental spillage and leakage during transportation, leaks/fires in transformers, capacitors, or other PCBs containing products. These PCBs released into the environment do not readily degrade and remain for a very long duration. The lighter type of PCBs can be transported to distant places by air and in areas with snow and deep-sea water (e.g., the Arctic). PCBs in the form of solid particles or vapor ultimately settle back as dust into sediments to soil and water or in the form of rain. PCBs that bind strongly to soil are not generally carried deep into the soil with rain. Lighter PCBs leave the soil *via* evaporation, and being in a gas form, they can accumulate in the leaves and roots of the plant. The volatile nature of PCBs is the main reason for their global distribution and bioaccumulation in the food chain (Tomza – Marciniak et al., 2019).

According to India's Ministry of Environment, Forests & Climate Change, "the use of PCBs in any form shall be completely prohibited" by 2025. PCBs have never been produced in India but are used in many industrial applications, mainly electric transformers. The data on the transformers containing PCBs were inventoried and showed that around 9837 tons of PCBs exist in the country. Iron and steel industries are the major contributors to POPs such as PCB and PAH. There are reports on the presence of PCBs congeners and PAH in agricultural, municipal, and industrial wastes in industrial soil, such as the Bhilai steel plant, Chattisgarh, India. (Patel et al., 2015; Kumar et al., 2014; Nayak et al., 2021). In India, PCBs are widely distributed in food commodities (Kannan et al., 1992), water (Rajendran et al., 2005; Kumar et al., 2008), atmospheric air (Chakraborty et al., 2010), soils (Kumar et al., 2011), and biota including humans (Tanabe et al., 1998; Monirith et al., 2003). The researcher also investigated the contamination levels of PCBs in India collected from different samples, including mussels from the seashore (Ramu et al., 2006) and breast milk (Subramanian et al., 2007; Devanathan et al., 2009).

### **1.2. Toxicity Profile of PCBs**

PCBs are categorized into two distinct types depending on their structural properties and toxicity. One group consists of 12 congeners that are considered dioxin-like (dl-PCBs) due to their

similarity in structure and toxicity with polychlorinated dibenzo-*p*-dioxins having coplanar configuration (Fig. 1.2). Coplanar congeners consist of four or more chlorine atoms at both *para* and *meta* positions, such as 3,3',4,4'-tetrachlorobiphenyl (PCB-77), and 3,3',4,4',5,5'-hexachlorobiphenyl (PCB-169). They are comparable to that of dioxin (2,3,7,8-TCDD). The coplanar PCBs are identified to be amongst the most toxic POP. Globally, the abundance of coplanar PCB in the environment is significantly more than the dioxins (Tanabe et al., 1987). Hence, they are considered a major environmental menace than dibenzofurans and dioxins (Safe, 1990).

Due to a coplanar geometry and lipophilic nature, PCBs are responsible for the deleterious effect on human health (Fig 1.3).

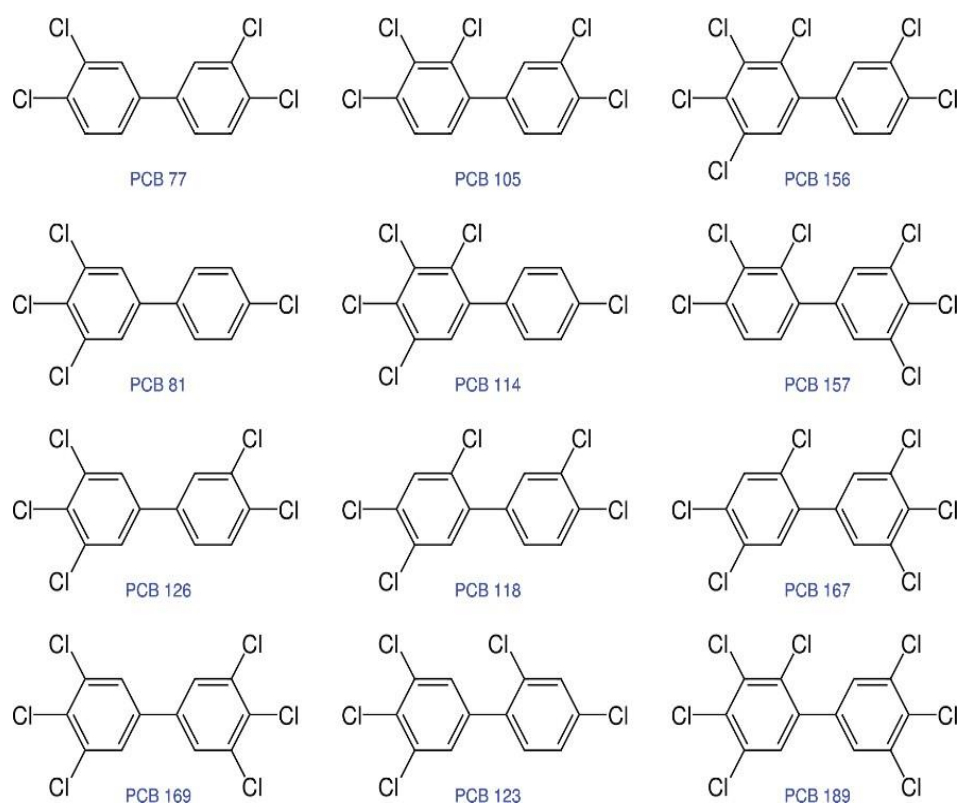


**Fig. 1.2.** Structure of various coplanar PCBs with various chlorination patterns.

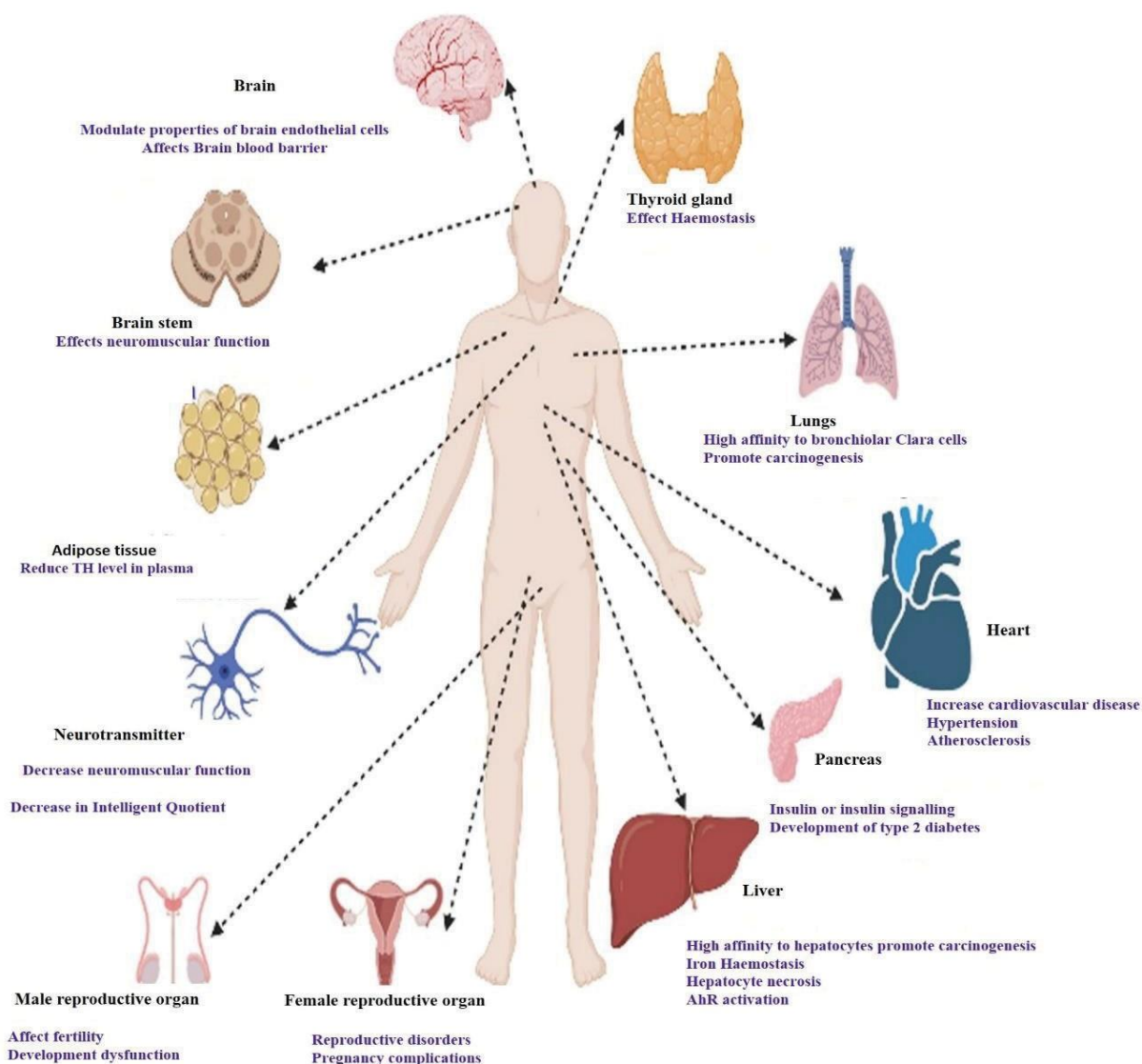


**Fig. 1.3.** Toxic effect of PCBs on the human body and the occurrence of different diseases (Carpenter et al., 2016). PCBs accumulate in adipose tissues, interact with several nuclear receptors, and disrupt the endocrine system. Toxic effects on the target site include effects on neuron development, reproduction, hormone homeostasis, thyroid hormone disorder, liver hypertrophy, and cancer through nongenotoxic mechanisms.

The lipophilic nature of PCBs makes them available for absorption by fatty tissue of human and animal body parts (Carpenter, 2006). Recent studies have revealed the effect of various PCBs on the human body and the occurrence of different diseases, such as diabetes, cardiovascular disease (Pascual, 2020; Silverstone et al., 2012; Yang et al., 2017), thyroid dysfunction (Lerro et al., 2018), hypertension (Pavuk et al., 2019; Raffetti et al., 2020a), and Parkinson disease (Goldman et al., 2016; Raffetti et al., 2020b).

The co-planar PCB possesses high binding affinity with the aryl hydrocarbon receptor (AhR). When the body comes in contact with the co-planar PCBs and gets accumulated in the fatty tissue, they activate the AhR, thereby forming a ligand-receptor complex. After translocated into the nucleus, it induces cytochrome P4501A1 (CYP1A1) genes leading to toxic effects. The second group of PCBs includes 197 non-dioxin-like congeners (Ndl-PCBs) with one or more chlorine atoms at the *ortho* position, thereby reducing the planarity and toxicity (Carpenter, 2006). Fig. 1.4. represent some examples of this class of PCBs.

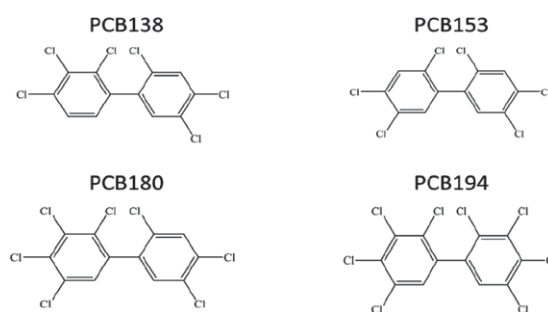


**Fig. 1.4.** The structure of planar PCBs consists of one or more chlorine atoms at the ortho-position.

### 1.3. Remediation of PCBs

Owing to their recalcitrant nature, the environmental elimination of PCBs has been challenging. Some reports disclose the disadvantages of chemical/physical methods of PCB degradation when compared to other methods. Chemical/physical strategies lead to problems in operational aspects, high cost, and partial degradation resulting in the addition of harmful end products (Trinh et al., 2019; Kvasnicka et al., 2020). Hence, developing a safe, effective, and economical degradation methodology for PCBs is urgently required. Bioremediation, a biological process of removing or modifying pollutants, seems to be the most promising method in recent times (Sharma et al., 2018).

---

### 1.3.1. Bioremediation

Organisms may alter organic contaminants such as PCBs without negatively impacting the environment. Bioremediation utilizes microorganisms (bacteria) and fungi that can degrade various contaminants, including PCBs, in collaboration with higher plants. Depending on the site, cost, and concentration of contaminants, bioremediation can either be *in-situ* or *ex situ*. *Ex-situ* bioremediation strategy includes bioreactors and land cultivating and fertilizing the soil, while *in-situ* bioremediation incorporates bioventing, and bio-stimulation. *In-situ* bioremediation technologies are sustainable as compared to *ex-situ* bioremediation. *In-situ* bioremediation neither requires groundwater pumping, transport /deposition of contaminated soil, treatment, nor discharge to recipients. Nonetheless, due to the eco-friendly characteristics of bioremediation, it has been approved to be the most reliable and efficient technology in remediating contaminated sites. Bacterial and plant-assisted bioremediation and combination approaches would further improve the effectiveness of bioremediation.

#### 1.3.1.1 Phytoremediation

Phytoremediation is considered to be one of the eco-friendly and cost-effective bioremediation methods. It involves the remediation of pollutants from the environment by the plant. There are several reports on the enhanced degradation of the organic pollutant in vegetative soil as compared to non-vegetative soil (Kurzawova et al., 2012; Tu et al., 2011). Plants are autotrophic organisms; therefore, they do not utilize these pollutants as energy sources. Also, plants can uptake some of the pollutants with the help of roots from the soil and transform them into reduced toxic forms *via* different metabolic pathways. The three main processes involved in phytoremediation are phytoextraction, phytotransformation, and rhizoremediation (Fig 1.5). Plant parts such as leaves aid in volatilizing organic compounds into the air, known as phytovolatilization, whereas bioremediation mediated by roots is referred to as rhizoremediation. Phytoextraction/phytoaccumulation is the uptake of pollutants inside the plant tissues, while the phytotransformation process involves enzymatic transformations of the accumulated compound. Some of the reported plants in phytoremediation include *Medicago*, *Brassica*, *Cucurbita*, and *Festuca* (Singer et al., 2003; Secher et al., 2013; Qin et al., 2014; Xu et al., 2010).

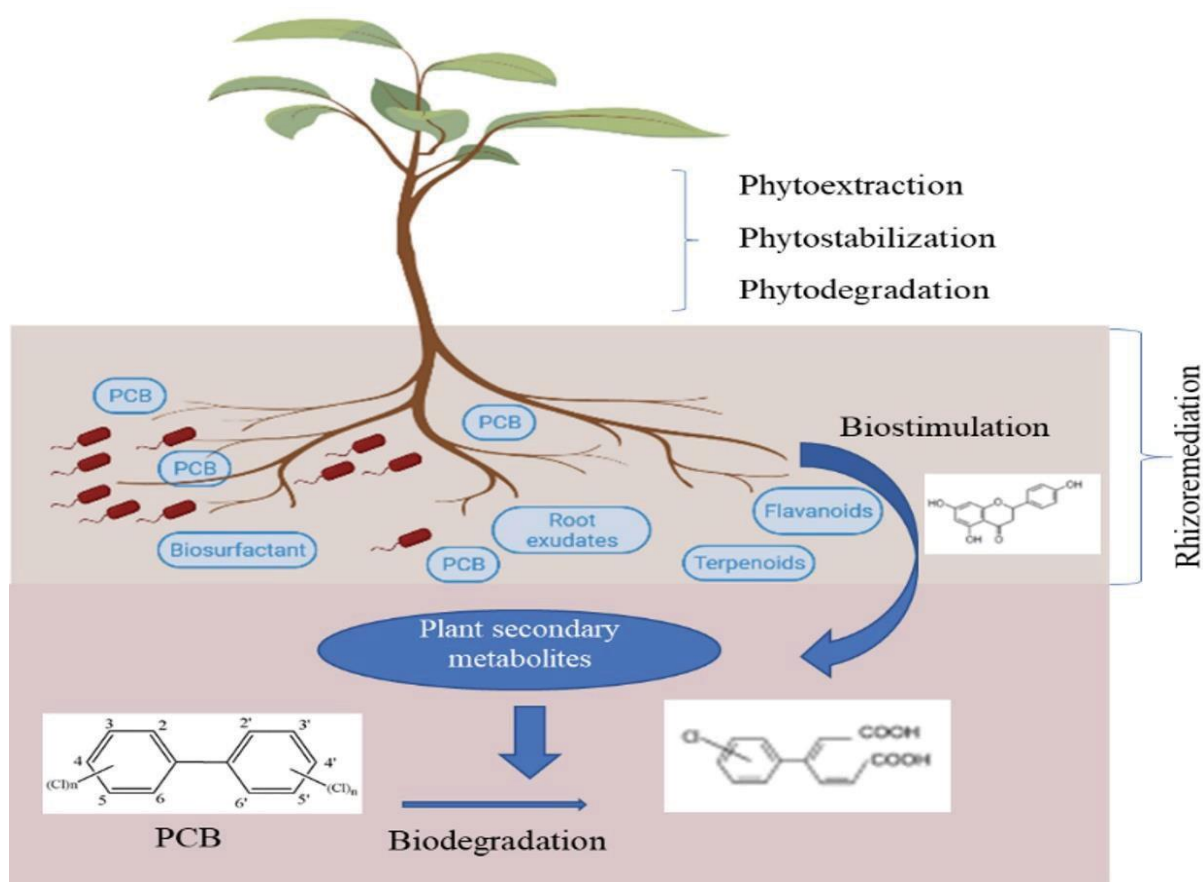


**Fig. 1.5.** Phytoremediation of PCBs involving phytoextraction, phytostabilization, phytodegradation, bio-stimulation, and rhizoremediation. Plant-microbe beneficial interactions play an important role in the bioremediation of contaminated soil. Many plant species can grow in PCB-contaminated soils. Plant Growth Promoting Rhizobacteria (PGPR) helps the plant by promoting plant growth. Plant, in turn, secretes secondary metabolites to enhance the growth of bacteria in the contaminated soil. The phytoextraction process includes uptakes of PCB from soil to plant tissues, where they are transformed by plant enzymes *via* the phyto-transformation process. Rhizoremediation takes into account the capability of indigenous bacteria to uptake and degrade PCB.

### 1.3.1.2 Mycoremediation

There is limited knowledge of PCB degradation and the existence of fungi in PCB-contaminated soils. *Fusarium solani*, *Penicillium digitatum*, *P. chrysogenum*, and *Scedosporium apiospermum* have been found to show growth and degradation properties in PCB-supplemented mineral media with glucose (Tigini et al., 2009). But, without glucose, they could not utilize PCBs for their growth. Fungi are mainly reported for the degradation of low-chlorinated PCB congeners. However, some strains also degrade high-chlorinated congeners under anaerobic conditions. Some fungal strains are known to be associated with plant roots which enable them to carry out PCB



degradation. Amongst the various fungi types, white rot fungi have been the centre of research related to PCB degradation (Cajthaml, 2015). White rot fungi easily degrade low-chlorinated biphenyls and hexa-PCB to benzoic acid (Hong et al., 2012; Takagi et al., 2007). Besides white rot fungi, several other fungi are also reported as PCB degraders. An example of such fungi includes *Phanerochaete chrysosporium*, which has been reported to reduce PCB concentration in different Aroclors blends (Gomes et al. 2013; Yadav et al. 1995). Most fungi have non-specific degradation abilities since they use intracellular enzymes such as dehydrogenases (Cvancarova et al., 2012) and extracellular enzymes such as peroxidases, laccases, etc. that are usually utilized for catalyzing other types of reactions (Hong et al., 2012).

### **1.3.1.3 Bacteria-mediated bioremediation**

Bacteria, omnipresent with the ability to thrive in the PCB-contaminated environment, are the most extensively studied organism for bioremediation of PCB compared to plants (Section 1.3.1.1) and fungi (Section 1.3.1.2). Moreover, they degrade lower and high PCB congeners through different metabolic pathways. Bacterial mechanisms of PCB degradation include anaerobic, aerobic co-metabolism, and aerobic degradation metabolism (Passatore et al., 2014). Bacteria can utilize PCBs as a single carbon source for their growth. Literature reveals significant reports on Gram-negative bacteria, namely *Pseudomonas*, *Sphingomonas*, and *Burkholderia* genera, that belong to  $\gamma$ - and  $\beta$ -subclasses of proteobacteria to degrade PCBs. However, very few Gram-positive bacteria like *Rhodococcus* and *Bacillus* species are known to degrade PCBs. The biochemical degradation pathways of PCBs have been investigated and described for the genera mentioned above. Bacteria *Rhodococcus* sp. RHA1 has been identified as an efficient PCB degrader with a reasonable growth rate in soil contaminated with PCB (Leigh et al., 2006). In a similar study, three aerobic bacteria were isolated from contaminated soil in Nigeria. They showed growth on all mono-chlorinated biphenyls (CBs) and di-CBs with 68 to 100% reduction (Adebusoye et al., 2007). Researchers have also attempted to develop combinations of various bacteria that combine the PCB-degrading potential of individual bacteria. Table 1.2 provide a summary of bacteria and their consortia that degrade PCBs.

#### **1.3.1.3.1. Bacteria-assisted phytoremediation**

Bacteria are present ubiquitously in PCB-contaminated environments, but the majority are still incapable of degrading PCBs due to the lack of sustaining nutrients. The rhizoremediation strategy uses the capability of plant roots to enhance the growth and PCB degrading efficiency of

microbes found in its rhizospheric soil. Toussaint et al. reported that PCB-degrading *R. erythropolis* U23A was isolated from the PCB-contaminated rhizospheric region. The root exudates supported bacterial growth and activated their ability to metabolize PCBs (Toussaint et al., 2012). Gentry et al. (2004) further reported new remediation technology approaches that increased the activity of exogenous bacteria and/or genes when introduced into the contaminated environment. These approaches comprise (1) gene bioaugmentation, (2) bioaugmentation, 3) rhizosphere bioaugmentation, and phyto-augmentation. Gentry et al. (2001) reported the application of bioaugmentation with an enhanced 3-chlorobenzoate (3-CB) degradation rate. PCBs uptake, and translocation have also been studied in various plant species. Many plant species, including *Cucurbita pepo*, *C. pepo* ssp. *Pepo*, *Beta vulgaris*, *Brassica rapa*, *Zea mays*, *B. oleracea* var. *capitata*, *Daucus carota*, are capable of growing in PCB-contaminated sites and favoring the indigenous PCB-degrading microbial population (Fries and Marrow, 1981; Low et al., 2010). Bittsanszky et al. (2011) have highlighted the PCBs accumulation potential of plant roots and shoots of different species of Cucurbitaceae. Amongst all, *Tall fescues* (roots) had the best potential to accumulate significant levels of PCBs and, therefore, were an excellent phytoaccumulator. Different plants such as *B. juncea*, *Avena sativa*, *Brachiaria decumbens*, and *Medicago sativa* has been reported to uptake and induce degradation of PCBs by rhizospheric microorganisms in contaminated soil (Pino et al., 2019). The most common plant species used for bioremediation studies are from the genera *Panicum*, *Festuca*, *Brassica*, *Nicotiana*, *Medicago*, and *Cucurbita*. *Brassica nigra* was also capable of enhanced PCB elimination in soil contaminated with Aroclor 1242 (Singer et al., 2003). Table 1.3 summarizes bacteria/ fungi that degrade PCBs in collaboration with plants.

Plants release secondary metabolites from roots, resulting in improved microbial degradation of PCBs (Aken et al., 2010). Plant secondary metabolites such as sugar, alcohol, and organic acids are readily available energy and electron sources for aerobic and anaerobic bacteria. Also, the complex aromatic compounds such as flavonoids, phenolics, terpenes, etc., released in the root exudates possess structural analogy with the PCB, further aid in microbial colonization of roots and act as inducers for degrading genes (Leigh et al., 2006; Jha et al., 2015) in microbial pathways.



**Table 1.2.** Summary of bacteria and their consortia that degrade PCBs.

Bacteria	Biphenyl/ PCB	%Degradation (duration)	Reference
<b>Anaerobic bacteria</b>			
<i>Dehalococcoides mccartyi</i> CBDB1	Aroclor 1260	64% (after 4 months)	Adrian et al (2009)
<i>Dehalobacter</i>	Aroclor 1260	PCB dechlorination	Wang & He (2013)
<i>Dehalococcoides mccartyi</i> JNA	Aroclor 1260	51% and 20% (hexa- hepta CBs after 124 days)	LaRoe et al (2014)
<i>Dehalococcoides mccartyi</i>	PCB-180	10.6–4.8%	Xiang et al (2020)
<b>Aerobic Gram-negative bacteria</b>			
<i>Alcaligenes</i> sp. JB1	Aroclor 1242	24% (2,2',3,3'-TetraCB)	Cammandeur et al (1995)
<i>Sphingobium fuliginis</i> HC3	CBs, DiCBs, and TriCBs	80.7% (within 24 h)	Hu et al (2015)
<i>Pseudomonas</i> sp.	2,4 DiCB	90%	Jayanna & Gayathri (2015)
<i>Mesorhizobium</i> sp. ZY1	3,3',4,4'-TetraCB	62.7% (within 10 days)	Teng et al (2016)
<i>Sinorhizobium meliloti</i> NM	3,3',4,4'-TetraCB	100% (within 9 days)	Wang et al (2016)
<i>Burkholderia xenovorans</i>	4-CB	98%	Bhattacharya et al (2017)
<i>Paraburkholderia xenovorans</i> LB400	Aroclor 1248	76% (within 7 days)	Xiang et al (2020)
<b>Aerobic Gram-positive bacteria</b>			
<i>Rhodococcus</i> sp. RHA1	Congeners of PCB 48	80-100% (within 3 days)	Seto et al (1995)
<i>Arthrobacter</i>	Aroclor 1242	15% (within 15 h)	Gilbret & Crowley (1997)
<i>Rhodococcus</i> sp. MAPN-1	DiCB& Biphenyl	95; 15% (within 7 days)	Sandhu et al (2020)
<b>Consortia</b>			
<i>R. pyridinivorans</i> SS2 and <i>R. ruber</i> SS1	Biphenyl	83.2; 71.5% (within 84 h)	Wang et al (2018)
<i>Pseudomonas</i> sp. and <i>Comamonas</i> sp.	4-CB	4-CB (within 12 h)	Xing et al (2020)

Another important feature of rhizoremediation is the occurrence of bacteria closely associated with the root region of the plants growing in the contaminated sites. They are known for their plant growth-promoting (PGP) properties and contaminant-degrading ability. Various researchers, namely Arslan et al. (2017), Leigh et al. (2006), and Xiang et al. (2020) have documented the rhizospheric partnership of indigenous PCB-degrading microorganisms found in

contaminated sites. PGP bacteria provide numerous benefits to plants in different ways, such as helping the plant protect against plant pathogens, synthesizing phytohormone and chelators, and stimulating the degradation of PCBs before it damages plant growth (Ma et al., 2011). Similarly, plants growing in contamination zones have been reported to produce compounds similar to biphenyl in their root exudates. Recent research reports that combining PGPR and specific contaminant-degrading bacteria can remove complex contaminants. Several reviews describe the extensive application of PGPR in phytoremediation and rhizoremediation (Lucy et al., 2004; Ma et al., 2011).

#### **1.3.1.3.2. Fungi-assisted phytoremediation**

There are very few reports on fungi-based phytoremediation (Qin et al., 2014). Strains belonging to the genus *Acaulospora* (*Acaulospora leaves*) and *Glomus* (namely *G. caledonium*, and *G. mosseae*) have been reported to be effective in the biodegradation of Aroclor 1242 in collaboration with plants of *Cucurbita* genus (Table 1.3). However, certain limitations should be addressed. The main limitation concerning PCB degradation is the peculiarity of different PCB congeners. In the long term, PCB is strongly bounded to the soil and is less bioavailable to the plant root and bacteria/fungi.

#### **1.4. Bio-stimulation of aerobic organisms**

Bio-stimulation involves modifying the environment to stimulate the growth of existing bacteria capable of pollutant degradation. Modification can be done by adding co-substrates, surfactants, or inducers. Strategies to encourage aerobic remediation of PCBs consist of bio-stimulation with competent PCB-degrading bacteria. Biphenyl and various plant secondary metabolites (PSM), like isoprenoid, flavonoid, etc., have been found to act as both carbon and energy sources. They have been shown to be effective inducers of PCB-degrading activity. For bio-stimulation of PCB degradation, several parameters such as optimum salt concentrations, pH, and nutrient availability (macro and microelements, mineral sources N/P/K) have been reported to accelerate PCB biodegradation in soil (Fava et al., 2003). Biphenyls, chlorobiphenyls, and some analogues of PCBs are reported to be inducers of PCB aerobic biodegradation in soils (Pieper and Seeger, 2008).

**Table 1.3.** Summary of bacteria/ fungi assisted phytoremediation of PCB.

Plant(s)	Bacteria/Fungi	Degradation	Reference
<i>Mentha spicata</i>	<i>Arthrobacter</i> sp. strain B1B	PCB	Gilbert & Crowley (1997)
<i>B. nigra</i>	<i>Rhodococcus</i> sp. ACS, <i>Ralstonia eutropha</i> H850	PCB	Singer et al (2003)
<i>Pinus nigra</i> L.	<i>Rhodococcus</i> sp. <i>Arthrobacter</i> sp. <i>Microbacterium</i> sp.	PCB congener	Leigh et al (2006)
<i>Armoracia rusticana</i>	<i>Achromobacter xylosoxidans</i> <i>Hydrogenophaga palleronii</i> , <i>Methylobacillus flagellatus</i>	Biphenyl	Uhlik et al (2009)
<i>B. napus</i>	--	PCB	Javorska et al (2009)
<i>M. sativa</i> L.	<i>Rhizobium meliloti</i>	PCB congener	Xu et al (2010)
<i>Bidens cernua</i> , <i>C. pepo</i> , <i>D. carota</i> , <i>Chenopodium album</i> , <i>Rumex crispus</i> , <i>Plantago major</i>	--	PCB	Ficko et al (2011)
<i>Festuca arundinacea</i>	<i>Burkholderia xenovorans</i> LB400	PCB	Secher et al (2013)
<i>C. pepo</i> , <i>C. moschata</i> , <i>C. maxima</i> , <i>C. sativus</i>	<i>Acaulospora laevis</i> , <i>Glomus caledonium</i> , & <i>Glomus mosseae</i>	Aroclor 1242	Qin et al (2014)
<i>Astragalus sinicus</i> L.	<i>Mesorhizobium</i> sp. ZY1	PCB	Teng et al (2016)
<i>Morus alba</i>	<i>Rhodococcus</i> sp. MAPN-1	Biphenyl/ PCB	Sandhu et al (2020)

The bioavailability of PCBs for bacteria is restricted due to their hydrophobic nature. Therefore, the efficiency of PCB biodegradation could be enhanced by producing certain surfactants. Biosurfactant aids in increasing the surface area of organic compounds such as PCBs, thus making them bioavailable to bacteria.

Biosurfactants are metabolic products secreted by several bacterial and fungal species when grown on hydrophobic substrates. Biosurfactants are associated with cell-wall and are secreted externally. The excreted biosurfactant can be used for solubilization of PCB from the soil, thereby enhancing PCBs' remediation. Examples include rhamnolipids, surfactin, sophorolipids, and

alasan, produced by *Candida bombicola*, *P. fluorescens*, and *Bacillus subtilis*, respectively. In addition to the added advantage of an enhanced ability to degrade pollutants due to the ready availability of biosurfactants (Moran et al., 2000; Rahman et al., 2002), these compounds are eco-friendly and safe. It also reduces the lag time before the removal of chlorine. *In-situ* augmentation of biosurfactant-producing bacteria and direct application of biosurfactants to the contaminated site (Cho et al., 2004; Field and Sierra-Alvarez, 2008) can enhance PCB bioremediation.

### **1.5. Co-metabolism of PCBs by biphenyl-degrading bacteria**

Co-metabolism is the process where a second carbon source or the inducer is required to biodegradation non-growth substrate such as PCB by the bacterial cell. Bacteria undergo PCB co-metabolism either anaerobically or aerobically. Anaerobic co-metabolism consists of reductive dehalogenation. PCBs with more than four chlorine molecules act as electron acceptors and undergo dehalogenation. However, aerobic bacterial degradation takes place with low-chlorinated PCBs. The enzymes involved in the upper pathway of biphenyl degradation possess a wide range of substrate specificity, resulting in the oxidation of various PCB congeners. It has been reported that aerobic bacteria undergo the co-metabolism of PCB congeners when the bacterial cells are pre-grown on biphenyl. Ahmed and Focht (1973) reported that two species of *Achromobacter* co-metabolically degrade mono and dichlorobiphenyls to chlorobenzoates. The co-metabolism of PCBs expressing the upper biphenyl degradation pathway has been extensively investigated. Furukawa and co-workers reported isolation and enrichment of *Alcaligenes* sp. strain Y42, and *Acinetobacter* sp. strain P6, using biphenyl and 4-chlorobiphenyl as a sole carbon source for co-metabolism of 36 PCB congeners (Furukawa et al., 1978). *Acinetobacter* sp. strain P6 and *Alcaligenes* sp. strain Y42 were able to metabolize 33 and 23 compounds, respectively.

### **1.6. Mechanism of bioremediation**

The mechanism of PCB bio-remediation has been widely studied. It mainly involves anaerobic and aerobic degradation by bacteria through the biphenyl catabolic pathway, as mentioned in the above section. Due to the difficulty in growing and maintaining anaerobic bacteria, a limited number of anaerobic PCBs dechlorinating degraders have been studied. *D. mccartyi* strains are the most preferred microorganisms for reductive dechlorination. However, there are many reports on the isolation of aerobic PCB-degrading bacteria (Sharma et al., 2018; Harkness et al., 1993).

### 1.6.1. Anaerobic bioremediation

Anaerobic biodegradation does not need O<sub>2</sub> for the degradation of highly chlorinated PCBs. The slow growth of anaerobic bacteria consequently results in slow degradation processes. PCB congeners undergo anaerobic reductive dechlorination, where PCBs serve as an electron acceptor for the oxidation of organic carbon. Reductive dechlorination results in the release of chlorine from the biphenyl backbone preferentially at the *meta*- and *para*-positions. This process forms PCBs with ortho-substituted lesser chlorinated congeners (Fig 1.6). Thus, the decrease in the number of chlorines results in the formation of less toxic PCBs and in generating dechlorinated products. Less than five chlorinated PCBs so formed undergo an aerobic degradation mechanism and are easily degraded by aerobic bacteria (Demirtepe et al., 2015; Master et al., 2002). Anaerobic PCB-degrading bacteria such as *Dehalococcoides* and *Chloroflexi* are found to be present in the anaerobic contaminated environment such as sediments and flooded paddy fields (Abraham et al., 2002; Brown et al., 1988; Bedard et al., 2006; Chen et al., 2014; Furukawa & Fujihara, 2008; Zanaroli et al., 2012).

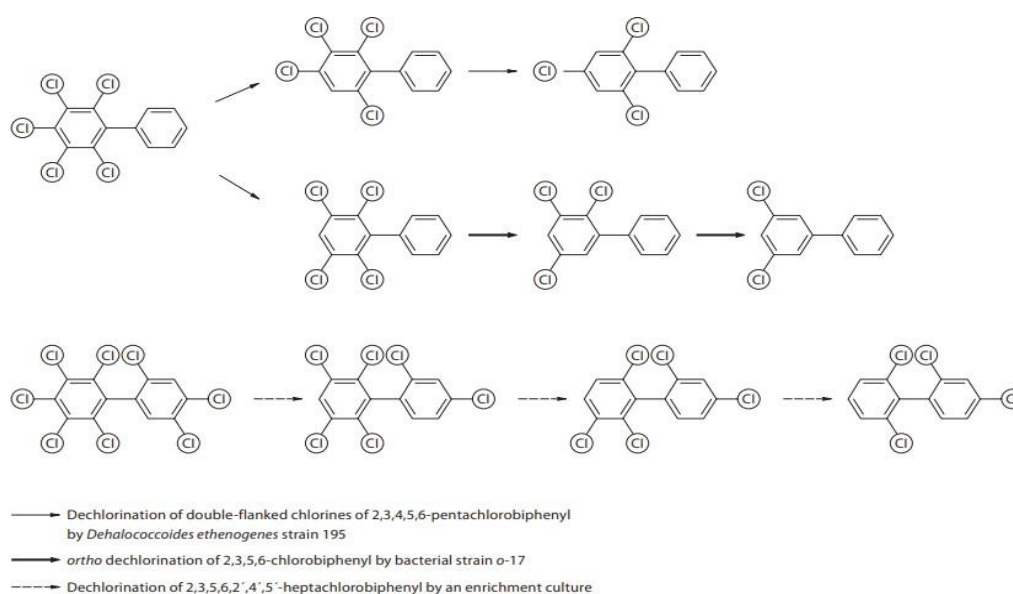


**Fig. 1.6.** Reductive dehalogenation of PCBs results in the release of chlorine from *meta*- and *para*-positions of biphenyl scaffold [Bedard et al., 2006; Fennell et al., 2004]. Anaerobic degradation of PCB occurs in highly chlorinated PCB i.e., with more than four chlorine atoms attached to a biphenyl scaffold. Under anaerobic conditions, 2,3,4,5,6-pentachlorinated PCB act as electron acceptors, releasing one chlorine atom in every step. Reductive dehalogenase (RDase) is the key enzyme catalyzing the PCB dechlorination process in *D. ethenogens*.

It has been reported that anaerobic PCB-degrading bacteria possess reductive dehalogenases (RDase) that catalyze the removal of chlorine molecules. However, RDase genes involved in PCBs dehalogenation lack proper characterization.

### 1.6.2. Aerobic bioremediation

Aerobic biodegradation requires O<sub>2</sub> for the growth and breakdown of organic compounds. Halogenated organic compounds such as PCB act as a source of carbon and energy for the bacteria. Dioxygenases are the main enzyme involved in the aerobic biodegradation of PCB. The aerobic Gram-negative PCB-degrading strains belong to different genera, mainly *Achromobacter*, *Burkholderia*, *Pseudomonas*, *Sphingomonas*, and *Acinetobacter*, while Gram-positive strains are from *Bacillus* and *Rhodococcus* genera. Whole genome sequence and characterization of PCB degrading bacteria, such as *B. xenovorans* LB400 and *R. jostii* RHA1, contributed to providing the overall metabolism, physiology, and their adaptative mechanism against PCB toxicity (Atago et al., 2016; Agullo et al., 2017). Aerobic bioremediation of PCBs involves the biphenyl upper degradation pathway (Pieper and Seeger, 2008; Pieper, 2005). Further, their respective benzoic acid product so formed is channeled through a lower degradation pathway converting into pyruvate and acetyl-CoA. Upper biphenyl degradation involves the following four major steps:

#### **Step1: Oxidation of Biphenyl by Biphenyl 2,3-Dioxygenases**

Biphenyl 2,3-dioxygenases (BphA) usually belong to the toluene/biphenyl branch of Rieske non-heme iron oxygenases (Gibson and Parales, 2000) where a ferredoxin and a ferredoxin reductase act as an electron transport system to transfer electrons from NADH to the terminal oxygenase. The terminal dioxygenase activates molecular oxygen to introduce it into the biphenyl molecule at the 2,3 position to obtain a 2,3-dihydro-2,3-diol (Aken et al., 2010). The biphenyl 2,3- dioxygenases are of crucial importance for the successful metabolism of PCBs. On the one hand, their dioxygenation regioselectivity determines the sites of attack by the subsequent metabolic pathway. On the other hand, their specificity determines the spectrum of PCB congeners that an organism can transform.

#### **Step 2: Dehydrogenation by *cis* -2,3-Dihydro-2,3-Dihydroxybiphenyl Dehydrogenases**

The second step in the PCB degradation pathway involves the dehydrogenation of *cis* -2,3- dihydro-2,3-dihydroxybiphenyls (biphenyl 2,3-dihydrodiol) to (chlorinated) 2,3- dihydroxybiphenyl (BphB) (Pieper and Seeger, 2008). (Fig. 1.7).



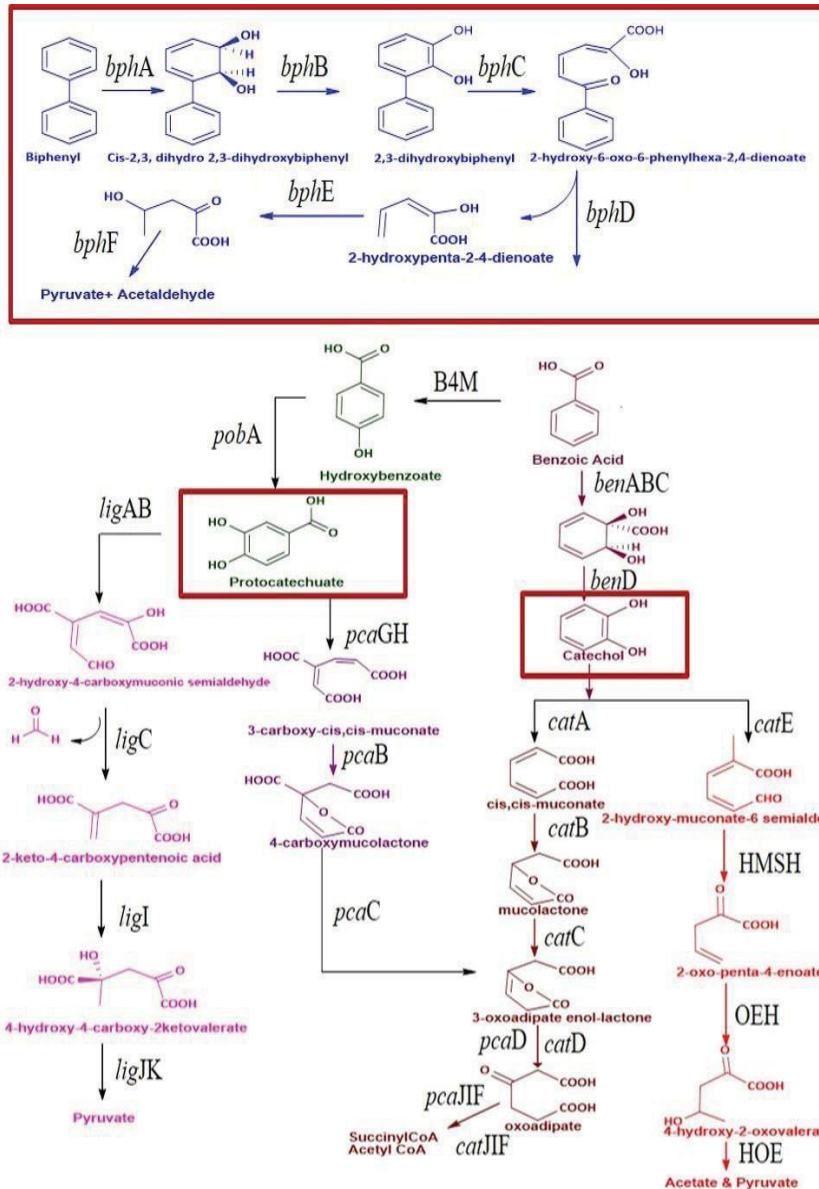


**Fig. 1.7.** The aerobic degradative pathway of biphenyl involves an upper degradation pathway where biphenyl is converted to benzoic acid. The benzoic acid product so formed is channeled through a lower degradation pathway converting into pyruvate and acetyl-CoA.

Blue, biphenyl degradation; red, benzoate degradation via catechol; pink, benzoate degradation via protocatechuate; enter central pathway via protocatechuate intermediate. Genes: *bphA* biphenyl 2,3-dioxygenase; *bphB*, cis-2,3-dihydroxybiphenyl-2,3-diol dehydrogenase; *bphC*, biphenyl-2,3-diol 1,2-dioxygenase; *bphD*, 2,6-dioxo-6-phenylhexa-3-enoate hydrolase; *bphE*, 2-hydroxypenta-2,4-dienoate hydratase; *bphF*, 4-hydroxy-2-oxovalerate aldolase; *benABC*, benzoate 1,2-dioxygenase; *benD*, 1,6-dihydroxycyclohexa-2,4-diene-1-carboxylate dehydrogenase; *catA*, catechol 1,2-dioxygenase; *catB*, muconate cycloisomerase; *catC*, muconolactone delta-isomerase; *catD*, 3-oxoadipate enol-lactonase; *catIJ*, 3-oxoadipate CoA-transferase; *catF*, 3-oxoadipyl-CoA thiolase; *catE*, catechol 2,3-dioxygenase; HSMH, 2-hydroxymuconate semialdehyde hydrolase; OEH, 2-oxopent-4-enoate hydratase, HOE, 4-hydroxy-2-oxovalerate aldolase; B4M, benzoate 4-monooxygenase; *pobA*, 4-hydroxybenzoate 3-monooxygenase; *ligAB*, protocatechuate 4,5-dioxygenase; *ligC*, 2-hydroxy-4-carboxymuconate semialdehyde hemiacetal dehydrogenase; *ligI*, 2-pyrone-4,6-dicarboxylate lactonase; *ligJ*, 4-oxalomesaconate hydratase; *ligK*, 4-hydroxy-4-methyl-2-oxoglutarate aldolase; *pcaGH*, protocatechuate 3,4-dioxygenase; *pcaB*, 3-carboxy-cis,cis-muconate cycloisomerase; *pcaC*, 4-carboxymuconolactone decarboxylase.

This step is catalyzed by the enzyme *cis*-2,3-dihydro-2,3-dihydroxybiphenyl dehydrogenase.

### **Step 3: Second oxidation by 2,3-Dihydroxybiphenyl 1,2-Dioxygenases**

The second dioxygenase, 2,3-dihydroxy-biphenyl dioxygenase (BphC) cleaves the 2,3-dihydroxylated ring between carbon atoms 1 and 2. Oxidation results in the formation of meta-cleavage product 2-hydroxy-6-oxo-6-phenylhexa-2,4-dienoic acid (HOPDA).

### **Step 4: Hydrolysis by 2-Hydroxy-6-Phenyl-6-Oxohepta-2,4-Dienoate (HOPDA) Hydrolases**

The fourth step involves the hydrolysis of HOPDA by 2-hydroxy-6-phenyl-6-oxohepta-2,4-dienoate (HOPDA) hydrolase (BphD) to 2-hydroxypenta-2,4-dienoate and benzoate (Fig. 1.7).

**Lower Pathways for the Degradation of 2-Hydroxypenta-2,4-Dienoates and Benzoates:** The lower biphenyl catabolic pathway oxidizes 2-hydroxypenta-2,4-dienoate to pyruvate and Acetyl-CoA. 2-Hydroxypenta-2,4-dienoate is transformed by 2-hydroxypenta-2,4-dienoate hydratase (BphH), an acylating acetaldehyde dehydrogenase (BphI) and 4-hydroxy-2-oxovalerate aldolase (BphJ) into Acetyl-CoA, which enters the Krebs cycle. The benzoate degradative pathway can occur either via catechol formation or protocatechuate formation. In protocatechuate degradation pathway involves benzoate 4-monooxygenase (CYP450) and a 4-hydroxybenzoate 3-monooxygenase (PobA). After protocatechuate formation, protocatechuate 3,4-dioxygenase (PcaGH) and protocatechuate 4,5-dioxygenase (LigAB) results in complete mineralization *via* ortho and meta cleavage, respectively.

## **1.7. Adaptation strategies of PCBs degrading microorganisms**

### **1.7.1. Cell membrane modification**

Bacteria undergo modification in the cell membrane as an adaptation mechanism for survival. Hydrophobic pollutants such as PCBs, when in contact with the cytoplasmic membrane, alter the saturation of the bacterial membrane. Accumulation of PCBs results in increased fatty acid saturation of bacterial membranes (Zoradova et al., 2011). Further, it leads to significant functional imbalance and bacterial death. Fatty acids are the main constituents of membrane phospholipids. Modulating the number and position of double bonds of acyl chains by specific fatty acid desaturases plays a crucial role in preserving an appropriate dynamic state of the bilayer during environmental impact (Sajbidor, 1997). A correlation between an increase in the degree of saturation of membrane fatty acids and increased tolerance towards the toxic compounds in phenol-degrading strain *P. putida* P8 has been reported (Heipieper et al., 1992). This phenomenon



is thought to be the major long-time adaptive mechanism in microorganisms exposed to toxic aromatic compounds. Another membrane adaptation mechanism, such as *cis/trans* isomerization of unsaturated fatty acids (UFAs), has been observed under growth-inhibiting conditions. Steric differences between *cis* and *trans* configurations reduce membrane fluidity (Kabelitz et al., 2003). Changes in branched fatty acids can also be observed in an adverse environment (Chavez et al., 2006).

### **1.7.2. Production of Biosurfactants**

Another adaptive mechanism is the production of certain surface-active compounds like biosurfactants that aid in eliminating PCBs outside the cells (Ron and Rosenberg, 2001; Chakraborty and Das, 2016). Biosurfactants are generally categorized by their microbial origin, and their chemical composition includes glycolipids (rhamnolipids, trehalolipids, sophorolipids), lipopeptides/lipoproteins, and surfactin. Several PCB-degrading bacteria, such as *Pseudomonas* sp. (Pathiraja et al., 2019), *Rhodococcus* sp. (Petric et al., 2007), and *Bacillus* sp. (Gudina et al., 2015) are known to produce biosurfactants. Biosurfactants are reported to enhance the biodegradation of hydrophobic organic compounds (HOCs), including PCBs. Several studies have demonstrated the role of biosurfactants in solubilisation, and mobilization of PCB to the bacteria. They may be present on the surface of the bacteria or are extracellularly released into the environment. The uptake of organic compounds occurs directly through cellular contact with hydrophobic compounds or by micelles formation.

### **1.7.3. Efflux system**

The Efflux systems export toxic compounds through the cell membranes in a single-energy-coupled step with the help of complex transporters. It requires a cytoplasmic membrane export system, an outer membrane factor, and a membrane fusion protein (Amaral et al., 2014). It is reported that AcrAB–TolC is the primary multidrug efflux system that facilitates the efflux of pollutants such as PCB outside the cell. The efflux system transporters for organic compounds have been identified in multidrug-resistant Gram-negative bacteria belonging to the resistance-nodulation-cell division family (RND) of pumps encoded chromosomally. The sequence of AcrAB–TolC has been found to be conserved in all Gram-negative bacterial genomes and affect the accumulation and PCB degradation. Geng et al. (2012) have reported constitutive expression of multidrug efflux system AcrAB–TolC in *E. coli*, the major facilitator for the efflux of hydroxylated PCBs (HPCBs) out of the cell. HPCBs are known intermediates of PCBs. HPCBs

are more hydrophilic than the original PCBs, therefore easy to be removed. Therefore, it is an environmentally friendly process that uses microorganisms to degrade hazardous chemicals into non-toxic ones. Several studies indicated the importance of the physical properties of compounds (hydrophobicity and molecule charge) for determining the specificities of this mechanism. Microbes must import the compound into their cytosol to break down a compound. Eliminating toxic chemicals occurs by an uncontrolled efflux and accelerates the active extrusion of structurally unrelated compounds from the cytoplasm or the cytoplasmic membrane to the external space. Toxic organic pollutants may represent substrates for the efflux system. A typical RND efflux pump consists of three components: a transporter (efflux) protein trimer TtgB, an outer membrane protein trimer TtgC and a lipoprotein trimer TtgA. TtgB is located in the bacterium's inner (cytoplasmic) membrane, TtgC penetrates the periplasmic space to form a channel, and TtgA is a membrane fusion protein located in the periplasmic space and plays a role in stabilizing the interactions between the two other elements. Two paralogous SrpABC and TtgABC RND efflux pumps have been reported to be exporters of biphenyl intermediates of PAH into the extracellular medium (Yao et al., 2017; Yao et al., 2021). Further, it has been identified that biphenyl, 2-hydroxybiphenyl, 3-hydroxybiphenyl, and 2,3-dihydroxybiphenyl (2,3-DHBP) acts as an inducer of SrpABC.

#### **1.7.4. Polyphosphates (polyP)**

Polyphosphate (polyP) is a ubiquitous linear polymer with hundreds of orthophosphate residues (Pi) linked by high-energy phosphor anhydride bonds. Polyphosphate kinase (PPK) is the best-known enzyme that is reported to be present in polyP metabolism in bacteria. This enzyme catalyzes the reversible conversion of the terminal phosphate of ATP into polyP. Another enzyme, exopolyphosphatase hydrolyzes the terminal residues of polyP to liberate Pi (Kornberg et al., 1999). Several reports on PCB-degrading bacteria highlight the increased accumulation of polyP during the exponential growth phase when supplied with biphenyl as the sole carbon source. For example, *Pseudomonas* strain B4, and *B. fungorum* LB400 accumulated polyP in the presence of chlorobiphenyl in the exponential phase as an adaptive mechanism (Chavez et al., 2004).

#### **1.7.5. Stress response**

Another known response of bacterial cells to POPs presence is the production and overexpression of stress proteins (Agulló et al., 2007). A toxic environment acts not only on the envelope but usually affects the cell proteome. Additionally, physiological adjustments include induction of the

general stress protein GroEL and reactive oxygen species (ROS) to growth in PCB. Thus, it is concluded that PCB stress drives the synthesis of certain stress-resistant adaptations in bacteria for their survival in PCB-contaminated sites.

### 1.7. Genetic organization and biphenyl transcriptional regulation

Gram-negative and Gram-positive bacterial strains aerobically and anaerobically have been described (refer to section 1.6). Although a single cluster of biphenyl degradation (*bph*) genes is present in most biphenyl-degrading bacterial isolates studied to date, certain strains appear to have multiple sets of degradation genes, some of which function in the degradation of multiple aromatic hydrocarbon substrates.

The structure and organization of the *bph* gene of some bacteria are found to be similar, while it differs in others, indicating that the *bph* gene cluster undergoes rearrangement. *bph* genes have been found on bacterial chromosomes, plasmids, or transposable elements in different biphenyl degraders. The genes encoding enzymes for biphenyl degradation are clustered and termed a *bph* gene cluster, which can be divided into four types based on the arrangement/order of genes. The first type of *bph* gene cluster consists of *bphA1*, *bphA2*, *bphA3*, *bphA4* (biphenyl dioxygenase), *bphB* (cis-2,3-di-hydro-2,3-dihydroxybiphenyl dehydrogenase/dihydrodiol dehydrogenase), *bphC* (2,3-dihydroxybiphenyl 1,2-dioxygenase) and *bphD* (2-hydroxy-6-oxo-6-phenylhexa-2,4-dienoate HOPDA hydrolase). Genes encoding enzymes of the biphenyl upper pathway (*bph*) were first cloned from *P. pseudoalcaligenes* KF707 (Furukawa and Miyazaki, 1986) and later from *Burkholderia* sp. LB400 (Mondello, 1989). The first typical *bph* gene cluster was observed in *Burkholderia* sp. LB400 (Hofer et al., 1994) and *P. pseudoalcaligenes* KF707 (Furukawa and Miyazaki, 1986), with *bphR*, *bphA1*, *bphA2*, *bphA3*, *bphA4*, *bphB*, *bphC*, *bphK*, *bphH*, *bphJ*, *bphI*, *bphD* genes. In both strains, the genes namely *bphA1*, *bphA2*, *bphA3*, *bphA4*, *bphB*, *bphC*, and *bphD* are organized in an operon, with genes *bphK* encoding a glutathione S- transferase and enzymes involved in the transformation of 2-hydroxypenta-2,4-dienoate released during hydrolysis of HOPDA to form benzoate (2- hydroxypenta-2,4-dienoate hydratase, *bphH*; acetaldehyde dehydrogenase, *bphJ*; 4-hydroxy-2-oxovalerate aldolase, *bphI*) localized between *bphC* and *bphD* (Hofer et al. 1994) (Fig. 1.8).

The second type of *bph* gene cluster with *bphS*, *bphE*, *bphG*, *bphF*, *bphA1*, *bphA2*, *bphA3*, *bphB*, *bphC*, *bphD*, *bphA4* genes was reported in *A. georgiopolitanum* KKS102 (Kikuchi et al., 1994) and *Alcaligenes eutrophus* A5 (Merlin et al., 1997; Mouz et al., 1999). The third cluster type

includes *bphA1*, *bphA2*, *bphA3*, *bphA4*, *bphC*, *bphB*, *bphS*, *bphT* genes observed in *Rhodococcus* sp. RHA1 (Masai et al., 1995). *bphD* in this strain is replaced by two-component signal transduction systems *bphT* and *bphS* (Takeda et al., 2004).

Recently, a fourth, novel type of *bph* cluster was discovered in *Rhodococcus* sp. R04 (Yang et al., 2007) and *Rhodococcus* sp. K37 (Taguchi et al., 2007) with the order *bphB*, *bphC*, *bphA1*, *bphA2*, *bphA3*, *bphA4*, *bphD*, which differed from that of other biphenyl degraders reported previously. Genes *bphB*, *bphC*, *bphA1*, *bphA2*, *bphA3*, *bphA4*, *bphD* encoding enzymes involved in PCB degradation upper and lower pathway converting it to acetyl-CoA are found to be located on the same operon.

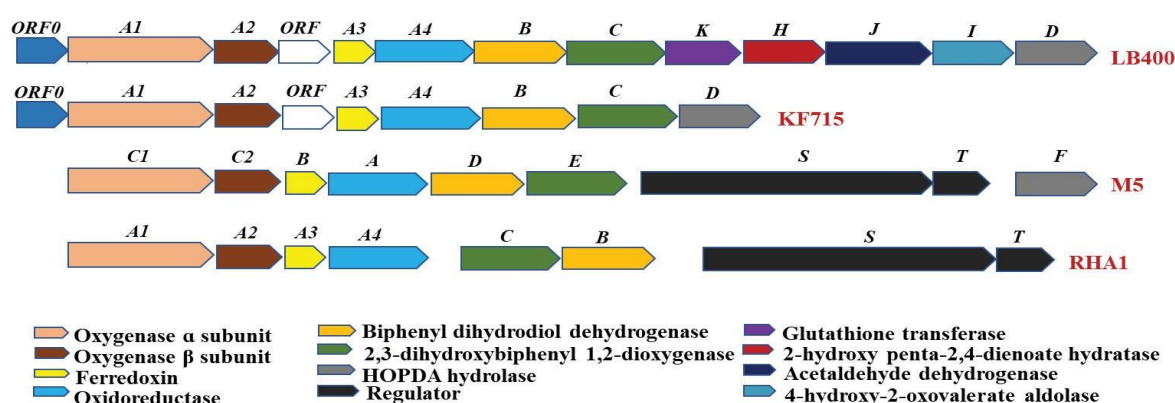


**Fig. 1.8.** Genetic organization of *bph* gene cluster of *Burkholderia* sp. LB400, *P. putida* KF715, *Rhodococcus* sp. M5 and *Rhodococcus* sp. RHA1 (adapted from Furukawa et al., 2004).

The *bphC1*, *bphC2*, *bphB*, *bphA*, *bphD*, *bphE* gene cluster and a distally located *bphF* gene in M5 (see Fig. 1.8) encode the first four enzymes for the degradation of biphenyl to benzoate and 2-hydroxy-penta-2,4-dienoate. A pair of regulatory elements (*bphS* and *bphT*) is situated between *bphE* and *bphF*, identified as genes encoding new members of the two-component signal transduction proteins (Wang et al., 1995).

For the origin of PCBs-degrading genes, aromatic ring dioxygenases evolved from a common ancestor, as evidenced by toluene dioxygenase, benzene dioxygenase, naphthalene dioxygenase and biphenyl dioxygenase (Harayama and Kok, 1992). It also could be postulated that many degraders of aromatics might be involved in the degradation of plant lignin, which is massively distributed in the environment (Furukawa 1994).

### Transcriptional regulation of *bph* genes

Two regulatory systems include regulatory genes *bphR1* and *bphR2* in *P. pseudoalcaligenes*

KF707 are involved in the regulation *bph* gene cluster, *bphR1*-*bphA1*, *bphA2(orf3)* *bphA3*, *bphA4*, *bphB*, *bphC*, *bphX0*, *bphX1*, *bphX2*, *bphX3*, and *bphD*.

The *bphR1* gene is located just upstream of *bphA1* but *bphR2* is separated from the other *bph* genes. The BphR1 protein belongs to the GntR family, and the BphR2 protein belongs to the LysR family. The BphR2 protein positively regulates the *bphA1*, *bphA2*, *bphA3*, *bphA4*, *bphB*, *bphC* genes and allows biphenyl to convert to HOPDA. The BphR1 protein binds with HOPDA and activates the transcription of the *bphR1* gene itself. The BphR1 protein is also involved in expressing the *bphX* region and *bphD*. Thus, there are two regulatory systems as follows: (i) *bphR1*-dependent transcription for *bphR1* itself, *bphX0*, *bphX1*, *bphX2*, *bphX3*, and *bphD* and (ii) *bphR2*-dependent transcription for *bphA1*, *bphA2(orf3)*, *bphA3*, *bphA4*, *bphB*, and *bphC*. In this regulatory system, it is believed that the BphR2 protein first activates the transcription of *bphA1*, *bphA2(orf3)*, *bphA3*, *bphA4*, *bphB*, and *bphC* to convert biphenyl to the meta-cleavage compound (HOPDA), which binds to BphR1 to activate this protein. The activated BphR1 protein binds to the promoter-operator regions of *bphR1* itself and to *bphX0*, *bphX1*, and *bphD* to promote the transcription of these genes (Fig. 1.9).

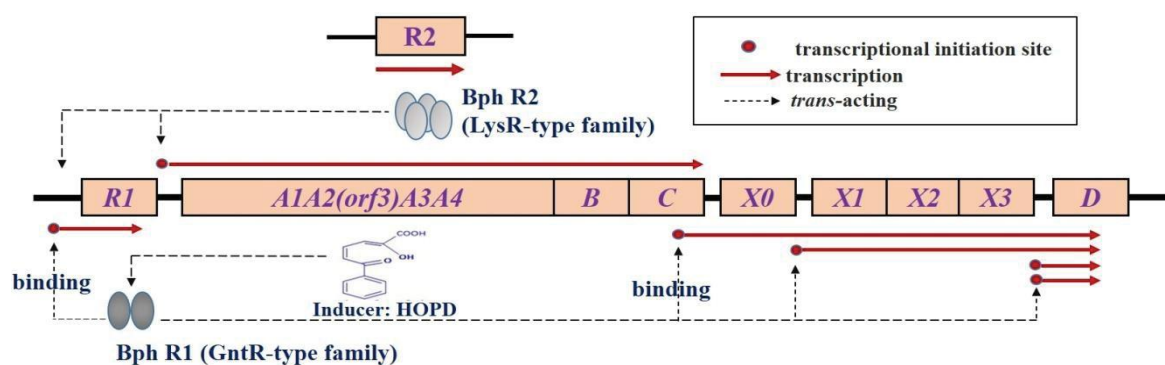


**Fig. 1.9.** Transcriptional regulation of *bph* genes in *P. pseudoalcaligenes* KF707 (adapted from Watanabe et al., 2003). In *P. pseudoalcaligenes* KF707 *bph* genes are likely to be regulated by two regulatory systems: *bphR2*-dependent transcription for *bphA1A2(orf3)-bphA3A4BC* and *bphR1*-dependent transcription for *bphR1* itself, *bphX0X1X2X3*, and *bphD*. The BphR1 protein, belonging to the GntR-type family, is required to express *bphR1* itself and *bphX0X1X2X3D*, while the BphR2 protein belongs to the LysR-type family. In these systems, BphR2 first activates the transcription of *bphA1A2(orf3)-bphA3A4BC* to convert biphenyl to HOPD, which binds to BphR1 to activate this protein. The activated BphR1 then promotes the transcription of *bphX0X1X2X3* and *bphD*.

The transcription of the *bph* locus of *Burkholderia* sp. strain LB400, whose *bph* genes are very similar to those of KF707, was investigated (Fig. 1.10). In this system, the ORF0 protein (corresponding to KF707 BphR1) mediates the activation of the *bphA1* promoter. It is reported to

have a glutathione transferase gene (*bphK*), two ORFs (*ORF0* and *ORF1*), and three promoters (p1, p2, and p3) (Erickson and Mondello, 1992). Promoter p1 and p2 are located directly upstream *ORF0*, is activated by biphenyl. The locus contains ten cistrons encoding enzymes for degrading biphenyls to benzoates, pyruvates, and acetyl-CoA. It should be noted that the regulatory mechanisms of the *bph* genes are different between *P. pseudoalcaligenes* KF707 and *Burkholderia* sp. strain LB400, even though the *bph* genes of these two strains are nearly identical.

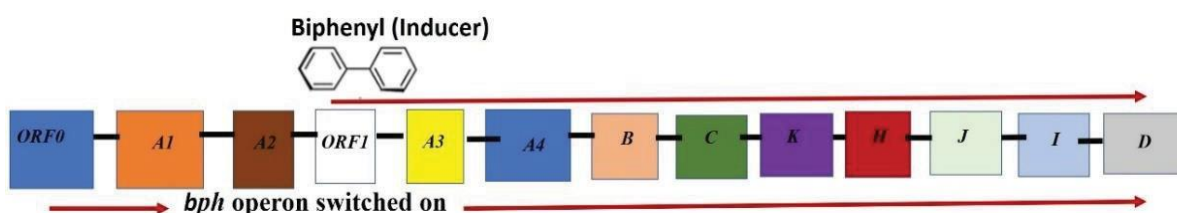


**Fig. 1.10.** Transcriptional regulation of *bph* genes in *Burkholderia* sp. strain LB400 via activation of *bphA1* promoter in the presence of biphenyl. PCB degradation by strain LB400 is greatest when the cells are grown with biphenyl as the sole carbon and energy source. It consists of glutathione transferase gene (*bphK*), two ORFs (*ORF0* and *ORF1*), and three promoters (p1, p2, and p3). The expression of *bphK* is coregulated with the expression of genes responsible for the catabolism of biphenyl.

## 1.9. Molecular approaches to study microorganisms for bioremediation

### 1.9.1. Cultivation-dependent approach

The isolation and characterization of pure cultures have been crucial for developing and interpreting molecular analysis. The recovery of isolates that are representative of the microorganisms responsible for the bioremediation process can be invaluable. These isolates provide the opportunity to investigate their biodegradation reactions and other aspects of their physiology likely to control their growth and activity in contaminated environments. The conventional method for obtaining novel enzymes by cultivation and subsequent screening of pure culture strains is a standard and robust approach. However, with the advances in molecular microbial ecology, it has become apparent that a large portion of environmental microorganisms cannot be easily cultured in the laboratory using standard methods. The cultivation-dependent approaches have isolated many cultivable PCB-degraders, including *Pseudomonas* sp., *Alcaligenes eutrophus* H850, *R. globerulus* P6, and *B. xenovorans* LB400 (Hong et al., 2009; Gorris et al., 2004). The isolation of the bacteria provided important insights into the physiological properties and mechanisms of these PCB-degrading microbes. In addition, PCB-



degrading genes and biodegradation pathways have been identified with the aid of these isolates. For example, the oxidation of biphenyl to 2,3-dihydroxybiphenyl is catalysed by biphenyl dioxygenase encoded by *bphA* genes. It is the initial step of PCB aerobic mineralization and the rate-limiting step of the PCB degradation pathway. Bio-remediator microorganisms are useful in various methods for dechlorinating chlorinated biphenyls (PCBs), including anaerobic dechlorination of ortho- and double-flanked chloro- substituents of PCBs. However, there is a large gap between microorganisms capable of utilizing PCBs or BP in nature and those cultivated in the laboratory. Moreover, doubt remains whether these bacteria or genes are truly active or functional for PCBs or BP degradation in the microbial communities of PCB-contaminated sites. Bioremediation methods may employ consortia of effective microbial species, e.g., aerobic and anaerobic species, to dechlorinate corresponding PCB mixtures containing widely varying and significant numbers of PCB congeners. However, no such patent has been reported on the bioformulation development based on the consortium, answering all the bottlenecks related to poor PCB degradation.

### **1.9.2. Cultivation-independent approaches**

Studies of the diversity of microbial communities reveal that most bacteria from the environment are currently not cultivable (99%). Although degradation of PCB by isolated microbes is well characterized to a certain extent, as discussed earlier, knowledge on the role of uncultivable microbes in PCB bioremediation is very limited. Assessments of the biodiversity of a broad range of habitats revealed that the cultivability of strains does not follow a statistical distribution but is related to phylogeny. With the advent of culture-independent/metagenome approaches, the exploration of unveiled genetic resources in the environment has rapidly increased. Whole genome metagenomic sequencing has helped explore the potential of culturable and unculturable microorganisms. It has been possible to develop models that are needed for predicting microbial activity under various bioremediation strategies. The metagenomic approach has resulted in identifying the bacteria and the genes encoding the enzymes in different biodegradation pathways (Fang et al., 2010; Garrido-Sanz et al., 2018; Behera et al., 2020). Culture-independent approaches clarified potential microbial roles; however, culture-based studies are still needed to comprehend microbial characteristics and phenotypes. Metagenomics has boosted industrial production systems and enzyme bioprospecting (Madhavan et al., 2017). To date, very few

metagenomes analysis of PCB-contaminated sites has been done. Also, there are no studies conducted on PCB-contaminated soil from steel industries.

### **1.10. Gaps in Existing Research**

Over the past few years, the ability of bacteria to degrade a broad range of PCBs both anaerobically and aerobically has been investigated. However, applying microbial-based bioremediation to treat PCB-contaminated soil is not widely practiced. The following are the gaps in the existing research:

**1. Lack of metagenomic study:** Very few reports on metagenomic data related to PCB degradation by bacterial population and analysis of their PCB degrading potential. Despite several years of research on PCB biodegradation, the exploration of microbial communities in PCB-contaminated areas and their potential for biodegradation is limited. There are several reports of PCB contamination in industrial sites in India, but no reports on the metagenomic analysis of PCB-contaminated sites have been conducted so far. Microbial communities enriched in bacteria can thrive by degrading pollutants. The PCB-contaminated site increases the growth of specific microbial degraders, illustrated by the strong adaptation and bioremediation ability of such indigenous bacteria (refer to sections 1.9.2 & 1.7).

**2. Poor studies on Steel Industry contamination:** Some studies on aerobic and anaerobic microorganisms capable of degrading a broad range of PCBs have been conducted over the last decade. But there is very scarce information about the aerobic PCB degradation activity of the bacteria isolated, especially from the steel industry. The effectiveness of complete mineralisation or bioremediation is determined by a number of factors, such as PCB degrader in the contaminated environment, maintaining the PCB degrading bacterial communities in environmental conditions, the nature of the PCB mixture, the severity of contamination and bioavailability of PCBs. Therefore, identifying suitable microorganisms capable of surviving under a PCB-contaminated environment while producing biosurfactants would accelerate PCB solubility and subsequent degradation. In the present work, we also aim to conduct a whole genome sequence analysis of the best bacterial isolate in PCB degradation.

**3. Lack of mechanistic/interaction studies:** The knowledge of both synergistic and antagonistic relations between bacteria and the mechanisms of this cooperation among them in PCB degradation studies is still not fully understood. Due to the complexity of commercial PCB



mixtures with varying degrees of chlorination, a single bacterium cannot degrade all or even most of the PCB congeners present in contaminated environments. A particular strain of microorganisms may degrade one or more compounds. Sometimes, for the degradation of a single compound, the synergetic action of a few microorganisms (i.e., a consortium of microbes) may be more efficient. Based on the information on the PCB degradation potential of individual microbes and the metabolites produced, the bioformulation of bacterial consortia would be a more practical approach for the biodegradation of PCB in soil.

**4. Lack of Bioformulation development:** Very few attempts by various research groups have been made to deliver the PCB-degrading bacteria in the form of bioformulation. Moreover, the research has been mainly confined to the laboratories, and no successful PCB degradation reports exist. Also, there are very few reports on combinational strategies/work for using both conventional and metagenomic approaches.

### **1.11. Aim**

Considering the above potential gaps in the existing research, the present thesis aims at "Molecular and Functional Characterization of Polychlorinated Biphenyl (PCB) Degrading Bacteria concerning Bioremediation." It would involve a wide array of studies that include metagenomics, molecular biology techniques, and bioformulation preparation. The proposed research will elucidate the composition of microbial communities of PCB-polluted soil, their adaptation mechanisms, the identification of the effective PCB degrader, and the interactions among populations and the genes involved in the degradative pathway employing culture- dependent and culture-independent methods.

### **1.12. Objectives**

- 1.** Analysis of metabolic potential and bacterial diversity of PCB-degrading bacteria using a metagenomic approach
- 2.** Enrichment, isolation, and characterization of PCB-degrading bacteria
- 3.** Optimization of consortia-based bacterial bioformulation for enhanced PCB degradation

## **Chapter II**

# **Analysis of Metabolic Potential and Bacterial Diversity of PCB Degrading Bacteria Using a Metagenomic Approach**

---

## 2.1 Introduction

The contaminated soil environment consists of the genetic, species, and metabolic diversity of microbial degraders. However, only a minor fraction of POP-degrading bacteria can be obtained using a culture-dependent method. Furthermore, it has been reported that enrichment of these cultures under lab conditions is less efficient in biodegradation than indigenous bacteria in the contaminated soil (Isaac et al., 2013; Isaac et al., 2015). To date, information related to taxonomic and functional interaction amongst the microbial communities during the biodegradation process within the contaminated environment is skewed. The recent development of powerful culture-independent metagenomic approaches and the advancement of next-generation sequencing (NGS) technology provides a comprehensive insight into the entire microbial community and their metabolic capabilities inhabiting contaminated sites. Several metagenomics studies conducted on PCB-contaminated soil samples (Leewis et al., 2016; Garrido-Sanz et al., 2018; Zhang et al., 2019) have highlighted the role of microbial interaction that plays a pivotal part in the bioremediation of these POPs. However, most of these studies are based on the 16S rRNA gene sequence, which does not highlight the metabolic potential of resident microorganisms. Therefore, the present study aimed to investigate taxonomic diversity and their metabolic potential to degrade POPs by employing Oxford Nanopore Technology (ONT). ONT is sensitive and can detect very low abundant microbial members that are otherwise missed in the metagenome (Jain et al., 2016).

The PCBs congeners have been reported to be present in the waste sites of the industrialized area of the Bhilai steel plant in India (Yadav et al., 2016). The primary source of pollution of steel industries includes sinter, coke, and blast furnace (Jiun-Horng et al., 2007). Therefore, the present study aimed to investigate and provide an insight into the diversity of the bacterial community and metabolic potential of the dominant bacterial community in the contaminated soil collected from nearby regions of this steel plant (one of Asia's biggest steel plants) in Chhattisgarh, India, and to correlate their functional characteristics to the biodegradation pathways.

## 2.2 Materials and methods

### 2.2.1 Study site and sampling

The soil samples were collected from 3 different sites, i.e., normal soil (Metagenomic Bhilai; MGB-1), a sludge site (Metagenomic Bhilai; MGB-2), and a dry soil waste site (Metagenomic Bhilai; MGB-3) from the polluted area near the Bhilai steel plant, Chhattisgarh (21.1915°N,

81.4041°E), in India (Fig. 2.1). Soil samples were collected in sterile containers from a depth of about 0 to 10 cm of two sampling sites. The soil samples were randomly collected from three areas of each site and pooled for further analysis. It was then transported on an ice pack and stored at 4 °C (to be used immediately) in the lab for analysis.



**Fig. 2.1.** Map illustrating the sampling location of three soil samples (Metagenomic Bhilai MGB-1, MGB-2 and MGB-3) collected from a polluted site near Bhilai steel plant, Chhattisgarh (India).

#### 2.2.1.2. Extraction and determination of PCB in sediments

PCBs were extracted following He et al. (2015) with minor modifications. Briefly, 5 g each of MGB-1, MGB-2, and MGB-3 was added into 50 mL Milli Q (MQ) water and homogenized by vortexing for 15 min. After allowing it to stand for 30 min, 10 mL of acetone and hexane (1:1; v/v) was added and vortexed for 3 min. Further, 2g NaCl was added, shaken vigorously for 2 min, and centrifuged at 4000 x g for 5 min. The supernatant was subjected to further solid-phase extraction (SPE) of PCBs using a bond elute cartridge as per the manufacturer's instruction (Agilent Technologies, USA). Further, the sample elution was performed with methanol and hexane (1:1; v/v) in 5 mL MQ water by centrifuging for 2 min at 1000 x g. The final elute was then collected through a Polytetrafluoroethylene (PTFE) filter (0.22 μ) in a separate vial and concentrated to 1 mL with nitrogen gas (Weiland-Brauer et al., 2017).

GC-MS/MS (Model: TQ8040, Shimadzu, Japan) was used to qualitatively analyze PCBs potentially present in the MGB-1, MGB-2, and MGB-3 samples. The analysis was carried out using RTX-5 column (30 m × 0.32 mm × 0.25 μm) in Scan/SIM mode. GC conditions were set at 40°C with a 2 min hold and 10°C/min increment upto 80°C, then 6 °C/min up to 225°C with 10

min hold. The PCB-contaminated soil samples (MGB-2 & MGB-3) were carried forward for further analysis.

### 2.2.2. Physicochemical parameters of the PCB-contaminated soil samples

Physicochemical parameters such as pH, electrical conductivity, organic C, N, P, Mg, K, Na, Cl, Ca, S, Zn, Fe, Cu, and Mn of MGB-2 and MGB-3 soil samples were estimated using the standard protocol at the National Horticultural Research and Development Foundation, Nasik, India.

### 2.2.3 Metagenome sequencing and analysis

#### 2.2.3.1 DNA extraction and processing for metagenome

DNA extraction from MGB-2 and MGB-3 was done using Powersoil<sup>®</sup> DNA Isolation Kit (Qiagen, USA) following the manufacturer's instructions. The metagenomic DNA was checked for integrity by agarose gel (1%) using a BioRad Gel documentation system and was quantified by Qubit 3.0 Fluorometer (Invitrogen, USA).

#### 2.2.3.2 Preparation of library and whole metagenome sequencing

Metagenomic DNA extracted from the collected soil (MGB-2 and MGB-3) and were outsourced for whole genome metagenome sequencing from Genotypic Pvt. Ltd. Bangalore. Metagenomic DNA was end-repaired using NEBnext ultra II kit (New England Biolabs, USA) and cleaned up with 1x AmPure beads (Beckmann Coulter, U.S.A.). Native barcode ligation was performed with NEB blunt/TA ligase using NBD103 and cleaned with 1x AmPure beads. Qubit quantified barcode ligated DNA samples were pooled at an equimolar concentration to attain a 1 µg pooled sample. Adapter ligation (BAM), library mix cleaning, and sequencing library elution were done as per Kumar et al. (2021) and were further used for whole-genome sequencing. The whole- genome library was prepared using a Native Barcoding kit (EXP-NBD103). Barcode sequences are detailed in Table 2.1.

**Table 2.1.** Barcode used for sequencing

S.No	Sample ID	Barcode name	Sequences
1	SO_8116_MGB2	NB08	ACGTAACCTGGTTTGTTCCTGAA
2	SO_8116_MGB3	NB09	AACCAAGACTCGCTGTGCCTAGTT

The sequencing was performed using SpotONflow cell (R9.4) on MinKNOW 2.1v18.05.5 with a 48h sequencing protocol (Laver et., 2015) on GridION X5 Oxford Nanopore Technology, UK.

#### 2.2.3.3 Data processing and analysis

The Nanopore raw reads (*fast5* format) were base-called (*fastq5* format) and demultiplexed using Albacore v2.3.1 and were uploaded to MG-RAST server (version 4.0.3) for taxonomic and functional analysis. Functional annotation was done using SEED subsystems to predict the abundance of genes assigned to metabolic pathways in soil. The sequenced reads were interpreted using a multisource non-redundant ribosomal RNA database for taxonomic diversity. They were determined using the contigLCA algorithm against the M5NR database for samples analyzed *via* whole-genome sequencing (WGS) (MG-RAST metagenome MGB-2 and MGB-3 identification numbers = mgm4822000.3, mgm4822001.3). The interpretation was based on E-value cut-off =  $1 \times e^{-5}$  and sequence identity of 60% (Randle-Boggis et al., 2016; Brumfield et al., 2020). Raw reads of whole genome metagenome shotgun sequence of MGB-2 and MGB-3 were deposited to the NCBI Sequence Read Archive under Bio Project PRJNA765179 with the accession numbers SRR16004303 and SRR16004304, respectively.

#### **2.2.2.4. Statistical analysis**

Various alpha diversity indices were calculated to study species richness and evenness of the MGB-2 and MGB-3 using PAST4.03 software. The principal component analysis (PCA) plot was constructed using Bray-Curtis matrices with R studio v3.1.2. Comparison of samples MGB-2 and MGB-3 was made using Statistical Analysis of Metagenomic Profiles software (Parks and Beiko, 2010) with a two-sided G-test (w/Yates'+ Fischer's). Comparative metagenome analysis was done mainly with RefSeq and SEED subsystem to obtain genus/functional abundance. Cytoscape software v3.7.1 was used to generate networking plots to study the interaction of microbial communities of MGB-2 and MGB-3 involved in xenobiotic biodegradation pathways.

### **2.3 Results and discussions**

#### **2.3.1 Determination of PCB residues in MGB-2 and MGB-3**

Cities with long industrial history contribute to adding organic pollutants to soil (Jiang et al., 2018; Ontiveros-Cuadras et al., 2019). Hence, we examined the presence of various PCBs in MAPB-1, MGB-2, and MGB-3 by GC-MS/MS. GC-MS/MS triple quadrupole allows detection at very low (femtogram) limits of analyte in the matrix through the use of greater selectivity with selected reaction monitoring (SIM) mode (Ayriss et al., 1997). Based on the data obtained from GC-MS/MS analysis, various PCBs in MGB-2 and MGB-3 were identified. The structure of identified PCBs in MGB-2 and MGB-3 are given in Fig 2.2.



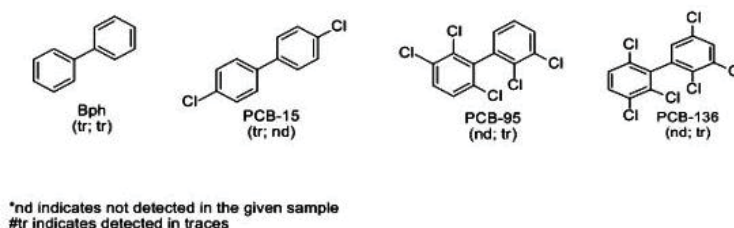


**Fig. 2.2.** Structure and relative abundance of the PCB identified in MGB-2 and MGB-3. Bph, PCB-15, PCB-95, and PCB-136 represent biphenyl, 1,1'-biphenyl, 4,4'-dichloro, biphenyl, 1,1'-biphenyl 2,2',3,3',5,6-pentachloro and 1,1'-biphenyl 2,2',3,3',6,6'-hexachloro respectively.

MGB-1 was not found to be contaminated with PCB; therefore, this soil sample was not used for further studies. MGB-2 and MGB-3 were found to be contaminated with PCBs such as biphenyl, 4,4'-dichloro, biphenyl, (PCB-15) in MGB-2 (Fig. 2.3A) and biphenyl, 2,2',3,5',6-pentachloro, biphenyl (PCB-95), and 2,2',3,3',6,6'-hexachloro, biphenyl (PCB-136) in MGB-3 (Fig. 2.3B) (Aydin et al., 2014). It is well-studied that the carcinogenic risk increases with the molecular weight or the aromatic ring of PAHs (Yang et al., 2002) and with the chlorine atoms in the case of PCBs (Cogliano, 1998). However, the data on the source of PCBs has been scarce in industrial regions, as they are added into the atmosphere as side products of the manufacturing and incineration process. The present study highlights the presence of PCB in the nearby soil of the steel industry along with other organic contaminants such as PAH and benzene.

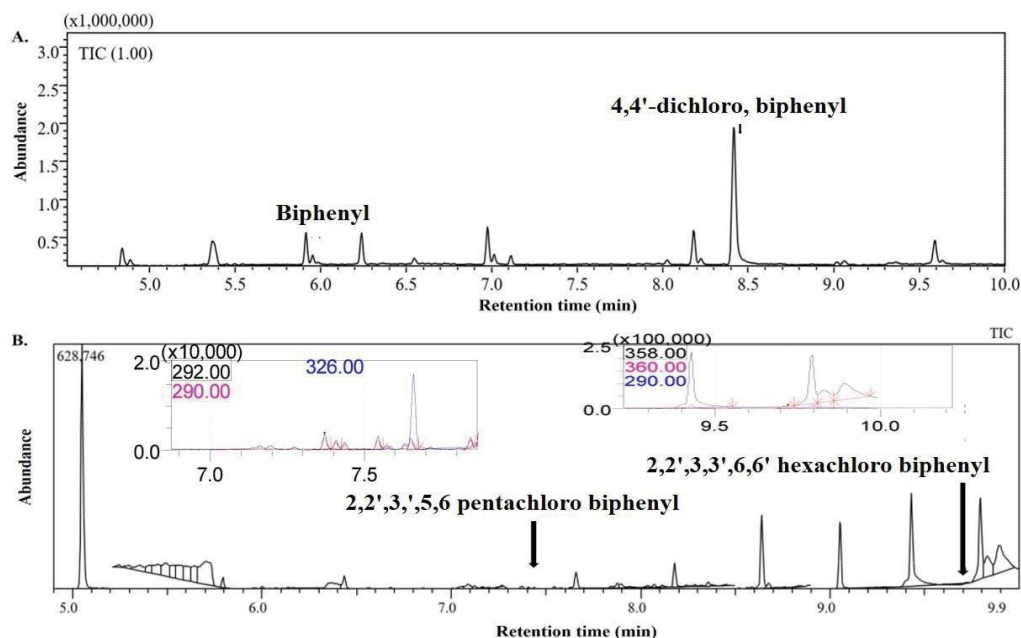


**Fig. 2.3.** GC-MS/MS-based identification of PCB in MAPB-2 and MGB-3 soil sample (A) Biphenyl and 1,1'-Biphenyl 4,4'-dichloro- identified at Rt 5.9 and 8.4 min respectively, in MAPB-2 while (B) 1,1'-Biphenyl 2,2',3,3',5,6-pentachloro- and 1,1'-Biphenyl 2,2',3,3',6,6'-hexachloro- was identified at 7.4 and 9.7 min *via* SIM mode respectively, in MAPB-3.

The present results corroborate with previous studies conducted on the Bhilai steel plant (Raipur, Chhattisgarh) soil, reporting the presence of PCBs ranging from mono-chlorinated to octa-chlorinated biphenyl in the sludge (Patel et al., 2015). From the data on organic contaminants, it appears that the high carbon content in MGB-2 and MGB-3 mentioned in the previous section could correlate with PCB in the soil samples.

### **2.3.2. Physico-chemical analysis of the MGB-2 and MGB-3**

Various environmental factors, including nutritional status and other parameters, such as pH, salinity, presence of metals, and different physicochemical parameters, determine microbial community structure and function. Therefore, the physicochemical properties of the MGB-2 and MGB-3 soil samples were determined and are summarized in Table 2.2. The sample MGB-3 was richer in terms of macronutrients such as carbon (C), nitrogen (N), and phosphorus (P) which can significantly influence the composition of the microbial community. The organic carbon content, representing the energy flow in the carbon cycle, was 0.85% (slightly high) in MGB-2 and 1.39% (high) in MGB-3 compared to reference values. Our results indicated high carbon content in the samples because aromatic organic hydrocarbons such as PCBs and PAHs were present in the contaminated soil. Industrial soil and effluent are considered sources of organic contaminants, including PCBs (Cai et al., 2007). Because of the hydrophobic nature of these PCBs, they tend to bind with the soil and hence add to the organic carbon content of the soil. The sample MGB-3 had very high nitrogen and phosphorus content (N, 734 kg ha<sup>-1</sup>; P, 56.9 kg ha<sup>-1</sup>, respectively), whereas MGB-2 had moderate nitrogen (430 kg ha<sup>-1</sup>) and low phosphorus (17.66 kg ha<sup>-1</sup>) content. MGB-3 exhibited high P and low C/P ratios, indicating the possibility of higher microbial diversity than MGB-2.

Several studies have confirmed that soil with high microbial diversity has high P and low C/P ratios. In contrast, the environment with less P and high C/P ratios shows microbial diversity (Delgado-Baquerizo et al., 2017). A higher level of these micronutrients in MGB-2 can be due to the high-water content in the sample. Further, these results indicate that MGB-2 and MGB-3 can support diverse microbial communities. Overall, micronutrients, including Na and Mn, and macronutrients K and Mg, were higher in MGB-2 than in MGB-3. The K (1232 kg ha<sup>-1</sup>) and Mg (768 kg ha<sup>-1</sup>) were higher than the reference value in MGB-2. The availability of inorganic nutrients serves structural as well as catalytic functions. Therefore, bacterial communities' total taxonomic and functional profiles are predominantly driven by the availability of C, N, and P, and to some extent, by the presence of inorganic nutrients, i.e., Ca, K, and Mg (Nicolitch et al., 2019).



**Table. 2.2.** Physio-chemical parameters of the contaminated soil sample MGB-2 and MGB-3 from polluted near the Bhilai steel plant

Soil testing parameter	MGB-2	MGB-3	Reference value
pH	7.83	7.69	V. acidic < 5.0, Acidic 5.0 < 6.0, Normal 6.0 - 8.0, Alkaline 8.0 < 9.0
Electrical Conductivity (dSm <sup>-1</sup> )	0.21	0.183	<1.0 Normal
Organic Carbon (%)	0.85	1.39	< 0.5 Low, 0.50 - 0.75 Medium, > 0.75 - High
Nitrogen (kg ha <sup>-1</sup> )	430	734	< 280 Low, 281 - 560 Medium, > 560 High
Phosphorous (kg ha <sup>-1</sup> )	17.66	56.9	< 22 Low, 23 - 56 Medium, > 56 High
Potassium (kg ha <sup>-1</sup> )	1232	336	< 112 Low, 113 - 280 Medium, > 280 High
Calcium Carbonate (%)	7.2	7.6	< 1 Low, 1 - 5 Normal, 5-10 Sufficient, > 10 Harmful
Available Calcium (ppm)	640	960	< 500 Low, 500 -1000 Normal, >1000 Sufficient
Magnesium (ppm)	768	576	< 250 Low, 250 - 500 Normal, >500 Sufficient
Available Sodium (ppm)	138	126.5	Up to 400 Normal, 400 - 700 Problem may occur, > 700 Harmful
Chloride (ppm)	11.92	7.95	Up to 350 Normal, 350 - 1050 Slightly problem, > 1050 Harmful
Sulphur (mg kg <sup>-1</sup> )	16.37	25.37	< 10 Low, 10 -50 Normal, 50 High
Zinc (mg kg <sup>-1</sup> )	1.218	3.267	< 0.6 Low, 0.61- 5.0Medium, >5.1 High
Iron (mg kg <sup>-1</sup> )	8.372	14.98	< 4.5 Low, 4.6 -24 Medium, >25 High
Copper (mg kg <sup>-1</sup> )	1.286	1.575	< 0.2 Low, 0.3 -1.5 Medium, >1.5 High
Manganese (mg kg <sup>-1</sup> )	44.12	17.44	< 2.0 Low, 2.1 - 29 Medium, >30 High
Water Holding Capacity (%)	46	43.81	< 20 Low, 20 -50 Medium, > 50 High

The result of the metal analysis indicated that the MGB-3 had a comparatively higher metal content (Zn, Cu, and Fe) than the MGB-2 (Table 2.2). The result also showed a high percentage of Mn (44.12 mg kg<sup>-1</sup>) in MGB-2 and Fe (14.98 mg kg<sup>-1</sup>) in MGB-3, providing a suitable environment for microbes to undergo anaerobic biodegradation. The high metal content in both samples could be due to the additives used in a steel factory. The presence of the metals in a soil sample can limit many microbial species, whereas they can support the survival and growth of metal-tolerant species. The presence of metals is in accordance with several reports highlighting heavy metals and organic contaminants such as PCB from iron and steel industrial soil sites (Bano et al., 2018). In addition, Mn (IV) and Fe (III) are known to act as terminal electron acceptors that efficiently remove aromatic compounds from the soil. In biodegradation studies, Fe is the most widely found cofactor involved in deoxygenation reactions. It has been reported that Fe- containing dioxygenases are incorporated into the active site either as the iron centre, Rieske [2Fe- 2S] cluster or as heme prosthetic group during PCB biodegradation (Langenhoff et al., 1996).

### 2.3.3 Metagenomic analysis

#### 2.3.3.1 Whole genome sequencing and assembly summary

The metagenomic approach provides a complete picture of biodegradation *vis-a-vis* microbes present within the environment and the functional genes involved in the bioremediation of contaminants. Whole-genome metagenomics analyses study taxonomic diversity and elucidate the metabolic pathways required for understanding pollutant degradation (Bouhajja et al., 2016). Therefore, the present study conducted a whole-genome metagenomics analysis of soil samples from the Bhilai steel plant industrial area. To date, no reports on metagenomics studies have been undertaken for contaminated soil of the Bhilai steel plant region. We used the ONT platform for community analysis to enable the unbiased assembly of complete genome sequencing (Cummings et al., 2017).

Nanopore GridION X5 generated real-time, long-read, high-fidelity DNA sequence data. The downstream analyses of the total number of reads are detailed in Table 2.3. MG-RAST statistical analysis of the dataset provided 275,844 sequences (totaling 539,360,072 bp; average length 1,955 bp) for MGB-2 and 193,221 (totaling 532,031,111 bp; average length 2,753 bp) for MGB-3. The mean GC percent was  $58 \pm 7$  and  $58 \pm 9\%$  for MGB-2 and MGB-3, respectively. As described in the previous section, the datasets were used for various taxonomic, ecological, and functional analyses.

**Table 2.3.** Total number of unassembled and assembled reads used for downstream analyses

S.no	Dataset	MGB-2	MGB-3
1.	bp Count	539,360,072 bp	532,031,111 bp
2	Sequences Count	275,844	193,221
3	Mean Sequence Length	$1,955 \pm 3,850$ bp	$2,753 \pm 4,578$ bp
4	Mean GC percent	$58 \pm 7$ %	$58 \pm 9$ %
5	Artificial Duplicate Reads: Seq. Count	0	0
6	Post QC: bp Count	539,360,072 bp	532,031,111 bp
7	Post QC: Sequences Count	275,844	193,221
8	Post QC: Mean Sequence Length	$1,955 \pm 3,850$ bp	$2,753 \pm 4,578$ bp
9	Post QC: Mean GC percent	$58 \pm 7$ %	$58 \pm 9$ %
10	Processed: Predicted Protein Features	586,053	514,069
11	Processed: Predicted rRNA Features	1,450	1,531
12	Alignment: Identified Protein Features	115,880	123,629
13	Alignment: Identified rRNA Features	403	382
14	Annotation: Identified Functional Categories	Undefined	undefined

### 2.3.3.2 Analysis of sequence data for the extent of microbial diversity

The horizontal rarefaction curve indicated the significant sampling depth, representing sufficient sample coverage in both samples for diversity analysis. The rarefaction curves showed that the species richness has plateaued to the right (Fig. 2.4), indicating the saturation of sequencing reads. Therefore, the probability of finding more OTUs (by further sequencing) is negligible.

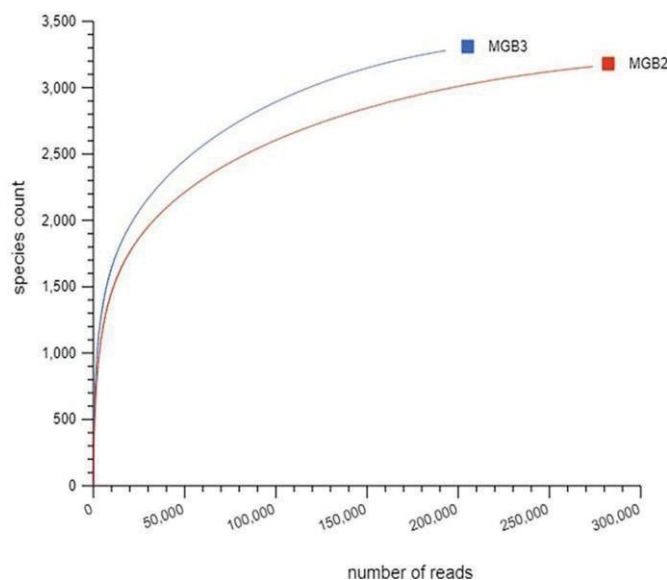


**Fig. 2.4.** Rarefaction curve represented species richness indicating the function of a number of reads (y-axis) per MGB-2 and MGB-3 (x-axis).

The standard alpha diversity indices, such as Chao, Simpson, and Shannon indices depicted in Table 2.4, suggest equivalent overall diversity in both samples. Alpha diversity indices highlighted the diversity within MGB-2 and MGB-3 metagenome, including richness and evenness measurements. Shannon and Simpson's diversity indexes (1-D) were calculated to check the richness and evenness of the microbe community in MGB-2 and MGB-3. The higher the value for this index (ranges from 0 to 1), the higher the species diversity. Simpson 1-D for bacteria was found to be 0.9957 and 0.9964 for MGB-2 and MGB-3, respectively, indicating its richness in diversity of both the metagenome. Chao-1 represents the abundance of species belonging to MGB-2 and MGB-3. The taxonomic analysis showed 1839 and 1884 species in MGB-2 and MGB-3, respectively, indicating higher species richness in MGB-3, which is also evident from Chao-1 and Shannon's diversity data.

Beta diversity among MGB-2 and MGB-3 based on Bray-Curtis dissimilarity (Fig. 2.5) defined the overall distribution pattern of bacterial communities in these samples, with principal coordinates showing 98.7%, bacterial communities' similarity, in the number of microbes found

**Table 2.4.** Alpha diversity for bacterial, archaea, and Eukaryota communities in the polluted site near the Bhilai steel plant

Domain	Bacteria		Archaea		Eukaryota		Total Diversity	
	MGB-2	MGB-3	MGB-2	MGB-3	MGB-2	MGB-3	MGB-2	MGB-3
Sample	MGB-2	MGB-3	MGB-2	MGB-3	MGB-2	MGB-3	MGB-2	MGB-3
Simpson_1-D	0.9957	0.9964	0.9788	0.9798	0.9847	0.987	0.9959	0.9966
Shannon_H	6.175	6.25	4.12	4.139	4.638	4.743	6.267	6.341
Evenness_e^H/S	0.3456	0.3689	0.7075	0.7298	0.4921	0.5338	0.3057	0.3232
Brillouin	6.155	6.23	4.03	4.034	4.492	4.614	6.244	6.318
Menhinick	3.247	3.168	1.849	2.024	4.17	3.856	3.972	3.91
Margalef	114.7	115.1	11.17	11.34	26.66	26.61	141.9	143.6
Equitability_J	0.8532	0.8624	0.9225	0.9293	0.8674	0.8831	0.841	0.8488
Fisher_alpha	204.5	204.4	18.06	18.8	54.35	52.45	262	264.4
Berger-Parker	0.02676	0.0224	0.05917	0.04873	0.04574	0.04471	0.02608	0.02184
Chao-1	1414	1429	87	86.33	266	267.1	1839	1884

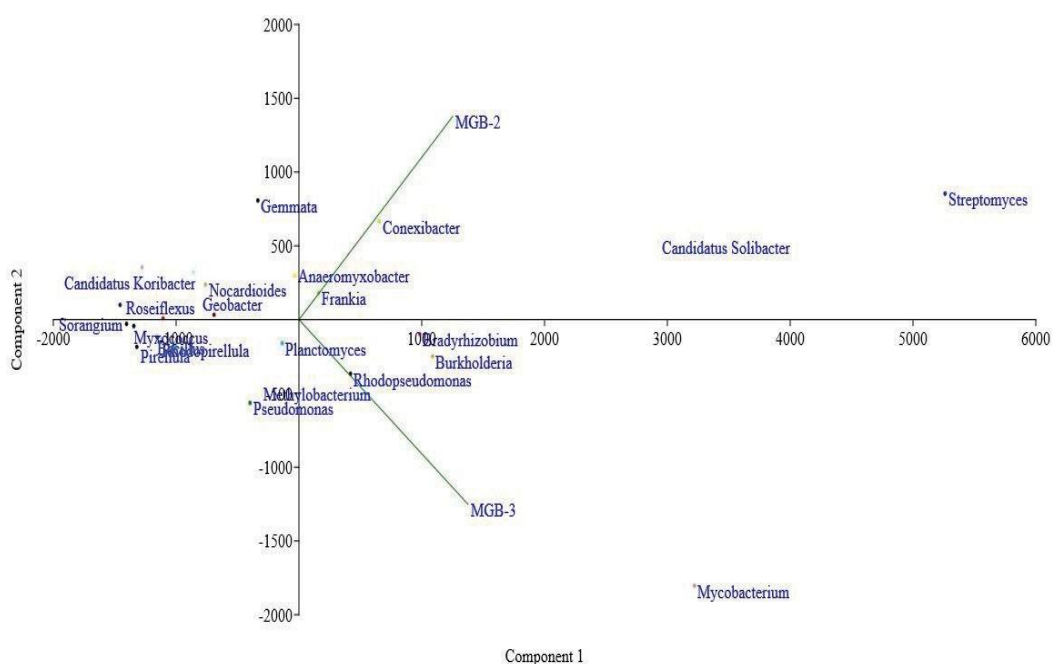


**Fig. 2.5.** Taxonomic analysis of beta diversity of MGB-2 and MGB-3 on Bray-Curtis dissimilarity indicating the abundances of microbes shared between MGB-2 and MGB-3 and the number of microbes found in each metagenome. The first PC (Principle component) accounts for most of the variance, and the first eigenvector (principal axis) has all positive coordinates. It probably means that the two metagenomes are positively correlated, and the first PC represents a "common genus." All genera in MGB-2 and MGB-3 have positive values in the PC1 axis, while genera depicted in MGB-2 are positive in PC2 and MGB-3 are negative. Component 1 and Component 2 represents the PC1 and PC2 axis. in MGB-2 and MGB-3. MGB-3 has more scattered or variation of bacterial community than MGB-2.

### 2.3.3.3. Taxonomic diversity of microbial communities

The collected samples were explored for taxonomic diversity and functional potential. ONT and MG-RAST database search provided detailed microbial taxonomy of MGB-2 and MGB-3. The differences were noticeable at the domain level, where MG-RAST derived reads accounted majorly for bacteria (97.4%; 97.5%) followed by eukaryote (1.4%; 1.5%), archaea (1.2%; 0.9%), and virus (0.02%; 0.04%) in MGB-2 and MGB-3 respectively. The abundance of bacteria at the level of phylum, order, class, family, and genus in the two samples is shown in the Krona plot (Fig. 2.6 A-B). Among bacteria, phylum *Proteobacteria* (45.0%; 50.0%) was the most predominant, followed by *Actinobacteria* (22.1%; 19.5%) and *Firmicutes* (6.3%; 5.4%) in both MGB-2 and MGB-3 samples. The predominance of these phyla in soils contaminated with PCB is consistent with the results of other authors who have reported the enrichment of *Proteobacteria* and *Acidobacteria* due to exposure to individual PCB congeners (Correa et al., 2010). Similar results were also reported by Macedo et al. (2007), who revealed the predominance of *Proteobacteria* identified in a biofilm formed on a slide containing a layer of PCB. This can be explained by the fact that these groups have well-known PCB degraders (*Rhodococcus*, *Arthrobacter*, *Corynebacterium*, *Sphingomonas*, *Pseudomonas*, *Acinetobacter*, etc.). While in another study, the biodiversity of PCB-contaminated soils was dominated by *Actinobacteria* (42.79%) and *Firmicutes* (42.32%) phyla, and others in smaller proportions such as *Proteobacteria*, *Gemmatimonadetes*, *Chloroflexi*, and *Bacteroidetes* (Cervantes-González et al., 2019). Both samples included all six classes of *Proteobacteria*, namely, *Alphaproteobacteria* (18.6%; 22.4%), *Betaproteobacteria* (8.8%; 10.7%), *Deltaproteobacteria* (8.2%; 7.1%), *Epsilon proteobacteria* (0.3%; 0.3%), *Gamma proteobacteria* (7.2%; 8.9%) and *Zeta proteobacteria* (0.04%; 0.03%) with the difference in their relative abundance, which indicates the presence of diverse members playing a vital role in photosynthesis, nitrogen fixation, sulfur, and phosphorus metabolism (Zhou et al., 2020). At the class level, *Actinobacteria* (26.2%) was observed to be dominant in MGB-2, while *Alphaproteobacteria* (22.1%) in MGB-3.

A.

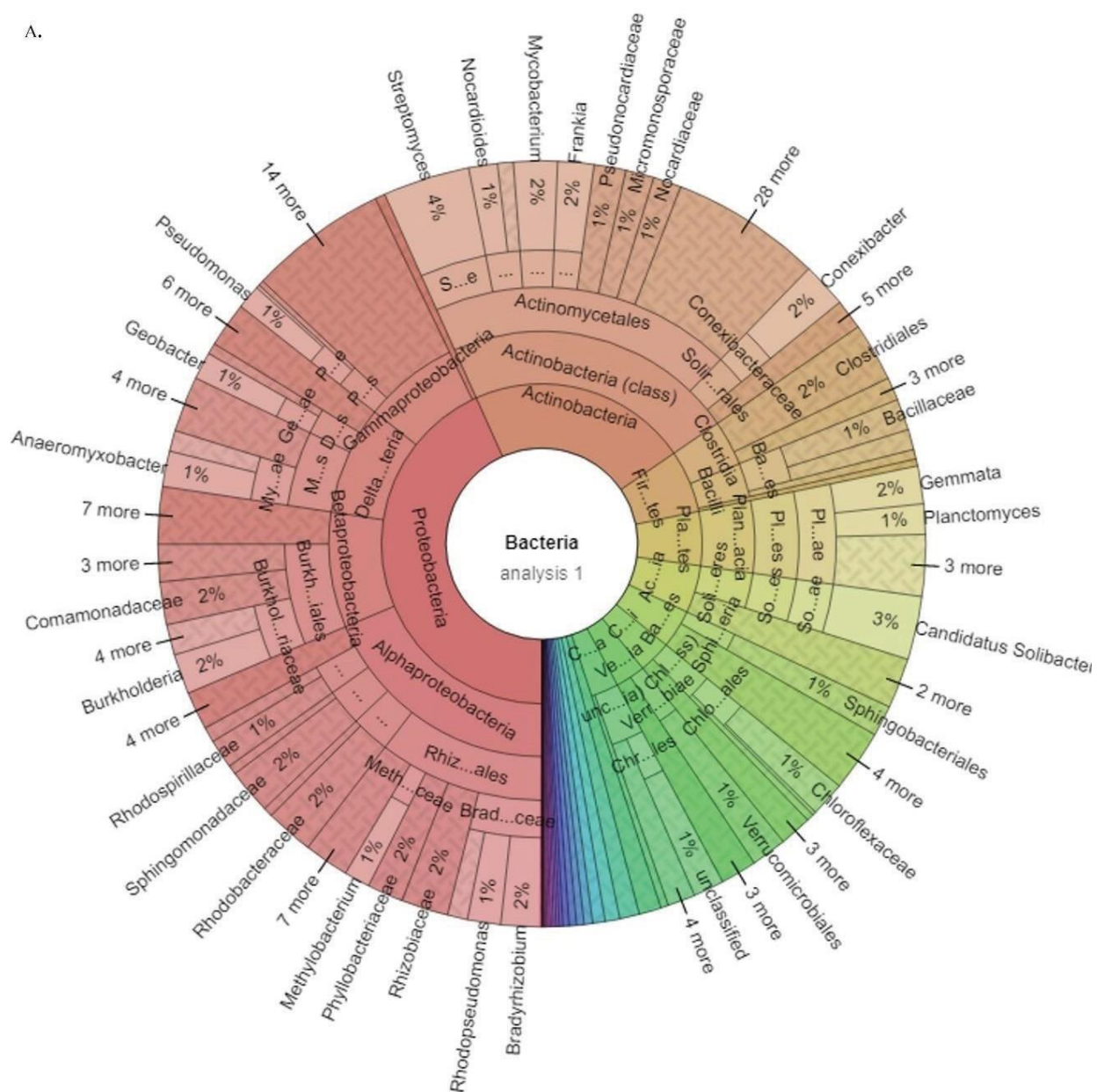


**Fig. 2.6.** (A) Krona plot demonstrating the relative abundance of taxa of bacteria across phylum to genus level hierarchy of MGB-2. Among bacteria, phylum *Proteobacteria* (45.0%), *Actinobacteria* (22.1%), and *Firmicutes* (6.3%), while *Streptomyces* (3.7%) and *Candidatus Solibacter* (2.7%) were the most predominant genera in MGB-2.



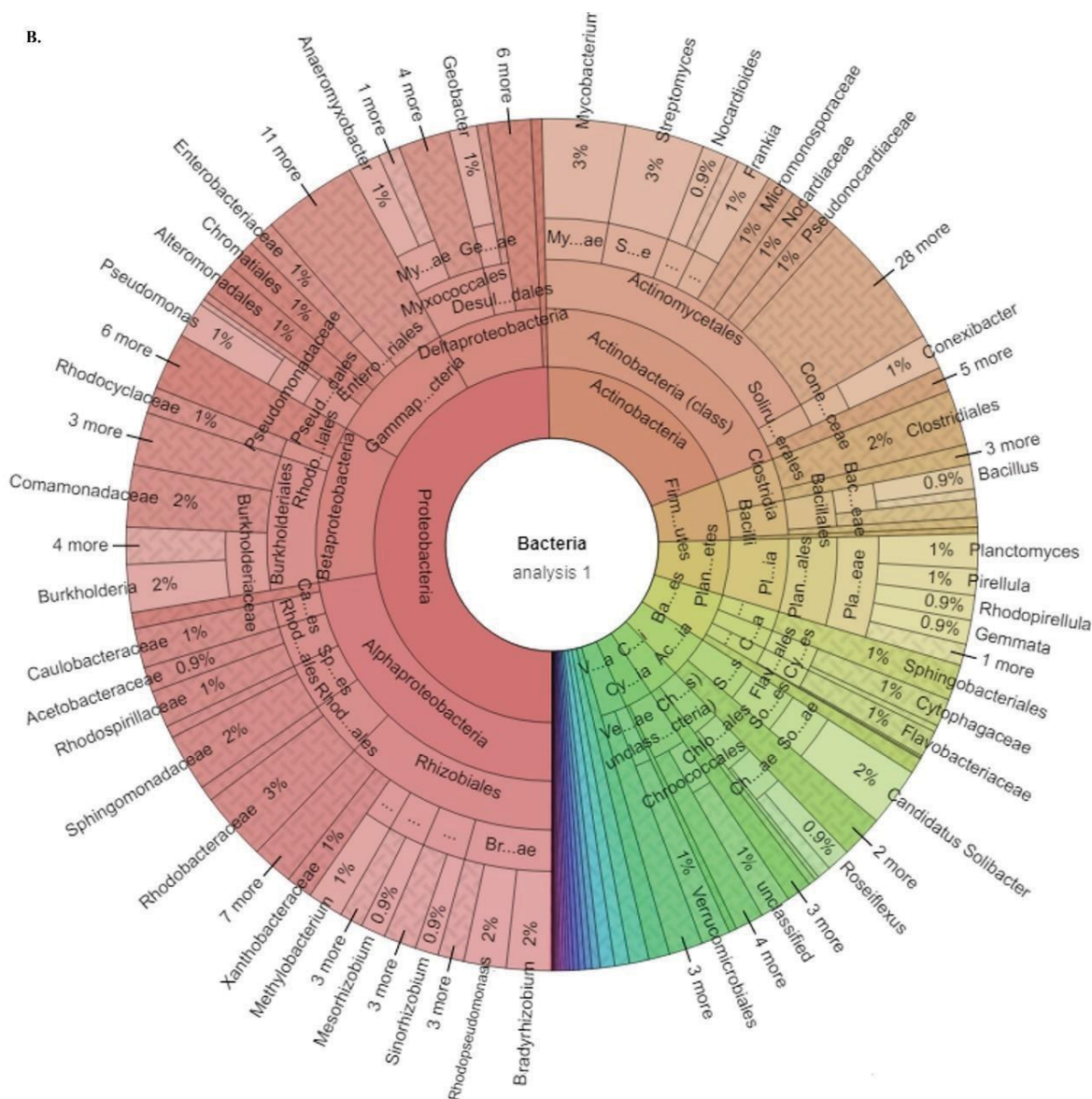


**Fig. 2.6.** (B) Krona plot demonstrating the relative abundance of taxa of bacteria across phylum to genus level hierarchy of MGB-3. Among bacteria, phylum *Proteobacteria* (50.0%), *Actinobacteria* (19.5%), and *Firmicutes* (5.4%), while *Mycobacterium* (3.1%) and *Streptomyces* (3.0%) were the most predominant genera in MGB-3.

Statistical Analysis of Metagenomic Profiles (STAMP) with G-test (w/Yates'+ Fischer's) two-way comparison showed the degree of closeness and difference across MGB-2 and MGB-3 at the class level. The analysis showed close similarities in both metagenomes but differences in relative abundance. Among the classes, *Actinomycetales* (85.7%; 88.4%) were distinctly observed in MGB-2 and MGB-3, followed by *Solirubrobacterales* (8.6%; 6.7%). The bacterial community composition in the two samples was similar at the genus level, but they differed in relative abundance. *Streptomyces* (3.7%) and *Candidatus Solibacter* (2.7%) were the most predominant genera in MGB-2, while in MGB-3, it was *Mycobacterium* (3.1%) and *Streptomyces* (3.0%). It has been reported that the structure and abundance of microbial communities shift in soil contaminated with PCB (Petric et al., 2011). There is an alteration in the abundance of bacteria on exposure to different PCB congeners (Correa et al., 2010). For instance, *Mycobacterium* is the dominant genus in PAH-contaminated soil (Cheung et al., 2001; Li et al., 2015).

RefSeq annotations at the highest taxonomic classification, i.e., at the genus level, possess a significant abundance level with  $p < 1 \times 10^{-5}$  for *Streptomyces*, *Candidatus Koribacter*, *Gemmata*, *Conexibacter*, *Anaeromyxobacter* and *Nocardioides* in MGB-2, while *Hypomicrobium*, *Pseudomonas*, *Mycobacterium*, *Roseomonas*, and *Methylobacterium* with  $p < 1 \times 10^{-5}$  in MGB-3. The correlation coefficient ( $r^2$ ) indicated a linear relationship between MGB-2 and MGB-3, as depicted on the scatter plot (Fig. 2.7).

The presence of the dominant genera in samples suggests the potential for degrading organic pollutants by the members of these genera. For instance, *Anaeromyxobacter* is capable of anaerobic respiration and possesses genes involved in reductive dechlorination processes at the contaminated site (Stanford et al., 2002). Similarly, members of *Mycobacterium*, *Bradyrhizobium*, *Burkholderia* (Goris et al., 2004; Jorge et al., 2006), and *Pseudomonas* (Wittich et al., 1999; Hatamian-Zarmi et al., 2009) are well-known aromatic pollutant degraders in contaminated soils (Seo et al., 2009).

Within the metagenome of MGB-2 and MGB-3, *Archaeal* communities showed a dominance of *Euryarchaeota* (76.7%; 81.3%) at the phylum level, followed by *Crenarchaeota* (13.7%; 13.2%) *Thaumarchaeota* (8.7%; 4.8%) and *Korarchaeota* (0.9%; 0.7%). The class *Halobacteria* within the phylum *Euryarchaeota* have been reported to be associated with biphenyl and PAH degradation and their degradative abilities (Al-Mailem et al., 2010; Al-Mailem et al., 2017). At the genus level, relative abundance for methane-producing *Methanosarcina* (10.5%; 12.1%) *Methanoculleus* (3.7%; 3.2%), ammonia-oxidizing



*Nitrosopumilus* (5.9%; 3.3%), Sulfur reducing bacteria like *Thermococcus* (4.3%; 4.7%), unclassified (derived from *Euryarchaeota*) (4.3%; 4.2%), *Pyrococcus* (3.9%; 3.3%), and *Sulfolobus* (3.6%; 3.3%) dominated in both MGB-2 and MGB-3.

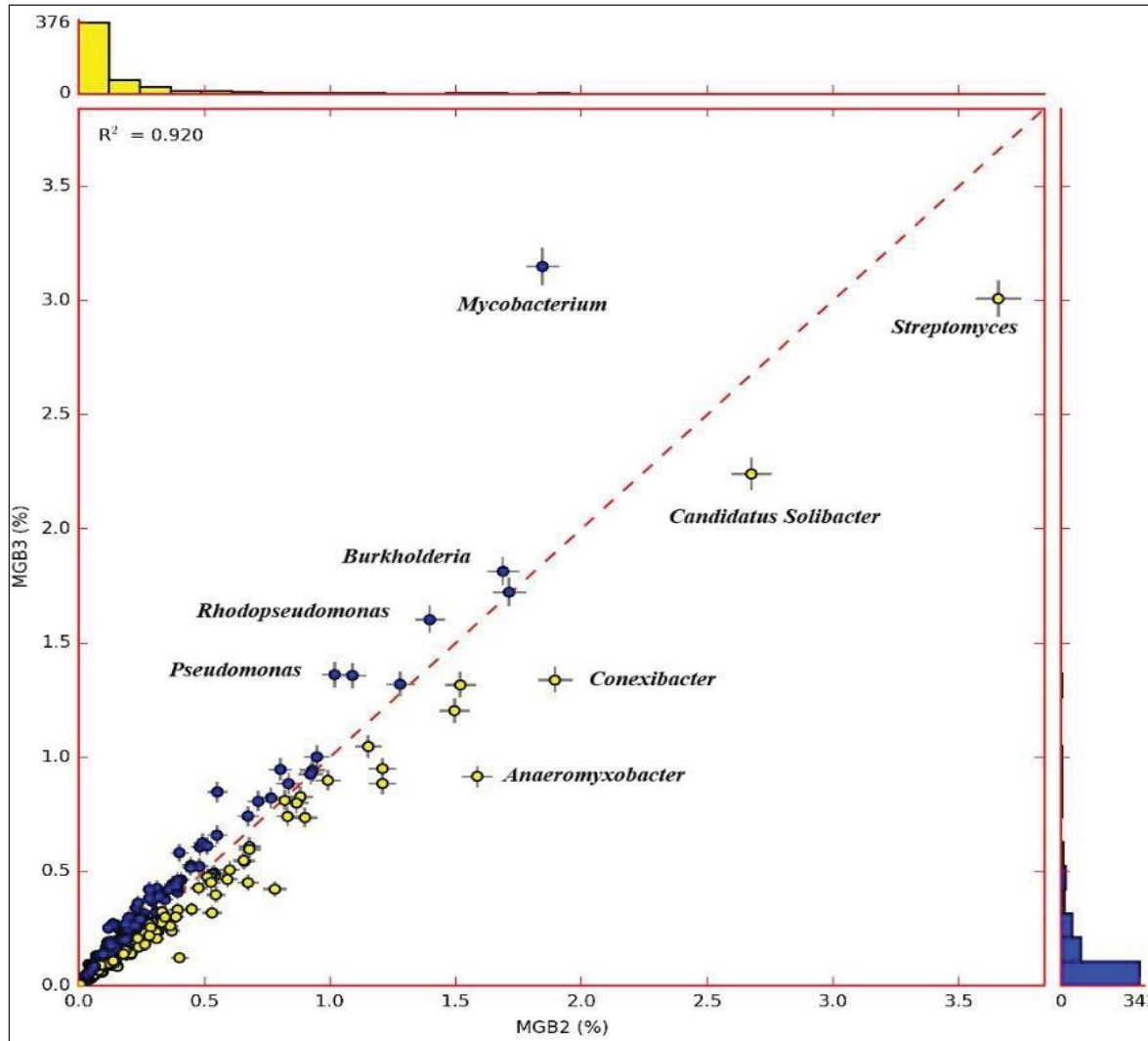


**Fig. 2.7.** The scatter plot indicates the linear relationship between the dominance of genera between MGB-2 and MGB-3 metagenome. The difference between proportions (%) of *Mycobacterium* (1.8, 3.1,  $p < 1e^{-5}$ ), *Streptomyces* (3.6, 3.0,  $p < 1e^{-5}$ ), *Candidatus Solibacter* (2.6, 2.2,  $p < 1e^{-5}$ ), *Burkholderia* (1.6, 1.8,  $p = 3.32e^{-5}$ ), *Rhodopseudomonas* (1.3, 1.6,  $p < 1e^{-5}$ ), *Pseudomonas* (1.0, 1.4,  $p < 1e^{-5}$ ), and *Anaeromyxobacter* (1.6, 0.9,  $p < 1e^{-5}$ ) in MGB-2 and MGB-3, respectively with significant p values. The genera towards the linear line indicate a similar proportion of reads in the metagenome.

However, a two-way statistical comparison of *Archaea* at the genus level revealed *Nitrosopumilus* ( $p = 1.24 \times 10^{-4}$ ) and *Cenarchaeum* ( $p = 5.18 \times 10^{-3}$ ) in MGB-2 while *Methanobrevibacterium* ( $p=0.012$ ) in MGB-3 to predominate indicating more methanogenesis occurring in MGB-3 (Samson et al., 2019). The contaminated soil also possesses many members of *Methanosarcina*, *Halobacterium*, *Euryarchaeota*, and *Crenarchaeota* of uncultured genera. The diversity of *Archaea* is found to be higher within hydrocarbon-degrading communities in the contaminated environment than the non-contaminated counterpart (Zhang et al., 2012). Krzmarzick and his co-workers (2018) have highlighted the role and importance of *Archaea* in hydrocarbon degradation in extreme environments. The relative abundance of *Archaeal* communities was more in MGB-2, which may be associated with the higher soil moisture and POPs content.

Eukaryota microbial communities showed a predominance of phylum *Ascomycota* (20.5%; 23.6%), *Streptophyta* (18.5%, 17.0%), and unclassified (derived from *Eukaryota*) (12.1%; 12.2%) in MGB-2 and MGB-3, respectively. Several studies on contaminated soils have revealed the presence of *Ascomycota* as the most dominant eukaryotic phylum, as the indigenous *Ascomycete* can transform or remove pollutants (Aranda, 2016). Some of the *Ascomycete*'s strains, such as *Penicillium chrysogenum*, *P. canescens*, *P. citreosulfuratum*, and *Aspergillus jensenii*, reported to be isolated from historically PCB-polluted soils possessed good PCB biodegradation ability (Germain et al., 2021a; Germain et al., 2021b).

#### **2.3.3.4. Functional diversity and metabolic potential of MGB-2 and MGB-3**

The SEED subsystem analysis in MG-RAST assigned reads based on various functions that identified 60% of the total function constituting metabolisms of amino acid, carbohydrate, energy, lipid, cofactors, vitamins, biosynthesis of glycan, polyketides, terpenoids, xenobiotic biodegradation, and biosynthesis of secondary metabolites. The remaining 40% of functions include cellular processes, organismal systems, genetic & environmental processing, and human diseases (Fig. 2.8).

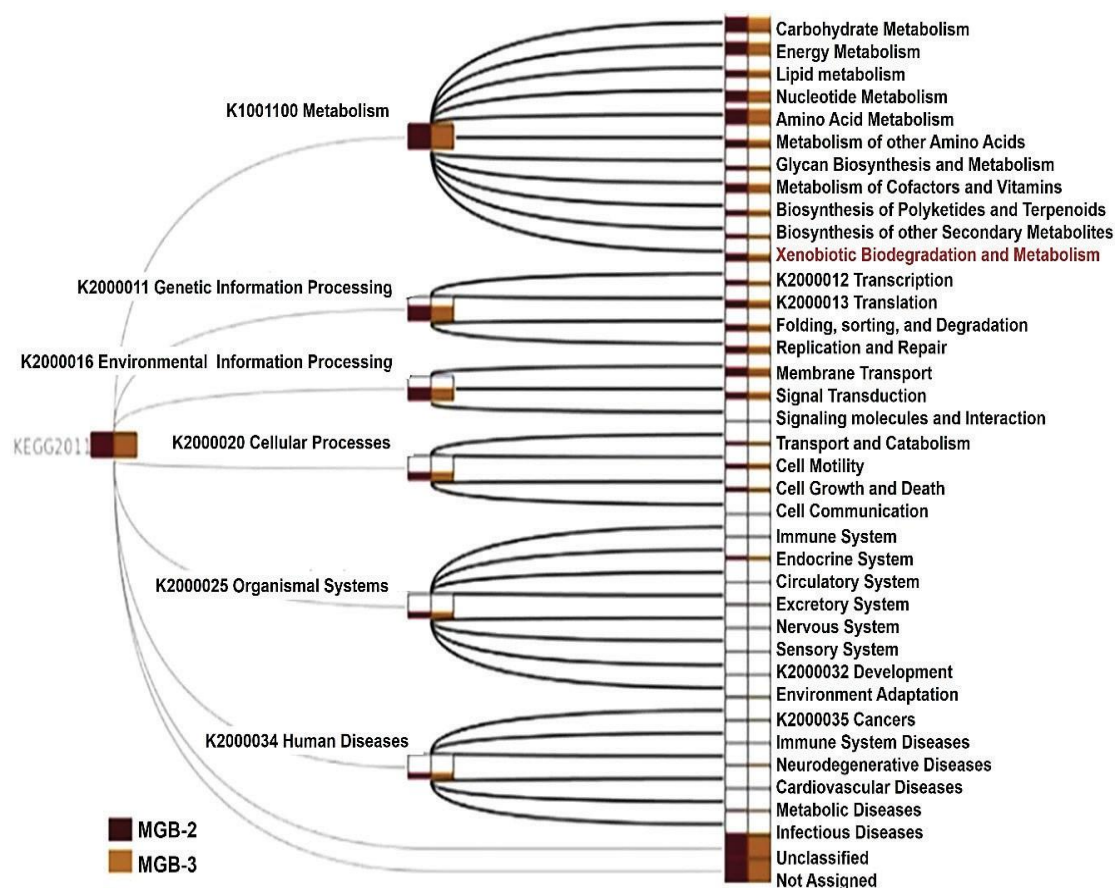


**Fig. 2.8.** SEED subsystem analysis in MG-RAST assigned reads in MGB-2 and MGB-3 based on various functions. MG-RAST assigned reads based on various functions consist of 60% of the total function metabolisms, and the remaining 40% of functions include cellular processes, organismal systems, genetic and environmental processing, and human diseases. Of this 60%, 2% accounts for xenobiotic biodegradation and metabolism.

#### 2.3.3.4.1 General metabolism of microbial community

Predicted genes from the MGB-2 and MGB-3 metagenome were used as input in the KEGG mapper for functional annotation. Annotated genes involved in methane, N, and S metabolism pathways were identified (Table 2.5 & 2.6). Comparative analysis of both the metagenome based on their metabolism at SEED level 1 revealed significant dominance of methane metabolism ( $p = 5.61 \times 10^{-4}$ ), citrate cycle ( $p = 1.62 \times 10^{-3}$ ), carbon fixation ( $p = 2.61 \times 10^{-3}$ ), pyruvate metabolism ( $5.80 \times 10^{-3}$ ), amino benzoate degradation ( $p = 0.031$ ), selenocompound metabolism ( $p = 0.038$ ), and benzoate degradation ( $p = 0.045$ ) in both samples. However, lipoic acid metabolism ( $p = 7.58 \times 10^{-4}$ ), drug metabolism ( $p = 7.81 \times 10^{-3}$ ), folate biosynthesis ( $p = 0.17$ ), fatty acid metabolism ( $p = 0.042$ ), and lysine degradation ( $p = 0.042$ ) were found to be comparatively high in abundance in MGB-3 (Fig. 2.9). The results indicated representation of active metabolism by bacteria belonging to genus

*Conexibacter*, *Candidatus Koribacter*, *Norcardiodes*, *Anaeromyxobacter* in MGB-2 and *Mycobacterium*, *Methylobacterium*, *Mezorhizobium*, *Pseudomonas*, *Burkholderia*, *Bradyrhizobium* in MGB-3 (Fig. 2.10).

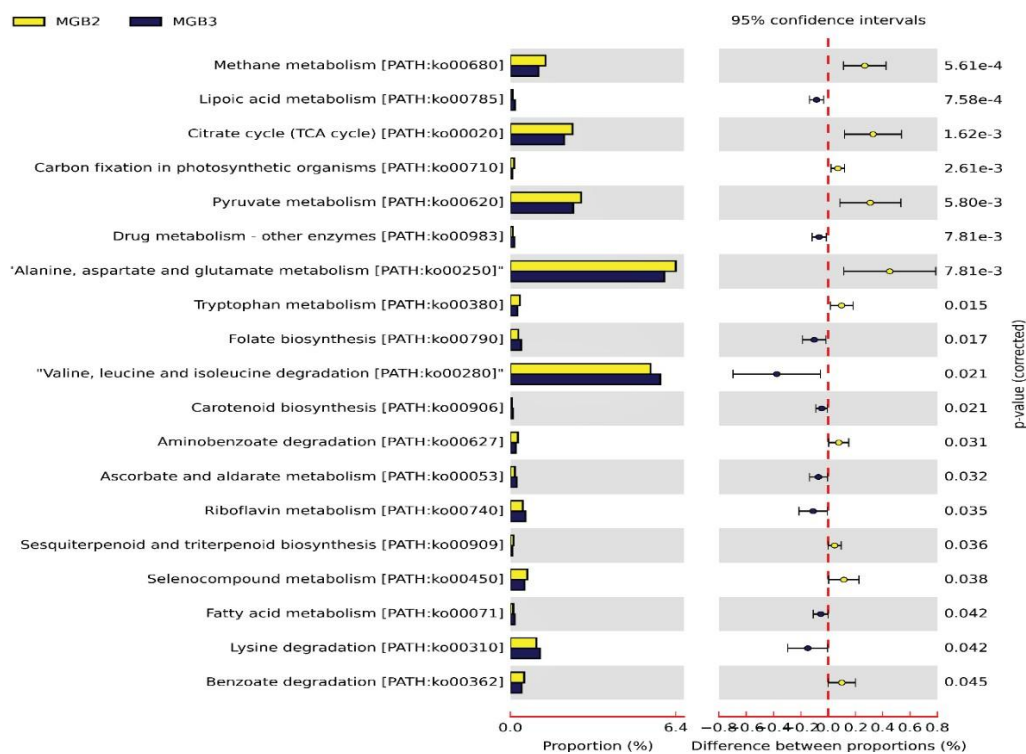


**Fig. 2.9.** Comparative analysis of potential metabolic pathways in the metagenome of MGB-2 and MGB-3 at SEED level using online available STAMP software. The graph highlights the relative dominance of methane (1.246, 0.267,  $p=5.61e^{-4}$ ), citrate cycle (1.158, 0.329,  $p=1.62e^{-3}$ ), pyruvate (1.127, 0.309,  $5.80e^{-3}$ ), benzoate degradation (1.232, 0.099,  $p=0.045$ ) in MGB-2 and lipoic acid (0.49, -0.85,  $p=7.58e^{-4}$ ), folate biosynthesis (0.751, -0.102,  $p=0.017$ ), fatty acid metabolism (0.662, -0.055,  $p=0.042$ ), and lysine degradation (0.870, -0.149,  $p=0.042$ ) in MGB-3.

**Table 2.5** Annotated gene and enzyme identified in metagenome MGB-2 and MGB-3 for methane metabolism

Metabolism	sublevel 3	gene	Enzyme identified
<b>Methane</b>	coenzyme M biosynthesis	<i>comE</i>	Sulfofpyruvate decarboxylase - beta subunit [EC 4.1.1.79]
	coenzyme M biosynthesis	<i>comA</i>	Phosphosulfolactate synthase [EC 4.4.1.19]
	Hydrogenases	<i>hoxF</i>	NAD-reducing hydrogenase subunit HoxF [EC 1.12.1.2]
	Hydrogenases	<i>hoxY</i>	NAD-reducing hydrogenase subunit HoxY [EC 1.12.1.2]
	CO Dehydrogenase	<i>cutL</i>	Carbon monoxide dehydrogenase form I, large chain [EC 1.2.99.2]
	H <sub>2</sub> : CoM-S-S-HTP oxidoreductase	<i>hdrA</i>	CoB--CoMheterodisulfide reductase subunit A [EC 1.8.98.1]
	CO Dehydrogenase	<i>coxS</i>	Carbon monoxide dehydrogenase small chain [EC 1.2.99.2]
	Hydrogenases	<i>hoxH</i>	NAD-reducing hydrogenase subunit HoxH [EC 1.12.1.2]
	CBSS-314269.3.peg.1840	<i>coxL</i>	Carbon monoxide dehydrogenase large chain [EC 1.2.99.2]
	CBSS-314269.3.peg.1840	<i>coxM</i>	Carbon monoxide dehydrogenase medium chain [EC 1.2.99.2]
	Methanogenesis from methylated	<i>mttB</i>	Trimethylamine: corrinoid methyltransferase [EC 2.1.1.250]
	Methanogenesis	<i>hdrC2</i>	CoB--CoMheterodisulfide reductase subunit C [EC 1.8.98.1]
	Serine-glyoxylate cycle	<i>mcH</i>	N (5), N (10)-methenyltetrahydromethanopterin cyclohydrolase [EC 3.5.4.27]
	Methanogenesis	<i>fhcD</i>	Formylmethanofuran--tetrahydromethanopterin N-formyltransferase [EC 2.3.1.101]
	One-carbon by tetrahydropterines	<i>mtdC</i>	Methylene tetrahydromethanopterin dehydrogenase [EC 1.5.99.9]
	Methanogenesis	<i>fwdA</i>	Formylmethanofuran dehydrogenase subunit A [EC 1.2.99.5]
	Methanogenesis	<i>fwdB</i>	Formylmethanofuran dehydrogenase subunit B [EC 1.2.99.5]

**Table 2.6** Annotated gene and enzyme identified in metagenome MGB-2 and MGB-3 for N and S metabolism

Metabolism	sublevel 3	gene	Enzyme identified	
<b>Nitrogen</b>	Denitrification	<i>nirS</i>	Cytochrome cd1 nitrite reductase [EC 1.7.2.1]	
	Denitrification	<i>nirK</i>	Copper-containing nitrite reductase [EC 1.7.2.1]	
	Denitrification	<i>norB</i>	Nitric-oxide reductase subunit B [EC 1.7.99.7]	
	Denitrification	<i>norC</i>	Nitric-oxide reductase subunit C [EC 1.7.99.7]	
	Denitrification	<i>nosZ</i>	Nitrous-oxide reductase [EC 1.7.99.6]	
	Denitrification	<i>norD</i>	Nitric oxide reductase activation protein NorD	
	Denitrification	<i>norQ</i>	Nitric oxide reductase activation protein NorQ	
	Denitrification	<i>qnoR</i>	Nitric-oxide reductase, quinol-dependent [EC 1.7.99.7]	
	Nitrate and nitrite ammonification	<i>nitH</i>	PolyferredoxinNapH (periplasmic nitrate reductase)	
	Nitrate and nitrite ammonification	<i>nirB</i>	Assimilatory nitrate reductase large subunit [EC:1.7.99.4]	
	Nitrate and nitrite ammonification	<i>nitH</i>	Nitrite reductase [NAD(P)H] small subunit [EC 1.7.1.4]	
	Nitrate and nitrite ammonification	<i>nosZ</i>	Ferredoxin--nitrite reductase [EC 1.7.7.1]	
	Nitrate and nitrite ammonification	<i>nrjE</i>	Cytochrome c-type heme lyase subunit nrjE [EC 4.4.1.-]	
	Nitrate and nitrite ammonification	<i>napB</i>	Nitrate reductase cytochrome c550-type subunit [EC 1.9.6.1]	
	Nitrate and nitrite ammonification	<i>nitH</i>	Nitrite reductase [NAD(P)H] large subunit [EC 1.7.1.4]	
	Nitrate and nitrite ammonification	<i>napA</i>	Periplasmic nitrate reductase precursor [EC 1.7.99.4]	
	<b>Nitrogen</b>	Nitrogen fixation	<i>nifN</i>	Nitrogenase FeMo-cofactor scaffold and assembly protein NifN [EC 1.18.6.1]
		Nitrogen fixation	<i>nifE</i>	Nitrogenase FeMo-cofactor scaffold and assembly protein NifE [EC 1.18.6.1]
Nitrogen fixation		<i>nifK</i>	Nitrogenase (molybdenum-iron) beta chain [EC 1.18.6.1]	
<b>Sulfur</b>		Inorganic Sulfur Assimilation	<i>cysN</i>	Sulfateadenylyltransferase, dissimilatory-type [EC 2.7.7.4]
		Inorganic Sulfur Assimilation	<i>cysH</i>	Phosphoadenylyl-sulfate reductase [thioredoxin] [EC 1.8.4.8]
		Inorganic Sulfur Assimilation	<i>siR</i>	Ferredoxin--sulfite reductase [EC 1.8.7.1]
	Inorganic Sulfur Assimilation	<i>papsR</i>	Adenylyl-sulfate reductase [thioredoxin] [EC 1.8.4.10]	
	Inorganic Sulfur Assimilation	<i>cysC</i>	Adenylylsulfate kinase [EC 2.7.1.25]	
Inorganic Sulfur Assimilation	<i>cysI</i>	Sulfite reductase hemoprotein beta-component [EC 1.8.1.2]		



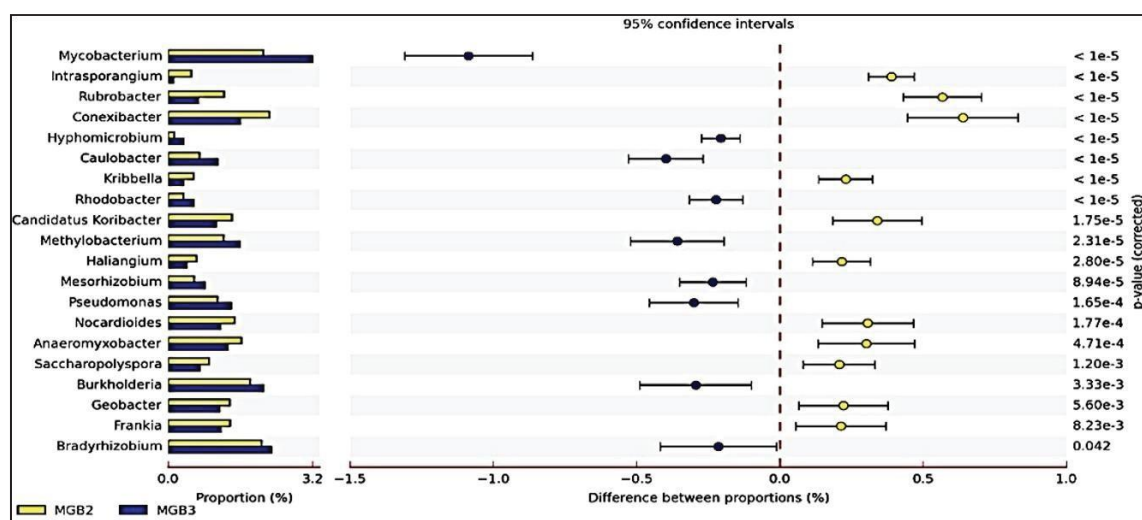
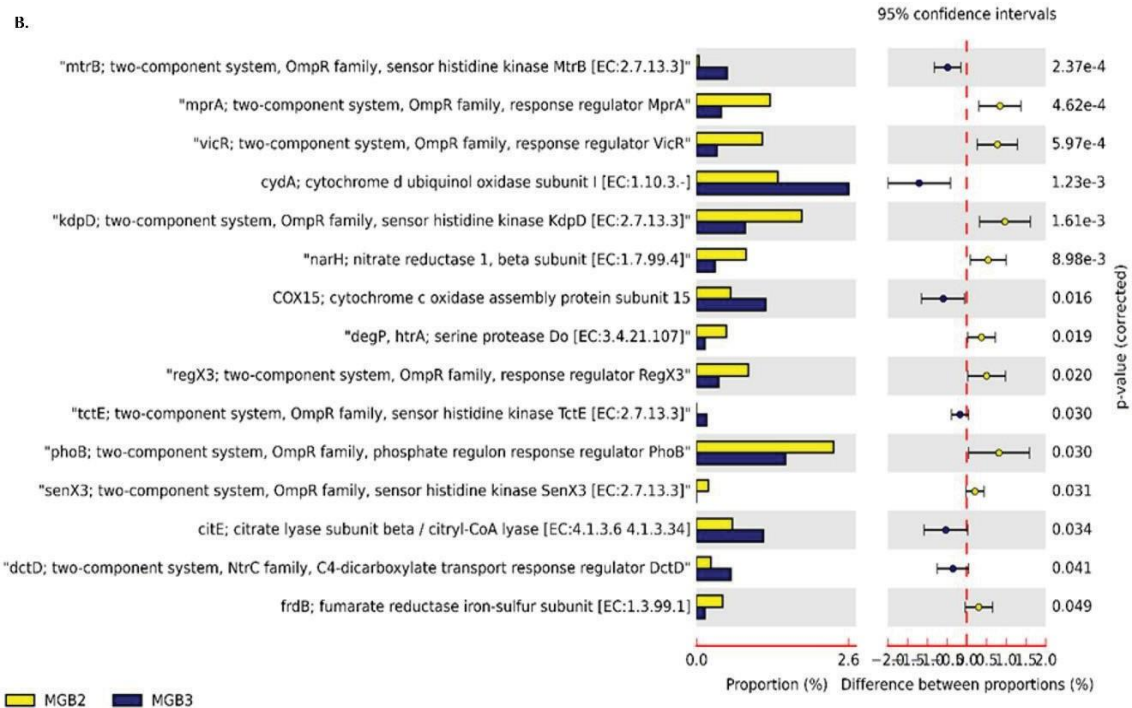
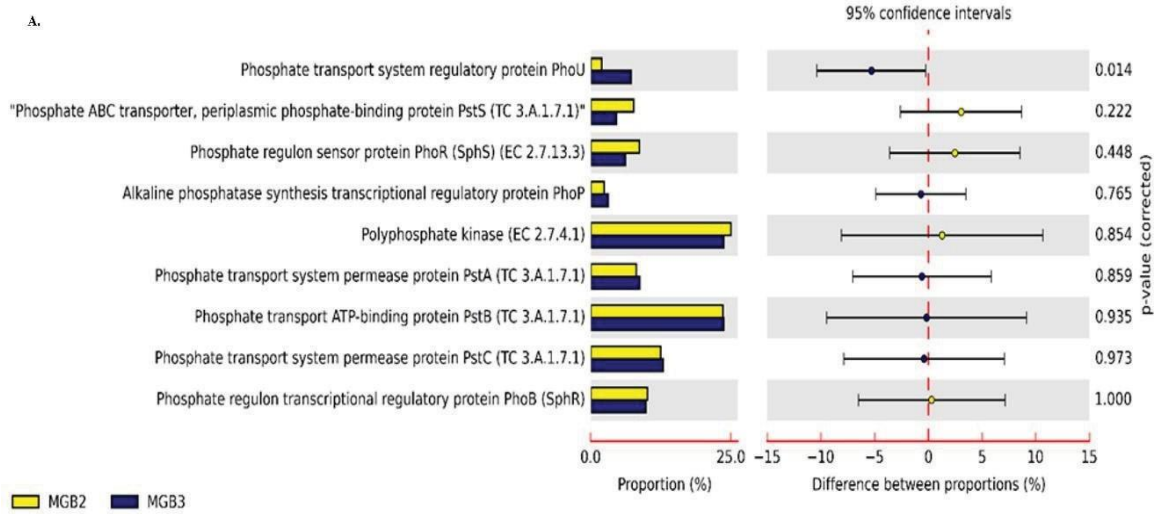


**Fig. 2.10.** Comparative analysis of metagenome MGB-2 and MGB-3 using STAMP SEED level based on genus level with RefSeq for metabolism. The data represents the ratio of proportion and the difference between the proportion (%) of *Mycobacterium* (0.65, -1.086,  $p < 1e^{-5}$ ), *Pseudomonas* (0.784, -0.300,  $p = 1.65e^{-4}$ ), *Nocardioides* (1.265, 0.306,  $p = 1.77e^{-4}$ ), *Anaeromyxobacter* (1.230, 0.302,  $p = 4.71e^{-4}$ ), and *Burkholderia* (0.861, -0.293,  $p = 3.33e^{-3}$ ) between MGB-2 and MGB-3 with significant p values.

The comparative analysis of gene sequences revealed the abundance of P transporter in MGB-2, which can correlate with the low P content than MGB-3. Various genes encoding proteins involved in phosphate-recycling mechanisms, such as *phnA*, *phnE*, *phnW* and *phnX*, (phosphonate transporters), *pstA*, *pstB*, *pstC*, and *pstS* (high-affinity phosphate transporters), and *phoR*, *phoA*, *phoP* and *phoD* (two-component systems) were detected across both the metagenome. The relative abundance of reads for phosphate mechanism in low phosphate-phosphorous environments indicated these mechanisms help them cope with such environments. Bacteria sense and respond to their environment through two-component systems. Moreover, bacteria can survive in metal-rich environments due to resistant genes toward toxic metals such as copper, lead, and nickel as a part of their defense mechanism, which is recruited further for cleaning the contaminated environments. The abundance of Mn content in MGB-2 can correlate with the significantly higher reads for Mn transporter in MGB-2 than in MGB-3. Also, a comparison between MGB-2 and MGB-3 of functional gene annotation using SEED subsystem for membrane transport revealed a significant level ( $p > 0.05$ ) of abundance for  $Na^+/H^+$  antiporters, and Mn transporter MntH, Mn ABC transporter SitD, TadA, Zn ABC transporter ZnuA (Fig. 2.11A-C). MGB-3 showed higher  $Na^+/H^+$  transporters that indicate the exchange of the ions across the membrane to maintain homeostasis.



## Chapter II



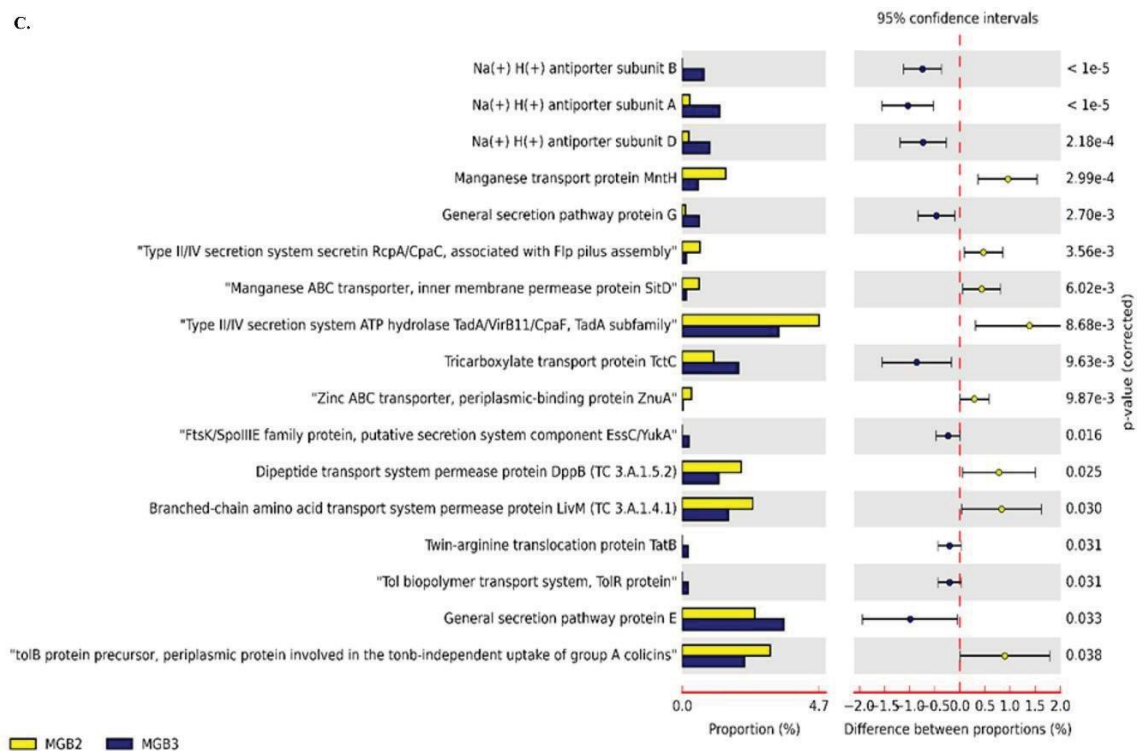


**Fig. 2.11.** Comparison between MGB-2 and MGB-3 of functional gene annotation using STAMP using SEED subsystems including (A) Phosphate transporter (B) two-component system (C) membrane transport. The data represents the ratio of proportion and the difference between the proportion (%) of the reads with significant  $p < 0.05$  under phosphate transport, two-component, and membrane transport systems in MGB-2 and MGB-3.

#### 2.3.3.4.2 Abundance of xenobiotics degradation and metabolism genes related to biodegradation

Overall, 708 (MGB-2) and 760 (MGB-3) annotated genes corresponding to 17 pathways linked with xenobiotic biodegradation and metabolism were identified, although with varying levels of abundance (Fig. 2.12) in both samples. The annotated pathways for degradation and metabolism of xenobiotic compounds, including POPs enlisted by the US Environmental Protection Agency, accounted for 2% of the 60 % of metabolic functions (Fig. 2.8).

The presence of reads for biphenyl degradation, dioxin degradation, and PAH degradation pathways can be further correlated with the presence of PCBs and PAHs as detected in the MGB-2 and MGB-3 samples (Fig. 2.13). Further, chlorocyclohexane and chlorobenzene [PATH: Ko00361], and benzoate [PATH: Ko00362] degrading pathways were most prominent in MGB-2 (33.76%; 37.39%) and MGB-3 (39.55%; 33.96%). In addition to these degradative pathways, dioxin [PATH: Ko00621] and PAH [PATH: Ko00624] degradation pathways were also observed in MGB-2 (3.27%; 2.54%) and MGB-3 (4.29%; 2.80%), respectively.

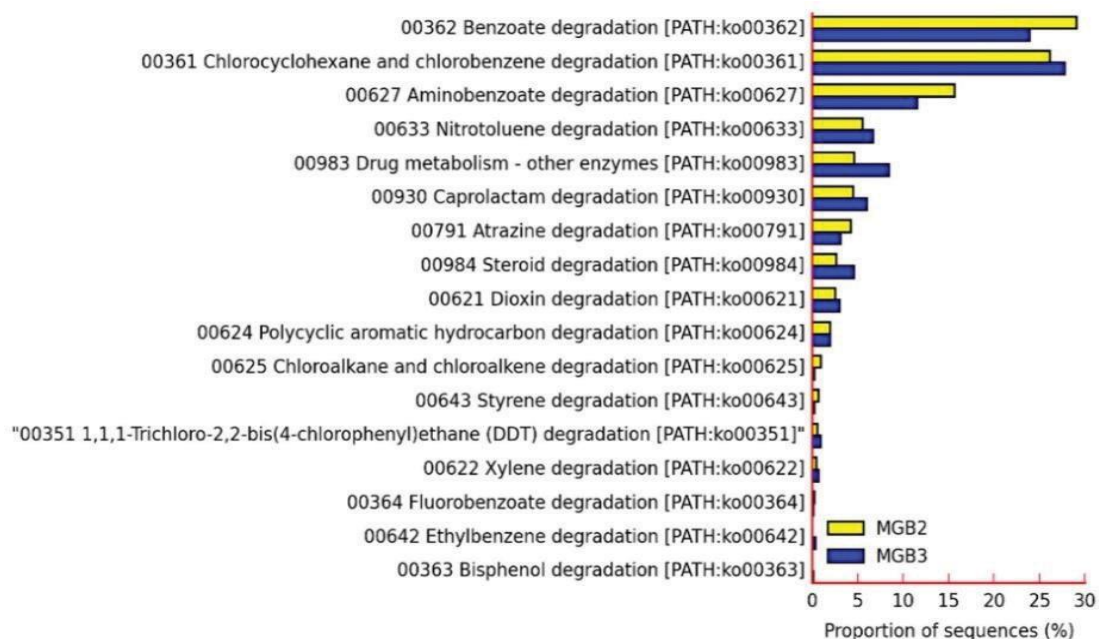


**Fig. 2.12.** Annotated pathways for xenobiotic degradation and metabolism accounted for metagenome MGB-2 and MGB-3

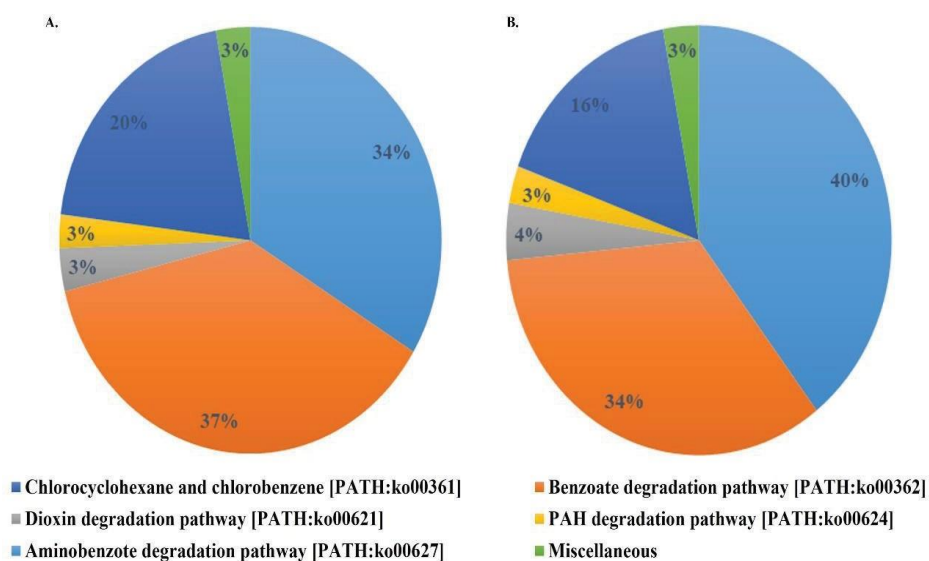


**Fig. 2.13.** Analysis of various xenobiotic biodegradation pathways in (A) MGB-2 and (B) MGB-3 at SEED subsystem level using MG-RAST assigned reads

Similar to our observations, the presence of chlorobenzene, PAH, PCB, and benzoate were found to be prominent contaminants of dye and steel industries (Yadav et al., 2016; Jiun-Horng et al., 2007). The annotated genes, namely *chqB*, *pcpB*, *pheA*, *clcD*, *hadL*, *bedC1/todC1*, *bphC*, *catA*, and *catB*, encoding enzymes highlighted the degradation of chlorocyclohexane and chlorobenzene compounds within the two communities (Table 2.7).

**Table 2.7.** Annotated enzyme and the assigned genera in metagenome MGB-2 and MGB-3 for chlorocyclohexane and chlorobenzene degradation pathway

<b>Pathway</b>	<b>Gene</b>	<b>Anotated Enzyme</b>	<b>Assigned bacteria in MGB-2</b>	<b>Assigned bacteria in MGB-3</b>
<b>Chlorocyclohexane and chlorobenzene degradation [PATH:ko00361]</b>	<i>chqB</i>	hydroxyquinol 1,2-dioxygenase [EC:1.13.11.37]	<i>Arthrobacter</i> , <i>Bradyrhizobium</i> <i>Burkholderia</i> , <i>Cupriavidus</i> <i>Variovorax</i> , <i>Verminephrobacter</i>	<i>Catenulispora</i> <i>Bradyrhizobium</i>
	<i>pcpB</i>	pentachlorophenol monooxygenase [EC:1.14.13.50]	<i>Rhodococcus</i>	<i>Anabaena</i> , <i>Burkholderia</i>
	<i>pheA</i>	phenol 2-monooxygenase [EC:1.14.13.7]	<i>Arthrobacter</i> , <i>Bradyrhizobium</i> , <i>Nocardia</i> , <i>Renibacterium</i> , <i>Rhodococcus</i> , <i>Rubrobacter</i>	<i>Agrobacterium</i> , <i>Arthrobacter</i> , <i>Azoarcus</i> , <i>Bradyrhizobium</i> , <i>Methylobacterium</i> , <i>Nocardia</i> , <i>Paracoccus</i> , <i>Rhodococcus</i> , <i>Rubrobacter</i>
	<i>pnpD</i>	maleylacetate reductase [EC:1.3.1.32]	<i>Bradyrhizobium</i> , <i>Polaromonas</i>	<i>Bradyrhizobium</i> , <i>Burkholderia</i> , <i>Polaromonas</i> , <i>Rhodococcus</i> , <i>Rhodopseudomonas</i>
	<i>clcD</i>	carboxymethylenebutenolidase [EC:3.1.1.45]	<i>Acidimicrobium</i> <i>Agrobacterium</i> , <i>Arthrobacter</i> , <i>Bradyrhizobium</i> , <i>Burkholderia</i> , <i>Candidatus</i> , <i>Cupriavidus</i> , <i>Desulfobacterium</i> , <i>Gemmatimonas</i> , <i>Methanoculleus</i> , <i>Polaromonas</i> , <i>Pseudomonas</i> , <i>Rhodococcus</i> , <i>Rhodopseudomonas</i> , <i>Sphingobium</i>	<i>Acetobacter</i> , <i>Acidimicrobium</i> , <i>Acidobacterium</i> , <i>Agrobacterium</i> , <i>Azoarcus</i> , <i>Beijerinckia</i> , <i>Bradyrhizobium</i> , <i>Burkholderia</i> , <i>Candidatus</i> , <i>Cellvibrio</i> , <i>Cupriavidus</i> , <i>Dechloromonas</i> , <i>Desulfobacterium</i> , <i>Flavobacterium</i> , <i>Gemmatimonas</i> , <i>Polaromonas</i> , <i>Rhodococcus</i> , <i>Sphingomonas</i>
	<i>hadL</i>	2-haloacid dehalogenase [EC:3.8.1.2]	<i>Beijerinckia</i> , <i>Bordetella</i> , <i>Burkholderia</i> , <i>Cupriavidus</i> , <i>Methylobacterium</i> ,	<i>Acidovorax</i> , <i>Anaeromyxobacter</i> , <i>Beijerinckia</i> , <i>Bordetella</i> , <i>Bradyrhizobium</i> ,

## Chapter II

---

		<i>Mycobacterium</i> , <i>Oligotropha</i> , <i>Rhodopseudomonas</i>	<i>Burkholderia</i> , <i>Candidatus</i> , <i>Chromobacterium</i> , <i>Mesorhizobium</i> , <i>Methylobacterium</i> , <i>Mycobacterium</i> , <i>Methylocella</i> , <i>Polaromonas</i> , <i>Rhodopseudomonas</i> , <i>Sorangium</i> , <i>Xanthomonas</i>
<i>dehH</i>	haloacetate dehalogenase [EC:3.8.1.3]	<i>Anabaena</i> , <i>Anaeromyxobacter</i> , <i>Azoarcus</i> , <i>Burkholderia</i> , <i>Chloroflexus</i> , <i>Cupriavidus</i> , <i>Kribbella</i> , <i>Mesorhizobium</i> , <i>Methylobacterium</i> , <i>Nocardiopsis</i> , <i>Micromonospora</i> <i>Psychromonas</i> , <i>Rhizobium</i> , <i>Rhodopseudomonas</i> , <i>Roseiflexus</i> , <i>Saccharopolyspora</i>	<i>Anabaena</i> , <i>Anaeromyxobacter</i> , <i>Bradyrhizobium</i> , <i>Burkholderia</i> , <i>Chloroflexus</i> , <i>Geodermatophilus</i> ,, <i>Mesorhizobium</i> , <i>Methylibium</i> , <i>Methylobacterium</i> , <i>Nocardiopsis</i> , <i>Psychromonas</i> , <i>Rhodopseudomonas</i> , <i>Roseiflexus</i> ,
<i>bedC1</i> <i>todC1</i>	benzene/toluene dioxygenase subunit alpha [EC:1.14.12.3 1.14.12.11]	<i>Mycobacterium</i>	<i>Mycobacterium</i>
<i>bphC</i>	biphenyl-2,3-diol 1,2- dioxygenase [EC:1.13.11.39]	<i>Rhizobium</i>	<i>Mycobacterium</i> , <i>Candidatus</i> , <i>Bradyrhizobium</i>
<i>catA</i>	catechol 1,2-dioxygenase [EC:1.13.11.1]	<i>Cupriavidus</i> , <i>Methylobacterium</i> , <i>Pseudomonas</i> , <i>Sphingobium</i> , <i>Streptomyces</i>	<i>Azospirillum</i> , <i>Bradyrhizobium</i> , <i>Burkholderia</i> , <i>Delftia</i> , <i>Mycobacterium</i> , <i>Pseudomonas</i> , <i>Rhizobium</i> , <i>Sphingomonas</i> , <i>Mycobacterium</i>
<i>catB</i>	muconate cycloisomerase [EC:5.5.1.1]	<i>Rhodopirellula</i>	<i>Mycobacterium</i>
<i>dmpB</i>	catechol 2,3-dioxygenase [EC:1.13.11.2]	<i>Arthrobacter</i> , <i>Bradyrhizobium</i> , <i>Brucella</i> , <i>Geobacillus</i> , <i>Meiothermus</i> , <i>Rubrobacter</i>	<i>Agrobacterium</i> , <i>Bradyrhizobium</i> , <i>Burkholderia</i> , <i>Meiothermus</i> , <i>Methylibium</i> , <i>Rhodococcus</i> ,

---

The above-mentioned enzymes suggest that chlorobenzene degradation is catalyzed *via* the *ortho*-cleavage pathway (Mars et al., 1999) and the *meta*-cleavage pathway (Mars et al., 1997) in

---

two metagenomes. The annotated reads for various genes, including *bphA*, *bphC*, *bphD*, *bphE*, and *bphF*, corresponding to the biphenyl degradation pathway, were identified in both samples (Table 2.8). The presence of *bphA* in both metagenomes MGB-2 and MGB-3 indicated biphenyl degradation assigned to genus *Mycobacterium* in both samples and *Polaromonas* in MGB-3. Biphenyl 2, 3-diol, 1, 2-dioxygenase (*bphC*) is another important enzyme that was noted in both the metagenome. The *bphC* genes were assigned to *Mycobacterium* in MGB-2, whereas *Alkalilimnicola*, *Mycobacterium*, and *Polynucleobacter* in MGB-3. Metabolic pathways of PCBs degradation by *Pseudomonas*, *Polaromonas*, *Mycobacterium*, and *Polynucleobacter* have been studied in detail (Weiland-Brauer et al., 2017; Langenhoff et al., 1996; Jorge et al., 2006; Hatamian-Zarmi et al., 2009; Komancova et al., 2003; Pagnout et al., 2007). The degradation pathway mainly of PAHs and PCBs is highlighted in the present study as the collected soil samples MGB-2 and MGB-3 were contaminated with these organic pollutants.

The annotated genes encoding enzymes required in the PAH degradation pathway in the MGB-2 and MGB-3 are listed in Table 2.8. The presence of genes encoding hydroxychromene-2-carboxylate isomerase (*nahD*), naphthalene dioxygenase (*nahAc*), salicylate hydroxylase (*nahG*), and other genes including *nidA*, *nidB*, *nidD*, *phdF*, *phdG*, *phdI*, and *phdJ* indicated the presence of a complete pathway of PAH degradation. The presence of reads for *nidA* gene could be correlated with pyrene degradation (Lu et al., 2019), which was found abundantly present in MGB-3 as detected by GC-MS/MS. Several reports indicate that *nidA* gene is responsible for synthesizing the large subunit of PAH dioxygenase involved in the degradation of PAHs such as phenanthrene, pyrene, and benzo[a]pyrene, etc. (Heider et al., 1998). The pathway analysis demonstrated that the enzymes involved in the PAH biodegradation pathway were affiliated with the members of genera *Pseudoalteromonas*, *Aromatoleum*, *Dechloromonas*, *Agrobacterium*, *Mesorhizobium* in MGB-2, while *Mycobacterium*, *Parvibaculum*, *Ruegeria*, *Burkholderia*, *Aromatoleum*, *Bradyrhizobium* in MGB-3 communities.



**Table 2.8.** Annotated enzyme and the assigned genera in metagenome MGB-2 and MGB-3 for Biphenyl/ PAH degrading pathway

Pathway	Gene	Annotated Enzymes	Assigned bacteria in MBG-2	Assigned bacteria in MBG-3
<b>Biphenyl degradation</b>	<i>bphA</i>	biphenyl 2,3-dioxygenase [EC:1.14.12.18]	<i>Mycobacterium vanbaalenii</i> PYR-1	<i>Mycobacterium vanbaalenii</i> PYR-1, <i>Polaromonas naphthalenivorans</i> CJ2
	<i>bphB</i>	cis-2,3-dihydrobiphenyl-2,3-diol dehydrogenase [EC 1.3.1.56]	nd	nd
	<i>bphC</i>	biphenyl-2,3-diol 1,2-dioxygenase [EC:1.13.11.39]	<i>Mycobacterium smegmatis</i> str. MC2 155	<i>Alkalilimnicola ehrlichii</i> MLHE-1, <i>Mycobacterium smegmatis</i> str. MC2 155, <i>Mycobacterium tuberculosis</i> KZN 1435, <i>Mycobacterium bovis</i> BCG str. Tokyo 172
	<i>bphD</i>	2,6-dioxo-6-phenylhexa-3-enoate hydrolase [EC:3.7.1.8]	<i>Nocardioides</i> sp. JS614	<i>Mycobacterium marinum</i> M, <i>Polynucleobacter necessarius</i> ,
	<i>bphE</i>	2-hydroxypenta-2,4-dienoate hydratase [EC 4.2.1.80]	nd	<i>Polynucleobacter necessarius</i>
	<i>bphF</i>	4-hydroxy-2-oxovalerate aldolase [EC 4.1.3.39]	<i>Carboxydotherrnus hydrogenoformans</i> , <i>Pseudomonas putida</i> F1, <i>Burkholderia</i> sp. 383	<i>Carboxydotherrnus hydrogenoformans</i> Z-2901, <i>Legionella pneumophila</i> str. Corby <i>Mycobacterium</i> sp. JLS, <i>Roseiflexus</i> sp. RS-1, <i>Arcobacter butzleri</i> , <i>Rhodococcus jostii</i> RHA1, <i>Streptosporangium roseum</i> DSM 43021 <i>Nocardioides</i> sp. JS614, <i>Nocardia farcinica</i> IFM 10152, <i>Eubacterium rectale</i> ATCC 33656, <i>Frankia</i> sp. EAN1pec



	<i>nahD</i>	hydroxychromene-2-carboxylate isomerase [EC:5.99.1.4]	<i>Agrobacterium tumefaciens</i> , <i>Aromatoleum aromaticum</i> , <i>Bradyrhizobium sp.</i> BTAi1, <i>Dechloromonas aromatic</i> ,	<i>Aromatoleum aromaticum</i> , <i>Bradyrhizobium sp.</i> BTAi, <i>Burkholderia xenovorans</i> , <i>Parvibaculum lavamentivorans</i> ,
	<i>nahAc</i>	naphthalene dioxygenase ferredoxin [EC:1.14.12.12]	<i>Pseudoalteromonas atlantica</i>	<i>Rhizobium leguminosarum</i> ,
	<i>nahG</i>	salicylate hydroxylase [EC:1.14.13.172]	<i>Mesorhizobium loti</i> <i>Anaeromyxobacter dehalogenans</i> , <i>Burkholderia cenocepacia</i> , <i>Dyadobacter fermentans</i> <i>Methylobacterium extorquens</i> ,	<i>Ruegeria pomeroyi</i> <i>Acidovorax citrulli</i> , <i>Bordetella bronchiseptica</i> , <i>Corynebacterium efficiens</i> , <i>Cupriavidus pinatubonensis</i> , <i>Delftia acidovorans</i> ,
PAH degradation	<i>nidA</i>	PAH dioxygenase large subunit [EC:1.13.11.-]	<i>Mycobacterium smegmatis</i> , <i>Polaromonas sp.</i> JS666,	<i>Polaromonas sp.</i> JS666, <i>Streptomyces coelicolor</i>
	<i>nidB</i>	PAH dioxygenase small subunit [EC:1.13.11.-]	<i>Pseudoalteromonas atlantica</i>	
	<i>nidD</i>	aldehyde dehydrogenase [EC:1.2.1.-]	nd	<i>Mycobacterium sp.</i> JLS
	<i>phdF</i>	extradiol dioxygenase [EC:1.13.11.-]	nd	<i>Mycobacterium sp.</i> JLS
	<i>phdG</i>	hydratase-aldolase [EC:4.1.2.-]		
	<i>phdI</i>	1-hydroxy-2-naphthoate dioxygenase [EC:1.13.11.38]	<i>Mycobacterium vanbaalenii</i>	<i>Mycobacterium vanbaalenii</i>
	<i>phdJ</i>	4-(2-carboxyphenyl)-2-oxobut-3-enoate aldolase [EC:4.1.2.34]	<i>Mycobacterium vanbaalenii</i> <i>Mycobacterium sp.</i> KMS, <i>Mycobacterium sp.</i> MCS	<i>Mycobacterium sp.</i> KMS <i>Mycobacterium vanbaalenii</i> <i>Mycobacterium sp.</i> MCS

The contribution of enzymes for degradation by different genera suggests synergistic degradation of these PAH. Further, the annotated gene/enzyme and the bacterial genera involved in the benzoate degradation pathway were identified in MGB-2 and MGB-3, as listed in Table 2.9. The presence of benzoate ligase in MGB-2 indicated anaerobic degradation of benzoate. Benzoate is the most common intermediate in the metabolism of aromatic compounds, and in the anaerobic condition, it is converted into benzoyl-CoA by benzoate ligase (Valderrama et al., 2012). The presence of genes encoding anaerobic degradation *via* benzoyl CoA (*badA*, *badD*, *badE*, *badF*, *badH*, *badI*, *hbaA*, *hbaB*, *hcrC*) and aerobic *via* protocatechuate (*ligAB*, *ligC*, *ligI*, *ligJ*, *pobA*, *pcaB*, *pcaC*, *pcaDF*, *pcaGH* and *pcaIJ*) catechol (*catE/dmpB*) indicates complete pathway for degradation of benzoate. Protocatechuate can be metabolized by protocatechuate 4, 5-dioxygenase (*LigAB*) or protocatechuate 3, 4-dioxygenase (*PcaGH*).

**Table 2.9.** Annotated gene/enzyme and the bacterial genera involved in the benzoate degradation pathway *via* benzoyl coA, protocatechuate and catechol pathways identified in MGB-2 and MGB-3

Pathway	Gene	Annotated Enzymes	Assigned bacteria in MBG-2	Assigned bacteria in MBG-3
	<i>benB/xylY</i>	benzoate/toulene1,2 dioxygenase beta subunit	<i>Rhodopseudomonas</i> <i>Rhodococcus</i>	<i>Geodermatophilus</i> , <i>Saccharopolyspora</i>
	<i>benC/xylZ</i>	benzoate/toulene 1,2 dioxygenase electron transfer component	<i>nd</i>	<i>Geodermatophilus</i> , <i>Mycobacterium</i> , <i>Saccharopolyspora</i>
	<i>benD</i>	2,3-dihydroxybenzoate decarboxylase [EC:4.1.1.46]	<i>Burkholderia</i> , <i>Rhodococcus</i> , <i>Rhodopseudomonas</i>	<i>Bordetella</i> , <i>Novosphingobium</i> , <i>Polaromonas</i> , <i>Rhizobium</i> , <i>Rhodopseudomonas</i> , <i>Xanthobacter</i>
	<i>pimC</i> <i>praC</i>	pimeloyl-CoA dehydrogenase [EC:1.3.1.62] 4-oxalocrotonate tautomerase [EC:5.3.2.-]	<i>Cupriavidus</i> <i>nd</i>	<i>Cupriavidus</i> <i>Candidatus</i> , <i>Methylocella</i>
	<i>aliA</i>	cyclohexanecarboxylate-CoA ligase [EC:6.2.1.-]	<i>nd</i>	<i>Conexibacter</i> , <i>Cupriavidus</i> , <i>Rhodopseudomonas</i> , <i>Verminephrobacter</i>
Benzoate degradation	<i>badA</i>	benzoate-CoA ligase [EC:6.2.1.25]	<i>Achromobacter</i> , <i>Aromatoleum</i> , <i>Azoarcus</i> , <i>Burkholderia</i> , <i>Comamonas</i> , <i>Cupriavidus</i> , <i>Delftia</i>	<i>Albidiferax</i> , <i>Amycolatopsis</i> , <i>Aromatoleum</i> , <i>Azoarcus</i> , <i>Bradyrhizobium</i> , <i>Cupriavidus</i> , <i>Leptothrix</i> , <i>Rhodomicrobium</i>
	<i>badD</i>	benzoyl-CoA reductase subunit [EC:1.3.7.8]	<i>Rhodopseudomona</i> , <i>Thauera</i>	<i>Rhodopseudomonas</i>
	<i>badE</i>	benzoyl-CoA reductase subunit [EC:1.3.7.8]	<i>Magnetospirillum</i> , <i>Rhodomicrobium</i>	<i>nd</i>
	<i>badF</i>	benzoyl-CoA reductase subunit [EC:1.3.7.8]	<i>Magnetospirillum</i> , <i>Rhodomicrobium</i> , <i>Rhodopseudomona</i> , <i>Thauera</i>	<i>Magnetospirillum</i> , <i>Rhodomicrobium</i>
	<i>badH</i>	2-hydroxycyclohexanecarboxyl-CoA dehydrogenase [EC:1.1.1.-]	<i>Cupriavidus</i> , <i>Magnetospirillum</i> , <i>Nocardioides</i>	<i>Alicyclobacillus</i> , <i>Aromatoleum</i> , <i>Bordetella</i> , <i>Rhodopseudomonas</i>
	<i>badI</i>	2-ketocyclohexanecarboxyl-CoA hydrolase [EC:3.1.2.-]	<i>nd</i>	<i>Cupriavidus</i> , <i>Leptothrix</i> , <i>Polaromonas</i>

## Chapter II

<i>hbaA</i>	4-hydroxybenzoate-CoA ligase [EC:6.2.1.27 6.2.1.25]	<i>Bradyrhizobium</i> , <i>Magnetospirillum</i> , <i>Rhodopseudomonas</i>	<i>Bradyrhizobium</i>
<i>hbaB</i> , <i>hcrC</i>	4-hydroxybenzoyl-CoA reductase subunit gamma [EC:1.3.7.9]	<i>Magnetospirillum</i> , <i>Rhodopseudomonas</i>	nd nd
<i>hbaC</i> , <i>hcrA</i>	4-hydroxybenzoyl-CoA reductase subunit alpha [EC:1.3.7.9]	<i>Rhodopseudomonas</i> , <i>Thauera</i>	<i>Brevundimonas</i> , <i>Azoarcus</i> <i>Brevundimonas</i> ,
<i>ligAB</i>	protocatechuate 4,5-dioxygenase [EC 1.13.11.8]	<i>Rhodopseudomonas</i> , <i>Acidimicrobium</i> , <i>Burkholderia</i> , <i>Nakamurella</i> , <i>Novosphingobium</i> , <i>Pseudoalteromona</i> , <i>Xanthomonas</i>	<i>Marinomonas</i> , <i>Saccharomonospora</i>
<i>ligC</i>	2-hydroxy-4-carboxymuconate semialdehyde hemiacetal dehydrogenase [EC 1.1.1.312]	<i>Rhodopseudomonas</i>	<i>Brevundimonas</i>
<i>ligI</i>	2-pyrone-4,6-dicarboxylate lactonase [EC:3.1.1.57]	<i>Agrobacterium</i> , <i>Albidiferax</i> , <i>Arthrobacter</i> , <i>Bradyrhizobium</i> , <i>Novosphingobium</i> , <i>Rhodopseudomonas</i>	<i>Agrobacterium</i> , <i>Arthrobacter</i> , <i>Bradyrhizobium</i> , <i>Delftia</i> , <i>Polaromonas</i> , <i>Rhodopseudomonas</i>
<i>ligJ</i>	4-oxalomesaconate hydratase [EC 4.2.1.83]	<i>Arthrobacter</i> , <i>Asticcacaulis</i> , <i>Bradyrhizobium</i> , <i>Brevundimonas</i> , <i>Burkholderia</i> , <i>Cupriavidus</i> , <i>Burkholderia</i> , <i>Methylobacterium</i> , <i>Paracoccus</i> , <i>Pseudoalteromonas</i> , <i>Ralstonia</i> , <i>Rhizobium</i> , <i>Rhodopseudomonas</i> , <i>Sphingobium</i> , <i>Variovorax</i> , <i>Xanthomonas</i>	<i>Azoarcus</i> , <i>Brevundimonas</i> , <i>Burkholderia</i> , <i>Magnetospirillum</i> , <i>Methylobacterium</i> , <i>Novosphingobium</i> , <i>Paracoccus</i> , <i>Polaromonas</i> , <i>Rhizobium</i> , <i>Rhodopseudomonas</i> , <i>Verminephrobacter</i> , <i>Xanthomonas</i>
<i>pobA</i>	p-hydroxybenzoate 3- monoxygenase [EC:1.14.13.2]	<i>Amycolatopsis</i> , <i>Arthrobacter</i> , <i>Bacillus</i> , <i>Burkholderia</i> , <i>Candidatus</i> , <i>Caulobacter</i> , <i>Chelativorans</i> , <i>Delftia</i> , <i>Frankia</i> , <i>Herbaspirillum</i> , <i>Mesorhizobium</i> ,  <i>Novosphingobium</i> ,	<i>Agrobacterium</i> , <i>Amycolatopsis</i> , <i>Arthrobacter</i> , <i>Burkholderia</i> , <i>Candidatus</i> , <i>Magnetospirillum</i> , <i>Pseudomonas</i> , <i>Rhodopseudomonas</i> , <i>Saccharomonospora</i> , <i>Xanthomonas</i> ,  <i>Verminephrobacter</i>

## Chapter II

<i>pcaG</i>	beta-Carboxy-cis,cis-muconate [EC:1.13.11.3]	<i>Bradyrhizobium</i> , <i>Candidatus</i> , <i>Cupriavidus</i> , <i>Geodermatophilus</i> , <i>Sphaerobacter</i> , <i>Sphingomonas</i>	<i>Candidatus</i>
<i>pcaH</i>	protocatechuate 3,4-dioxygenase, beta subunit [EC:1.13.11.3]	<i>Acidiphilium</i> , <i>Amycolatopsis</i> , <i>Arthrobacter</i> , <i>Azospirillum</i> , <i>Burkholderia</i> , <i>Caulobacter</i> , <i>Klebsiella</i> , <i>Pirellula</i> , <i>Planctomyces</i> , <i>Polaromonas</i> , <i>Pseudomonas</i> , <i>Rhodopirellula</i> , <i>Rubrobacter</i> , <i>Saccharopolyspora</i> , <i>Spirosoma</i> , <i>Streptosporangium</i> , <i>Xanthobacter</i>	<i>Agrobacterium</i> , <i>Azorhizobium</i> , <i>Azospirillum</i> , <i>Burkholderia</i> , <i>Candidatus</i> , <i>Cupriavidus</i> , <i>Geodermatophilus</i> , <i>Klebsiella</i> , <i>Mesorhizobium</i> , <i>Planctomyces</i> , <i>Polaromonas</i> , <i>Pseudomonas</i> , <i>Rhodococcus</i> , <i>Rhodopirellula</i> , <i>Saccharopolyspora</i> , <i>Spirosoma</i> , <i>Streptomyces</i> , <i>Streptosporangium</i> , <i>Xanthomonas</i> ,
<i>pcaI</i>	3-oxoadipate CoA- transferase, alpha subunit [EC:2.8.3.6]	<i>Achromobacter</i> , <i>Arthrobacter</i> , <i>Kocuria</i> , <i>Serratia</i> , <i>Shewanella</i> , <i>Xanthomonas</i>	<i>Catenulispora</i> , <i>Mycobacterium</i>
<i>pcaJ</i>	3-oxoadipate CoA- transferase, beta subunit [EC:2.8.3. 6]	<i>Arthrobacter</i> , <i>Cupriavidus</i> , <i>Escherichia</i> , <i>Herbaspirillum</i>	<i>Nocardioides</i> , <i>Rhodopseudomonas</i> <i>Ruegeria</i> , <i>Streptomyces</i>
<i>pcaB</i>	3-carboxy-cis, cis- muconate cycloisomerase [EC:5.5.1.2]	<i>Cupriavidus</i> , <i>Deinococcus</i> , <i>Delftia</i> , <i>Frankia</i> , <i>Pseudomonas</i> , <i>Sinorhizobium</i> , <i>Xanthomonas</i>	<i>Albidiferax</i> , <i>Burkholderia</i> , <i>Chelativorans</i> , <i>Cupriavidus</i> , <i>Leptothrix</i> , <i>Meiothermus</i> , <i>Methylobacterium</i> , <i>Polaromonas</i> , <i>Ralstonia</i> , <i>Xanthomonas</i>
<i>pcaC</i>	4- carboxymuconolactone decarboxylase [EC:4.1.1.44]	<i>Beutenbergia</i> , <i>Bradyrhizobium</i> , <i>Burkholderia</i> , <i>Candidatus</i> , <i>Methylobacterium</i> , <i>Mycobacterium</i> , <i>Rhizobium</i> , <i>Rhodomicrobium</i>	<i>Amycolatopsis</i> , <i>Arthrobacter</i> , <i>Bradyrhizobium</i> , <i>Burkholderia</i> , <i>Frankia</i> , <i>Mycobacterium</i> , <i>Ralstonia</i> , <i>Rhodococcus</i> , <i>Rhodopseudomonas</i> , <i>Sinorhizobium</i>

## Chapter II

<i>pcaD</i>	3-oxoadipate enol-lactonase [EC:3.1.1.24]	<i>Burkholderia</i> <i>Rhizobium</i> , <i>Xanthobacter</i>	<i>Chelativorans</i> , <i>Cupriavidus</i> , <i>Methylobacterium</i> , <i>Mycobacterium</i> , <i>Rhizobium</i> , <i>Sinorhizobium</i> , <i>Thermomonospora</i>
<i>pcaF</i>	3-oxoadipyl-CoA thiolase [EC:2.3.1.174]	<i>Bradyrhizobium</i> , <i>Pseudomonas</i> , <i>Rhodopseudomonas</i>	<i>Bradyrhizobium</i> , <i>Sphingomonas</i>
<i>catA</i>	catechol 1,2-dioxygenase [EC:1.13.11.1]	<i>Cupriavidus</i> , <i>Methylobacterium</i> , <i>Pseudomonas</i> , <i>Sphingobium</i> , <i>Streptomyces</i>	<i>Azospirillum</i> , <i>Bradyrhizobium</i> , <i>Burkholderia</i> , <i>Mycobacterium</i> , <i>Pseudomonas</i> , <i>Rhizobium</i> , <i>Sphingomona</i> ,
<i>catB</i>	muconate cycloisomerase [EC:5.5.1.1]	<i>Rhodopirellula</i>	<i>Mycobacterium</i>
<i>catE</i> / <i>dmpB</i>	catechol 2,3- dioxygenase [EC:1.13.11.2]	<i>Agrobacterium</i> , <i>Bradyrhizobium</i> , <i>Burkholderia</i> , <i>Methylibium</i> , <i>Rhodococcus</i>	<i>Arthrobacter</i> , <i>Bradyrhizobium</i> , <i>Brucella</i> , <i>Geobacillus</i> , <i>Meiothermus</i> , <i>Rubrobacter</i>

Anaerobic degradation *via* benzoyl-CoA has also been documented in a variety of facultative anaerobes, including the denitrifying *Thauera* (Heider et al., 1998), *Magnetospirillum* strains (Meyer-Cifuentes et al., 2017), and the photoheterotroph *Rhodopseudomonas* (Egland et al., 1995). Similar to the above reports, we observed that enzymes involved in benzoate degradation are contributed possibly by members of genera *Aromatoleum*, *Arthrobacter*, *Burkholderia*, *Bradyrhizobium*, *Cupriavidus*, *Magnetospirillum*, *Methylobacterium*, *Rhodomicrobium*, *Rhodopseudomonas*, and *Polaromonas* in both the metagenome communities suggesting a synergistic degradation of benzoate. Analysis of functional gene annotation using SEED subsystem by STAMP for peripheral degradation pathway in MGB-2 and MGB-3 is shown in Fig. 2.14.

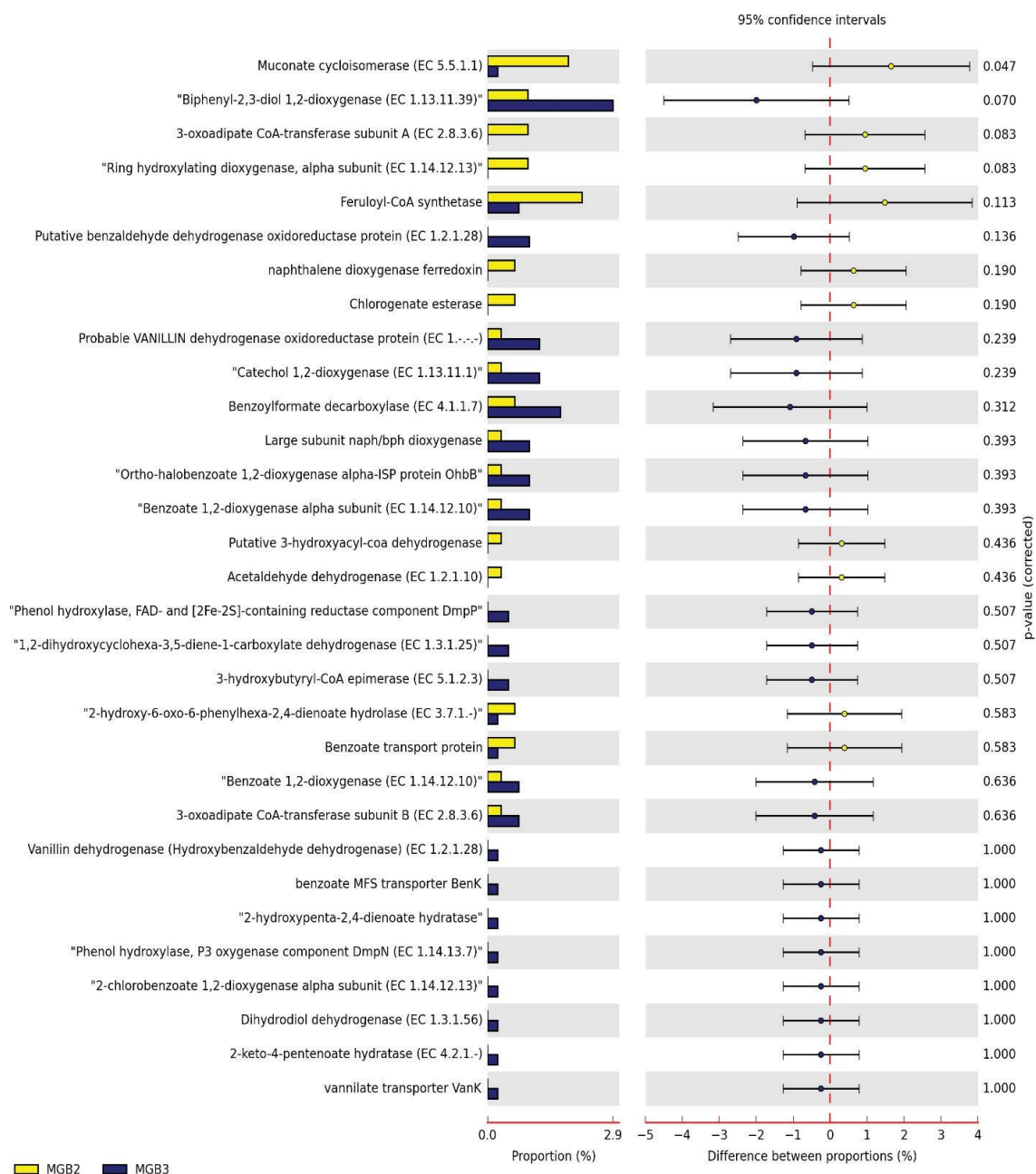


**Fig. 2.14.** Comparative analysis of metagenome MGB-2 and MGB-3 based on Peripheral aromatic degradation metabolism at SEED subsystem level by using STAMP. These enzymes depicted in the graph cleave the rings of aromatic compounds and represent groups in the peripheral aromatic degradation pathway, and transform the aromatic compounds into intermediary metabolites.



It revealed the abundance of muconate cycloisomerase ring hydroxylating dioxygenase, naphthalene dioxygenase, acetaldehyde dehydrogenase, 2-hydroxy-6-oxo-6-phenyl hexa-2,4-dienoate hydrolase, and benzoate transport protein in MGB-2. On the other hand, genes encoding biphenyl 2,3 diol dioxygenase, benzaldehyde dehydrogenase, *nap/bph* dioxygenase, *ortho*-halobenzoate 1,2- dioxygenase, phenol dioxygenase, and 1,2-dihydroxycyclohexa-3,5-diene-1-carboxylate dehydrogenase were abundant in MGB-3.

Similarly, a two-way comparison between MGB-2 and MGB-3 of functional gene annotation using the SEED subsystem for aromatic degradation revealed a significant level of abundance for benzoate ligase ( $p = 2.63 \times 10^{-3}$ ) and 4-hydroxy phenylacetate 3-monooxygenase ( $p = 8.93 \times 10^{-3}$ ) in MGB-2. The presence of 2-hydroxy cyclohexane carboxyl dehydrogenase with  $p = 2.39 \times 10^{-3}$  also indicated the anaerobic degradation of benzoate in MGB-3. However, aerobic degradation of biphenyl was also found in MGB-3, which is evident by the abundance of biphenyl-2, 3-diol 1, 2-dioxygenase with  $p = 0.035$  in MGB-3 (Fig. 2.15).

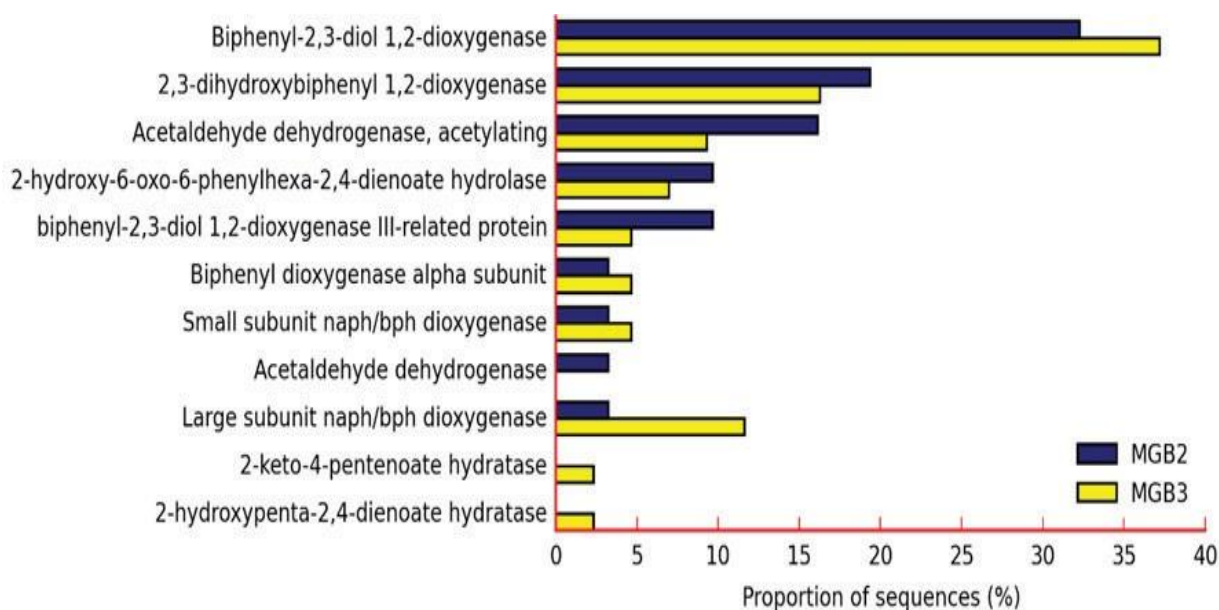


**Fig. 2.15.** Comparative analysis of metagenome MGB-2 and MGB-3 based on biphenyl degradation metabolism at SEED subsystem level by using STAMP.

Furthermore, a comparison between MGB-2 and MGB-3 at functional gene annotation using RefSeq for aromatic degradation revealed a significant level of abundance of *Acidothermus* ( $p=2.68 \times 10^{-3}$ ), *Nakamurella* ( $p=6.39 \times 10^{-3}$ ) in MGB-2, while *Mycobacterium* ( $p = 3.30 \times 10^{-3}$ ), *Leptothrix* ( $p=7.89 \times 10^{-3}$ ) and *Polynuclearbacter* ( $p=0.034$ ) in MGB-3 (Fig. 2.16).



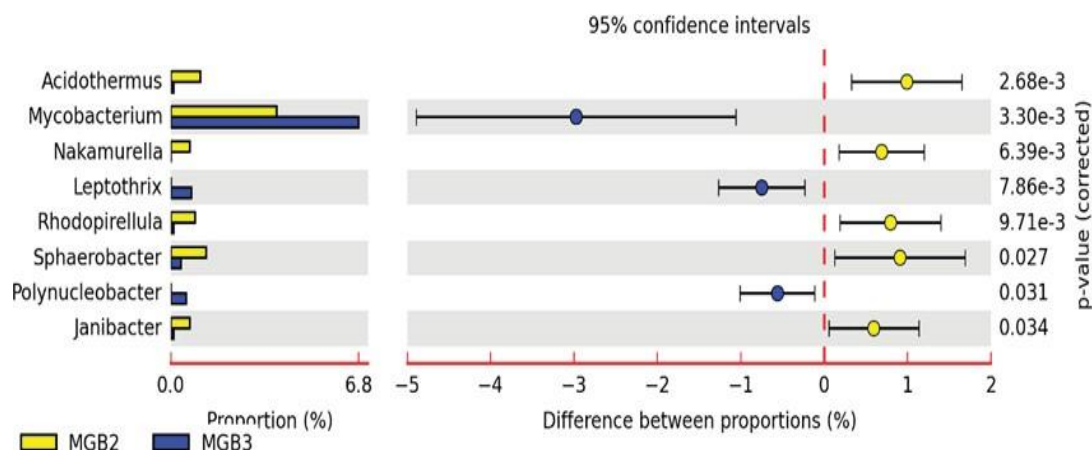


**Fig. 2.16.** Comparative analysis of metagenome MGB-2 and MGB-3 based on aromatic degradation metabolism at ReFSeq genus level by using STAMP.

Our findings suggest that biphenyl/ PCB and pyrene/phenanthrene (PAH) biodegradation pathways could be linked together *via* a common intermediate protocatechuate pathway and that it further undergoes complete degradation through the common protocatechuate branch of the  $\beta$ -keto adipate pathway. Therefore, complete biphenyl/PCB and PAH degradative pathways were reconstructed based on the annotated genes, as shown in Fig. 2.17. Cytoscape-based networking revealed microbial interaction in the xenobiotic biodegradation pathway. The key biodegraders in xenobiotic biodegradation pathways (aromatic halogenated, dioxin, PAH, PCB/biphenyl, catechol, protocatechuate, benzoyl-CoA) were found to be *Arthrobacter chlorophenolicus*, *Meiothermus ruber*, *Cupriavidus metallidurans*, *Burkholderia xenovorans*, *Rubrobacter xylanophilus*, *Bradyrhizobium* sp. BTAi1, *Bradyrhizobium japonicum*, *Sphingobium japonicum*, *Pseudomonas aeruginosa*, *Polaromonas* sp. JS666 and *Rhizobium leguminosarum* in MGB-2 (Fig. 2.18). In MGB-3 it was *Bradyrhizobium japonicum*, *Rhizobium leguminosarum*, *Mycobacterium* sp. K.M.S., *Polaromonas* sp. JS666, *Rhodopseudomonas palustris*, *Xanthobacter autotrophicus*, *Mycobacterium smegmatis*, *Burkholderia cenocepacia*, and *Burkholderia xenovorans* (Fig. 2.19). The abundance of these genes and genera in sample MGB-2 and MGB-3 suggests a higher degrading capacity in both the metagenome. However, the key biodegraders were found to be *Bradyrhizobium*, *Burkholderia*, *Mycobacterium*, and *Rhodopseudomonas* in both the metagenome.

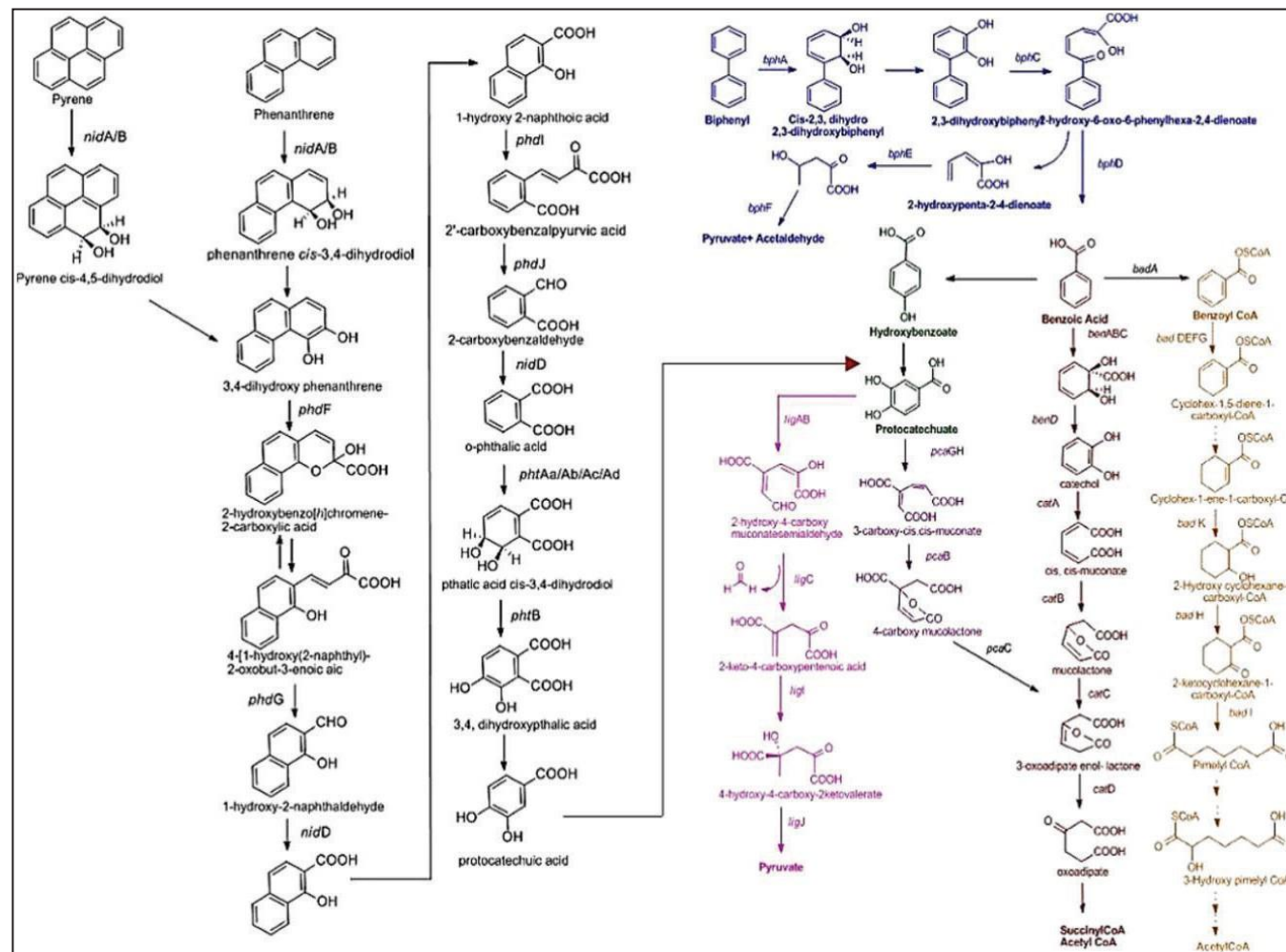


**Fig. 2.17.** Reconstruction of complete Biphenyl/PCB and PAH degradation pathways based on annotated genes identified., biphenyl degradation (Blue); benzoate degradation *via* catechol (red); benzoate degradation *via* protocatechuate (pink); benzoate degradation *via* benzoyl CoA degradation (orange); PAH degradation (Black) enters central pathway *via* protocatechuate intermediate. PAH, like pyrene and phenanthrene, produces a common degradation intermediate, i.e., 3,4 hydroxy phenanthrene, which gets converted into protocatechuate through a series of enzymes involved in the PAH degradation pathway. The upper biphenyl degradation pathway consists of the degradation of biphenyl to benzoic acid. The benzoic acid product so formed is channelled to a lower degradation pathway *via* protocatechuate converting into pyruvate and Acetyl-CoA.

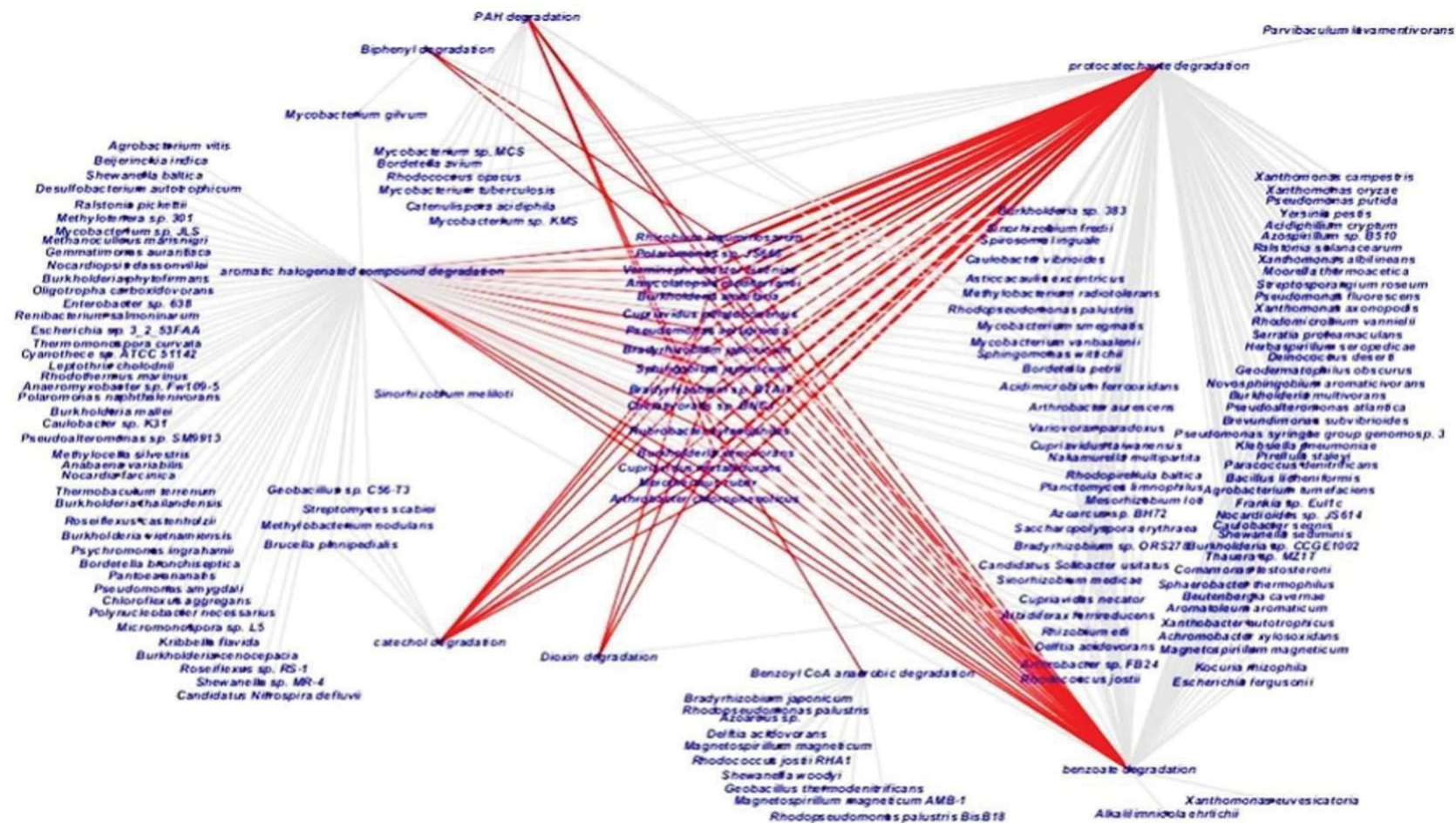


Fig. 2.18. Cytoscape-based networking depicted the interrelationship of key biodegraders in PAH, biphenyl, dioxin, halogenated, catechol, and protocatechuate pathways. Key biodegraders in metagenome MGB-2 are presented in the middle, and the interrelated pathways are given in red lines.



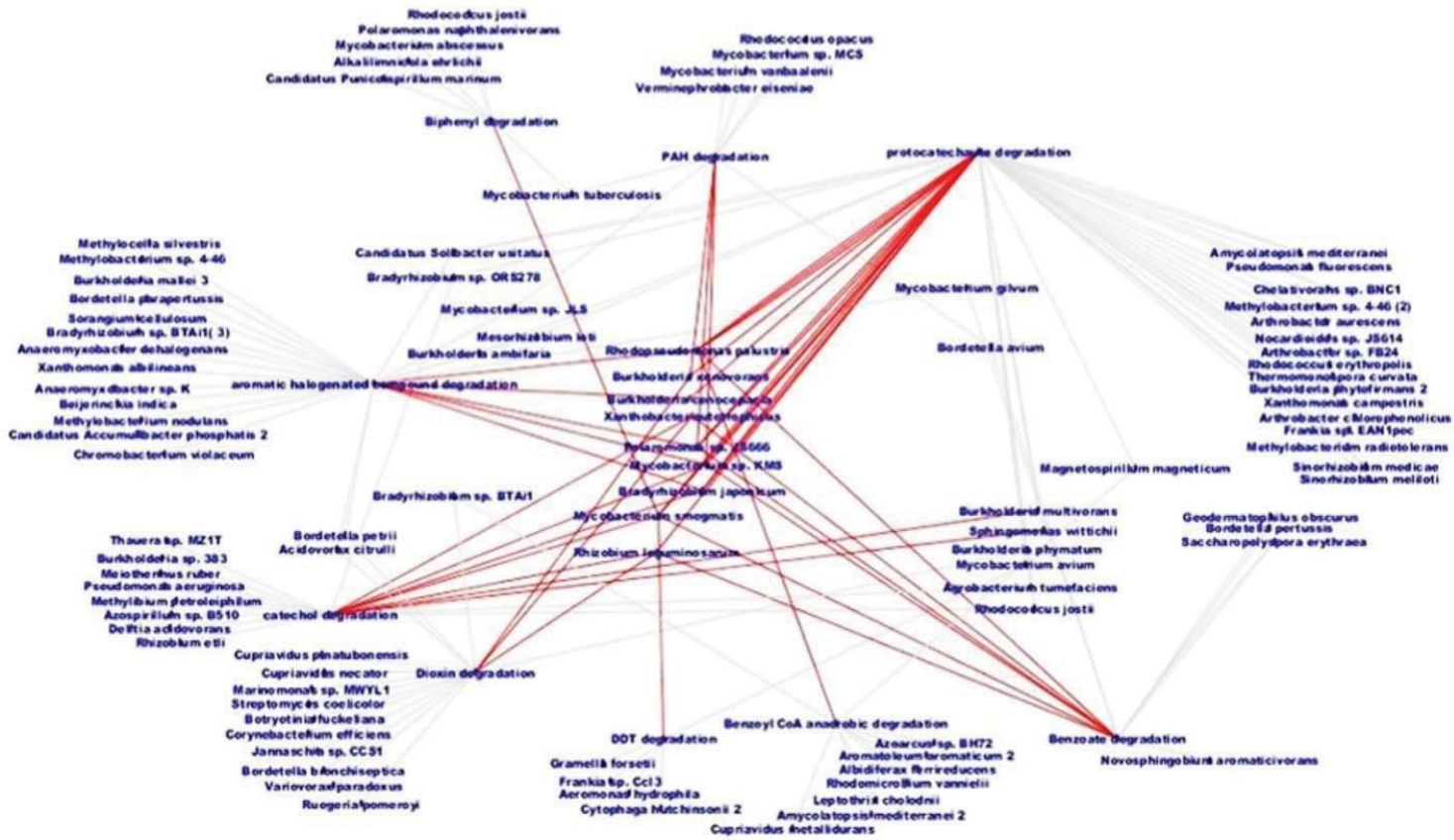


Fig 2.19. Cytoscape-based networking depicted the interrelationship of key biodegraders in PAH, biphenyl, dioxin, halogenated, catechol, and protocatechuate pathways. Key biodegraders in metagenome MGB-3 are presented in the middle, and the interrelated pathways are given in red lines.

**Chapter III**  
**Enrichment, Isolation, and**  
**Characterization of PCB-Degrading**  
**Bacteria**

### 3.1 Introduction

Polychlorinated biphenyls (PCBs) belong to a broad family of anthropogenic organic chemicals. They are among the harmful, persistent organic pollutants (POPs) listed under the Stockholm Convention (Zhu et al., 2022). Due to their physical and chemical properties, they are toxic and bioaccumulated through the food chain, posing a risk to human health and the environment (Pieper, 2005; Tomza-Marciniak et al., 2019). Bioremediation is considered the most promising approach for PCB decontamination from the environment due to its efficiency and cost-effectiveness (Tandlich et al., 2011). Bacteria play a significant role in the remediation of the PCB-contaminated environment. Many PCB-degrading bacteria have been isolated, including Gram-negative strains belonging to the genera *Achromobacter* (Hong et al., 2009), *Burkholderia* (Totevova et al., 2002; Goris et al., 2004), *Pseudomonas* (Hatamian-Zarmi et al., 2009; Kimura et al., 2018; Hirose et al., 2019; Thorat et al., 2020), *Ochrobactrum* (Murinova and Dercov, 2014a) and Gram-positive strains belonging to the genera *Rhodococcus* (Seto et al., 1995) and *Bacillus* (Shimura et al., 1999). These bacteria carry out biodegradation (through the metabolic pathway) using enzymes that convert organic pollutants into simpler compounds (Abramowicz, 1990). Biodegradation can be either through mineralization (where an organic pollutant acts as a sole carbon source) or by co-metabolism (where an inducer is required as the second carbon source, transforming the target pollutant simultaneously). There are several reports on using inducers for effective PCB degradation by bacterial strains belonging to the genera *Acinetobacter*, *Pseudomonas*, and *Rhodococcus* (Field and Sierra-Alvarez, 2008). The most common inducer used to improve PCB biodegradation is biphenyl, the basic scaffold of all PCB congeners (Luo et al., 2007; Luo et al., 2008). Biphenyl has been reported to induce ring cleavage hydroxylating dioxygenase enzyme that initiates the PCB degradation pathway. Aromatic ring cleavage genes have been used as markers for figuring out bacterial catabolic capabilities and have provided an interesting insight into the role played by the bacterium in response to PCB pollution. The rate-limiting step in aromatic hydrocarbon biodegradation is the large subunit of ARHD (Demaneche et al., 2004). It is one of the reasons why this enzyme has been chosen as an indicator gene in screening microbes with the ability to degrade aromatic hydrocarbons (Kimura et al., 2006, Kimura and Kamagata, 2009). The information about the functional and genetic diversity of ARHDs can provide the necessary basic knowledge for developing a microbial consortium for bioremediation technology (Yrjala et al., 2010).

Using glucose in combination with biphenyl has also been reported to improve cell survival (Zoradova-Murinova et al., 2012), increase biomass (Murinova et al., 2014), and, in turn, enhance PCB biodegradation. In addition to using an inducer, bioremediation is more effective when bacterial growth conditions such as pH, temperature, the concentration of the pollutant utilized (Parnell et al., 2010), and biosurfactant production are optimal. The efficiency of PCB degradation depends not only on the bacterial ability to degrade but also on the bioavailability of PCB (Mulligan, 2005). The bioavailability of the pollutant is influenced by bacterial chemotaxis in soil and the contaminants' affinity with the soil. Its strong hydrophobicity, and low biodegradability can limit the biodegradation efficiency of biphenyl. Bioavailability is well known to be one of the most crucial limiting factors for PCB bioremediation, which can be overcome by biosurfactants produced by bacteria. Biosurfactants improve the bioavailability of PCB to bacterial cells by detaching the strongly adsorbed PCB from the soil (Sifour et al., 2007). Thus, the biosurfactant-producing property of the bacterial strains plays a relevant role in the PCB's solubilization, making it bioavailable to bacteria for efficient degradation.

Another critical factor in the biodegradation process is the number and position of the chlorine atom attached to the biphenyl ring. It is reported that the rate of PCB degradation decreases with increasing chlorine content, indicating that highly chlorinated congeners are difficult to degrade (Kohler et al., 1988; Passatore et al., 2014). PCBs with one or two chlorines have been reported to biodegrade mainly at the *para* position *via* mineralization or co- metabolization. For instance, *Achromobacter xylosoxidans* IR08 degraded 4,4'-dichlorobiphenyl (diCB) metabolically (Ilori et al., 2008), while *Rhodococcus* sp. MAPB-1 (Sandhu et al., 2020) and *Rhodococcus* sp. WAY2 (Garrido-Sanz et al., 2020) degraded it co-metabolically. Similarly, it has been observed that bacteria exhibit no or reduced degrading ability for PCBs with four or more chlorine substitutions. For example, *Rhodococcus pyridinivorans* SS2 and *Rhodococcus ruber* SS1 efficiently degraded chlorobiphenyl, dichloro-, and trichloro-biphenyl but could not degrade tetrachloro- and hexachloro-biphenyl (Wang et al., 2016).

PCBs in commercial and environmental samples are complex mixtures of congeners. PCB-77 (3,3',4,4'-tetrachlorobiphenyl) is one of the major components of commercially available PCB blends and products. It is one of the most toxic coplanar congeners and is ubiquitous in the environment (Meggo et al., 2013). Structure-toxicity studies have revealed that it binds to aryl hydrocarbon receptor agonists (Ah), contributing significantly to its toxicity (Safe, 1994).



Moreover, its dioxin-like structure makes it highly resistant to biodegradation, and there are very few reports on its bioremediations (Liang et al., 2014).

As discussed in Chapter II, GC-MS/MS analysis showed that the soil samples collected from the nearby regions of the steel industry were contaminated with PCBs (Sandhu et al., 2022). Due to the complexity of the PCB congeners, a single bacterium cannot degrade all or even most of the PCB congeners present in the contaminated environment. Therefore, to increase biodegradation efficiency, the bacteria must possess biosurfactant, PGP-producing and chemotaxis properties, and biodegradation potential. Sometimes, for the degradation of a single compound, the synergetic action of a few microorganisms (i.e., a consortium of microbes) may be more efficient. Therefore, the objective of the current research was to isolate PCB degrading potential of the bacteria using biphenyl as substrates and to characterize selected bacterial isolates based on morphological, biochemical, molecular (ARHD gene expression), and analytical methods. Also, a tetrachlorobiphenyl PCB-77 was used as a model contaminant for the degradation study. Furthermore, this is the first report of these bacterial isolates using and degrading PCB-77. In addition to the characterization of PCB-degradation potential, we also tested plant growth-promoting properties of selected isolates which can be instrumental in the rhizoremediation process.

### **3.2 Materials and Methods**

#### **3.2.1 Chemicals and media**

LB medium, M9 medium (MM), and glucose were purchased from Himedia (Mumbai, India). Cetyltrimethylammonium bromide (CTAB), methylene blue, biphenyl, PCB-77 (3,4,3',4'-tetrachlorobiphenyl), acetone, ethyl acetate, hexane, methanol (Empure, GC grade) was purchased from Sigma Aldrich (St. Louis, MO, USA).

#### **3.2.2 Selective enrichment and isolation of microorganisms from PCB-contaminated soil**

The soil samples were collected at a 0-10 cm depth from the nearby site of Bhilai Steel Plant, Chhattisgarh, India, at latitude 21.1915°N and longitude 81.4041°E. Selective enrichments were made by inoculating 50 mL sterile MM with 10 g of PCB-contaminated soil samples. MM was supplemented with 1g mL<sup>-1</sup> biphenyl (*w/v*) as a sole carbon source and was incubated on a rotary shaker (150 rpm) at 30°C. After one week of acclimatization, 1% of the inoculum was transferred to fresh 50 mL of MM supplemented with 1% biphenyl, repeating up to three generations at a 7-day interval. Serial dilution was done from enriched diluent up to 10<sup>-6</sup>, and 100 µL from each

dilution was plated onto MM Agar medium supplemented with 1% (w/v) biphenyl as a carbon source. The plates were incubated at 30°C. The bacterial colonies of different morphotypes were further grown in MM supplemented with biphenyl. They were screened and selected based on their growth measured by optical density (OD) at 600 nm for further PCB degradation experiments.

### **3.2.3 Morphological and biochemical characterization of the selected PCB degrader**

#### **3.2.3.1 Morphological and Biochemical characterization**

The selected bacterial isolates were observed for different morphological characteristics such as shape, color, and colony pattern. These isolates were subjected to biochemical tests such as Gram staining, carbohydrate utilization, catalase, oxidase, starch hydrolysis, indole, methyl red, and Voges-Proskauer tests using biochemical test kits (HiMedia, Mumbai, India) according to the manufacturer's instructions. All the biochemical tests were done in triplicate using freshly grown bacterial isolates having OD<sub>600</sub> 0.4. The plates were kept at 30°C, and the growth was observed after 24 h of incubation.

#### **3.2.3.2 Antimicrobial susceptibility determination and antifungal activity**

To determine the antibiotic sensitivity of the four selected bacterial isolates, pure colonies of the culture were inoculated in fresh LB at 30 ±2°C for 15-16 h. The freshly grown bacteria suspension was swabbed evenly over the surface of the LA plate. The inoculated plates were allowed to dry for 15 min, followed by placing the antibiotic-containing disc diffusion disc over the plates. The susceptibility test of 4 antibiotics, namely, tetracycline (10 µg), gentamycin (30 µg), ampicillin (10 µg), and chloramphenicol (10 µg), was performed by disc diffusion method as described by Bauer et al. (1966). Plates containing the antibiotic disc were incubated at 30 ±2°C for 24 h. A zone of inhibition (ZOI) was measured after the incubation period. A disc without the antibiotic was placed within every plate as negative control.

A dual-culture assay examined the antifungal activity of selected bacterial isolates against the tested fungi *A. niger*, *A. flavus*, and *F. solani*. To prepare fungal inoculum, the fungal strains were cultured on PDA for 5 d at 28°C. The assay was based on inhibiting the fungal mycelia on PDA plates. Each tested bacterial isolate and negative control was streaked to the sides of the mycelium plug. The plates were sealed with Parafilm M and incubated at 28°C until mycelia in

the untreated controls spread onto the plates. Inhibition of the mycelial growth of the tested fungi was compared with the mycelial growth of the untreated control plates.

### 3.2.3.3 Test of PGPR properties

Selected bacteria MAPB-2, MAPB-6, MAPB-9, and MAPB-27 were further subjected to the test of PGPR properties like Indole acetic acid (IAA), siderophore production, phosphate solubilisation, 1-aminocyclopropane-1-carboxylic acid (ACC) deaminase ammonia, and hydrogen cyanide (HCN).

**IAA production Assay:** Selected bacterial isolates were inoculated in 5 mL of LB supplemented with 2.5 mM of tryptophan and incubated for 72 h at 30°C, 150 rpm. The uninoculated media was used as control. After incubation, 1.5 mL of each bacterial culture was transferred to 2 mL Eppendorf tubes and centrifuged at 10,000 g for 2 min. IAA production was determined by Salkowski method (Gang et al., 2019). A standard curve was plotted against different concentrations ( $\mu\text{g mL}^{-1}$ ) at 540 nm absorbance. The pink and reddish suspension produced indicates the bacterial production of IAA.

**Siderophore production Assay:** Siderophore production of the selected isolates was assayed by the chrome azurole S (CAS)- agar method (Schwyn and Neilands, 1987). The CAS agar plates were spot inoculated with a drop of 2  $\mu\text{L}$  of bacterial cultures. The plates were then incubated for 72 h at 30°C. The development of a yellow-orange halo around the bacterial colony indicates siderophore production.

**Phosphate solubilization Assay:** Tricalcium phosphate agar plates were prepared for phosphate solubilization assay. The medium ( $\text{g L}^{-1}$ ) consists of glucose (10g), yeast extract (2g), and agar (15g). After autoclaving, add sterile  $\text{K}_2\text{HPO}_4$  (5g/ 50 mL  $\text{H}_2\text{O}$ ) and  $\text{CaCl}_2$  (10g/100 mL  $\text{H}_2\text{O}$ ) 10% solutions to the medium before pouring them onto the Petri plates. 2  $\mu\text{L}$  of overnight grown bacterial culture was added onto freshly prepared tricalcium phosphate agar plates and incubated at 30°C for 7 d. A clear halo around the bacterial colony is an indication of tricalcium phosphate solubilization (Sylvester- Bradley et al., 1982).

**ACC deaminase Activity:** Dworkin and Foster (DF) salts medium (Dworkin and Foster, 1958) was used to determine the ACC deaminase activity of the selected isolates. The composition of DF salts medium (per litre) without nitrogen source consists of 4.0 g  $\text{KH}_2\text{PO}_4$ , 6.0 g  $\text{Na}_2\text{HPO}_4$ , 0.2 g  $\text{MgSO}_4 \cdot 7\text{H}_2\text{O}$ , 2.0 g glucose, 2.0 g gluconic acid and 2.0 g citric acid with trace elements: 1 mg  $\text{FeSO}_4 \cdot 7\text{H}_2\text{O}$ , 10 mg  $\text{H}_3\text{BO}_3$ , 11.19 mg  $\text{MnSO}_4 \cdot \text{H}_2\text{O}$ , 124.6 mg,  $\text{ZnSO}_4 \cdot 7\text{H}_2\text{O}$ , 78.22 mg  $\text{CuSO}_4$

5H<sub>2</sub>O, 10 mg MoO<sub>3</sub>. DF salt agar plates were prepared and 50 µL of ACC (0.5M) was spread onto the plates. Spot inoculation of each bacterial suspension on DF salt agar plates was done and incubated for 7 d at 30°C. Bacteria colonies will be observed if they are able to utilize ACC as an N source (Penrose and Glick, 2003).

**Ammonia production Assay:** Selected bacterial cultures were inoculated in 5 mL peptone water and were incubated for 72 h at 30°C. After the incubation period, 250 µL Nessler's reagent was added to each tube. The development of a brown-to-yellow color indicates a positive test for ammonia production (Cappuccino and Sherman, 1992).

**HCN production Assay:** Modified nutrient agar plates amended with 4.4 g L<sup>-1</sup> glycine were prepared. Selected bacteria isolates were streaked on modified agar plates. A Whatman filter paper no.1 pre-soaked in 2% sodium carbonate in 0.5% picric acid was placed on the top of the agar plate. The parafilm-sealed plates were then incubated for 4 d at 30°C. Orange-to-red color development indicated the presence of HCN production (Lorck, 1948).

#### **3.2.4. DNA isolation and 16 S rDNA identification of the selected PCB degrader**

The bacterial isolates were inoculated in 5 mL LB tubes and grown at 30°C for 16 h at 150 rpm shaking condition. Bacterial genomic DNA was isolated using the QIAamp kit (Qiagen, USA) and detected by agarose gel electrophoresis (1%; w/v). The DNA template (50 ng) of each isolate was used for the amplification of the 16S rRNA gene using universal primers 27F (5'-AGAGTTTGATCCTGGCTCAG-3') and 1494R (5'-CTACGGCTACCTTGTTACGA-3') with a thermal cycler (T100, BioRad, USA). The temperature conditions were set as follows: initial denaturation of 5 min at 94°C, 30 cycles of 1 min at 95°C, 1 min at 53°C and extension of 2 min at 72°C, and final extension of 5 min at 72°C. The amplicon was purified and sequenced using the dideoxy chain terminator method in the Department of Biochemistry, South Campus, Delhi University (New Delhi, India) DNA sequencing facility. The 16S rRNA sequence was compared with the National Centre for Biotechnology Information (NCBI) public database using the BLAST tool (<http://www.ncbi.nlm.nih.gov/BLAST/>) and was deposited in the NCBI/Gen Bank nucleotide sequence database (refer to accession number in Table 1).

The isolates showed good growth on MM supplemented with biphenyl and were further selected for biochemical, molecular, and biodegradation studies. The 16S rDNA sequences of MAPB-2, MAPB-6, MAPB-9, and MAPB-27 were further aligned with the reference sequence using MEGA XI to construct the phylogenetic tree (Tamura et al., 2021). Furthermore, to determine the taxonomic position of each strain, the 16S rRNA gene sequences were aligned with

the reference sequences available in the NCBI database. The phylogenetic tree was constructed using the Maximum likelihood method and Kimura 2-parameter model (Kimura, 1980) with a bootstrap test of 1000 replicates with Mega XI.

### **3.2.5. PCR amplification of ARHD**

The PCR reaction was performed to amplify the ARHD gene in the selected bacterial isolate MAPB-2, MAPB-6, MAPB-9, and MAPB-27 using specific primers based on gene information obtained from NCBI. Primers were designed using Primer3 software; the details are provided in Table 5.1. PCR amplification was carried out in a reaction volume of 25  $\mu$ L containing 2.5  $\mu$ L Taq DNA polymerase buffer (10X), 0.35  $\mu$ L of Taq DNA polymerase (3U), 0.3  $\mu$ L dNTP (2.5 mM each), 1.0  $\mu$ L of primer (10 mM each) and 3  $\mu$ L (50 ng) of the template. Thermocycler T100 (BioRad, Germany) was set for an initial denaturation step of 4 min at 95°C, followed by 25 cycles of denaturation at 94°C for 30 s, annealing at the respective temperature for each pair of primers for 45 s (Table 2), extension at 72°C for 30 s and a final extension step at 72°C for 5 min. The PCR amplicon was analyzed on a 1.5% agarose gel under a UV gel documentation unit (Biorad, USA). The amplicon was purified and sequenced using the dideoxy chain terminator method in the DNA sequencing facility of AgriGenome Pvt. Ltd., Kochi. Amplified sequences were compared with the National Centre for Biotechnology Information (NCBI) public database using the BLAST tool (<http://www.ncbi.nlm.nih.gov/BLAST/>) and were deposited in the NCBI/Gen Bank nucleotide sequence database

### **3.2.6. Analysis of ARHD gene expression by quantitative PCR (qPCR)**

#### **3.2.6.1. Bacterial growth conditions**

The time and biphenyl concentration-dependent gene expression of ARHD was analyzed using qPCR. The bacterial cultures of selected isolates MAPB-2, MAPB-6, MAPB-9, and MAPB-27 were grown in MM supplemented with different concentrations (100-300 mg L<sup>-1</sup>) of biphenyl. The bacterial cultures were collected at 72 h and 120 h of the incubation period.

#### **3.2.6.2. Extraction of RNA and cDNA synthesis**

After incubation, bacterial culture was pelleted by centrifugation at 10,000  $\times$ g at 4°C for 8 min. Total RNA was extracted as per the modified Trizol method (Rio et al., 2010) and stored at -80°C. The integrity of RNA was verified by 1% agarose gel electrophoresis. The RNA was checked for its purity and concentration using a Nano-drop spectrophotometer (Simplinano, USA). The cDNA

was prepared as a template for reverse transcription as follows: The reaction mixture contained Verso enzyme mix 1  $\mu\text{L}$ , dNTP mix 2  $\mu\text{L}$  (500  $\mu\text{M}$  each), RNA primer 1  $\mu\text{L}$ , RT enhancer 1  $\mu\text{L}$ , 5 $\times$  cDNA synthesis buffer 4  $\mu\text{L}$ , template (1  $\mu\text{g}$ ) and RNase-free water to make up to 20  $\mu\text{L}$ . The reaction mixture was incubated at 42°C for 30 min after which the enzyme was inactivated at 95°C for 2 s. cDNA was stored at -20 °C for further gene expression studies.

### **3.2.6.3. qPCR analysis for expression of ARHD**

A set of 16S rRNA primers and genus-specific primers targeting the ARHD of the degradation pathway were used for RT-qPCR assays. The melting curve and efficiency of the selected primer set were evaluated by RT-qPCR using a CFX96 Real-time detection system (BioRad, USA). The reaction mixture contains 2X Power SYBR Green Master mix (Applied Biosystems™), 1  $\mu\text{L}$  each of forward and reverse primer, 1  $\mu\text{L}$  of cDNA template, and nuclease-free water to make up to 10  $\mu\text{L}$ . The cycling conditions of an initial step of 5 min at 95 °C, followed by 40 cycles of denaturation at 94 °C for 30 s, annealing at 57 °C for 45 s, and elongation at 72°C for 5 min. The gene expression level was determined as the fold change in accordance with the 2<sup>- $\Delta\Delta\text{C(T)}$</sup>  method (Livak and Schmittgen 2001).

### **3.2.7. Biosurfactant production and characterization**

#### **3.2.7.1. Test for biosurfactant production**

The biosurfactant production of each isolate was tested using a semi-quantitative CTAB agar assay according to the method of Perfumo et al. (2006). CTAB agar plates ( $\text{L}^{-1}$ ) were prepared by adding 0.2 g of CTAB, 0.005 g of methylene blue to MM containing 20 g of glucose, 1 g of yeast extract, 2 g of peptone, 0.1 g of  $\text{CaCl}_2$ , and 15 g of agar. The plates were inoculated with 20  $\mu\text{L}$  culture and incubated at 30°C for 48 h. The formation of dark blue halos around the colonies confirmed the production of biosurfactants as extracellular glycolipids by bacterial isolates.

#### **3.2.7.2. Production and characterization of biosurfactants**

For the production and characterization of biosurfactants, modified Bushnell-Haas (BH) broth ( $\text{g L}^{-1}$ ) with  $\text{MgSO}_4$  (0.2 g),  $\text{CaCl}_2$  (0.02 g),  $\text{KH}_2\text{PO}_4$  (1.0 g),  $\text{K}_2\text{HPO}_4$  (1.0 g),  $\text{NH}_4\text{NO}_3$  (1.0 g),  $\text{FeCl}_3$  (0.05 g) was prepared. BH broth was supplemented with 1.5  $\text{g L}^{-1}$   $\text{NaNO}_3$  and 2% glycerol. The medium was inoculated with isolates and kept for 7 d at 30°C, 150 rpm for incubation. After incubation, the suspension was centrifuged at 6400 g for 30 min. The supernatant was collected



and acidified to pH 2 with HCl (6N). The acidified supernatant was kept overnight at 4°C to precipitate the biosurfactant. An equal volume of chloroform and methanol (2:1; v/v) was added to the supernatant and vigorously shaken for 10 min to extract the biosurfactant produced. The organic layer was collected and evaporated by a rotary evaporator (Tripathi et al., 2020). The supernatant was tested for its emulsifying activity and drop collapse assay. At the same time, a crude biosurfactant was used for further characterization using Attenuated total reflectance - Fourier transform infrared spectroscopy (ATR- FTIR), High-performance thin layer chromatography (HPTLC), and GC-MS/MS techniques.

### 3.2.7.3 Emulsification and drop collapse assay

Further characterization of the biosurfactant was performed by calculating the emulsification capacity. The methodology up to the centrifugation process is the same as mentioned in section 3.2.5.3. After centrifugation, the supernatant was collected, and mixed with petrol (1:1%) in a test tube. The solution was vortexed for 1 min and kept at room temperature for 24 h. The  $E_{24}$  emulsification index was calculated for the selected isolates, as indicated below.

$$\text{Emulsification Index } E_{24} (\%) = \frac{\text{Height of the emulsion layer (cm)}}{\text{Total height of the solution (cm)}} \times 100$$

A qualitative drop collapse test was performed by adding 10  $\mu\text{L}$  of petroleum and 10  $\mu\text{L}$  of supernatant to the surface of the oil. The shape of the drop on the oil surface was observed after 3 min. The culture supernatant that makes the oil drop collapse was scored as positive, and the drops that remained beaded indicated a negative score. Distilled water was used as negative control (Jimoh and Lin, 2019).

### 3.2.7.4. Analysis of biosurfactant by HPTLC, ATR-FTIR, and GC-MS/MS

To determine the type of biosurfactant, 10  $\mu\text{L}$  of the crude extract was separated on silica gel TLC plates (F<sub>254</sub>; Merck, Germany) using HPTLC (Camag, Switzerland) equipped with Software Vision CATS. The solvent system used was a mixture of chloroform, methanol, and acetic acid in the ratio of 6.5:1.5:0.2 (v/v/v). The bands were visualized by a TLC scanner under 254 nm, 366 nm, and white light after anisaldehyde derivatization to detect carbohydrates. The plates were air-dried, dipped in anisaldehyde reagent acetic acid: sulphuric acid: *p*-anisaldehyde (100: 2: 1; v/v/v), and heated for 15 min at 110°C. The retention factor ( $R_f$  value) of each band was determined.

Characterization of functional groups in the biosurfactant produced by the selected isolates was done by ATR-FTIR (Bruker, Germany). Analysis of the IR spectra at the mid-infra-red region of 400-4000  $\text{cm}^{-1}$  was carried out by OPUS software 7.0 in transmittance mode.



GC-MS/MS analysis was performed to reveal the fatty acid composition of the produced biosurfactant. Extract (1  $\mu\text{L}$ ) was injected into the RTX-5Sil column with an initial temperature maintained at 50°C for 2 min, then programmed to 80°C at a rate of 10°C/min (5 min). The rate was increased further by 5°C/min up to 100°C with a hold of 1 min and the final increase with 15°C/min to 280°C with a hold of 5 min. The flow rate was 1 mL/min. The injection and detector temperatures were set at 200°C and 230°C, respectively. The MS scan range was kept at 45-500  $m/z$ .

### **3.2.8. Optimization of growth parameter for potential PCB-degrading bacterial isolates**

Optimization of growth parameters includes the biphenyl concentration, glucose concentration, pH, and temperature for the growth of the selected isolates.

#### **3.2.8.1 Effect of different concentrations of biphenyl and glucose on bacterial growth**

The effect of varying biphenyl concentration on the growth of the selected bacterial isolates was determined by inoculating 1% ( $v/v$ ) of the grown culture (OD 0.6) to MM. Biodegradation experiments were carried out in two different parallel sets. The first set consisted of isolates grown in various biphenyl concentrations (i.e., 10, 50, 100, 200, 300, 400, and 500  $\text{mg L}^{-1}$ ) for 48 h. The biphenyl concentration that showed maximum growth for all the selected isolates was used for the second experimental set with different glucose concentrations (0.1, 0.2, 1, 2, and 3%,  $w/v$ ). Glucose is the carbon source that bacteria most easily utilize and therefore was used to promote growth in biphenyl-supplied media and to enhance degradation.

#### **3.2.8.2 Effect of different pH and temperature on bacterial growth**

The concentration of biphenyl and glucose at which maximum bacterial growth was obtained from the previous experiment was further used to optimize the growth conditions at different temperatures ranging from 20 to 40°C with 5°C intervals and pH (4 to 9) with 150 rpm shaking conditions. The growth of MAPB-2, MAPB-6, MAPB-9, and MAPB-27 was monitored by measuring the OD<sub>600</sub> after 48 h of the incubation period. All experiments were performed in triplicate.

### **3.2.9. Growth curve of the selected PCB-degrading bacterial isolates**

Bacterial cultures were grown in LB and MM supplemented with biphenyl (200  $\text{mg L}^{-1}$ ) to examine the growth of selected bacteria under controlled conditions. 250 mL Erlenmeyer flasks

containing 100 mL sterile LB and MM supplemented biphenyl (200 mg L<sup>-1</sup>) media were used for each bacterial culture to develop their growth curves. Flasks were inoculated with 10% (v/v) overnight grown bacterial cultures in liquid LB broth as the seed and incubated at 30°C, 150 rpm in a shaker incubator. To measure the growth of the bacteria, the OD of the media was measured every 2 h, and 24 h intervals for LB and MM supplemented biphenyl (200 mg L<sup>-1</sup>) grown bacterial cells, respectively, at 600 nm using Thermo Scientific™ Multiskan™ GO microplate spectrophotometer. The doubling time of bacteria was calculated in each condition by plotting a graph of log (OD) vs. time (h) using the following equation:

$$\text{Doubling time (Td)} = \ln(2) / \text{growth rate (r)}$$

Where,

$$N(t) = N(0) e^{rt} \text{ or } r = \ln [N(t)/N(0)]/t$$

N(t) = No. of cells at time t

N(0) = no. of cells at time 0

r = growth rate

t = time (h)

### **3.2.10. Chemotaxis assays towards the metabolites produced during biphenyl biodegradation**

Recent studies have highlighted movement of bacteria towards chemo-attractants such as PCB (Parales and Harwood 2002) to aids in biodegradation of contaminants present in the soil. The chemotaxis of the selected bacterial isolates was studied by modified drop assays (Samanta et al., 2000). The medium used for the drop assay consisted of MM containing 0.30% agar and 1 mM PCB intermediates like biphenyl, dihydroxy biphenyl (DHB), benzoate, and catechol as sole carbon sources. MAPB-2, MAPB-6, MAPB-9, and MAPB-27 were grown in LB at 30°C up to the log phase (OD<sub>600</sub> 0.4). After that, the bacterial cells were centrifuged at 8,000 X g for 10 min. The pellet was washed twice with MM and suspended in the drop assay medium. It was then poured into Petri plates. Chemotactic rings were assessed for PCB intermediates, i.e., biphenyl, DHB, benzoic acid, and catechol by placing the crystals of intermediates (1 mM) at the centre of the plates. Glucose was used as a positive control. The plates were incubated for 24 h at 30°C. The turbid rings observed around the centre after incubation indicates the positive chemotactic movement of the bacteria towards the chemoattractant compound.

### **3.2.11. Study of cellular morphology by scanning electron microscopy (SEM)**

The SEM analysis of the selected isolates was performed to observe the effect of biphenyl on the cell morphology of the selected isolates. The isolates were grown in LB and MM supplemented with biphenyl 200 mg L<sup>-1</sup> in the presence of 0.2% glucose and incubated for 72h at 30°C. After the incubation period, the smear was prepared on the glass slide and was fixed with 2.5% (v/v) glutaraldehyde solution for an hour. The fixed bacterial cell was then subjected to gradual ethanol dehydration, i.e., 50-100% (v/v), with 10 min intervals each for drying. The gold sputter coating to the fixed bacterial cells was done for 30 sec. The bacterial cells were then observed under 20 kV SEM (FEI™ Thermo Fischer Scientific, Apreo) at different magnification power.

### 3.2.12. Degradation of Biphenyl and PCB congener(s)

#### Biphenyl biodegradation assay

To investigate the difference in the biphenyl degradation by the selected isolates, two different sets of experiments were carried out. The first set consisted of 200 mg L<sup>-1</sup> biphenyl as the sole carbon source in 20 mL MM inoculated with 10% inoculum. The tubes were cultured at 30°C, 150 rpm for 48 h of incubation. The second set consisted of 0.2% glucose as a co-substrate and 200 mg L<sup>-1</sup> biphenyl with optimized growth parameters.

#### Biodegradation assay with PCB-77

PCB-77 congener was used for PCB biodegradation assay as it is one of the most toxic coplanar congeners and is widely used in commercially available blends such as Aroclor (Venkatachalam et al., 2008). For the PCB-77 assay, the inoculating medium was MM supplemented with 50 mg L<sup>-1</sup> biphenyl dissolved in acetone. Media was inoculated with selected isolates and incubated at 30°C for 48 h. After incubation, inoculation media was centrifuged, and the pellet was washed with phosphate buffer (pH 7.4). The bacterial pellet was resuspended with MM, and 10% of the culture inoculum was added to assay media containing MM supplemented with PCB-77 (50 mg L<sup>-1</sup>). The flasks were incubated for 7 days at 30°C, 150 rpm.

After the incubation period, the sample was extracted with hexane three times to determine the biodegradation percentage. The hexane layer was collected and evaporated by a rotary evaporator. The concentrated extracts were resuspended with isooctane. 1 µL extract of each sample was used for GC-MS/MS analysis using a GC-MS/MS TQ8040 (Shimadzu, Japan). The separation of biphenyl and PCB-77 was performed on an SH-RXi-5SiIMS fused silica column with dimensions of 30 m × 0.32 mm × 0.25 µm. The column temperature was programmed from 80°C (1 min hold) to 150°C at 25°C/min and finally to 280°C at 4°C/min (2 min hold). The carrier

gas was helium, and the column flow rate was 1mL/min. The areas of specific peaks in the chromatogram of the samples were measured and compared to those of control samples supplemented with biphenyl/PCB-77 without inoculum. The residual biphenyl was estimated by plotting the calibration curve of biphenyl at different concentrations. The percentage of biphenyl/PCB-77 degradation was calculated as follows.

$$\text{Percent degradation (\%)} = \frac{\text{Peak area of control} - \text{Peak area of biphenyl / PCB-77}}{\text{Peak area of the control}} \times 100$$

The residual biphenyl/PCB-77 was estimated by plotting the calibration curve of biphenyl/PCB-77 at different concentrations. The biphenyl calibration curve was prepared using different concentrations of standard solutions (50, 100, 150, and 200 mg L<sup>-1</sup>;  $y = 35124x + 900526$ ,  $R^2 = 0.9897$ ). The recoveries of biphenyl from the spiked samples were in the range of 96.98-99.10%. The calibration curve of PCB-77 was constructed with different concentrations of 50, 100, 150, and 200 mg L<sup>-1</sup> ( $y = 28025x - 617466$ ,  $R^2 = 0.9871$ ). The recoveries of PCB-77 from the standards were in the range of 90–96. The metabolites of PCB-77 degradation by the selected isolates were identified and quantified by using peak area integration. The areas of specific peaks in the chromatogram were analyzed by using the NIST14 library.

### 3.3 Results and discussion

#### 3.3.1 Selective enrichment and isolation of microorganisms from PCB-contaminated soil

Repetitive enrichment and subsequent subculturing of soil in MM with biphenyl at 30°C for 7 days resulted in the isolation of 33 morphologically distinct bacteria. All 33 bacterial isolates were identified by 16S rRNA gene sequencing analysis, and the nucleotide sequences were deposited in the NCBI GenBank database (Table 3.1). Most isolated bacteria belong to phylum *Firmicutes*, followed by *Proteobacteria* and *Actinobacteria*. The abundance of these phyla in PCB-contaminated soil is in accordance with the other reported studies, such as the predominance of *Firmicutes* and *Proteobacteria* in aged soil contaminated with PCB (Cervantes-González et al., 2019); and the enrichment of *Proteobacteria* and *Acidobacteria* in the presence of PCB congeners and Aroclor 1224 (Correa et al., 2010).

**Table 3.1.** Thirty-three bacterial strains isolated from PCB contaminated soil and sequence deposited with provided accession no. in NCBI database

Isolates	Percent identity	Percent coverage	Closest type strain	NCBI Accession No.
MAPB1	99.72	100	<i>Pseudomonas plecoglossicida</i> NBRC 103162 <sup>T</sup>	MK512369.1
MAPB2	100	100	<i>Pseudomonas aeruginosa</i> JCM5962 <sup>T</sup>	MK512370.1
MAPB3	97.93	100	<i>Ochrobactrum anthropi</i> ATCC 49188 <sup>T</sup>	MK512371.1
MAPB4	100	100	<i>Pseudomonas plecoglossicida</i> DSM 15088 <sup>T</sup>	MK512372.1
MAPB5	100	100	<i>Pseudomonas monteilii</i> CIP 104883 <sup>T</sup> ; AF064458 <sup>T</sup>	MK512373.1
MAPB6	99.30	100	<i>Pseudomonas plecoglossicida</i> FPC951 <sup>T</sup>	MK512374.1
MAPB7	99.43	99	<i>Brevibacterium iodinum</i> DSM 20626 <sup>T</sup>	MK512375.1
MAPB8	99.57	96	<i>Pantoea dispersa</i> LMG2603 <sup>T</sup> ; DQ504305 <sup>T</sup>	MK512376.1
MAPB9	100	100	<i>Ochrobactrum anthropi</i> ATCC 49188 <sup>T</sup>	MK512377.1
MAPB10	99	100	<i>Bacillus amyloliquefaciens</i> NBRC 15535 <sup>T</sup>	MW227569.1
MAPB11	99.79	99	<i>Bacillus stratosphericus</i> 41KF2a <sup>T</sup> ; AJ831841 <sup>T</sup>	MW227570.1
MAPB12	98.75	100	<i>Lysinibacillus composti</i> NCCP-36 <sup>T</sup> ; AB547124 <sup>T</sup>	MW227571.1
MAPB13	99.50	100	<i>Bacillus cereus</i> ATCC 14579 <sup>T</sup> ; AE016877 <sup>T</sup>	MW227572.1
MAPB14	100	100	<i>Bacillus aryabhattai</i> B8W22 <sup>T</sup>	MW227573.1
MAPB15	98.34	99	<i>Solibacillus silvestris</i> HR3-23 <sup>T</sup> ; AJ006086 <sup>T</sup>	MW227574.1
MAPB16	100	100	<i>Bacillus thuringiensis</i> IAM 12077 <sup>T</sup> ; ATCC 10792 <sup>T</sup>	MW227575.1
MAPB17	100	100	<i>Bacillus cereus</i> ATCC 14579 <sup>T</sup> ; AE016877 <sup>T</sup>	MW227576.1
MAPB18	100	100	<i>Bacillus paramycoides</i> MCCC 1A04098 <sup>T</sup>	MW227577.1
MAPB19	99.79	100	<i>Bacillus aryabhattai</i> B8W22 <sup>T</sup> ; EF114313 <sup>T</sup>	MW227578.1
MAPB20	98.54	100	<i>Bordetella petrii</i> DSM 12804 <sup>T</sup> ; AJ249861 <sup>T</sup>	MW227579.1
MAPB21	99.79	100	<i>Staphylococcus pasteurii</i> ATCC 51129 <sup>T</sup>	MW227580.1
MAPB22	98.96	99	<i>Pseudomonas aeruginosa</i> JCM 5962 <sup>T</sup> ; DSM50071 <sup>T</sup>	MW227581.1
MAPB23	99	100	<i>Bacillus cereus</i> ATCC 14579 <sup>T</sup> ; AE016877 <sup>T</sup>	MW227582.1
MAPB24	99.79	99	<i>Paenibacillus illinoisensis</i> JCM 9907 <sup>T</sup> ; AB073192 <sup>T</sup>	MW227583.1
MAPB25	99.38	100	<i>Bacillus amyloliquefaciens</i> NBRC 15535 <sup>T</sup>	MW227584.1
MAPB26	98	100	<i>Bacillus velezensis</i> strain CR-502 <sup>T</sup>	MW227585.1
MAPB27	100	100	<i>Bacillus megaterium</i> NBRC 15308 <sup>T</sup> ; IAM 13418 <sup>T</sup>	MW227586.1
MAPB28	99.79	100	<i>Bacillus aryabhattai</i> B8W22 <sup>T</sup> ; EF114313 <sup>T</sup>	MW227587.1
MAPB29	100	100	<i>Bacillus subtilis</i> DSM10 <sup>T</sup> ; AJ276351 <sup>T</sup>	MW227588.1
MAPB30	99.79	100	<i>Bacillus subtilis</i> DSM10 <sup>T</sup> ; AJ276351 <sup>T</sup>	MW227589.1
MAPB31	92.48	99	<i>Domibacillus indicus</i> strain SD111	MW227590.1
MAPB32	100	99	<i>Bacillus cereus</i> ATCC 14579 <sup>T</sup> ; AE016877 <sup>T</sup>	MW227591.1
MAPB33	99.79	99	<i>Paenibacillus illinoisensis</i> JCM 9907 <sup>T</sup> ; AB07319 <sup>T</sup>	MW227592.1

Each isolate was separately screened to assess its ability to biodegrade biphenyl as a sole carbon and energy source. After 7 d, based on prominent growth on biphenyl ( $1\text{mg L}^{-1}$ ), as indicated by optical density (OD) in biphenyl, four bacterial isolates, namely MAPB-2, MAPB-6, MAPB-9, and MAPB-27, were selected for further biodegradation studies.

The strains MAPB-2, MAPB-6, MAPB-9, and MAPB-27 were identified as *Pseudomonas aeruginosa*, *Pseudomonas plecoglossicida*, *Brucella anthropi*, and *Priestia megaterium*, respectively. *P. aeruginosa* and *Ochrobactrum anthropi* have been previously reported to utilize lower chlorinated biphenyls, such as the diCB, as the sole carbon source. In contrast, *P. plecoglossicida* and *Bacillus megaterium* have been reported for their PCB degradation potential for the first time. Initial tree(s) for the heuristic search were obtained automatically by applying Neighbor-Joining and BioNJ algorithms to a matrix of pairwise distances estimated using the Maximum Composite Likelihood (MCL) approach and then selecting the topology with a superior log likelihood value. Investigation of the 16S rRNA gene tree showed that strain MAPB-2 is a member of the genus *Pseudomonas*, forming a cluster with *Pseudomonas aeruginosa* DSM50071<sup>T</sup> and *Pseudomonas aeruginosa* ATCC 10145<sup>T</sup> (Fig. 3.1A). Then strain MAPB-6 is a member of the genus *Pseudomonas*, forming a cluster with *Pseudomonas plecoglossicida* NBRC 13162<sup>T</sup> and *Pseudomonas plecoglossicida* FPC951<sup>T</sup> (Fig. 3.1B). The strain MAPB-9 is a member of the genus *Brucella*, forming a cluster with *Brucella anthropi* ATCC 49188<sup>T</sup> and *Brucella anthropi* NBRC 15819<sup>T</sup> (Fig. 3.1C). In contrast, strain MAPB-27 is a member of the genus *Priestia*, forming a cluster with *Priestia megaterium* ATCC 14581<sup>T</sup> and *Priestia aryabhattai* B8W22<sup>T</sup> (Fig. 3.1D). *Ochrobactrum* and *Bacillus* have been reclassified into the genus *Brucella* (Hordt et al., 2020) and *Priestia* (Gupta et al., 2020), respectively. The degradation of PCBs by various species of genera *Pseudomonas*, *Ochrobactrum*, and *Bacillus*, such as *Pseudomonas* sp. 2 (Komancova et al., 2003), *Ochrobactrum* sp. NP04 (Pathiraja et al., 2019), *O. intermedium* (Liz et al., 2009), *B. anthropi* (Horvathova et al., 2018), and *Bacillus* sp. have been reported in earlier studies. However, this is the first report of *P. plecoglossicida* and *P. megaterium* as potential PCB degraders. These two species were known to degrade organophosphate pesticides (Borji et al., 2014; Bhadbhade et al., 2002).



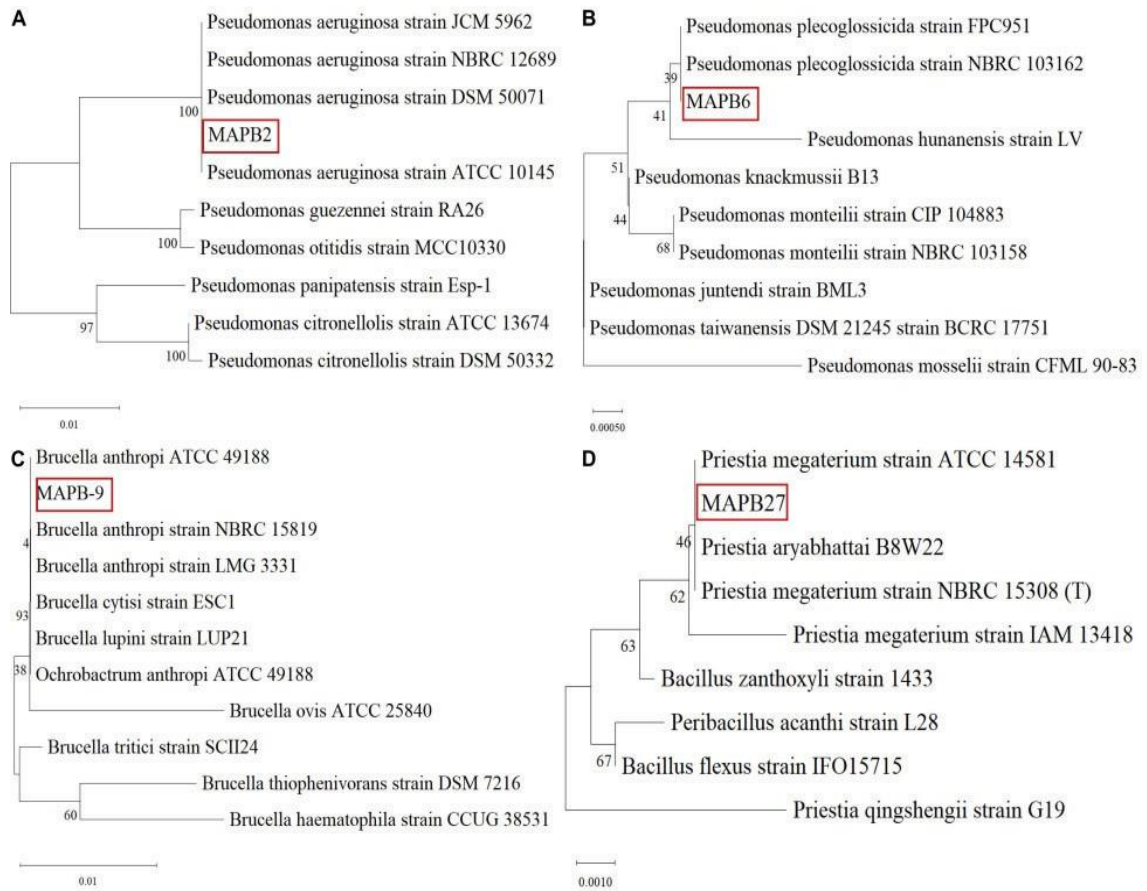


**Fig. 3.1.** Phylogenetic tree by Maximum Likelihood method and Kimura 2-parameter model based on 16S rRNA gene sequences (A) MAPB-2, (B) MAPB-6, (C) MAPB-9, and (D) MAPB-27. Bootstrap values (expressed as percentages generated from 1000 replicates) are shown at branch points.



### 3.3.2 Morphological and Biochemical characterization of the selected PCB degrader

The morphological and biochemical properties of the four selected bacterial isolates were carried out, and details are highlighted in Table 3.2. MAPB-2, 6, and 9 were Gram-negative, whereas MAPB-27 was Gram-positive. Based on morphology, the MAPB-2, MAPB-6, MAPB-9, and MAPB-27 isolates were different rod-shaped with blue-green, pale, white, and white colonies on LB agar plates (Fig. 3.2A), respectively. The presence of bluish-green pyocyanin pigment of isolate MAPB-2 is the characteristic feature of *P. aeruginosa*. All the isolates could grow on MM with biphenyl as a sole source of carbon (Fig. 3.2B). Different carbon utilization tests showed that isolates differed in their use of carbon sources, as provided in Table 3.2. All the isolates grew aerobically and showed positive results for catalase, whereas negative results for Voges Proskauer, methyl red, and indole test. MAPB-2, MAPB-6, and MAPB-9 showed negative results to *O*-nitrophenyl- $\beta$ -D-galactopyranoside (ONPG) and H<sub>2</sub>S production, while MAPB-27 showed a positive for the above tests. MAPB-2 showed positive results for phenylalanine deamination and citrate test. MAPB-6 showed a positive response to the Ornithine test. MAPB-9 indicated lysine, ornithine, phenylalanine deamination, nitrate reduction, and citrate test. However, MAPB-27 showed positive results for ONPG, H<sub>2</sub>S production, and citrate test.

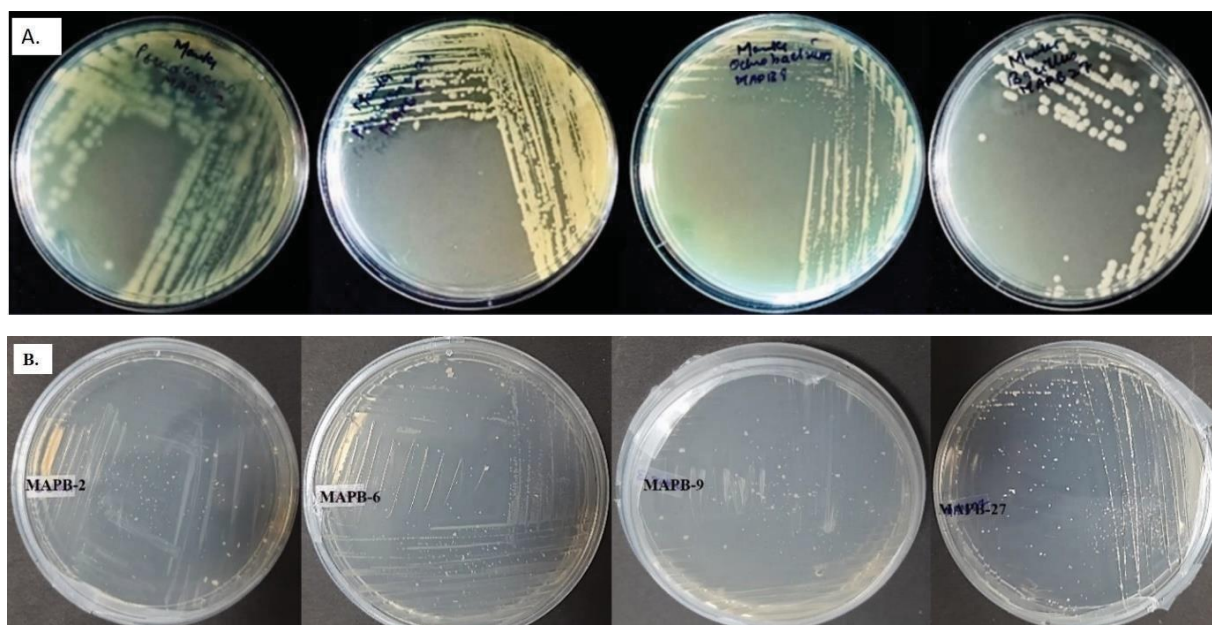


**Fig. 3.2.** Growth and colony morphology of selected bacterial isolates on (A) LB and (B) MM supplemented with biphenyl.

**Table 3.2.** Morphological and biochemical properties of the screened PCB-degrading bacterial isolates

Screened bacterial isolates	MAPB-2	MAPB-6	MAPB-9	MAPB-27
<b>Morphological properties</b>				
<b>Shape</b>	rods	rods	short rods	long rods
<b>Gram strain</b>	-	-	-	+
<b>Color</b>	bluish green	green	pale white	white
<b>Biochemical test</b>				
<b>ONPG</b>	-	-	-	+
<b>Lysine</b>	-	-	+	-
<b>Ornithine</b>	-	+	+	-
<b>Urease</b>	-	-	+	-
<b>Phenylalanine Deamination</b>	+	-	-	-
<b>Nitrate reduction</b>	-	-	+	-
<b>H<sub>2</sub>S production</b>	-	-	-	+
<b>Citrate</b>	+	-	+	+
<b>Voges Proskauer</b>	-	-	-	-
<b>Methyl red</b>	-	-	-	-
<b>Indole</b>	-	-	-	-
<b>Carbohydrate utilization test</b>				
<b>Malonate utilization</b>	+	+	+	-
<b>Esculin hydrolysis</b>	-	-	+	+
<b>Arabinose</b>	+	-	-	-
<b>Xylose</b>	+	-	-	-
<b>Adonitol</b>	-	-	-	-
<b>Rhamnose</b>	-	-	-	-
<b>Cellobiose</b>	-	-	-	-
<b>Melibiose</b>	-	-	-	-
<b>Saccharose</b>	-	-	-	-
<b>Raffinose</b>	-	-	-	+
<b>Trehalose</b>	-	-	-	+
<b>Glucose</b>	+	-	-	+
<b>Lactose</b>	-	-	-	+
<b>Oxidase</b>	+	-	+	-
<b>Catalase</b>	+	+	+	+

‘+’ indicate positive response while ‘-’ indicates negative response

### 3.3.2.1 Antimicrobial susceptibility determination and antifungal activity

The zone of inhibition (ZOI) test was performed to check the susceptibility of MAPB-2, MAPB-6, MAPB-9, and MAPB-27 towards four antibiotics (Fig. 3.3). No ZOI was observed for MAPB-2, MAPB-6, and MAPB-9 when exposed to ampicillin (10  $\mu$ g) indicating these isolates to be resistant to this antibiotic. Ampicillin resistance could be due to the production of  $\beta$ -lactamase by these bacterial isolates, which cleaves the  $\beta$ -lactam ring of ampicillin to inactivate it. Based on measured ZOI, all four selected isolates were sensitive to gentamycin (30  $\mu$ g) with 24 mm, 23 mm, 18 mm, and 28 mm ZOI for MAPB-2, MAPB-6, MAPB-9, and MAPB-27, respectively. MAPB-6 (14.0 mm) and MAPB-9 (18.0 mm) showed intermediate response towards tetracycline (10  $\mu$ g). No or very less ZOI was observed with chloramphenicol (10  $\mu$ g) for MAPB-2, MAPB-6, and MAPB-9, indicating resistance to chloramphenicol. The chloramphenicol resistance in *Pseudomonas* could be due to chloramphenicol inactivating enzyme acetyltransferase and multidrug efflux pumps (Westbrock-Wadman et al., 2004). MAPB-27 was sensitive to all three antibiotics except for ampicillin (10  $\mu$ g) which showed intermediate resistance. In general, antibiotic resistance mechanisms could be due to pumping the antibiotic out of the cell before it reaches its site of action *via* efflux pumps, protection of the ribosomal binding site, resulting in decreased affinity, or alterations in cell envelope permeability, resulting in reduced drug uptake.

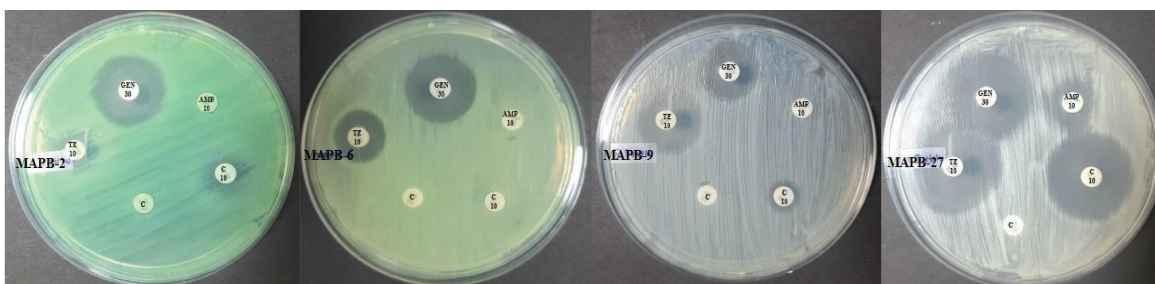


**Fig. 3.3.** Sensitivity of selected isolates towards different antibiotics (A) MAPB-2, (B) MAPB-6, (C) MAPB-9, and (D) MAPB-27.

The antifungal activity of MAPB-2, MAPB-6, MAPB-9, and MAPB-27 against *Aspergillus niger*, *A. flavus*, and *Fusarium solani* is depicted in Fig. 3.4 (A-C). All four isolates could inhibit the growth of *Aspergillus niger* (Fig. 3.3A). It was observed that MAPB-2 and MAPB-6 could control the spread of all three fungal mycelia compared to the control. Some reports revealed that the siderophores producing pseudomonads limit plant pathogens' growth, reducing their ability to colonize plant roots (Couillerot et al., 2009). In addition, they also induce plant systemic

resistance and help in suppressing/ controlling fungal pathogens *via* the production of antifungal compounds and lytic enzymes. There are numerous reports of *Pseudomonas* sp. (Haas et al., 2000; Laue et al., 2000), *Ochrobactrum* sp. (Sowndhararajan et al., 2013), and *Bacillus* spp. (Fira et al., 2018) suppress phytopathogens and act as biocontrol.

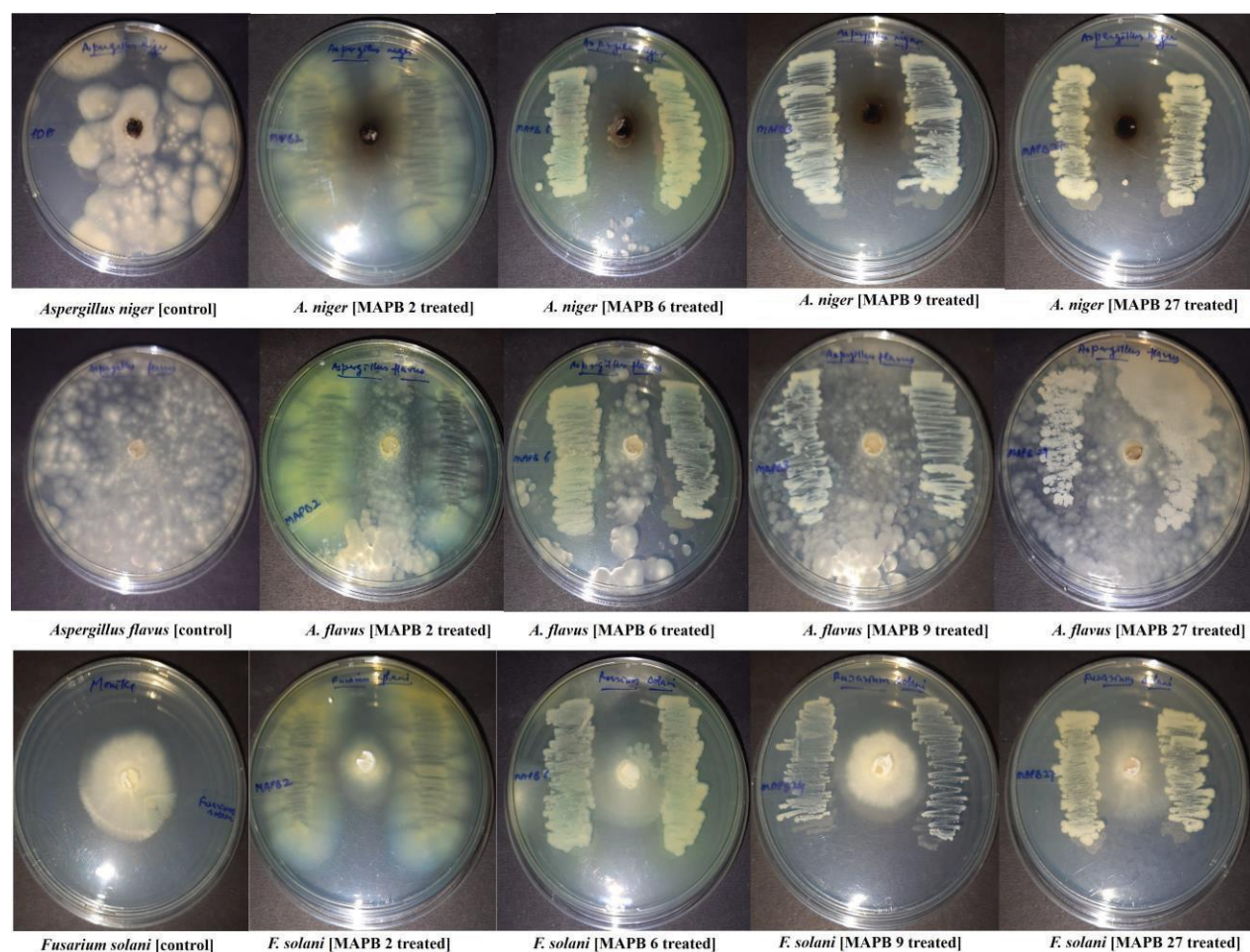


**Fig. 3.4.** Antifungal properties of the selected isolates MAPB-2, MAPB-6, MAPB-9, and MAPB-27 against (A) *Aspergillus niger*, (B) *A. flavus* and (C) *Fusarium solani*.

### 3.3.2.2. Test of PGPR properties of the selected isolates

Plants and microbe interactions play a significant role in accelerating phytoremediation. PGPR involves good bacteria that promote plant growth and help remediate different contaminants in the environment. The plant, in turn, allows these PGPR to grow and proliferate in the contaminated soil by secreting secondary plant metabolites. Plant secondary metabolites have a structural analogy with the PCBs, thereby helping induce PCB-degrading genes in associated bacteria. Several reports have been of PGP activities in bacteria from polluted soils (Franchi et al., 2016;



Thijs et al., 2016; Croes et al., 2013) when growing under phytotoxic and stress conditions. To explore the ability of the selected bacterial isolates to promote plant growth, different PGP properties, such as the production of IAA, siderophore, inorganic phosphate solubilization, ACC deaminase, ammonia production, and HCN production, were assessed (Table 3.3). *Pseudomonas* sp. MAPB-2 and MAPB-6 exhibited 8.25 and 11.25  $\mu\text{g mL}^{-1}$  IAA production and 1.2 and 1.6 mm siderophore zone, respectively. A clear halo observed around the bacterial culture of MAPB-2, MAPB-6, MAPB-9, and MAPB-27 indicated a positive response to phosphate solubilization. MAPB-2, MAPB-6, and MAPB-9 showed ACC deaminase activity and ammonia production. Several researchers have reported PGP traits such as siderophore (Sulochana et al., 2014; Omidvari et al., 2010), IAA production (Wagi and Ahmed, 2019; Hwang et al. 2022; Rahmoune et al., 2017), phosphate solubilization (Rawat et al., 2021), ACC deaminase (Nascimento et al., 2019; Chinnaswamy et al., 2018), and ammonia production (Deshwal and Kumar, 2004) by *Pseudomonas*, *Ochrobactrum*, and *Bacillus* sp. Therefore, considering PGP traits, MAPB-2 and MAPB-6 were found to be promising candidates.

**Table 3.3.** PGPR properties of the selected isolates

Selected isolates	IAA ( $\mu\text{g mL}^{-1}$ )	Siderophore	Phosphate solubilization	ACC deaminase	Ammonia producing	HCN producing
MAPB-2	8.25	++ (1.2)	+	+	+++	+++
MAPB-6	11.25	+++ (1.6)	+	+	++	-
MAPB-9	7.83	+ (0.3)	+	+	+	++
MAPB-27	7.21	-	+	-	+	-

+, - indicates Positive and negative response

When grown in contaminated soil, the plant undergoes nutritional and phytotoxicity stress (Vergani et al., 2017). Several biphenyl-utilizing rhizobacteria have been isolated, showing PGP traits such as IAA production and ACC deaminase activity. Bacterial IAA stimulates root proliferation, promoting plants' uptake of nutrients and water (Lambrecht et al., 2000). Siderophores chelate iron and other metals and contribute to disease resistance by limiting the supply of essential trace minerals in natural habitats. ACC deaminase activity lowers ACC levels in plant cells and protects the plants by decreasing stress hormone levels (Glick, 2010). Therefore, these results indicated that isolates MAPB-2, MAPB-6, MAPB-9, and MAPB-27 have considerable potential to support plant adaptation and growth in the biphenyl-supplemented media.

### 3.3.3. PCR amplification of ARHD

Aerobic degradation of biphenyl is initiated by ARHD, i.e., biphenyl dioxygenase (BDO), which converts biphenyl to 2,3-dihydroxy-1-phenylcyclohexa-4,6-diene (dihydrodiol compound) (Iwasaki et al., 2006). This enzyme has been reported to incorporate two hydroxyl groups on the aromatic ring, resulting in the opening of the aromatic ring (Furukawa et al., 2004; Iwai et al., 2011; Baldwin et al., 2003). BDO is a key enzyme that primarily determines the substrate specificity of PCB degradation. PCR amplification of this enzyme and its expression in selected isolates was done. PCR confirmed the presence of the ARHD gene with an amplified product size of approximately 157, 199, 161, and 202 bp in MAPB-2, MAPB-6, MAPB-9, and MAPB-27, respectively (Table 3.4). Sequencing and BLASTn analysis of the amplified products confirmed the presence of the dioxygenase gene in all the selected isolates.

**Table 3.4.** Details of the ARHD gene in the selected bacterial isolate MAPN-2, MAPB-6, MAPB-9, and MAPB-27 designed using Primer3 software

Isolates	Primer	Primer Sequence	Annealing temp.(°C)	Amplification size (bp)
<i>P. aeruginosa</i> MAPB-2	PA-ARHD F	5'-GGCCAGGCCGAAGGACTATAT-3'	57	185
	PA-ARHD R	5'-GTGCCGAGGGTATTCAGGTA-3'		
<i>P. plecoglossicida</i> MAPB-6	PP-ARHD F	5'-AGAAGCTTTTACCCCTGCCCT-3'	57	199
	PP-ARHD R	5'-GGAACGCATGAATCTGTCCC-3'		
<i>B. anthropi</i> MAPB-9	BA-ARHD F	5'-GACCAGCTGGAGAAGCAGAT-3'	57	161
	BA-ARHD R	5'-TGAACCCCTTCGACAGATTC-3'		
<i>P. megaterium</i> MAPB-27	PM-ARHD F	5'-ACCGCACGTATTTTGGCATT-3'	57	202
	PM-ARHD R	5'-CACCCTCACACGCTTCAAA-3'		

### 3.3.4. RNA extraction and reverse transcription polymerase chain reaction (RT-qPCR)

The relative expression level of the ARHD gene was checked after treating the cultures with various concentrations (100, 200, and 300 mg L<sup>-1</sup>) of biphenyl for 72 h and 120 h. At 72 h, the expression of ARHD increased with increased concentration of biphenyl in all isolates except MAPB-2 (Fig. 3.5). On increasing biphenyl concentration (100, 150, and 200 mg L<sup>-1</sup>), the ARHD gene showed a significant ( $p < 0.001$ ) up-regulation up to 76.6, 59.5, and 5.5- folds in MAPB-6, MAPB-9, and MAPB-27, respectively. However, in the case of *P. aeruginosa* MAPB-2, the fold change was more at 100 mg L<sup>-1</sup> concentration than 200 mg L<sup>-1</sup> and 300 mg L<sup>-1</sup>. The upregulation in MAPB-2, MAPB-6, MAPB-9, and MAPB-27 might be attributed to stress induced by biphenyl



at 100, 200, and 300 mg L<sup>-1</sup> to initiate the biphenyl degradation pathway through increased expression of ARHD. Contrary to the results of 72 h treatment, the expression of ARHD decreased at 120 h with increased concentration of biphenyl in all isolates except in the isolate MAPB-27. In MAPB-2, biphenyl concentrations upregulated the ARHD gene expression by 40.7, 1.9 and 2.4-fold change with 100, 200, and 300 mg L<sup>-1</sup> respectively, for 72 h (Fig. 3.5A). However, the increase in biphenyl concentrations to 100, 200, and 300 mg L<sup>-1</sup> upregulated the ARHD gene expression to 50.6, 16.8, and 3.2 folds in MAPB-6; 0.7, 0.6, 1.0 folds in MAPB-9 and 9.6, 53.8, 62.6 folds in MAPB-27, respectively (Fig. 3.5B-C). This study has shown significant expression activity of the tested genes at different biphenyl concentrations and times. Some reports highlight the expression of ARHD is enhanced in *Pseudomonas* sp. KKS102 in the presence of biphenyl (Ohtsubo et al., 2000).

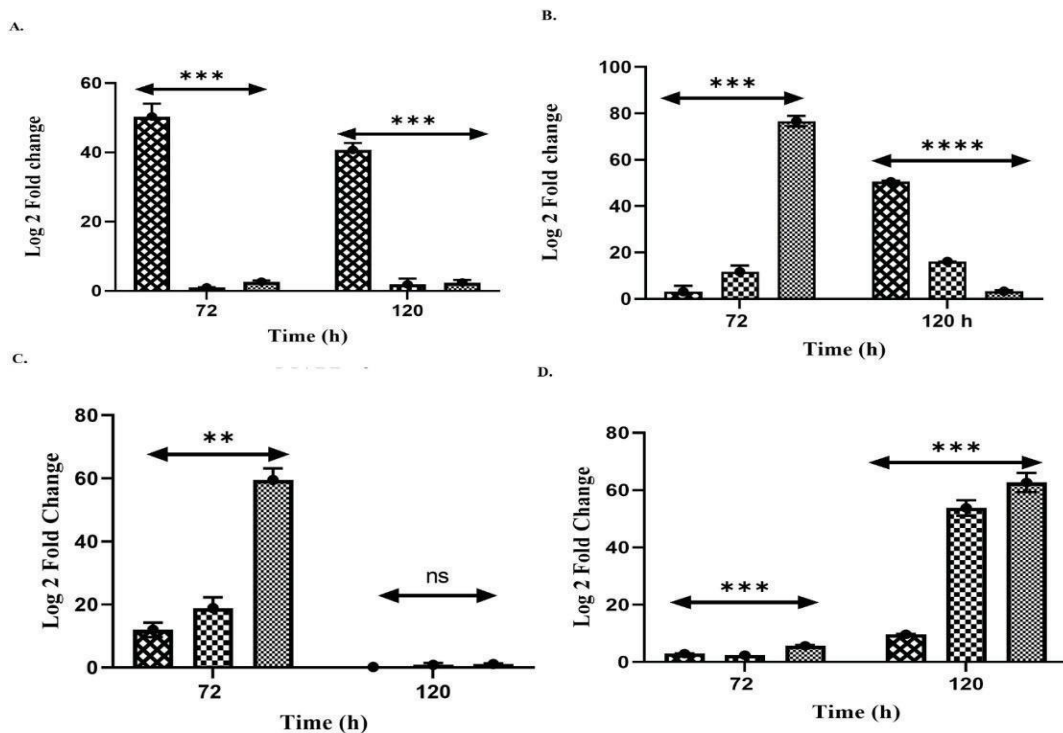


**Fig. 3.5.** Biphenyl-induced gene expression of ARHD by the selected isolates at different concentrations (100-300 mg L<sup>-1</sup>) supplemented in MM and incubated for 72 and 120 h. An increase in biphenyl concentrations from 100 to 300 mg L<sup>-1</sup> highly upregulated the ARHD gene expression in MAPB-6, MAPB-9, and MAPB-27. (A) ARHD gene expression was 56.1-fold and 40.7-fold at 100 mg L<sup>-1</sup> for 72 and 120 h, respectively, by MAPB-2 (B) ARHD gene expression was 76.6 at 300 mg L<sup>-1</sup> for 72 h, while 50.6-fold change at 100 mg L<sup>-1</sup> for 120 h by MAPB-6 (C) ARHD gene expression upregulated to 59.5-fold and 1.0-fold at 300 mg L<sup>-1</sup> for 72 and 120 h, respectively by MAPB-9 (D) ARHD gene expression upregulated to 5.5-fold and 62.6-fold at 300 mg L<sup>-1</sup> for 72 and 120 h, respectively by MAPB-27.

As shown in Fig. 3.5D, the expression level of the ARHD gene significantly increased over time in MAPB-27, i.e., from 72 to 120 h time interval, indicating that benzoate metabolism might be involved in MAPB-27 biphenyl-mediated degradation. Our study shows that the regulation of the ARHD gene is remarkably different in the selected PCB-degrading bacterial isolates. The ARHD gene in MAPB-2 is expressed more at 72 and 120 h with 100 mg L<sup>-1</sup> biphenyl. In contrast, the expression of ARHD in MAPB-6, MAPB-9, and MAPB-27 is more at 72 h with a higher concentration, i.e., 300 mg L<sup>-1</sup>. These results indicate that available inducer biphenyl and physical environmental conditions, i.e., concentration and time of incubation, affect ARHD expression in the selected PCB-degrading bacteria. Master and Mohn (1998) also reported substantial differences in the effects of physical and chemical environmental conditions on the genetic regulation of PCB degradation in different bacteria.

### **3.3.5. Biosurfactant production and characterization**

#### **3.3.5.1 CTAB agar plate assay for screening of the biosurfactant**

Bacterial biosurfactant-producing property is one of the most important features in biodegradation. The biosurfactant enhances PCB availability from the contaminated soil, increasing biodegradation rates (Laszlova et al., 2018). The CTAB-methylene blue agar plate method is a semi-quantitative screening assay for determining the production of glycolipid biosurfactant. The anionic surfactant produced by the bacteria interacts with the cationic surfactant CTAB, resulting in a dark blue insoluble ion pair with CTAB and methylene. The blue halo around the bacterial colonies indicated that the selected isolates could produce biosurfactants (Walter et al., 2010).

#### **3.3.5.2 Emulsification index and drop collapse assay of biosurfactant**

The efficacy of biosurfactants produced by MAPB-2, MAPB-6, MAPB-9, and MAPB-27 was tested against petroleum oil. *P. aeruginosa* MAPB-2, *P. Plecoglossicida* MAPB-6, and *B. anthropi* MAPB-9 exhibited emulsifying activity of 66%, 57%, and 51%, respectively. However, *B. megaterium* MAPB-27 showed the least emulsification at 44%. In addition, all isolates showed a positive response to the drop collapse assay, as the supernatant led to the expansion of the water by reducing interfacial tension, increasing the drop size.

#### **3.3.5.3 HPTLC and ATR-FTIR characterization of the biosurfactants**

The biosurfactant consists of a hydrophobic moiety that includes fatty acid, while the hydrophilic moiety can be carbohydrate, phosphate, carboxylic acid, alcohol, and amino acid. Therefore, for further characterization of the biosurfactant, the extracted biosurfactant was analyzed by HPTLC

and ATR-FTIR spectroscopy providing information on functional groups, bonds, and molecular nature (Aparna et al., 2012; Ibrahim, 2018). In HPTLC analysis under short UV (254 nm), two bands at  $R_f$  0.91 and 0.72 (as black spots) were observed, indicating monorhamnolipid and dirhamnolipid (Bhat et al., 2015), while at long UV (366 nm), blue fluorescent bands were observed with  $R_f$  values of 0.54, 0.72, and 0.91 in all the four isolates. The HPTLC plate was derivatized with anisaldehyde reagent. It showed a pinkish-black band with an  $R_f$  value of 0.91 in MAPB-2 and MAPB-6 (Fig. 3.6). The bands with an  $R_f$  value of 0.91 indicated the presence of carbohydrate moiety with *p*-anisaldehyde (Belgacem et al., 2015).

The FTIR spectra showed broad and significant peaks at 3357, 3382, 3367, and 3362  $\text{cm}^{-1}$  corresponding to -OH stretching of the glycolipid in MAPB-2, MAPB-6, MAPB-9, and MAPB-27, respectively, while peaks at 2900-2800  $\text{cm}^{-1}$  represented aliphatic -CH<sub>3</sub> and -CH<sub>2</sub> vibrations. The major peaks found to be present at 1637, 1635, 1641, and 1636  $\text{cm}^{-1}$  in MAPB-2, MAPB-6, MAPB-9, and MAPB-27 were due to -C=O (ester group) of the lipids, respectively. The vibration at 1351, 1445, 1448, and 1440  $\text{cm}^{-1}$  represented -C-H group bending, while peaks at 527, 526, 518, and 622  $\text{cm}^{-1}$  corresponded to stretching vibrations of glycosidic bonds (Fig. 3.7A-D).

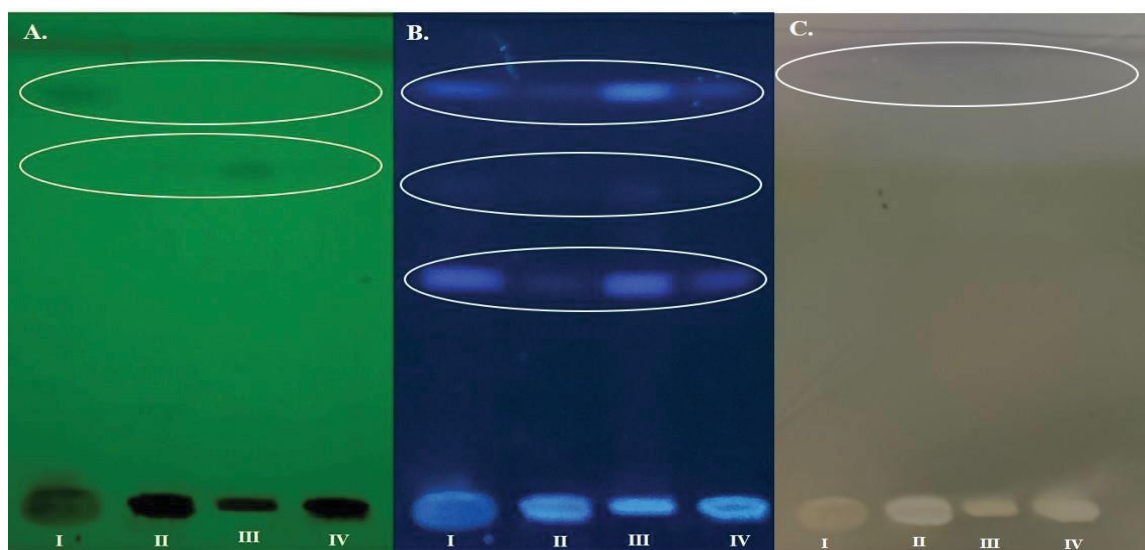


**Fig. 3.6** Visualization of the biosurfactant produced by MAPB-2 (I), MAPB-9 (II), MAPB-6 (III), and MAPB-27 (IV) by HPTLC. The TLC plates were visualized under (A) In short UV (254 nm), 0.72 (as black spots) observed indicates dirhamnolipid, and (B) In 366 nm wavelength, encircled component with fluorescence having  $R_f$  values of 0.54, 0.72, and 0.91 indicates the ester present in the biosurfactant (C) shows TLC plates derivatized with anisaldehyde indicated the presence of carbohydrate moiety showing the pinkish-black band with an  $R_f$  value of 0.91 in MAPB-2 and MAPB-6.

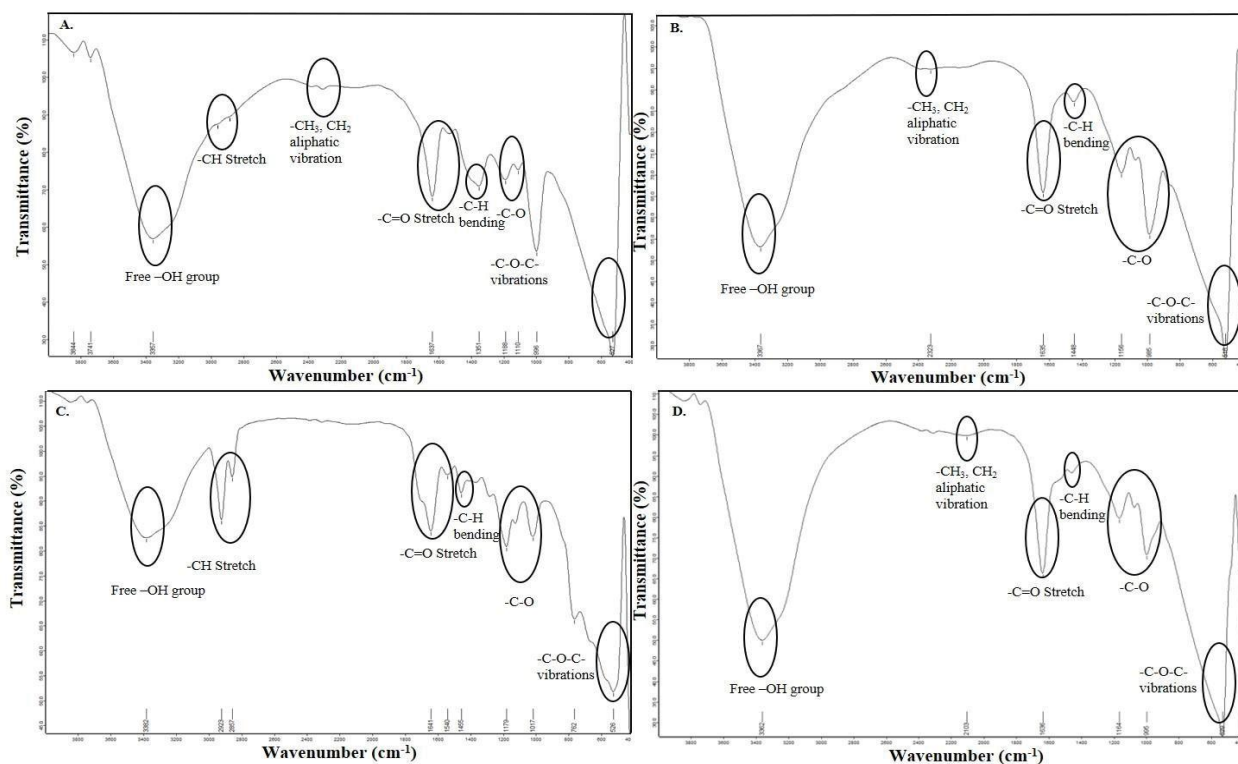


**Fig. 3.7.** ATR-FTIR-based structural characterization of the biosurfactant produced by (A) MAPB-2, (B) MAPB-6, (C) MAPB-9, and (D) MAPB-27.

Compared to previous reports (Ashitha et al., 2020; Bhawsar and Singh, 2016), these main chemical structure groups were in line with the structural characteristics of rhamnolipid. These data suggest that the biosurfactant belongs to the glycolipid class. *Pseudomonas* and *Bacillus* are the most studied genera for biosurfactant production (Gudina et al., 2015), with examples such as *Pseudomonas* BSB1 and BSB2, *Burkholderia* sp. WYAT7, *P. aeruginosa* NGB4. Similar band patterns have been reported in the above species, with wave numbers used to determine the chemical nature of the biosurfactants.

#### 3.3.5.4 GC-MS/MS analysis and characterization of the biosurfactant

The GC-MS/MS analysis identified different lipids/fatty acids with biosurfactant properties. GC-MS/MS analysis and characterization of identified biosurfactants from MAPB-2, MAPB-6, MAPB-9, and MAPB-27 are shown in Table 3.5. The main components of the fatty acid found in the four strains were the ascorbic acid analogs, L-(+)-Ascorbic acid 2,6-dihexadecanoic acid, Dodecane, 2,4-Di-tert-butylphenol, *n*-Nonadecanol-1, 1,2-benzenedicarboxylic acid ester, and Tetratetracontane. However, Octadecanoic acid (Stearic acid; C18:0) was identified in MAPB-2, MAPB-6, and MAPB-27. Octadecanoic acid is a surface-active agent and was found to be one of the major components derived from fatty acids produced by *Pseudomonas*, which has excellent

surfactant properties (Klein et al., 2013). Furthermore, 2-Octenoic acid, *cis*-, 10-Undecenoic acid, and methyl ester were also found as the fatty acid component of the biosurfactant produced by *P. MAPB-2* and *MAPB-6* (Sakthipriya et al., 2015).

**Table 3.5.** GC-MS/MS analysis and characterization of the identified compound from biosurfactant

R <sub>t</sub>	Name of the Compound	Molecular weight	Chemical Formula	Isolates MAPB			
				2	6	9	27
5.31	2-Hexanol, 2-methyl-	116.2	C <sub>7</sub> H <sub>16</sub> O	X	X	✓	X
8.05	Decanoic acid, hexyl ester	256.4	C <sub>16</sub> H <sub>32</sub> O <sub>2</sub>	X	✓	X	X
9.41	1-Nonen-4-ol	142.2	C <sub>9</sub> H <sub>18</sub> O	X	X	✓	X
10.19	Octanoic acid, octyl ester	256.4	C <sub>16</sub> H <sub>32</sub> O <sub>2</sub>	X	✓	X	X
17.02	Dodecane	170.3	C <sub>12</sub> H <sub>26</sub>	✓	✓	✓	✓
17.57	2-Pentenoic acid, 4-hydroxy-	116.1	C <sub>5</sub> H <sub>8</sub> O <sub>3</sub>	X	X	✓	X
19.10	1-Decanol, 2-hexyl-	242.4	C <sub>16</sub> H <sub>34</sub> O	X	✓	X	X
20.34	Dodecane, 2,6,11-trimethyl-	212.4	C <sub>15</sub> H <sub>32</sub>	✓	X	X	X
20.36	Tetradecane	198.3	C <sub>14</sub> H <sub>30</sub>	X	X	✓	X
20.38	Heptadecane, 8-methyl-	254.4	C <sub>18</sub> H <sub>38</sub>	X	✓	X	X
21.35	1-Undecanol	172.3	C <sub>11</sub> H <sub>24</sub> O	X	X	✓	X
21.52	2,4-Di-tert-butylphenol	206.3	C <sub>14</sub> H <sub>22</sub> O	✓	✓	✓	✓
22.12	Hexadecane, 2,6,10,14-tetramethyl-	282.5	C <sub>20</sub> H <sub>42</sub>	✓	✓	✓	X
22.12	Pentadecane, 3-methyl-	226.4	C <sub>16</sub> H <sub>34</sub>	✓	X	✓	X
22.33	1-Hexadecanol	242.4	C <sub>16</sub> H <sub>34</sub> O	✓	X	X	X
22.34	n-Tridecan-1-ol	200.3	C <sub>13</sub> H <sub>28</sub> O	X	✓	✓	✓
22.41	Eicosane	282.5	C <sub>20</sub> H <sub>42</sub>	✓	✓	✓	✓
23.62	Hexacosane	366.7	C <sub>26</sub> H <sub>54</sub>	✓	X	X	X
23.67	Tetradecane, 5-methyl-	212.4	C <sub>15</sub> H <sub>32</sub>	✓	✓	✓	X
23.68	Pentadecane, 8-hexyl-	296.5	C <sub>21</sub> H <sub>44</sub>	X	X	✓	X
23.84	Heptadecane, 2-methyl-	254.4	C <sub>18</sub> H <sub>38</sub>	✓	✓	✓	X
24.02	n-Nonadecanol-1	284.5	C <sub>19</sub> H <sub>40</sub> O	✓	✓	✓	✓
22.43	Octadecane, 5-methyl-	268.5	C <sub>19</sub> H <sub>40</sub>	X	✓	X	✓
24.58	1,2-Benzenedicarboxylic acid ester	278.3	C <sub>16</sub> H <sub>22</sub> O <sub>4</sub>	✓	✓	✓	✓
24.99	Hentriacontane	436.8	C <sub>31</sub> H <sub>64</sub>	✓	X	X	X
25.84	trans-2-Undecen-1-ol	170.2	C <sub>11</sub> H <sub>22</sub> O	✓	X	✓	✓
26.53	Nonadecane, 9-methyl-	282.5	C <sub>20</sub> H <sub>42</sub>	X	✓	X	✓
26.54	Heptadecane, 2,3-dimethyl-	268.5	C <sub>19</sub> H <sub>40</sub>	✓	✓	✓	X
26.61	Tridecanol, 2-ethyl-2-methyl-	242.4	C <sub>16</sub> H <sub>34</sub>	X	X	✓	X
26.62	Heneicosane, 5-methyl-	310.6	C <sub>22</sub> H <sub>46</sub>	✓	✓	✓	X
26.75	Octadecanoic acid (Stearic acid)	284.4	C <sub>18</sub> H <sub>36</sub> O <sub>2</sub>	✓	✓	X	✓
26.92	n-Tetracosanol-1	354.6	C <sub>24</sub> H <sub>50</sub> O	X	✓	✓	X
26.97	Heneicosane	296.5	C <sub>21</sub> H <sub>44</sub>	✓	✓	✓	X
27.12	1-Heneicosanol	354.6	CH <sub>3</sub> (CH <sub>2</sub> ) <sub>2</sub>	✓	✓	X	✓
27.65	Hexadecen-1-ol, trans-9-	240.4	C <sub>16</sub> H <sub>32</sub> O	✓	X	X	X
28.44	Tetratetracontane	619.2	C <sub>44</sub> H <sub>90</sub>	X	✓	✓	✓
30.37	Tetracontane	563	C <sub>40</sub> H <sub>82</sub>	✓	X	X	X
35.66	E-3-Pentadecen-2-ol	226.4	C <sub>15</sub> H <sub>30</sub> O	X	X	✓	X

1-Hexadecanol and Hexadecen-1-ol, trans-9-, 1-Heneicosanol, 1-Dodecanol, and 1-Octanol, were found to be fatty alcohol components of the nonionic biosurfactant identified in



MAPB-2. 1-Hexadecanol, *n*-Tridecan-1-ol, *n*-Tridecan-1-ol, and *n*-Tridecan-1-ol were identified as the primary fatty alcohol components of biosurfactant produced by MAPB-2. Fatty acid components decanoic acid, Octanoic, Heptadecane, and fatty alcohol Decanol were found to be specific to the biosurfactant extract of MAPB-6. While 2-hexanol, 2-methyl-, *n*-Tridecan-1-ol, *n*- Nonadecanol-1, Tridecanol, 2-ethyl-2-methyl-, *n*-Tetracosanol-, *trans*-2-Undecen-1-ol were found to be the primary fatty alcohol in MAPB-9. 4-hydroxy- 2-pentenoic acid, is an  $\alpha$ -alkyl hydroxy fatty acid identified in biosurfactant produced by MAPB-9. A similar type of fatty acid and alcohol component of the biosurfactants was observed by *Burkholderia* sp. (Ashitha et al., 2020) and *P. aeruginosa* (Bhawsar and Singh, 2016). Therefore, considering biosurfactants, MAPB-2 and MAPB-6 were good biosurfactant producers, followed by MAPB-9 and MAPB-27. The improved PCB degradation (Aroclor 1248) spiked soil by bacterial surfactant rhamnolipid was demonstrated earlier by Cho et al. (2004). Thus, the detailed characterization done with different analytical techniques such as HPTLC, ATR-FTIR, and GC-MS/MS have highlighted the presence and nature of the biosurfactant produced by the selected isolates.

### 3.3.6. Optimization of growth parameter for PCB-degrading bacterial isolates

Before conducting the biodegradation study, optimizing the growth parameters for efficient PCB degradation is crucial. Various studies have been undertaken on optimizing growth conditions for enhanced biodegradation efficiency (Khanpour-Alikelayeh et al., 2020). Several environmental factors, such as the contaminant concentration, inducers' presence, pH, and temperature, can alter bacterial growth, which, in turn, influences biodegradation efficiency. The optimum biphenyl concentration for bacterial growth varied for different isolates showing the best growth by MAPB-2, MAPB-6, and MAPB-9 at 200 mg L<sup>-1</sup> concentrations and 50 mg L<sup>-1</sup> by MAPB-27 (Fig. 3.8A). The differences in the growth pattern of individual bacterial isolates concerning different biphenyl concentrations may be due to different adaptive mechanisms. It has been reported that biphenyl degradation ability gets stimulated *via* induction of the biphenyl catabolic enzymes. It has been reported that adding cometabolite, such as glucose, provides an alternative nutrient, resulting in increased growth during PCB biodegradation. Adding glucose as a cometabolite improved the PCB-degrading property of the bacterial isolates *via* growth stimulation.



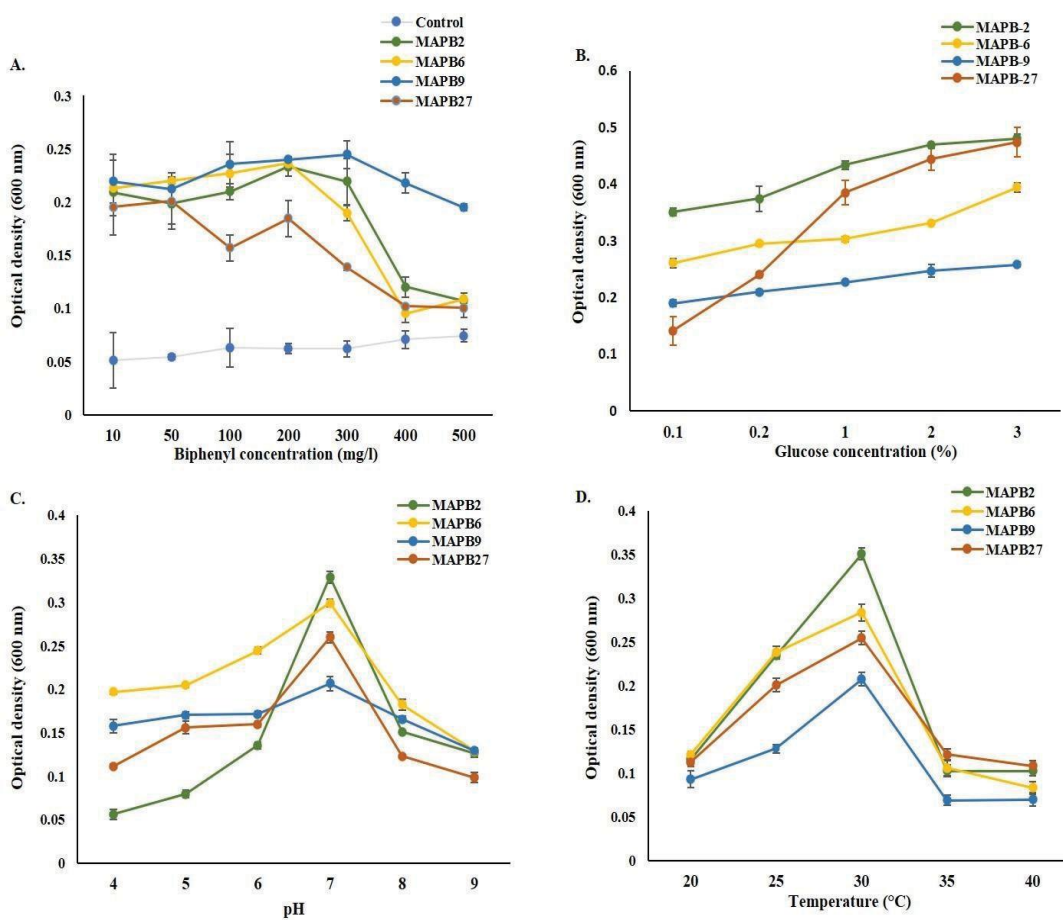


**Fig. 3.8.** Optimization of the growth parameter for potential PCB degrading bacterial isolates grown in minimal medium in 48 h (A) biphenyl concentration range (10-500 mg L<sup>-1</sup>) (B) glucose conc. (0.1-3%) with 200 mg L<sup>-1</sup> biphenyl (C) pH (4-9) and (D) Temperature (20-40°C).

In addition, the best growth was observed at a glucose concentration of 3% in MM supplemented with 200 mg L<sup>-1</sup> biphenyl for all the selected bacterial isolates (Fig. 3.8B). Nevertheless, it was also observed that the biodegradation rate decreases with a high amount of co-metabolite, as it is more rapidly utilized than PCB by bacteria (Bidlan and Manonmani 2002).

Therefore, 0.2% glucose concentration was selected for further experiments, as it also supported the growth of these isolates in low glucose concentration in the presence of 200 mg L<sup>-1</sup> biphenyl. The optimum pH for PCB degradation was 7 for all the isolates (Fig. 3.8C), which tallies previous studies reporting near-neutral pH as the most favourable for the bacterial degradation of chlorinated pollutants such as PCB (Fang et al., 2010). The reduced growth at acidic or alkaline pH strongly infers that a slight alteration greatly influences bacterial growth in the pH of the medium (Khopade et al., 2012).

As observed for the pH, the same pattern was also detected for the optimization of temperature. The temperature ranges between 20 and 40°C, as shown in Fig. 3.8D. Bacterial growth was severely suppressed at temperatures 20, 35, and 40°C, while 25 and 30°C were the optimum for growth. From these optimization studies, it appears that variation in the growth parameters directly affects the growth of the isolates and, indirectly, the biodegradation rate.

The overall result indicated that optimization of pH and temperature aids in promoting bacterial growth in MM with 200 mg L<sup>-1</sup> biphenyl concentration and 0.2% glucose as a co- substrate. Therefore, the growth parameters of pH 7.0 and temperature 30°C were selected for the biodegradation studies of biphenyl.

### 3.3.7. Analysis of the growth curve

The growth curve of the selected isolates MAPB-2, MAPB-6, MAPB-9, and MAPB-27 was plotted between time (h) and OD<sub>600</sub> in three different LB and MM supplemented with biphenyl as shown in Fig. 3.9 and 3.10, respectively. In LB media, the growth pattern was the same for MAPB-2, MAPB-6, and MAPB-27, while MAPB-9 was a slow grower. The cell doubling time in the exponential growth phase was 0.86, 0.90, 1.23, and 0.69 h for MAPB-2, MAPB-6, MAPB-9, and MAPB-27, respectively (Fig. 3.9A). However, the mean growth rate constant (k) was found to be 1.16, 1.10, 0.81, and 1.44 h<sup>-1</sup> for MAPB-2, MAPB-6, MAPB-9, and MAPB-27, respectively (Fig. 3.9B). The growth pattern of all four isolates in MM-supplemented biphenyl (200 mg L<sup>-1</sup>) media was similar to that observed in the LB medium. However, the cell doubling time in biphenyl-supplemented MM medium was 38.28, 43.86, 33.64, and 20.87 h for MAPB-2, MAPB-6, MAPB-9, and MAPB-27, respectively (Fig. 3.10).

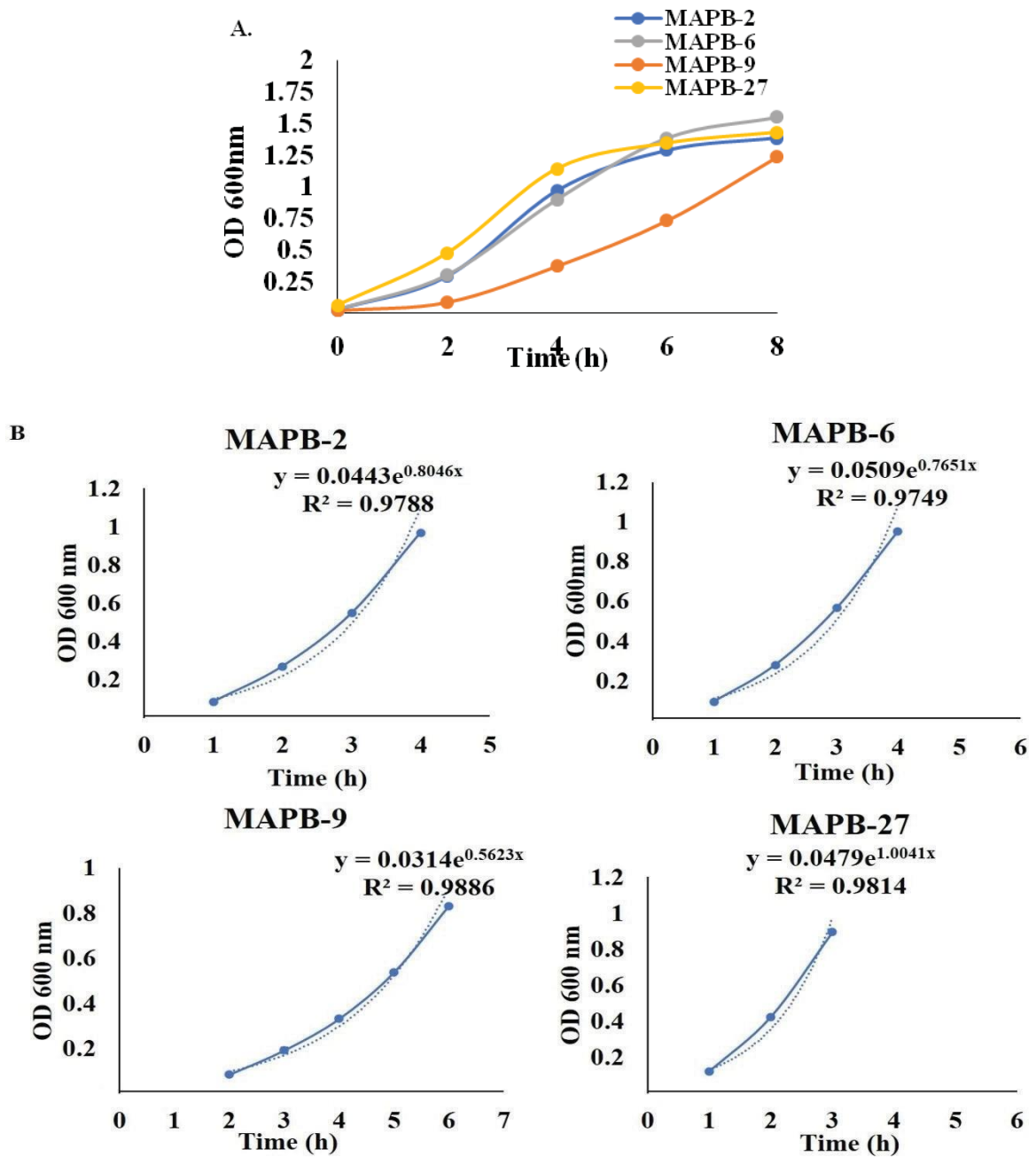


**Fig. 3.9.** Growth curve of selected isolates on (A) LB media (B) growth pattern of MAPB-2, MAPB-6, MAPB-9, and MAPB-27 graph depicting the exponential phase.

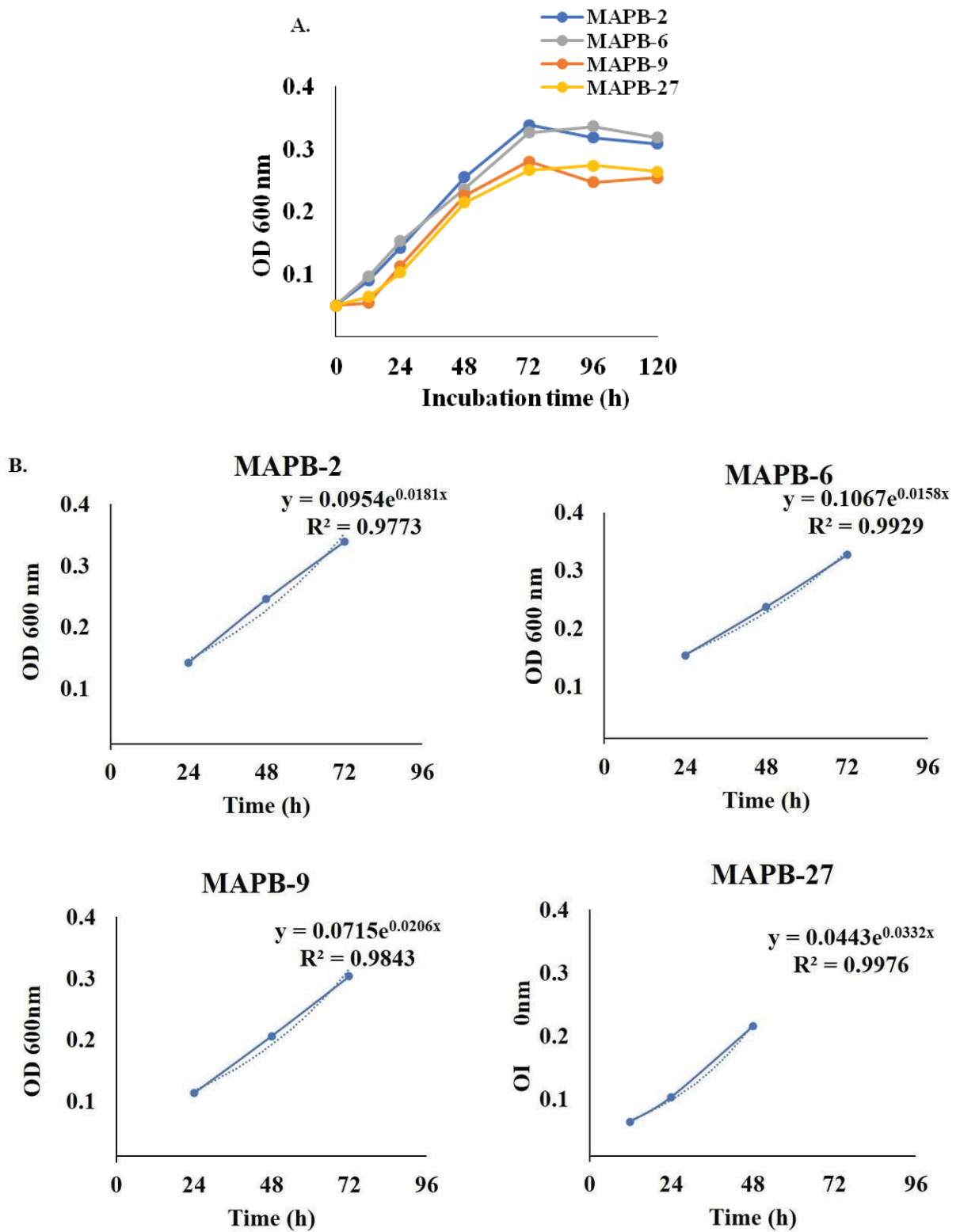


**Fig. 3.10.** Growth curve of selected isolates on (A) biphenyl-supplemented MM media (B) growth pattern of MAPB-2, MAPB-6, MAPB-9, and MAPB-27 graph depicting the exponential phase.

### 3.3.8. Chemotactic responses of MAPB-2, MAPB-6, MAPB-9, and MAPB-27 towards DHB, biphenyl, benzoate, catechol, and glucose

Chemotaxis helps the bacteria to come in contact with the pollutant and utilize it. Thus, this property of chemotaxis plays an important role in bioremediation (Pandey and Jain, 2002; Parales et al., 2015; Marx and Aitken, 1999). Strains MAPB-2, MAPB-6, MAPB-9, and MAPB-27 were tested for chemotaxis toward PCB intermediates and glucose by drop assay. For the assays, the chemoattractant is placed in the centre of the semi-solid agar plate resulting in a formation concentration gradient. The bacteria growth around the chemoattractant indicated chemotaxis. Drop assays showed that strain MAPB-2, MAPB-6, MAPB9, and MAPB-27 showed chemotaxis toward four tested PCB intermediates, *i.e.*, degradation intermediates of upper (biphenyl, dihydroxy biphenyl) and lower (benzoate, and catechol) biphenyl degradation pathways (Fig. 3.11).

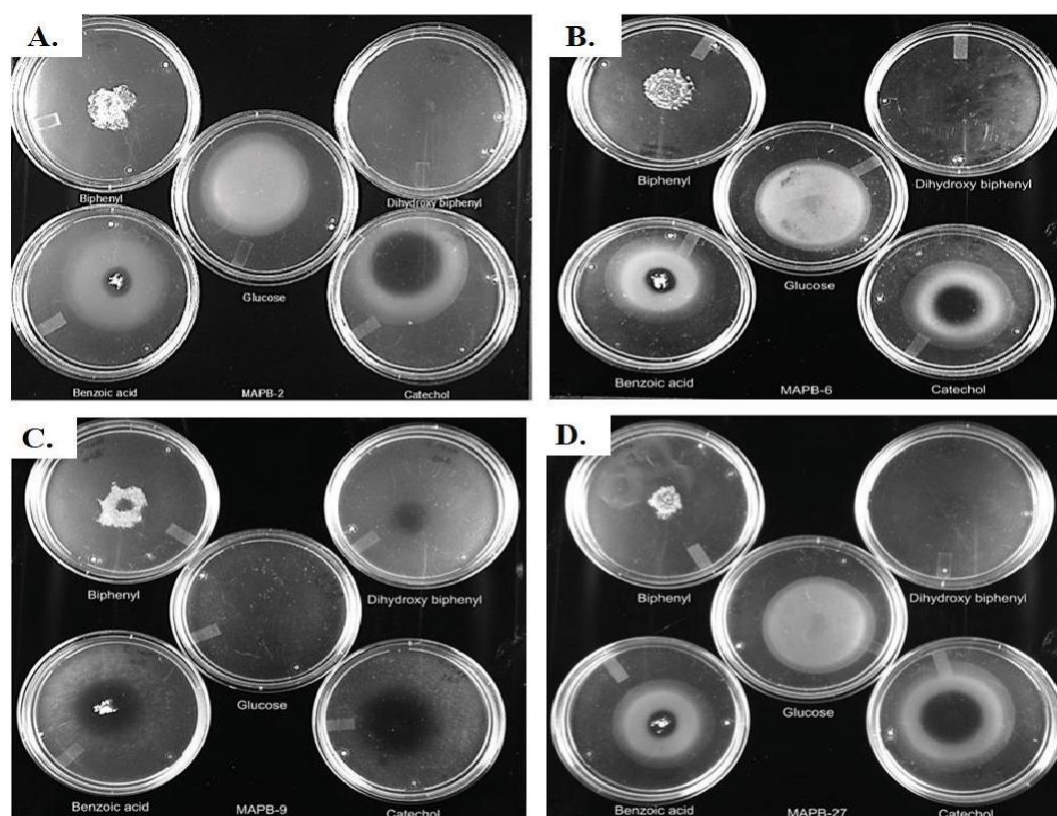


**Fig. 3.11.** Chemotaxis of the selected isolates by drop assay in the presence of intermediates of upper (biphenyl, dihydroxybiphenyl) and lower (benzoic acid, catechol) biphenyl degrading pathway (A). *P. aeruginosa* MAPB-2 (B). *P. plecoglossicida* MAPB-6 (C). *B. anthropi* MAPB-9 (D). *P. megaterium* MAPB-27.

Biphenyl-grown cells MAPB-2, MAPB-6, MAPB-9, and MAPB-27 resulted in bacterial growth ring in the centre of the plates around the biphenyl, dihydroxy biphenyl, benzoate, and catechol. These results indicated the positive movement of the bacterial isolates toward all the substrates but with a difference in growth towards the centre. Different intermediates, such as benzoate and CBAs, are produced in biphenyl/PCB degradation (Potrawfke et al., 1998). The chemotaxis of *Pseudomonas* spp. (Toussaint et al. 2012; Gordillo et al., 2007) and *Rhodococcus* sp. (Yun et al., 2009) toward chemical compounds has been previously reported. There are studies conducted on the chemotactic response by PCB-degrading bacteria towards benzoate, biphenyl (Wu et al., 2003), PCBs (Tremaroli et al., 2010), and CBA (Harwood et al., 1990). However, our data indicate that MAPB-2, MAPB-6, MAPB-9, and MAPB-27 showed chemotaxis toward biphenyl intermediates, dihydroxy biphenyl, benzoate, and catechol.

### **3.3.9. Study of cellular morphology by Field emission scanning electron microscopy (FESEM)**

The effect of biphenyl on the cellular morphology of selected isolates was analyzed by FESEM. The bacterial isolates showed normal morphology in the LB medium. The enlarged image of all the bacterial isolates MAPB-2, MAPB-6, MAPB-9, and MAPB-27 (10,000 X and 50,000 X) in LB and MM, supplemented with biphenyl, is depicted in Fig. 3.12-3.15. The average cell size was found to be 1.950, 1.975, 1.748, and 4.975  $\mu\text{m}$  for MAPB-2, MAPB-6, MAPB-9, and MAPB-27, respectively, when grown in LB medium. At the same time, it was found the cell size reduced to 1.268, 1.566, 1.563, and 4.758  $\mu\text{m}$  for MAPB-2, MAPB-6, MAPB-9, and MAPB-27 in biphenyl-treated conditions, respectively. Thus, cell size decreased in all the selected bacterial isolates when grown in MM supplemented with biphenyl compared to cells grown under a nutrient-rich LB medium. The biphenyl-treated cells showed the reduced size and increased secretion of exopolysaccharide layer and membrane vesicle-like structure on MAPB-9 and MAPB-27 surface (Fig. 3.14D and 3.15C) when grown in MM medium. Similar to our observation, *Pseudomonas* sp. IH-2000 (Kobayashi et al., 1999) and *P. putida* DOT-T1E (Ramos-González et al., 2001) produced membrane vesicles when toluene was added to the culture medium. The above study suggested that vesicle formation was a specific response of this strain to remove toluene. These physiological observations were in accordance with changes in *Burkholderia xenovorans* LB400 during early stationary-phase biphenyl-grown cells (Parnell et al., 2006). Due to exposure to organic compounds such as biphenyl, PCBs, and toluene, membrane separation, size reduction,



and formation of vesicles in a bacterial cell often indicate stress conditions. Depending upon the origin of these extracellular vesicles, they are classified into outer membrane vesicles (OMVs) and membrane vesicles (MVs) from Gram-negative and Gram-positive bacteria, respectively (Bose et al., 2020). The difference in assemblage pattern amongst the selected bacterial isolates was observed. In MAPB-2, the bacterial cell adheres to one another in pairs (Fig. 3.12A), while in MAPB-6, bacterial cells are attached as in biofilm, and a tube-like structure is observed in cells grown in LB (Fig. 3.13B). MAPB-9 cells showed a packed arrangement in a layer of bacterial cells lying one above another (Fig. 3.14D), whereas, in MAPB-27, they are arranged in pairs (Fig. 3.15C). Diplobacillus arrangement observed in MAPB-2, MAPB-6, and MAPB-27 revealed cell division.

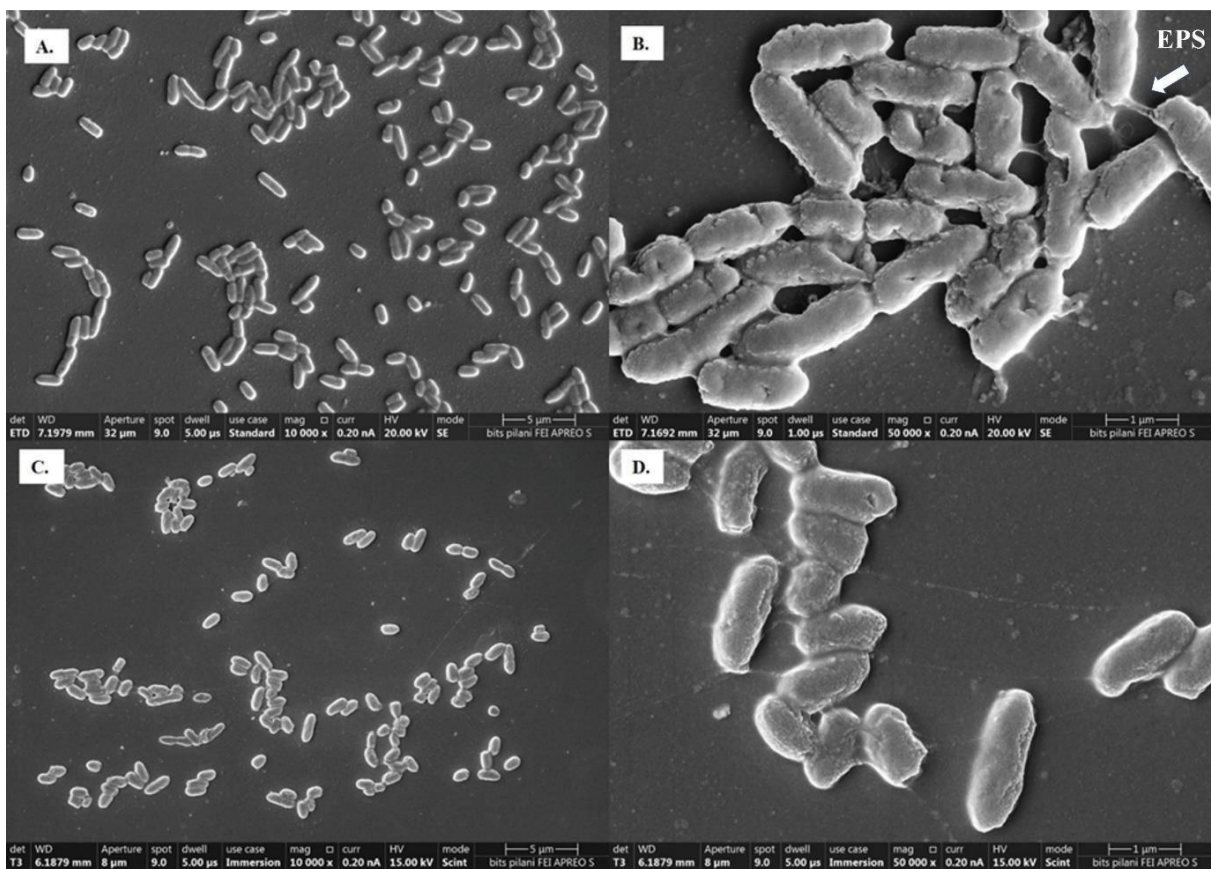


**Fig. 3.12.** FESEM image of MAPB-2 grown in (A) LB medium, 10, 000X (B) LB media, 50 000X, arrow indicates EPS production (C) MM with biphenyl, 10, 000X (D) MM with biphenyl, 50,000X.

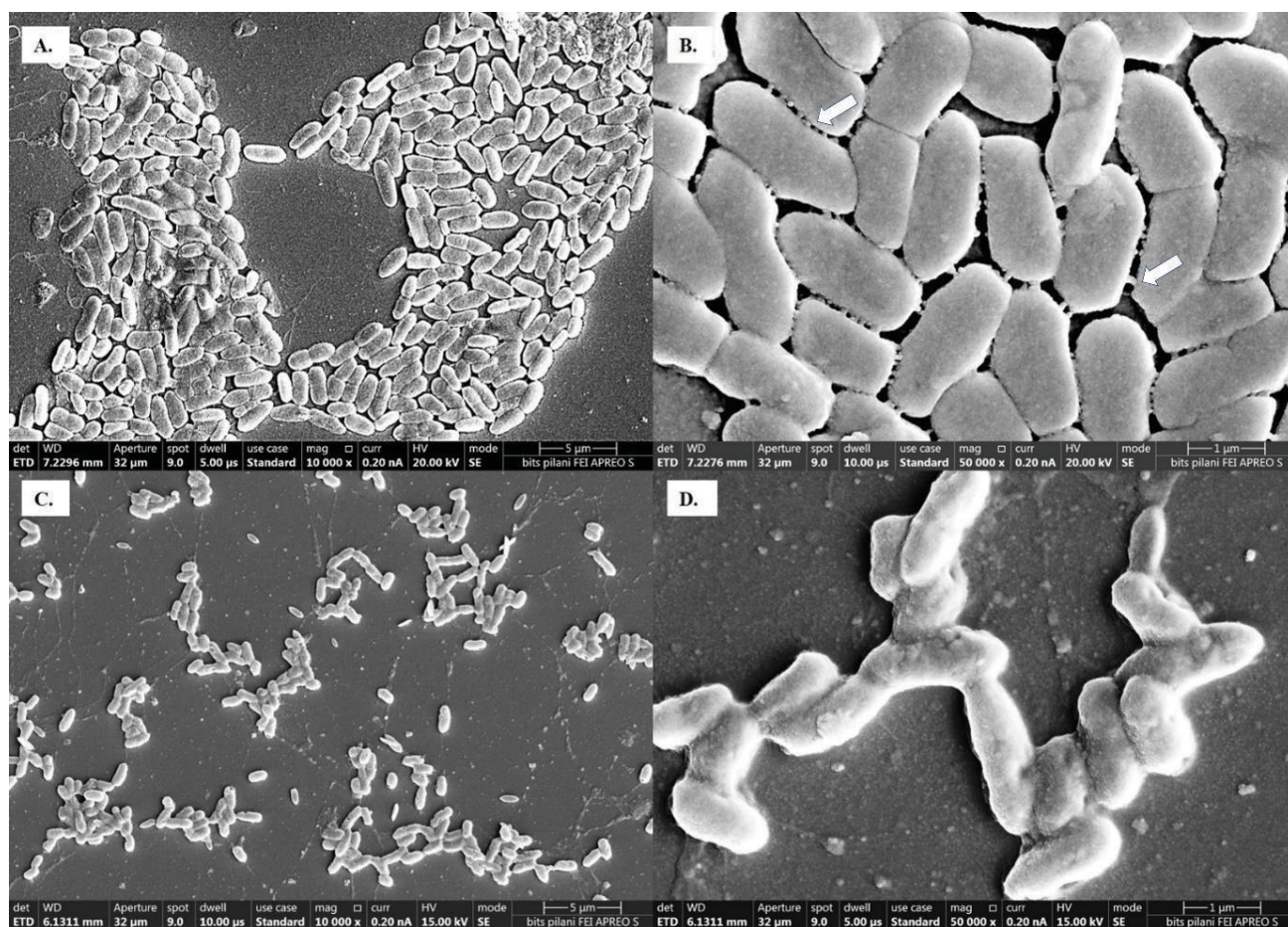


**Fig. 3.13.** FESEM analysis of MAPB-6 grown in (A) LB media, 10,000X (B) LB media, 50 000X, arrow indicates tube-like appendages and (C) MM with biphenyl, 10,000X (D) MM with biphenyl, 50,000X, EPS secretion observed.



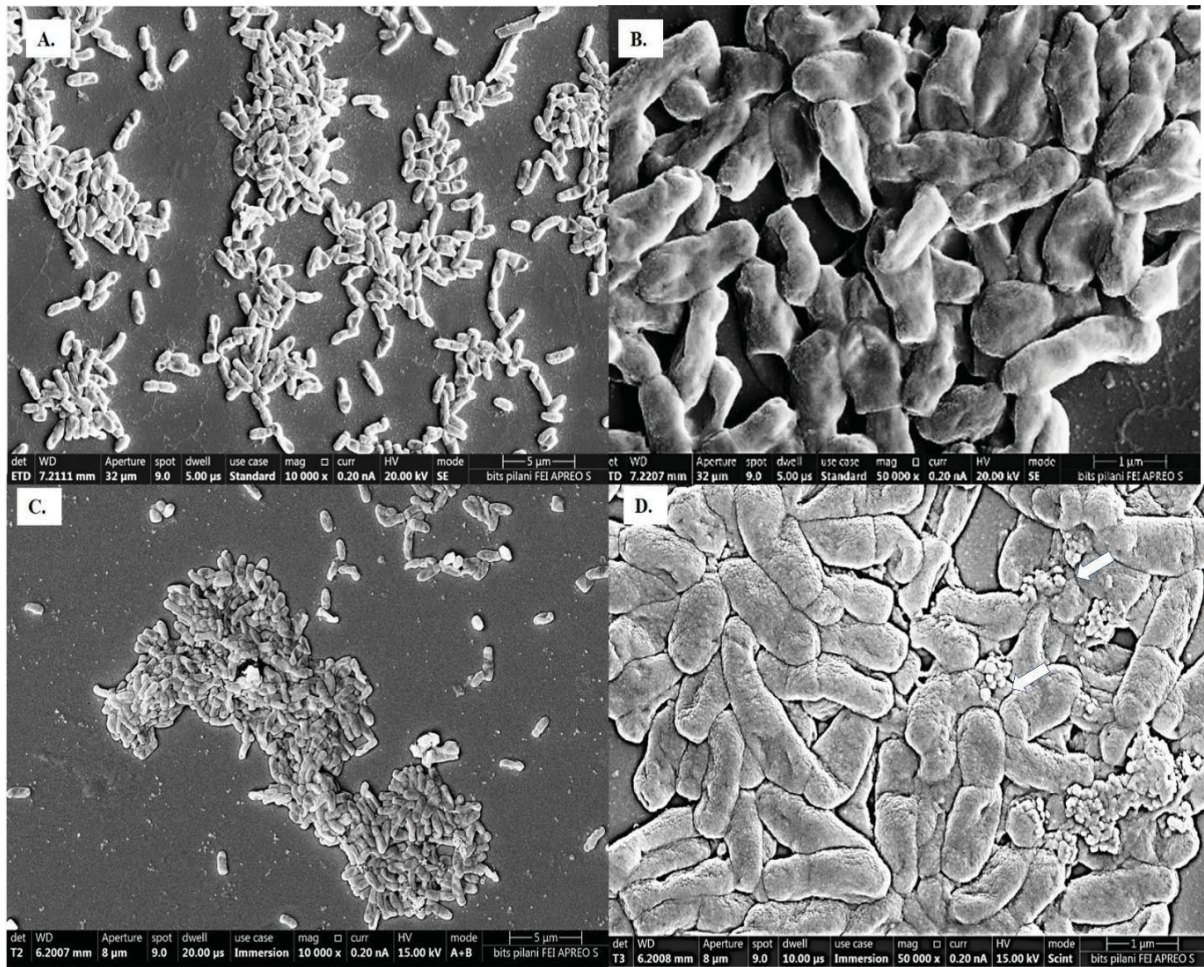


**Fig. 3.14.** FESEM analysis of MAPB-9 grown in (A) LB media, 10,000X (B) LB media, 50 000X, and (C) MM with biphenyl, 10,000X (D) MM with biphenyl, 50,000X, arrow indicates outer membrane vesicles.

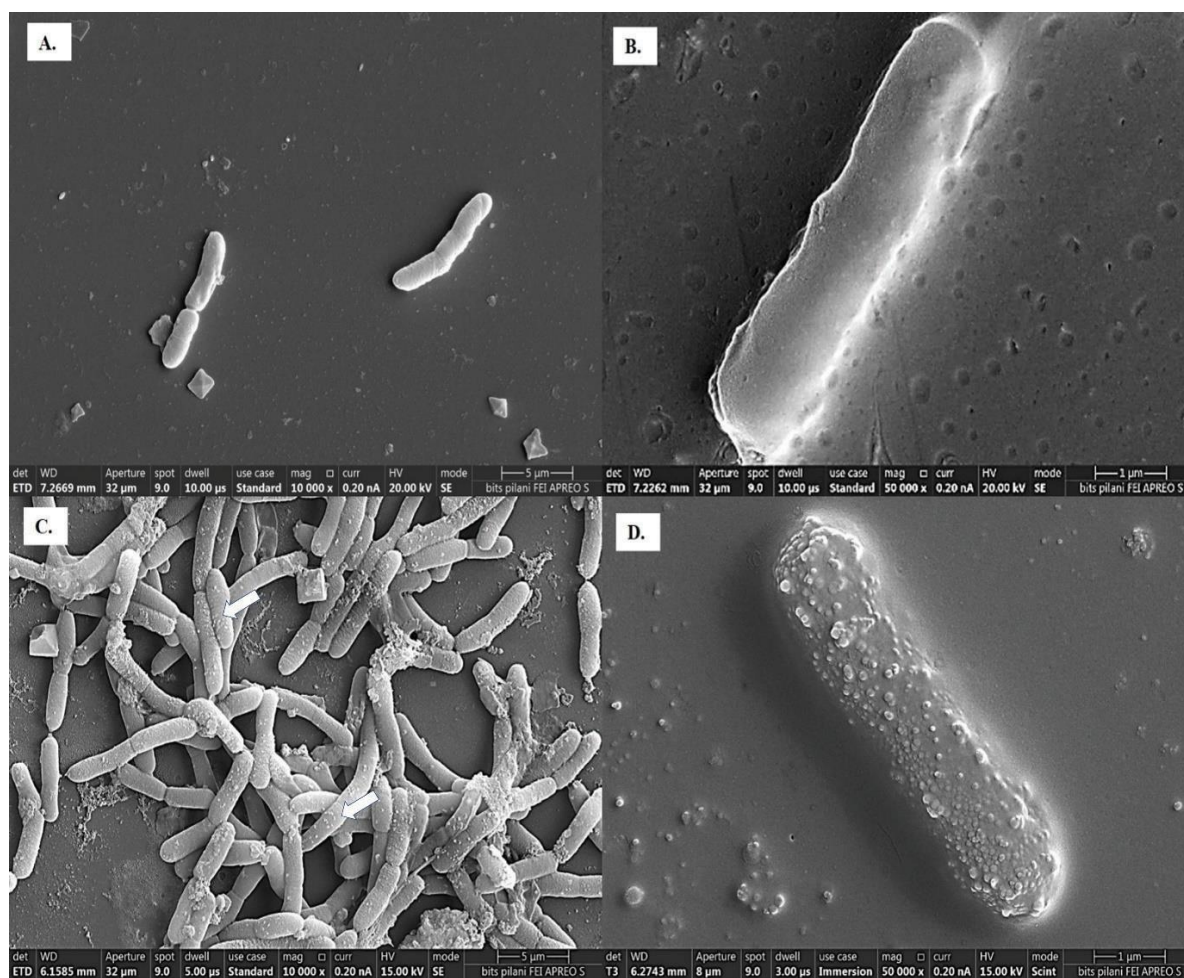


**Fig. 3.15.** FESEM analysis of MAPB-27 grown in (A) LB media, 10,000X (B) LB media, 50 000X and (C) MM with biphenyl, 10,000X arrow indicates membrane vesicle (D) MM with biphenyl, 50 000X, membrane vesicle observed.

### 3.3.10. Biodegradation assay with biphenyl

To measure the efficiency of biphenyl and PCB-77 degradation, the selected bacterial isolates were subjected to GC-MS/MS analysis for the percentage degradation of the pollutants. 200 mg L<sup>-1</sup> biphenyl was used as the sole carbon source in the growth medium. The percentage of biphenyl degradation was achieved up to 66.15, 62.06, 57.02, and 56.55% by *B. anthropi* MAPB-9, *P. aeruginosa* MAPB-2, *P. plecoglossicida* MAPB-6, and *P. megaterium* MAPB-27, respectively (Fig. 3.16).

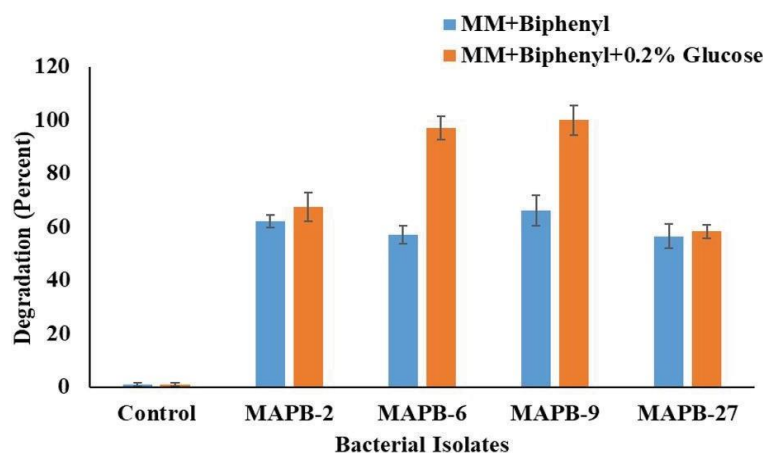


**Fig. 3.16.** Quantitative estimation of biphenyl degradation by GC-MS/MS. The selected bacterial isolates were grown in MM supplemented with 200 mg L<sup>-1</sup> biphenyl alone and with 0.2% glucose at 30°C for 48 h, 150 rpm.

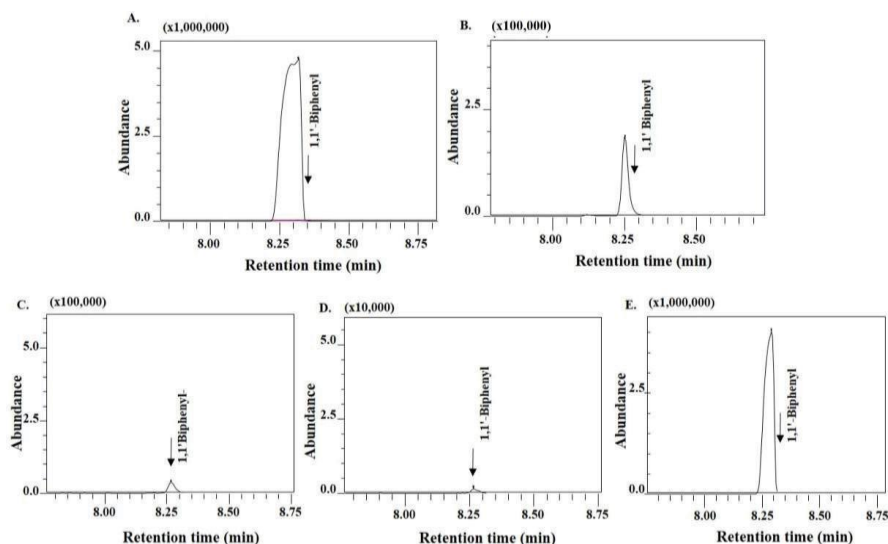


**Fig. 3.17.** GC-MS/MS Chromatogram of biphenyl degradation under optimized conditions. (A) control without inoculum (B) *P. aeruginosa* MAPB-2 showing 67.5% (C) *P. plecoglossicida* MAPB-6 showing 97.1% (D) *B. anthropi* MAPB-9 showing 100% (E) *P. megaterium* MAPB-27 showing 58.3% degradation. Biphenyl (200 mg L<sup>-1</sup>) supplemented MM with the addition of 0.2% glucose was kept at 30°C for 48h, 150 rpm.



However, the biphenyl degradation efficiency increased with the addition of co-substrate glucose (0.2%) to the culture medium showing a percentage degradation of 100, 97.1, 67.5, and 58.3% by MAPB-9, MAPB-6, MAPB-2, and MAPB-27 respectively (Fig. 3.16 & 3.17) in 48 h. Thus, the present study revealed that each isolate behaved differently with respect to its biphenyl degrading potential when used as the sole source or co-metabolically with glucose.

Our results are similar to previous studies, which indicated the PCB degrading ability of different bacteria, such as *Dyella ginsengisoli* LA-4 could degrade 95% biphenyl ( $100 \text{ mg L}^{-1}$ ) in 36 h (Li et al., 2009), *Achromobacter* sp. BP3 showed 100% biphenyl ( $50 \text{ mg L}^{-1}$ ) in 24 h (Hong et al., 2009), and *Mycobacterium* sp. PYR-1 degrades 98% biphenyl ( $80 \text{ mg L}^{-1}$ ) in 72 h (Moody et al., 2002). However, the studies mentioned above did not test the degradation property in the presence of co-metabolite. A similar study by Murinova et al. (2014) highlighted that adding glucose as a co-metabolite enhanced bacterial growth and PCB biodegradation. The present study highlighted the enhanced biodegradation due to glucose in the biphenyl-supplemented MM.

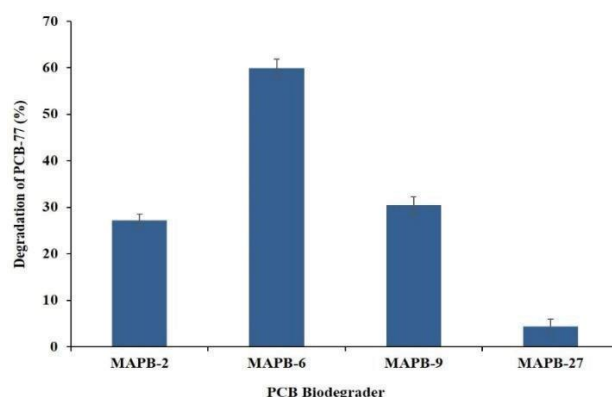
Also, results revealed the percent of biphenyl degradation by MAPB-9 increased from 66.15 to 100% in glucose-supplemented media after 48h. *B. anthropi* MAPB-9 was identified to be the efficient degrader. Therefore, it appears that the efficiency and amount of PCB degradation depend not only on the type and concentration of the carbon source/inducer but also on the genetic setup of the bacterial isolate (Murinova et al., 2014).

### 3.3.11. Biodegradation assay with PCB-77

Biphenyl, with more than two chlorine per molecule, is mostly considered to be recalcitrant and is usually biodegraded *via* co-metabolism. PCB-77 consists of four chlorine molecules at meta- and para-positions. It is abundant within the food chain due to its extensive application in commercial blends such as Aroclor (Wang et al., 2016). Therefore, it is very important to explore the potential degrader for the degradation of such coplanar PCB. MAPB-2, MAPB-6, MAPB-9, and MAPB-27 were evaluated for degradation of PCB-77 in the presence of biphenyl as an inducer. Based on the GC-MS/MS analysis data, all the isolates degraded PCB-77 ( $50 \text{ mg L}^{-1}$ ) in 7 d, though with varied efficiency. MAPB-6 showed the highest degradation of PCB-77 (59.89%), followed by MAPB-9 (30.49%), MAPB-2 (27.19%), and MAPB-27 (4.43%) as depicted in Fig. 3.18. There are reports that, in the absence of an inducer, potent PCB-degrading bacteria such as *Rhodococcus* sp. RHA1 (0%), *P. pseudoalcaligenes* KF707 (0%), and *Burkholderia xenovorans* LB400 (6%), exhibited no or very low degradation of PCB-77 (Sakai et al., 2005). To our knowledge, this is the first study



highlighting the capability of *P. aeruginosa*, *P. plecoglossicida*, *B. anthropi*, and *P. megaterium* in degrading PCB-77 with reasonable efficiency.

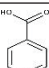
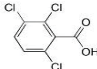
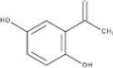
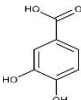


**Fig. 3.18.** Percentage degradation of PCB 77 ( $50 \text{ mg L}^{-1}$ ) by MAPB-2, MAPB-6, MAPB-9, and MAPB-27 kept at  $30^\circ\text{C}$  for 7 d. The areas of specific peaks in the chromatogram of the samples were measured and compared to those of control samples supplemented with PCB-77 without inoculum.

#### Analysis of metabolites produced during PCB-77 degradation

There is very less information related to PCB-77 metabolite detection. However, benzoic acid and 3,3',4 trichloro benzoic acid were detected in MAPB-2 at  $R_t$  4.9 and 27.8 min, respectively. 3,4-Dihydroxybenzoic acid, 3TMS and Dihydroxyacetophenone, 2TMS at 38.9 and 38.3 min in MAPB-6; 3,4-Dihydroxybenzoic acid, 3TMS at 41.2 min in MAPB-9 while 3,4- Dihydroxybenzoic acid, 3TMS at 37.9 min in MAPB-27 as shown in Table 3.6.

**Table 3.6.** GC-MS/MS Mass spectral features of metabolites identified during PCB-77 degradation by the selected isolates

Metabolites	Structure	Isolates	$R_t$	Mass spectra
Benzoic acid		MAPB-2	4.9	194,179,135,105,77,51
3,4,4' Trichloro benzoic acid		MAPB-2	18.9	256, 186,150,93,75
Dihydroxyacetophenone		MAPB-6 MAPB-27	38.3 37.9	152,137,109
3,4- Dihydroxybenzoic acid		MAPB-6 MAPB-9	38.9 41.2	355,249,193,105,73,45

PCBs, undergo dehalogenation to lower chlorinated biphenyl and further form chlorobenzoic acid metabolite. This chlorobiphenyl is further converted into hydroxybenzoic acid and dihydroxybenzoic acid (Plotnikova et al., 2012). Bedard and his co-workers (1987) have

reported chlorinated benzoic acid and chlorinated acetophenone intermediate metabolites from

oxidation of PCB congeners. *Rhodococcus* sp. RHA1 and *Phanerochaete chrysosporium* are well-known PCB degraders, but they still exhibit no or low degradation of di-para-chlorine-substituted congeners such as PCB-77 (Sakai et al., 2005). However, it is not clear whether these metabolites arise from common or independent metabolic pathways.

In conclusion, *P. aeruginosa* MAPB-2, *P. plecoglossicida* MAPB-6, *B. anthropi* MAPB-9, and *P. megaterium* MAPB-27 isolated from PCB-contaminated soil showed high biphenyl and PCB-77 degradation ability. Isolates MAPB-2, MAPB-6, MAPB-9, and MAPB-27 could tolerate up to 500 mg L<sup>-1</sup> biphenyl. Optimized growth conditions led to 100% improved biphenyl biodegradation by MAPB-9 with 200 mg L<sup>-1</sup> biphenyl, while 97.1 for MAPB-2 within 48h, respectively. The study is the first report of effective PCB-77 degradation with 59.89%, 30.49%, 27.19%, and 4.43% degradation by MAPB-6, MAPB-9, MAPB-2, and MAPB-27 respectively, using biphenyl as inducers. In addition to biodegradation potential, the isolates were also found to be capable of producing biosurfactants and PGPR traits. The biosurfactant-producing property of these isolates can be attributed to good PCB degradation. Thus, results highlighted the degradation potential of the selected bacteria and found them promising candidates for bioremediation of environments contaminated with biphenyl/PCBs.

## **Chapter IV**

# **Metabolite Profiling of Selected Bacterial Isolates Grown in Biphenyl-Supplemented Minimal Media**

#### 4.1. Introduction

As discussed in chapter 1, bacteria degrade biphenyl/ PCB congeners through aerobic or anaerobic degradation pathways (Taguchi et al., 2007; Gibson and Parales 2000). The complete mineralization of the biphenyl pathway consists of the upper and lower biodegradation pathways (Arai et al., 1998). The biphenyl-degrading bacteria lack a complete catabolic pathway (Pieper, 2005), which results in the accumulation of dead-end products, thereby inhibiting the growth of bacterial cells during the biodegradation process (Eklund, 1985). Benzoic acid and chlorobenzoic acid (CBA) have been identified as the dead-end intermediates (Adebusoye et al., 2008) involved in the biphenyl degradation pathway. However, it could be transformed by other bacteria that possess benzoate catabolic enzymes (Vrana et al., 1996). Therefore, identifying the metabolites formed during the biodegradation process is very important.

Metabolite profiling aims to identify metabolites/intermediates produced during the metabolic processes. It determines the total concentration or relative level of the metabolites that accumulate in the predefined group, such as organic acids, amino acids, and carbohydrates. In contrast, targeted metabolite analysis determines the profiling of the metabolites involved in a particular pathway. Metabolite analysis requires specialized extraction procedures, separation techniques, and specific detection methods. GC-MS/MS is the preferred technique for separating low molecular weight metabolites that are either volatile or can be converted into volatile compounds through chemical derivatization before analysis. Derivatization enhances volatility and reduces the polarity of carboxyl (-COOH), amine (-NH<sub>2</sub>), thiol (-SH), and polar hydroxyl (-OH) groups (Halket and Zaikin, 2003).

PCB and biphenyl are known to induce stress responses in bacteria (Storz and Hengge-Aronis, 2000; Chavez et al., 2006). There are few reports on the effect of nutritional stress on growth behaviours and metabolomic profiles of biphenyl/PCB-degrading bacteria (Zoradova et al., 2011; Murinova and Dercova, 2014b). Therefore, the present study aimed to analyze metabolites produced during biphenyl degradation in the four selected isolates (*P. aeruginosa* MAPB-2, *P. plecoglossicida* MAPB-6, *B. anthropi* MAPB-9, and *P. megaterium* MAPB-27). These metabolites include the by-products of biphenyl catabolism and those produced in response to stress induced by biphenyls or PCBs. The metabolomic profiles of these selected isolates grown in biphenyl-supplemented MM were analyzed and compared using GC-MS/MS-based metabolomics. Further, metabolite enrichment analysis was performed to confirm the active

metabolism in the selected bacterial isolates. To our knowledge, this study is the first to investigate metabolomics profiles of the selected bacterial isolates using a GC-MS/MS-based metabolomics approach.

## **4.2. Materials and Methods**

### **4.2.1. Metabolomic analysis of selected bacterial isolates grown in biphenyl-supplemented minimal medium (MM)**

#### **4.2.1.1 Bacterial culture and growth condition**

Experiments were carried out to investigate metabolites in the biphenyl degradation by the selected isolates. The selected bacterial isolates were grown up to the late log phase (OD<sub>600</sub> 0.8) at 30°C, 150 rpm in a shaker. After incubation, the suspension was aseptically transferred to a 15 mL falcon and centrifuged at 8000 ×g for 10 min. The cell pellet was collected and washed twice with MM. The pellet was resuspended in 1 mL of MM to be used as the inoculum. A 0.5 mL cell suspension was added to 4.5 mL of MM supplemented with biphenyl (200 mg L<sup>-1</sup>) and was incubated at 30°C, 150 rpm in a shaker for 72 h in 30 mL screw-capped vials. After incubation, the metabolomic profile of the individual bacterial isolates grown in biphenyl-supplemented was examined. Control was set as MM supplemented with 0.2% glucose inoculated with the selected isolates.

#### **4.2.1.2. Extraction and derivatization of metabolites produced in biphenyl-supplemented MM**

After incubation, the sample was extracted to identify the metabolites produced during biphenyl degradation. The cultivation media was acidified with HCl (6N) to attain a pH of 2, and the sample was extracted three times with ethyl acetate. The ethyl acetate was collected and evaporated by a rotary evaporator.

The extracts were derivatized with 100 µL of bis-(trimethylsilyl) trifluoroacetamide (BSTFA) at 37°C for 60 min and with trimethylchlorosilane (TMCS); (99:1, v/v) at 60°C for 15 min (Hu et al., 2015) and were analyzed by GC-MS/MS TQ8040 (Shimadzu, Japan).

#### **4.2.1.3. GC-MS/MS condition for the separation of the metabolites produced in biphenyl-supplemented MM**

The separation of metabolites produced in biphenyl-supplemented MM was performed on RXi-5SilMS fused silica column with dimensions of 30 m × 0.32 mm × 0.25 µm. The column



temperature was programmed from 50°C (2 min hold) to 80°C at 10°C/min (5 min hold), 100°C rise at 5°C/min (1 min hold), and finally to 300°C at 15°C/min (10 min hold). The carrier gas was helium, and the column flow rate was 1mL/min. The injection and the detector temperatures were 280°C and 300°C, respectively. Compounds separated by gas chromatography were detected by MS operating in full scan mode from  $m/z$  45 to 500 at a scan rate of 1.68 scans. $s^{-1}$ . Metabolites were identified by the mass spectral NIST14 library provided with GC-MS/MS TQ8040.

#### 4.2.1.4. Metabolite set enrichment analysis

Metabolite set enrichment analysis was performed to identify the active metabolism in the biphenyl-grown bacterial cell. The Metabolite identified with GC-MS/MS was converted into a KEGG identifier and was used as input for analysing metabolite by MetaboAnalyst 5.0 software. It is an online software for metabolomic data. For enrichment analysis, well-annotated KEGG ID compounds (i.e., those in pathway libraries & metabolite sets) are mapped.

#### 4.2.2. Statistical analysis

All the experiments were done in triplicates, representing data in  $\pm$  standard error mean. GC-MS/MS software GC-MS/MS Lab solution was used to identify the Metabolite produced by the selected isolates grown in biphenyl-supplemented. MetaboAnalyst 5.0 online software analysis of the metabolites was used for mapping the pathway. The one-tailed test was performed, and a  $p$ -value below 5% is considered a statistically significant result.

### 4.3. Results and discussion

#### 4.3.1. Metabolomics analysis of the selected isolates in biphenyl-supplemented MM

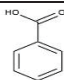
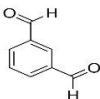
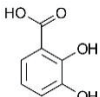
##### Metabolites for biphenyl degradation

Metabolites produced during the biphenyl degradation were extracted and analyzed by GC-MS/MS after the derivatization with BSTFA-TCMS. Benzoic acid ( $m/z=194$ ) was identified as one of the major metabolites during the biphenyl degradation by MAPB-2, MABP-6, MAPB-9, and MAPB-27 at  $R_t$  17.5, 17.3, 17.6, and 17.3 min, respectively (Table 4.1). However, 3-hydroxybenzoic acid was identified in MAPB-2 eluting at  $R_t$  23.1min, while 2,3-dihydroxybenzoic acid was identified in MAPB-9 (25.5 min) and MAPB-27 (25.4 min). The aromatic ring of biphenyl is cleaved by enzyme dioxygenases and converted into 2,3-dihydroxy

biphenyl (2,3-DHB). Another *bphC* dioxygenase converts 2,3-DHB to 2-hydroxy-6-oxo-6-phenylhexa-2,4-dienoic acid (HOPDA), which is further cleaved into benzoic acid and 2-

hydroxypenta 2,4-dienoic acid. Benzoic acid is considered a dead-end metabolite product during biphenyl degradation (Murinova et al., 2014; Pieper and Seeger, 2008). Identifying benzoic acid in the extract confirms that biphenyl degradation occurs in all the selected bacterial isolates. In addition, identifying the hydroxylated benzoic acid (hydroxybenzoic in MAPB-2 and 2,3-hydroxybenzoic acid in MAPB-9 and MAPB-27) in the extracts reveals benzoic acid degradation *via* protocatechuate by *meta* cleavage pathway followed by upper biphenyl degradation pathway and channeled into central metabolism. Benzoic acid catabolic pathways, such as the  $\beta$ - keto adipate pathway, are widespread in the soil environment (Leewis et al., 2016).

**Table 4.1.** Mass spectral features of the TMS-derived metabolites generated from biphenyl

Metabolites	Structure	Isolates	Rt	Mass spectra
Biphenyl degradation				
Benzoic acid		MAPB-2	17.5	194,179,135,105,77,51
		MAPB-6	17.3	
		MAPB-9	17.6	
		MAPB-27	17.3	
3-hydroxy benzoic acid		MAPB-2	23.1	282,267,223,193,149,55
2,3 dihydroxy benzoic acid		MAPB-9	25.525.4	355,249,193,105,73,45
		MAPB-27		

#### 4.3.2. Metabolites identified for carbon, nitrogen metabolism, and fatty acid metabolism formed by the selected bacterial isolates grown in biphenyl-supplemented MM

In general, larger numbers of different metabolites were observed in biphenyl-grown bacterial isolates MAPB-2, MAPB-6, MAPB-9, and MAPB-27 (Table 4.2) than in their respective control. Different organic acid, fatty acid, sugar, and amino acid metabolites were identified by the mass spectral NIST14 library, as shown in Fig. 4.1. The accumulation of organic acids such as oxalic, glycolic, lactic, and 1,4-butanediol in the media, are known metabolites formed during tricarboxylic acid (TCA) cycle, glyoxylate shunt, pyruvate metabolism, propanoate metabolism, amino acid biosynthesis, and fatty acid metabolism as described below.

##### TCA, Glyoxylate, and dicarboxylate metabolism

Organic acid metabolites involved in the citric acid cycle were identified in the biphenyl-supplemented MM. Tricarboxylic acid metabolites identified in the extract were citrate, isocitrate, and *cis*-aconitate. Aconitic acid and itaconic acid identified in MAPB-6 extract are intermediates

---

of the tricarboxylic acid cycle. Dehydration of citric acid results in the formation of *cis*-aconitic acid which transports to the cytosol (Steiger et al., 2016), where it converts to itaconic acid by the enzyme *cis*-aconitic acid decarboxylase. In addition, the metabolites involved in the glyoxylate were also identified in the extract. The glyoxylate cycle and tricarboxylic acid cycle share five of the eight enzymes. The glyoxylate cycle bypasses the carbon dioxide-producing steps of the tricarboxylic acid cycle and is essential for bacteria's acetate and fatty acid metabolism. Several reports indicate that oxidative stress induces glyoxylate shunt in bacteria such as *P. aeruginosa* (Ahn et al., 2016). Bacteria such as *P. aeruginosa* are reported to utilize acetate and fatty acids as sole carbon sources through the glyoxylate pathway.

The glyoxylate shunt is up-regulated when acetyl-CoA is a direct product of a metabolic pathway, for example, *via* the degradation of acetate, fatty acids, and alkanes (Maloy et al., 1980). Metabolites such as acetate, glycine, succinate, citrate, glycolate, oxalate, *cis*-aconitate, (R, R)-tartaric acid, and ethylene glycol identified in the extract of selected isolates are well-known metabolites formed during glyoxylate pathway. A higher accumulation of some intermediates in the glyoxylate pathway, e.g., oxalic acid, was found in the biphenyl-supplemented culture (Fig. 4.1) than in control (Fig. 4.2.). Higher accumulation of oxalates has also been reported in many bacteria under stress. Oxalate has been reported to chelate metals, which may help to alleviate oxidative stress (Singh et al., 2008). Enrichment metabolite analysis showed that glyoxylate and dicarboxylate metabolism was active in all the selected bacterial isolates (Fig. 4.3A-D). Fatty acid biosynthesis metabolism is interconnected with the Glyoxylate pathway. When higher fatty acids are oxidized into acetyl-CoA without forming pyruvate, acetyl-CoA enters the glyoxylate cycle. Acetyl-CoA produced either from acetate or by  $\beta$ -oxidation of fatty acids enters into the TCA cycle. It condenses with oxaloacetate to form citrate, which further isomerizes to isocitrate, wherein isocitrate cleaves by isocitrate lyase to form glyoxylate and succinic acid. Succinic acid then metabolizes in the TCA cycle, while glyoxylate condenses with a second molecule of acetyl- CoA to form malate. In the case of MAPB-27 (Fig.4.3D), this metabolic pathway was most prominent than the other metabolism. Therefore, the observation highlights that selected bacteria grown in the biphenyl-supplemented MM combat stress (nutritional stress in this case) *via* glyoxylate pathway to provide cellular precursors from one available carbon source.

---

### Salicylic acid biosynthesis

Salicylic acid (SA) is a plant defense hormone that regulates various cellular processes. In addition, many bacterial spp. also produces SA as an intermediate compound, which ultimately incorporates into salicylate-based siderophores. The bacterial salicylate production is distinct from that of plants. Under an iron-deprived environment, salicylic acid biosynthesis is reportedly involved in producing ferric-ion-chelating molecules, salicyl-derived siderophores catecholate (Sritharan, 2016) especially in PGPR bacteria. Salicylic acid is a secondary metabolite produced by most bacteria (Mishra and Baek, 2021), such as *Pseudomonas*, *Bacillus*, *Achromobacter*, and *Mycobacteria* (Khan et al., 2018; Schalk et al., 2020). Salicylic acid was identified in MAPB- 6, while alkylated salicylic acid (6-[12(Z)-Nonadecenyl] salicylic acid) was found in MAPB-2, MAPB-9, and MAPB-27. The observation correlates with the results described in the previous chapter where MAPB-2 and MAPB-6 were found to be siderophore-producing bacteria. SA has also been reported as an inducer of PCB degradation and its potential to enhance the biodegradation of PCBs (Hu et al., 2014). The salicylate catabolic gene cluster is located about 6 kb downstream from the *bph* gene cluster in *P. pseudoalcaligenes* KF707, and *bph* and *sal* gene clusters were found to be cross-regulated.

### Sugar moieties and monosaccharide metabolites in EPS

EPS is the heterogeneous matrix of polymers that contain mainly long-chain polysaccharides, lipids, nucleic acids, and proteins (McSwain et al., 2005). EPS is synthesized intracellularly either during growth, late logarithmic, or stationary phase. They also accumulate extracellularly on the cell surface, protecting the bacterial cells by stabilizing membrane structure and serving as carbon and energy reserves. Some sugar moieties and molecules, such as fucopyranose, cellobiose, melibiose, and lactose, were identified in the MAPB-9 extract, while D-galactose and D-sorbitol in MAPB-6 and MAPB-27. D-galactose is the hydrolysis product of lactose and is reported as an exopolysaccharide (EPS) component of the biofilm matrix produced by *Bacillus* (Chai et al., 2012). We also observed rhamnopyranose, a sugar associated with rhamnolipid, a biosurfactant in MAPB-2 extract. Several biosurfactant-producing bacteria, such as *Pseudomonas*, *Ochrobactrum*, and *Bacillus*, have been isolated from contaminated environments (Joy et al., 2017). Moreover, the biosurfactant-producing property of the selected isolates has already been described in Chapter 3. Other metabolites such as lactate, L-rhamnose, D-sorbitol, and L-fucose have known metabolites in fructose and mannose metabolism.

**Table 4.2.** List of identified metabolites in MAPB-2, MAPB-6, MAPB-9, and MAPB-27 grown in biphenyl

Metabolites	Retention time (R <sub>t</sub> )			
	MAPB-2	MAPB-6	MAPB-9	MAPB-27
1,4-Butanediol	8.9	9.0	-	-
Lactic acid	11.5	11.7	11.7	11.6
Methoxyacetic acid	-	-	11.9	-
Hexanoic acid	11.9	12.2	12.2	12.0
Acetophenone	-	12.1	-	11.9
Glycolic acid	12.0	12.3	12.3	12.1
Hydracrylic acid	-	14.4	14.3	14.3
2-Hydroxybutyric acid	15.0	-	15.1	15.1
L-Norvaline	-	-	15.3	15.5
4-Hydroxybutanoic acid	-	-	-	16.1
Malonic acid	16.1	16.3	16.4	16.3
3-Hydroxyisovaleric acid	16.6	16.8	16.5	16.4
Arginine (ester)	17.0	-	17.0	-
Oxalic acid	17.1	-	17.3	17.2
Benzoic acid	17.5	17.3	17.4	17.3
Octanoic acid	-	-	17.8	-
Benzeneacetic acid	18.8	-	18.8	-
Butanedioic acid (succinic acid)	19.2	19.0	18.7	18.8
N-acetyl L-Alanine	19.0	-	-	-
N-acetylglycine	19.3	-	-	-
L-Asparagine	19.5	-	-	-
Salicylic acid	-	19.5	-	-
Nonanoic acid	-	19.8	19.9	19.7
2,6-Bis(tert-butyl)phenol	22.9	22.8	22.9	22.8
3-Hydroxybenzoic acid	23.0	-	-	-
Aconitic acid	-	25.2	-	-
Itaconic acid	-	25.5	-	25.5
2,3-Dihydroxybenzoic acid	-	-	25.4	25.4
Isovanillic acid	-	-	24.7	-
Citric acid	-	-	-	26.3
Levoglucozan	-	27.4	-	25.0
Dulcitol	27.5	-	-	-
D-Sorbitol	-	-	-	27.5
3-Methyladipic acid	-	29.8	29.8	-
N-Acetyltyrosine	-	-	-	29.4
D-(+)-Galactose	-	29.6	-	29.6
Dehydroabiestic acid	31.8	-	-	31.8
(R)-(+)-Citronellic acid	-	32.2	-	32.2
L-(+)-Rhamnopyranose	32.1	-	-	-
Fucopyranose	-	-	32.7	-
D-(+)-Cellobiose	-	-	33.1	-
D-Lactose	-	-	33.8	-
Melibiose	-	-	34.4	-
1-Monooleoylglycerol	34.5	-	-	32.4
6-[12(Z)- Nonadecenyl]salicylic acid	35.4	-	35.4	35.4

Onbasli and Aslim (2009) reported high production of EPS by *P. aeruginosa* B1, *P. fluorescens* B5, *P. stutzeri* B11, and *P. putida* B15 grown in MM supplemented with various organic pollutants (2,4-D, benzene, BTX, and gasoline) as sole carbon source.

Also, EPS containing the neutral sugars (glucose, galactose, and pyruvate) have been reported in *Pseudomonas* sp., such as *P. putida*, *P. fluorescens* when grown in an organic compound as a sole source in MM (Ludbrook et al., 1997). Royan et al. (1999) demonstrated that *P. mendocina*, when grown in sodium benzoate as the sole source of carbon, has EPS content composed of rhamnose, fucose, glucose, ribose, arabinose, and mannose. From the above discussion, it is clear that bacteria produce EPS under stress conditions. Furthermore, the production of biosurfactant help in the solubilization of biphenyl and PCBs, making them bioavailable for degradation (Franzetti et al., 2010, Chakraborty and Das, 2014). Thus, EPS and biosurfactants play an important role in degrading biphenyl and PCBs, further aiding in their bioremediation.

### **Fermentation products**

Fermentation is an anaerobic process in which bacteria use organic molecules as their final electron acceptor to produce fermentation end-products. Different fermentative products, such as lactic acid, malonic acid (propanedioic acid), 2,3-butanediol, acetoin, and butanedioic acid (succinic acid), were found in the extract of MAPB-2, MAPB-6, MAPB-9, and MAPB-27 grown in biphenyl-supplemented medium (Table 4.2). The selected bacteria are known to be facultative anaerobes; therefore, in the screw cap vials, there is a chance of low oxygen or anaerobic condition after some time. Fermentative lactic acid is converted to propanedioic acid (malonic acid). Also, acetoin is produced in an intermediate process of the fermentation of 2,3-butanediol and was identified in *P. megaterium* MAPB-27. Acetoin has been reported to be produced by *Bacillus* strains (Xiao and Xu, 2007). Butanoate metabolism and propionate metabolism found in the extract of MAPB-2, MAPB-6, and MAPB-27 indicate fermentation of peptides and amino acids accumulated in the media.

### **Amino acid metabolism**

Amino acid accumulation (Jozefczuk et al., 2010) is also reported in bacterial cells under stress. The amino acid accumulation could be either for the synthesis of new protective proteins (Jozefczuk et al., 2010) or due to increased degradation of the protein.



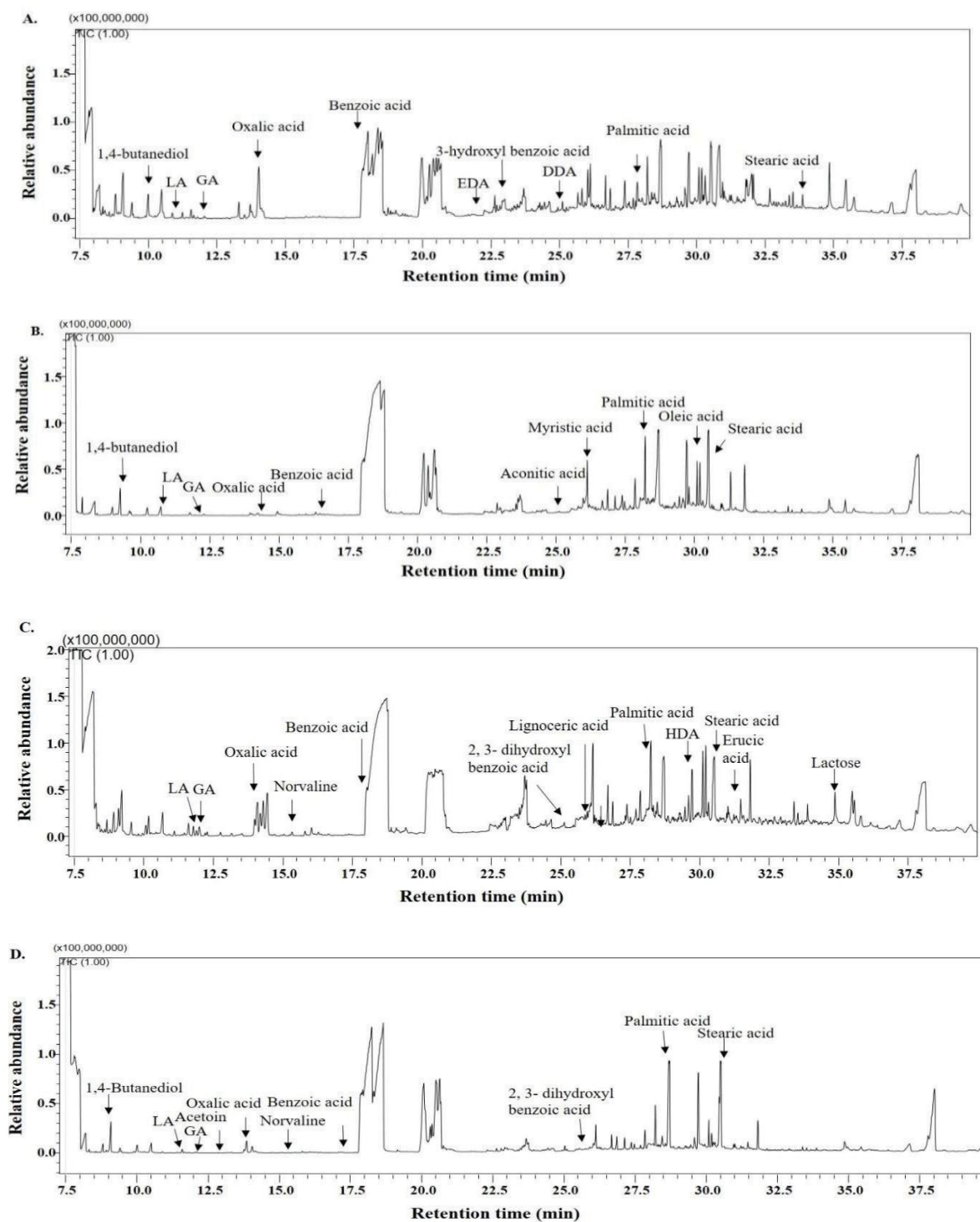


**Fig. 4.1.** GC-MS/MS analysis of the metabolites produced during biphenyl degradation by the selected bacteria grown on MM supplemented with 200 mg L<sup>-1</sup> biphenyl for 48 h. GC chromatograph represents the peaks of organic acids, fatty acids, and sugar, amino acids. (A) benzoic acid and 3-hydroxy benzoic acid intermediate produced by MAPB-2, (B) benzoic acid produced by MAPB-6, (C) benzoic acid and 2,3- dihydroxy benzoic acid intermediate produced by MAPB-9, and (D) benzoic acid and 2,3- hydroxybenzoic acid intermediate produced by MAPB-27.

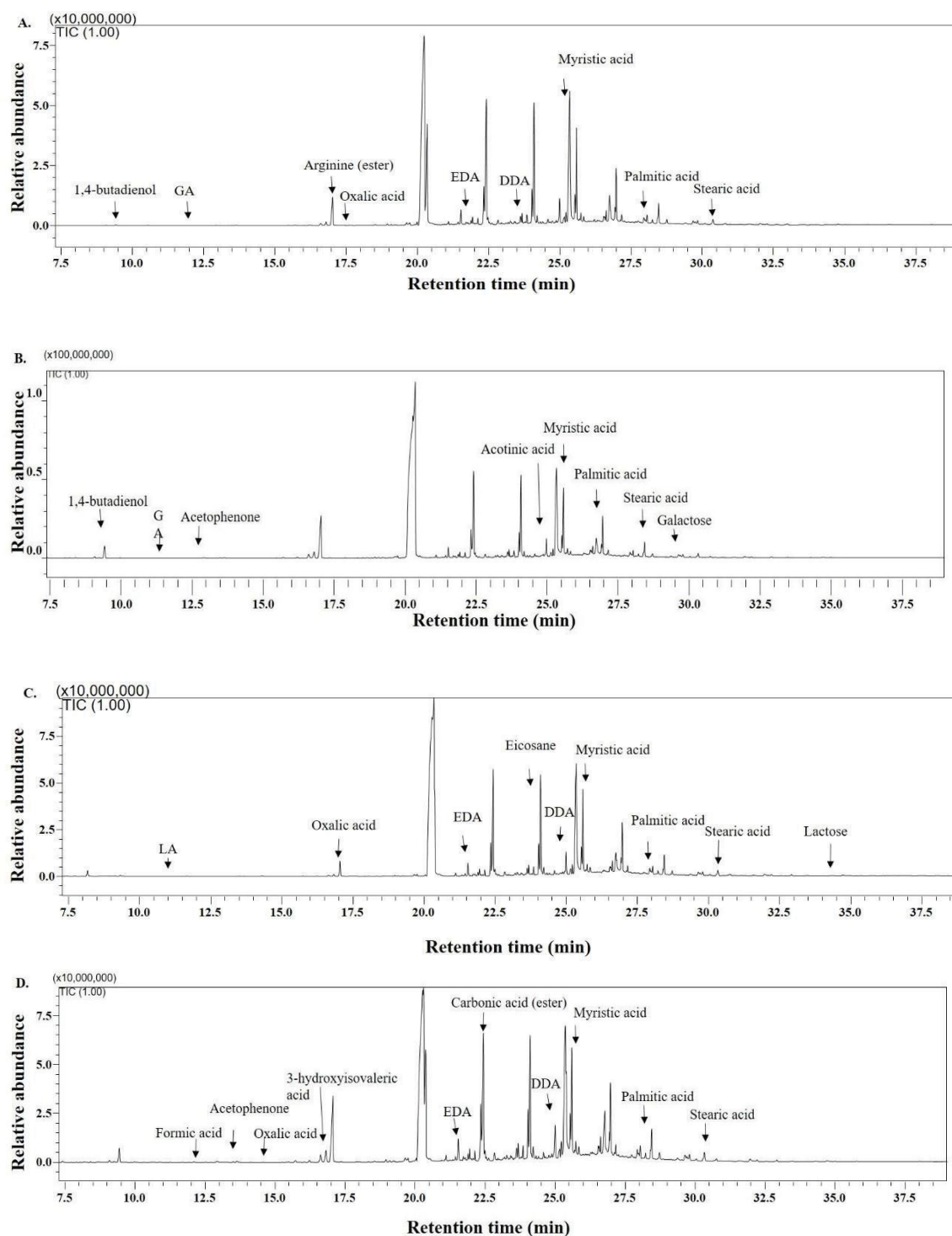


**Fig.4.2.** GC-MS/MS analysis of the metabolites produced by the selected bacteria grown on LB for 48 h. GC chromatograph represents the peaks of organic acids, fatty acids, and sugar, amino acids. (A) MAPB-2, (B) MAPB-6, (C) MAPB-9, and (D) MAPB-27. LA, GA, EDA, DDA, and HAD represent lactic acid, glycolic acid, 11,14-eicosadienoic acid, dodecenoic acid, and heptadecanoic acid, respectively.

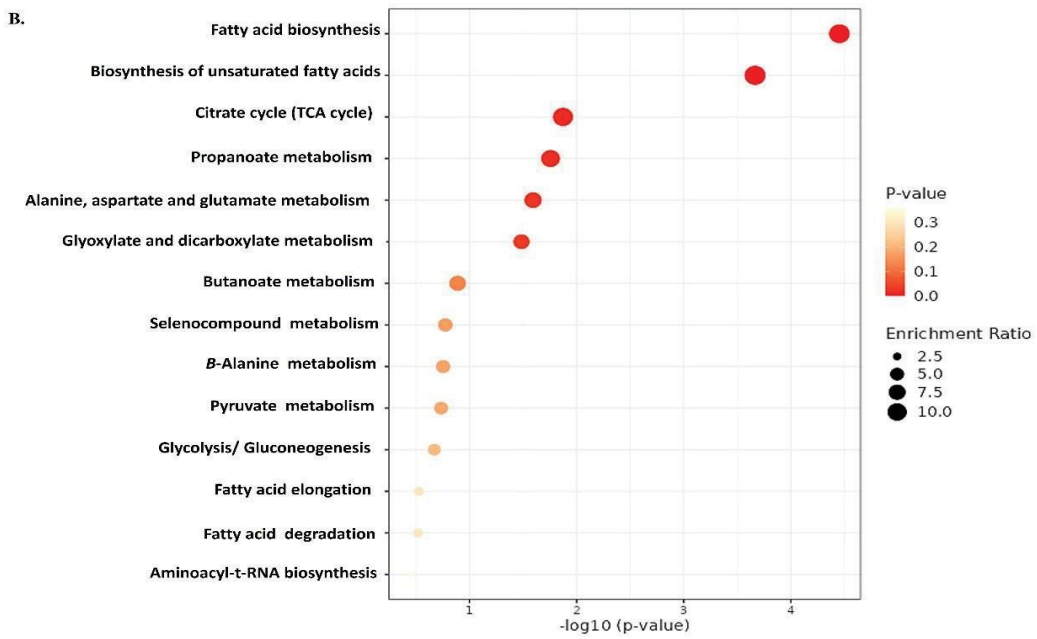
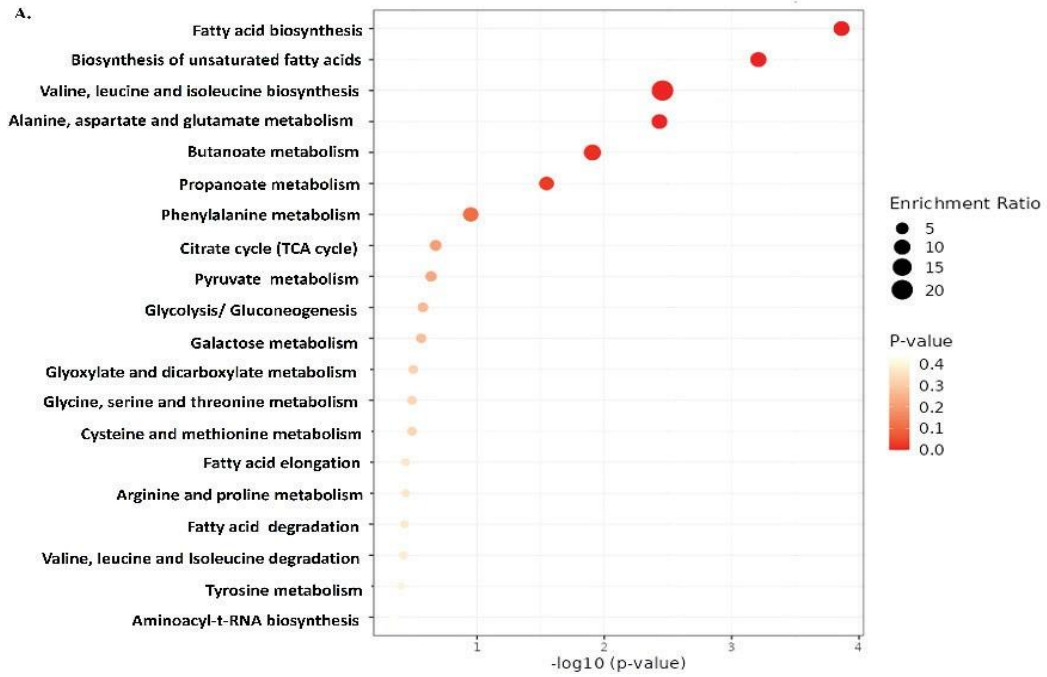
Metabolites such as glycine, 2-oxobutanoate, L-asparagine, citrate, and L-isoleucine identified in the extract are reported to be involved in amino acid biosynthesis metabolism. Acetyl derivative amino acids such as aceturic acid (N-acetyl lysine), N-acetyl L-alanine, and L-asparagine were present in MAPB-2. At the same time, N-acetyl tyrosine was identified in the MAPB-27 extract. 3-Hydroxyisovaleric acid is a by-product of leucine metabolism that was identified in all the isolates. MAPB-27. LA, GA, EDA, DDA, and HAD represent lactic acid, glycolic acid, 11,14-Eicosadienoic acid, dodecenoic acid, and heptadecanoic acid, respectively.

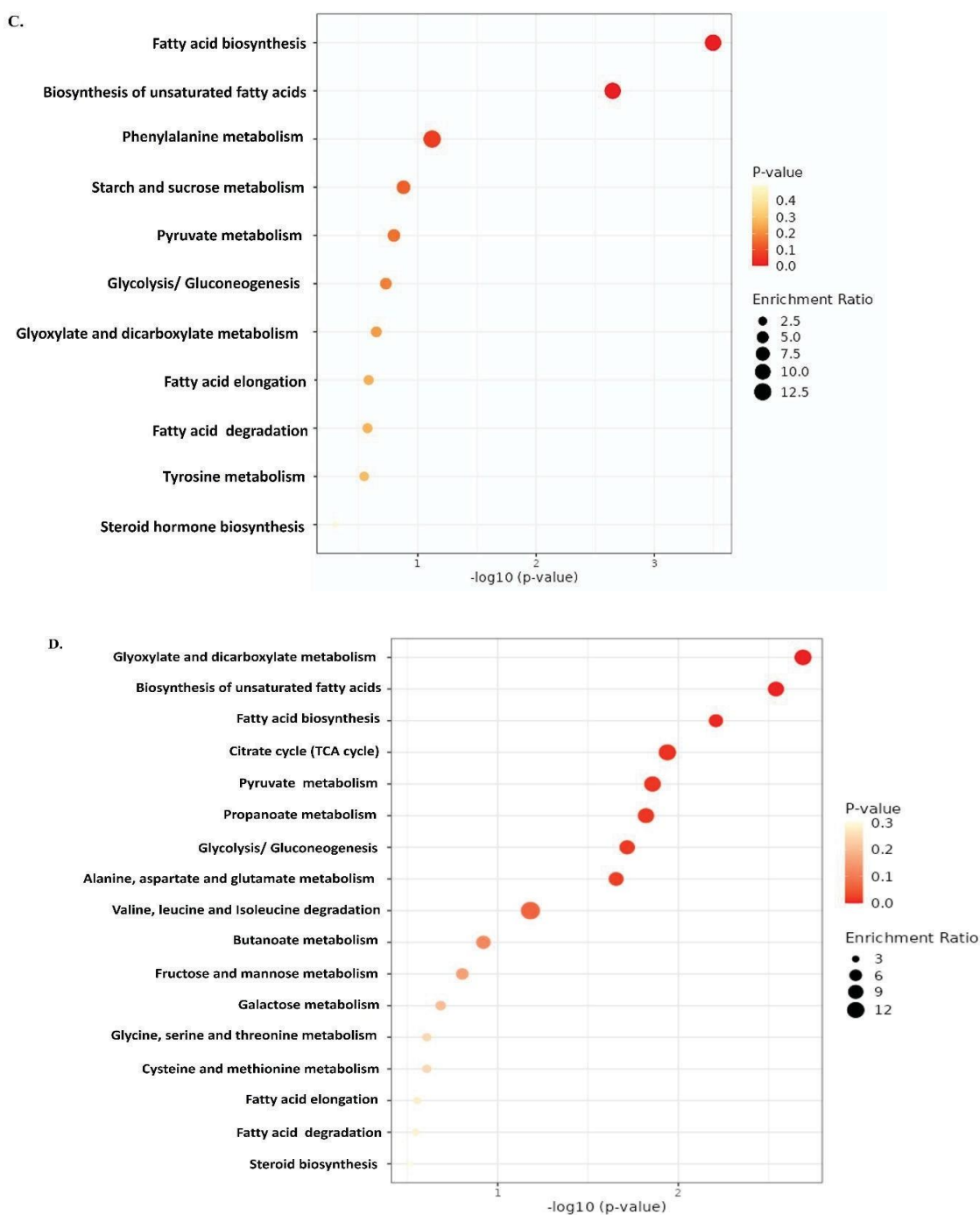
Glutamate, another amino acid, was present in all the selected isolates except MAPB-9. Glutamate metabolism is also found to be active in bacterial stress (Feehily and Karatzas, 2013), resulting in the accumulation of  $\gamma$ -aminobutyrate (GABA). Moreover, glutamate is a key metabolite that links nitrogen and carbon metabolism (Walker and Donk, 2016). Glutamate metabolism in bacterial stress responses results in glutamate decarboxylation (GAD) of glutamate to GABA. The by-product of the GAD system is GABA, which is the substrate of the GABA shunt pathway. This suggests that the GAD system might play a role in survival or growth under oxygen limitation. The role of the GAD system under anaerobic conditions might be linked with the acidification of the medium and the intracellular milieu that occurs during fermentation. The production of GABA during fermentation has been studied extensively in lactic acid bacteria (Siragusa et al., 2007). The lactic acid produced during fermentation by the bacteria lowers the pH. The acidic conditions created lead the lactic acid bacteria to utilize the GAD system and export GABA.

### **Fatty acid metabolism**

Fatty acids are essential membrane components and important sources of metabolic energy in all organisms. Thus, fatty acid degradation and biosynthesis pathways must be switched on and off according to the availability of fatty acids to maintain membrane lipid homeostasis (Zhang et al., 2008). As depicted in Fig. 4.3 (A-D), two main enriched metabolic pathways out of 25 metabolisms are fatty acid metabolism and glyoxylate and dicarboxylate pathway.

Biphenyl-induced stress increases saturation and changes in branched fatty acids in total lipids (TL). Alteration in the fatty acid composition of membrane lipids is one of the critical adaptation mechanisms of bacteria against organic compounds such as biphenyl. Bacteria undergo modification in the cell membrane as an adaption mechanism for survival.





A relatively higher abundance of saturated fatty acids was observed in the presence of biphenyl as compared to the control in all experimental sets. The TMS derivative stearic acid, palmitic, 11,14-eicosadienoic acid, and 5-dodecenoic acid (Z) were found in the extract of MAPB-2, MAPB-6, MAPB-9, and MAPB-27 showing a high percentage of fatty acid in the total lipid (Fig. 4.1.) than in control (Fig. 4.2). Previous report suggests that PCB accumulation results in increased fatty acid saturation of bacterial membranes (Zoradova et al., 2011).

Membrane stress responses modify the cell membrane by modulating the length, branching, and saturation of the fatty acid acyl chains, altering membrane lipid composition, and synthesizing proteins that modify or protect the membrane (Willdig and Helmann, 2021). The fatty acid profile of selected isolates is depicted in Fig. 4.4. It showed the presence of 11,14- eicosadienoic acid, 5-dodecenoic acid, tridecanoic acid, myristic, palmitic, and stearic at Rt 21.6, 24.2, 25.6, 26.4, 27.9, and 30.5 min, respectively in MAPB-2. MAPB-6 consist of palmitic acid, 8-octadecenoic acid, heptadecanoic acid, 11-octadecenoic acid (E), and stearic acid, at Rt 28.7, 29.2, 29.6, 30.3, and 34.4 min, respectively.

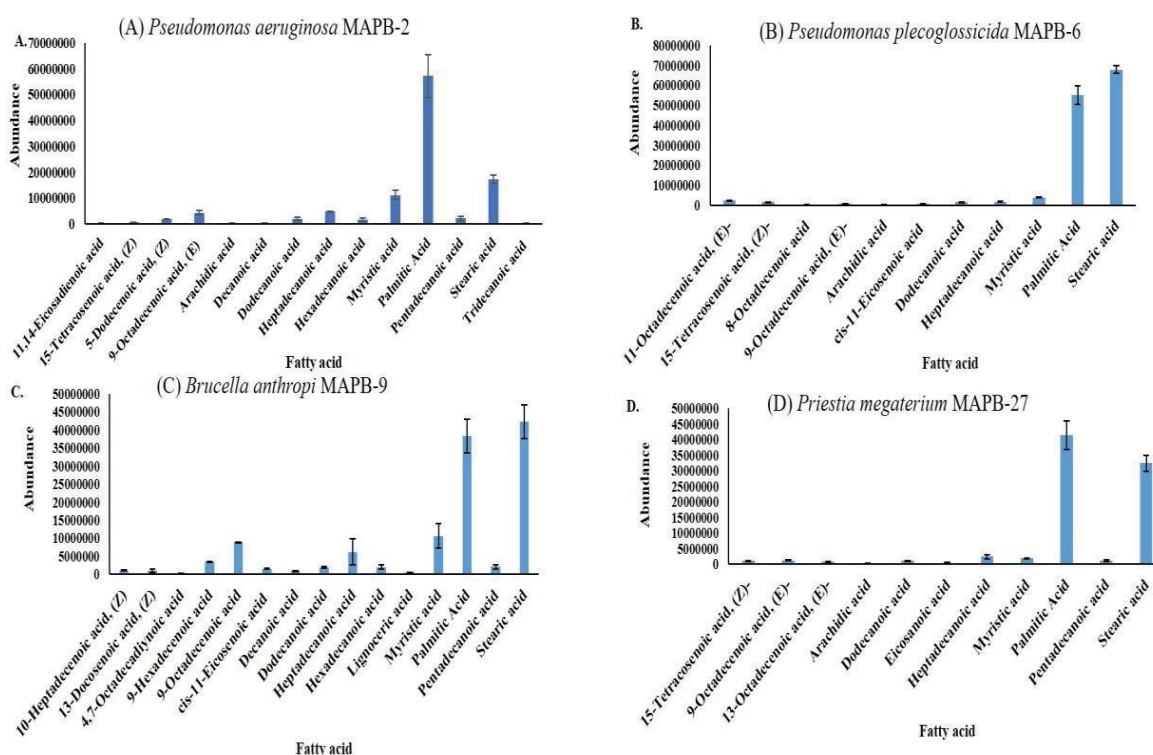


**Fig. 4.4.** GC-MS/MS fatty acid composition profile of the selected bacterial isolates during biphenyl degradation in biphenyl supplemented MM. (A) *P. aeruginosa* MAPB-2 (B) *P. plecoglossicida* MAPB-6 (C) *B. anthropi* MAPB-9 (D) *P. megaterium* MAPB-27.



MAPB-9 extract comprise of lignoceric acid, palmitic Acid, 9-octadecenoic acid, (E), stearic acid, 13-docosenoic acid at  $R_t$  26.5, 28.7, 30.3, 30.5, and 31.2 min, respectively. Myristic acid, palmitic acid, and stearic acid were identified at  $R_t$  26.6, 28.7, and 30.5 min, respectively, in the MAPB-27 extract. In all the extracts, the total lipid comprised of high levels of palmitic (C16:0) and stearic acid (C18:0) content, as shown in Fig. 4.4. Previous studies suggest that increased levels of stearic and palmitic acid, a fully saturated fatty acid, resulting in the stiffening of the cell membrane, thereby reducing its permeability to small molecules (Duldhardt et al., 2010) under stress. An increase in saturated fatty acids rather than unsaturated has been reported to be the most common adaptive response in the metabolism of toxic pollutants (Heipieper and de Bont, 1994). The possible reason for the relatively high abundance of saturated fatty acid identified in the extracts could be cell adaptation, including the bioavailability of the biphenyl to the bacterial cell for degradation. Therefore, the accumulation of fatty acids in all the selected bacterial isolate extracts is required to combat biphenyl-induced nutritional stress.

Fatty acid biosynthesis and biosynthesis of unsaturated fatty acid metabolism are found to be the most active metabolism in all the selected bacterial isolates. (Fig. 4.3A-D). The biosynthesis of unsaturated fatty acids is reportedly linked to the membrane fluidity in bacteria such as *E. coli* cells under environmental stress conditions (Janßen and Steinbuechel, 2014). Further, fatty acid degradation releases free acetyl-CoA, which can be reused for energy production via the TCA cycle or consumed to synthesize fatty acid.

Overall, the metabolomic profiling results and the metabolism enrichment analysis indicate that the selected bacteria showed an adaptive mechanism to survive under biphenyl-induced stress conditions. It has been reported that the evolution of metabolic pathways helps to regulate cellular function in response to nutrition and pollution stress (Storz and Hengge-Aronis, 2000). Thus, the present work identifies biphenyl-degraded metabolites by the selected bacterial isolates and other metabolites produced in metabolic processes in biphenyl-supplemented media. The study also indicated the enabled abilities of the isolates to utilize new substrates upon exposure to nutritional stress in the contaminated environment. The result also enhances the understanding of the essential cellular processes to predict the survival and activity of bacterial isolates exposed to such adverse conditions for selecting potential PCB degraders.

**Chapter V**

**Optimization of Consortia-Based Bacterial  
Formulation and Evaluation of  
Bioformulation for Enhanced PCB  
Degradation**

## 5.1. Introduction

PCBs' biodegradation ability is present mostly in bacteria isolated from PCB-contaminated sites. Several reports revealed that isolated bacteria are best-characterized PCB degraders with PCB degradation ability and adaptation to PCB-contaminated soil (Dudasova et al. 2014). As discussed in earlier chapters, PCBs are complex mixtures of various congeners in a sequestered form in the soil, thus making them difficult to bioremediate. To add to the woes, the varying degree of chlorination on the PCBs makes it more challenging for a single bacterium to degrade all or even most of the PCB congeners in the contaminated environments. Thus, a careful understanding of the individual bacterium for degradation potential is insufficient for successful bioremediation of such complex PCB congeners. Applying a combination of bacterial cultures could be a well-defined approach as it would have a higher degradation potential to remove a mixture of PCBs than a single bacterial culture (Horváthová et al., 2019). However, there is very scarce information on using bacterial consortia to remediate PCB-contaminated soil. A major challenge faced during the development of the bioremediation strategy is the response that is given by the bacterial consortia to the polluted environment. The bioremediation's success depends upon the consortia's ability to survive under harsh conditions such as pH, the presence of inhibitory compounds, osmotic stress, etc. Microencapsulation of bacterial consortia not only provides viability but also controls the release rate of microbes, purity of the strains encapsulated, genetic stability, etc. (Schoebitz et al., 2013; Dzionek et al., 2016; Bayat et al., 2015). Combining microbe and plant-mediated bioremediation approaches can be the most promising approach with enhanced PCB removal from the soil. *B. nigra* plant has been reported to support an increase in the microbial population in PCB-contaminated soil (Pino et al., 2019).

In previous chapters 3 & 4, we identified the potential degraders *P. aeruginosa* MAPB-2, *P. plecoglossicida* MAPB-6, *B. anthropi* MAPB-9, and *P. megaterium* MAPB-27 for biphenyl and PCB -77 degradation, along with their optimal growth conditions and possible metabolite formation. Our data indicated that adding biphenyl and PCBs increased the cell survival ability and adaptation responses of the bacterial isolates (Zoradova et al., 2011; Zoradova-Murinova et al., 2012). In addition to biodegradation ability, the selected bacterial isolates also possess PGPR properties that promote plant growth. Thus, the current chapter aimed to examine the effect of the selected PCB degraders individually and in combination when grown on a PCB congener mix. The development bioformulation by optimization of consortia from the selected bacteria, namely MAPB-2, MAPB-6, MAPB-9, and MAPB-27, that could degrade the PCB congeners was

prepared. The best consortium was selected and encapsulated in sodium alginate beads. Further, a pot study using the *B. nigra* plant was conducted to evaluate the developed bioformulation for its PCB congener's degradation efficiency.

## 5.2. Materials and methods

### 5.2.1. Preparation of bacterial culture for consortia of selected isolates

The PCB degradation ability of MAPB-2, MAPB-6, MAPB-9, and MAPB-27 and their consortia were examined. To examine the PCB congener biodegradation ability of the individual bacterial isolates, cell suspension of MAPB-2, MAPB-6, MAPB-9, and MAPB-27 was prepared as per section 4.2.1.1.

#### Biodegradation assay media:

For the biodegradation of PCBs by bacterial consortia, 10 % (v/v) inoculum was used. In consortia, an equal proportion of each isolate was used. A 0.5 mL resulting cell suspension was added to 4.5 mL MM supplemented with PCB congeners ( $1\text{mg mL}^{-1}$ ). The inoculum of individual isolates and consortia was prepared as shown in Table 5.1. and the isolates were co-cultivated in LB to investigate their compatibility among them. The monoculture and consortia were incubated at 30°C and 150 rpm. MM supplemented with PCB congeners without inoculum was used as a control. After 30 d of incubation, the contents were extracted using iso-octane to analyse the residual PCBs.

**Table 5.1.** List of bacterial isolates and their respective proportions used to prepare bacterial consortia for PCB congener degradation

Bioformulation	Bacterial isolate(s)	Ratio
1	MAPB-2	--
2	MAPB-6	--
3	MAPB-9	--
4	MAPB-27	--
5	MAPB-2+MAPB-6	1:1
6	MAPB-2+MAPB-9	1:1
7	MAPB-6 + MAPB-9	1:1
8	MAPB-2 + MAPB-6 + MAPB-9	1:1:1
9	MAPB-2 + MAPB-6 + MAPB-27	1:1:1
10	MAPB-2 + MAPB-9 + MAPB-27	1:1:1
11	MAPB-2+ MAPB-6+ MAPB-9+ MAPB-27	1:1:1:1
12	Control	Without inoculum

### 5.2.2. Biodegradation of PCB congener mix by consortia of the selected bacterial isolates

**GC-MS/MS analysis of PCB congener mix:** After incubation, the PCB congener mix was extracted from the MM media with isooctane. First, 10 mL of isooctane was added to each flask, and these were placed in an ultrasonic bath for 5 min to release the residual PCBs from the glass vial and the bacterial cell. The entire flask content was then moved to a separating funnel for intensive shaking. After the liquid phases settled, the water phase was released to the second separating funnel for the second extraction. The Isooctane phase was dehydrated using anhydrous  $\text{Na}_2\text{SO}_4$ .

PCB extracts were subsequently analyzed by GC-MS/MS with SH RTX-5Sil column (Shimadzu, Japan) with the following temperature program: Initial oven temperature 80°C (1 min hold) with 25°C/min increase to 150°C hold for 1min and 4°C/min to 280°C hold 2 min. Injection, ion source, and detector temperature were kept at 280°C, 280°C, and 300°C, respectively (Tu et al., 2010; Murinova et al., 2014). PCB congener mix (Certified reference material) SQC068-50g soil (Sigma-Aldrich, USA) was used. The PCB congener mix contained the following: Tri homolog [PCB 28 (2,4,4'-)], Tetra homolog [PCB 52 (2,2',5,5'-), PCB 77 (3,3',4,4'-), PCB 81 (3,4,4',5'-)], penta homolog [PCB 101 (2,2',4,5,5'-), PCB 105 (2,3,3',4,4'-), PCB 114 (2,3,4,4',5'-), PCB 118 (2,3',4,4',5'-), PCB 123 (2,3', 4,4', 5'-), PCB 126 (3,3',4,4',5'-)], hexa homolog [PCB 138 (2,2',3,4,4',5'-), PCB 153 (2,2',4,4',5,5'-), PCB 156 (2,3,3',4,4',5'-), PCB 157 (2,3,3',4,4',5'-), PCB 167 (2,3',4,4',5,5'), PCB 169 (3,3', 4,4', 5,5'-)], and hepta homolog [PCB 180 (2,2',3,4,4',5,5'-), PCB 189 (2,3,3', 4,4', 5,5' -)]. PCB congener mix degradation was evaluated *via* Selective Ion Monitoring (SIM) mode-based targeted selection of retention time and *m/z* for these PCB congeners.

### 5.2.3. Encapsulation of bacterial consortia in Ca-alginate beads

The calcium alginate bead encapsulation of bacterial consortium is required for bacterial survival and slow release of the entrapped bacteria into the soil (Bashan 2002). Bacterial inocula were prepared as per the protocol in section 5.2.1. Each bacterium's bacterial suspension was used to prepare bioformulation consisting of individual or consortia of selected isolates. 3% (*w/v*) sodium alginate suspension was prepared in autoclaved MM. The alginate solution and bacterium suspension (OD=0.8) were mixed thoroughly according to the method provided by Bashan et al., 1989 with slight modifications. For bioformulation of consortia, bacterium MAPB-2, MAPB-6, MAPB-9, and MAPB-27 in a ratio of 1:1:1:1 (*v/v*) and 1:1:2:2 (*v/v*) were added to the alginate solution. The suspension was then added to a sterile 20 mL syringe and extruded with a 31G

needle dropwise by using a syringe pump at a 120 mL/min flow rate. Dropwise suspension was added to sterile precooled 0.2M CaCl<sub>2</sub> solution with mild agitation. The bioformulations prepared were allowed to harden at room temperature. Beads without bacteria were kept as a control. The beads were stored at 4°C for the pot study experiment (Daâssi et al., 2014).

#### **5.2.3.1. Bacterial count and FESEM analysis of encapsulated bacterial consortia**

The viable bacterial count of the encapsulated MAPB-2, MAPB-6, MAPB-9, and MAPB-27 was performed. Bioformulated beads (100 mg) were resuspended in 10 mL phosphate buffer (pH 7.0) and homogenized for 20 min. The total bacterial count was determined by serial plate count method after 48 h incubation at 30°C. FESEM analysis of the surface of the alginate bead formulated bacterium and consortium was done from the above-homogenized suspension in section 5.2.3.1. Further protocol of alcohol dehydration and fixing was the same as reported in section 3.2.9.

#### **5.2.4. Evaluation of biodegradation potential of selected consortium and its effect on plant growth**

##### **5.2.4.1. Preparation of soil and PCB spiking**

A pot experiment was performed to evaluate the effectiveness of the selected consortium #11 for the biodegradation of PCB congeners and on the growth of *B. nigra* in soil spiked with PCB congeners. Each autoclaved pot was filled with PCB congener spiked sterile soil mix(1mg/g). Unspiked soil was used as a control. A different set of treatment and control groups were prepared and the detail is provided in Table. 5.2.

##### **5.2.4.2. Effect of bacterial bioformulation on the growth of *B. nigra***

Seeds were surface sterilized with 0.1% HgCl<sub>2</sub> for 2 min and washed three times with autoclaved MQ water. The sterilized seeds were soaked in pre-sterilized damp cotton Petri dishes and kept in the dark for three days for germination. After germination, the seeds were transferred to the PCB congener mix spiked soil. 100 mg encapsulated consortia were placed below the soil surface at an initial 1 x10<sup>8</sup> CFU/mL concentration. The pots were kept for 45 days in a growth chamber (Lab Tech, South Korea) maintained at 22/16°C with 16 h/ 8 h dark photoperiod with 70% relative humidity (Chekol et al., 2004).

**Table 5.2.** Preparation of bioformulation of selected isolates/consortia for PCB congener mix degradation in a pot experiment.



## Chapter V

Condition	Soil	Plant	Bioformulation
Treatment 1 (T1)	PCB congener spiked soil (300 mg/300g)	<i>B. nigra</i>	Consortium #11(1:1:1:1) <i>P. aeruginosa</i> MAPB-2 <i>P. plecoglossicida</i> MAPB-6 <i>B. anthropi</i> MAPB-9 <i>P. megaterium</i> MAPB-27
Treatment 2 (T2)	PCB congener spiked soil (300 mg/300g)	<i>B. nigra</i>	Consortium#11 (1:1:2:2) <i>P. aeruginosa</i> MAPB-2 <i>P. plecoglossicida</i> MAPB-6 <i>B. anthropi</i> MAPB-9 <i>P. megaterium</i> MAPB-27
Treatment 3 (T3)	PCB congener spiked soil (300 mg/300g)	-	Consortium#11 (1:1:1:1) <i>P. aeruginosa</i> MAPB-2 <i>P. plecoglossicida</i> MAPB-6  <i>B. anthropi</i> MAPB-9 <i>P. megaterium</i> MAPB-27
Treatment 4 (T4)	PCB congener spiked soil (300 mg/300g)	-	Consortium #11(1:1:2:2) <i>P. aeruginosa</i> MAPB-2 <i>P. plecoglossicida</i> MAPB-6 <i>B. anthropi</i> MAPB-9 <i>P. megaterium</i> MAPB-27
Treatment 3 (T5)	PCB congener spiked soil (300 mg/300g)	<i>B. nigra</i>	<i>P. aeruginosa</i> MAPB-2
Treatment 4 (T6)	PCB congener spiked soil (300 mg/300g)	<i>B. nigra</i>	<i>P. plecoglossicida</i> MAPB-6
Treatment 5 (T7)	PCB congener spiked soil (300 mg/300g)	<i>B. nigra</i>	<i>B. anthropi</i> MAPB-9
Treatment 6 (T8)	PCB congener spiked soil (300 mg/300g)	<i>B. nigra</i>	<i>P. megaterium</i> MAPB-27
Control 1 (C1)	PCB congener spiked soil (300 mg/300g)	-	-
Control 2 (C2)	Soil	<i>B. nigra</i>	-
Control 3 (C3)	PCB congener spiked soil (300 mg/300g)	<i>B. nigra</i>	-

Planted pots without consortia and individual encapsulated bacteria were used as control. After

incubation, the stem and roots were washed for length measurement. The total number of leaves

and buds was counted in each treated and control sample. At the end of the incubation period, soil samples were collected to determine the PCB congener degradation and microbial enumeration.

### **FESEM analysis and microbial enumeration**

Rhizospheric soil and root samples were analyzed for bacterial association with the root of the *B. nigra*. The protocol for the FESEM analysis was the same as reported in section 5.2.3.2. The microbial count was done as per the serial dilution plate count method.

### **5.2.5. Evaluation for PCB congener mix degradation by bioformulations in pot study experiment**

#### **PCB congener extraction and GC-MS/MS analysis**

After the incubation period, 100 g of soil spiked with PCB congeners was extracted with a mixture of n-hexane and acetone (1:1; v/v) and placed in an ultrasonic bath at 30 °C, 15 Hz for 20 min to release the residual PCBs from the bacterial cell. Further, residual PCBs in the sediment were extracted in n-hexane with a Soxhlet extraction apparatus kept at 40°C for 16 h. The solvent was collected and dehydrated by filtration *via* anhydrous Na<sub>2</sub>SO<sub>4</sub>. The solvent was then evaporated, and the concentrated extract was resuspended in isooctane. GC-MS/MS analysis was performed to determine the percent degradation of PCB congener. The GC conditions were the same as reported in section 5.2.2.

#### **Metabolite profiling of the treated and controlled samples**

Metabolite profiling of the treated and controlled samples of the pot study experiment was performed to identify the metabolite produced during PCB congener mix degradation. The extracts obtained in the above experiment were derivatized for GC-MS/MS analysis. Derivatization of the extract was done as per the protocol reported in section 4.2.1.3.

**GC-MS/MS conditions:** For metabolite profiling of the treated and controlled samples following temperature program with SH-RTX-5Sil column (Shimadzu, Japan) was used: Initial oven temperature 80°C (2 min hold) with 8°C/min increase to 160°C and 4°C/min to 270°C hold 10 min. Injection, ion source, and detector temperature were kept at 250°C, 250°C, and 270°C, respectively. Mass scans were given in the range of  $m/z$  30 to 600 (Tu et al., 2011). For SIM, the following temperature program was used with SH-RTX-5Sil column (Shimadzu, Japan): Initial oven temperature 60°C (1 min hold) with 15°C/min increase to 125°C and 8°C/min to 250°C hold

5 min. Injection, ion source, and detector temperature were kept at 270°C, 230°C, and 270°C, respectively. Mass scans were given in the range of  $m/z$  30 to 600.

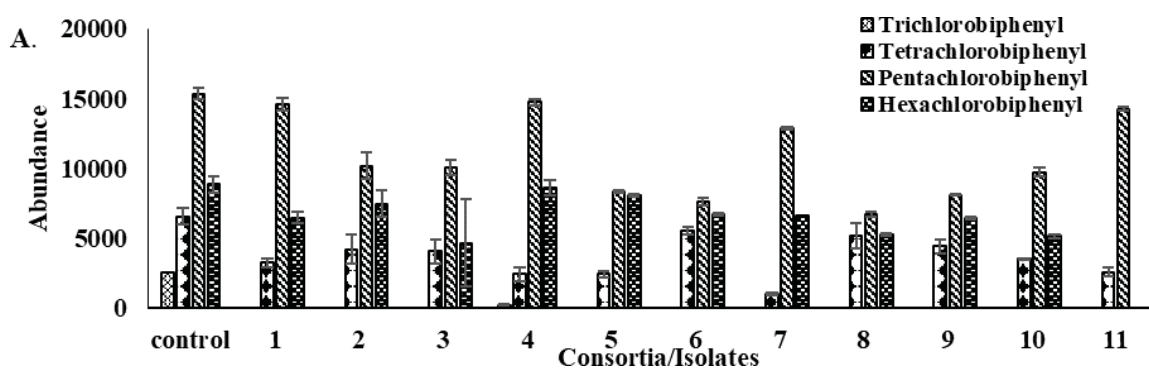
### 5.2.6. Statistical analysis

The results were expressed as mean  $\pm$  standard deviation (SD) of at least three independent experiments. Statistical analysis was performed using Graph Pad Prism5 software. The data were compared by one-way analysis of variance (ANOVA). Data were summarized as mean SD or <sup>ns</sup>  $p > 0.05$  or \* $p < 0.05$  or \*\* $p < 0.01$  as compared.

## 5.3. Results and discussion

### 5.3.1. Biodegradation of PCB congener mix by consortia of the selected bacterial isolates

Biodegradation of PCBs by isolates, MAPB-2, MAPB-6, MAPB-9, and MAPB-27, and their consortia, was studied by inoculation of the PCB congener mix supplemented MM. The biodegradability of PCB congener mix by the individual bacterial isolates varied. Although all the selected isolates were potential biodegrader as proved in previous chapters, there were differences in the biodegradation pattern of the various homologs of the PCB congener mix. PCB congeners are categorized into ten homolog groups and labeled from monochlorobiphenyls to decachlorobiphenyls based on the degree of chlorination in the biphenyl molecule (ATSDR, 2000). Biodegradation of individual PCB congeners was found to decrease by all the selected isolates with the increasing amount of chlorine on the PCB congeners (Fig. 5.1A & B).



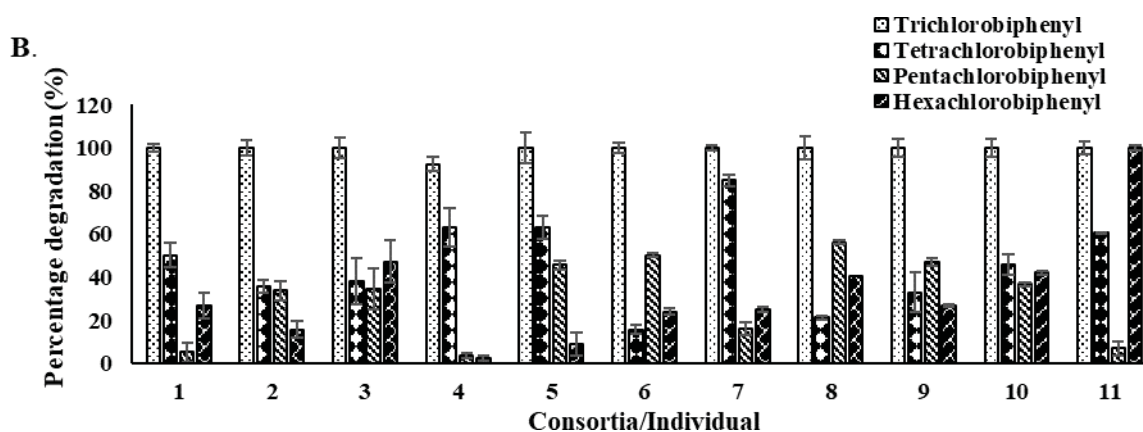


**Fig. 5.1.** Biodegradation of PCB congener mix by consortia and selected bacterial isolates. The number on X-axis refers to the isolate or consortia mentioned in Table 5.1. (A) Y-axis refers to the abundance of PCB congener. (B) Y-axis refers to the percent degradation of PCB congener. #1-4 consist of individual isolates MAPB-2, MAPB-6, MAPB-9, and MAPB-27, #5-7 isolates present in combination of two, #8-10 consist of three combination, while #11 consist of consortium of all the four bacteria.

All four isolates except *P. megaterium* MAPB-27 showed 100% degradation of trichlorobiphenyl. On the contrary, the degradation of pentachlorobiphenyls and hexachlorobiphenyls was minimal by all isolates (Fig. 5.1). Isolate *P. aeruginosa* MAPB-2 showed 50.3%, 5.1%, and 26.8 % degradation of tetrachlorobiphenyl, pentachlorobiphenyl, and hexachlorobiphenyl, respectively. *P. plecoglossicida* MAPB-6 degraded 35.8%, 33.7%, and 15.5 % of tetrachlorobiphenyl, pentachlorobiphenyl, and hexachlorobiphenyl, respectively. Isolate *B. anthropi* MAPB-9 degraded 38.2%, 34.3%, and 47.2 % of tetrachlorobiphenyl, pentachlorobiphenyl, and hexachlorobiphenyl, respectively, whereas isolate *P. megaterium* MAPB-27 degraded 92.5%, 62.9%, 3.7%, and 2.4 % of trichlorobiphenyl, tetrachlorobiphenyl, pentachlorobiphenyl, and hexachlorobiphenyl, respectively. Thus, MAPB-9 was found to be the best degrader among the four bacterial isolates. These results suggested the individual bacteria were capable of hydrolyzing the less chlorinated PCBs (Cl<sub>1-4</sub>) than the highly chlorinated PCBs (Cl<sub>≥5</sub>). Based on these results, it can be concluded that the higher the number of chlorines attached to the biphenyl rings, the more resistant the PCBs are to microbial biodegradation (Jing et al., 2018).

Combining different bacterial isolates was assumed to simulate the microbiological decomposition better than the individual bacterial isolates. Therefore, we used different consortia consisting of two, three, or four isolates based on their degradation and compatibility. As observed for individual isolates, all consortia showed 100% trichlorobiphenyl degradation and minimal

hexachlorobiphenyl degradation. Consortium #5, containing a combination of two isolates (MAPB-2 and MAPB-6), degraded 63.1%, 45.6%, & 8.9% of tetrachlorobiphenyl, pentachlorobiphenyl, and hexachlorobiphenyl, respectively. Similarly, consortium #6 (MAPB-2 and MAPB-9) degraded 15.7%, 50.2%, & 24.1% of tetrachlorobiphenyl, pentachlorobiphenyl, and hexachlorobiphenyl, respectively. With consortium #7 (MAPB-6 and MAPB-9), 100%, 84.9%, 15.9%, & 24.9% degradation of trichlorobiphenyl, tetrachlorobiphenyl, pentachlorobiphenyl, and hexachlorobiphenyl, respectively was observed. Consortium #10 (MAPB-2, MAPB-9, and MAPB-27) degraded 100%, 45.9%, 36.6%, & 42.0% of trichlorobiphenyl, tetrachlorobiphenyl, pentachlorobiphenyl, and hexachlorobiphenyl, respectively. As compared to all consortia used in present study, consortium #11 containing all four isolates was found to be the best PCB degrader wherein it showed 100%, 60.5%, 6.9%, & 100% degradation of trichlorobiphenyl, tetrachlorobiphenyl, pentachlorobiphenyl, and hexachlorobiphenyl, respectively. Biodegradation of the sum of six hexachlorobiphenyl congeners was less effective than that of four tetrachlorobiphenyls and six pentachlorobiphenyls. Hexachlorobiphenyl congeners were degraded to a comparable extent in consortium #11, while pentachlorobiphenyl was least degraded. It could be possible that hexachlorobiphenyl was converted into pentachlorobiphenyl and accumulated in the media. Thus, the biodegradation of PCB congener by consortia was more efficient than applying the selected individual isolates. The lowest efficiency of PCB congener biodegradation was observed with consortium #10 (Fig. 5.1) containing MAPB-2, MAPB-9, and MAPB-27. As expected, a two-member consortium was not efficient compared to other consortia. Consortium # 8 of MAPB-2, MAPB-6, and MAPB-9 with 1: 1: 1 (v/v/v) degraded only 21.1 %, 56.1 %, and 40.7 % of the four tetrachlorobiphenyls, six pentachlorobiphenyls, and six hexachlorobiphenyls, respectively. This result may probably be due to an antagonism between the isolates. Recently, Horvathova et al. (2018) have reported similar findings with a consortium of strains *Rhodococcus* sp. + *A. xylosoxidans*, and *Rhodococcus* sp. + *S. maltophilia*, (1: 1) that degraded approximately 80 % of the sum of seven PCB congeners and thus was found to be more efficient than the individual strains in the sediment.

### **Encapsulation of bioformulation with Ca-alginate beads**

Introduction of bacterial isolates degrading PCBs individually or as consortia are considered an effective strategy for the removal of PCBs from the soil. To avoid the hostile interaction of the indigenous microorganisms to a given environment from isolated bacteria, it is desirable to develop the bioformulation of bacterial consortia based on earlier cultured microorganisms.



Microencapsulation is one of the bioformulation techniques used to entrap various microbes in a polymeric matrix. Sodium alginate is commonly used to encapsulate microorganisms due to its lower cost, ease of biodegradability, and inertness (Dhamecha et al. 2019). It produces beads with good mechanical strength and chemical stability (Bouabidiet al. 2019) and helps maintain bacterial cell viability and slow release into the soil environment.

### **Microbial count of the encapsulated bacterium and consortium**

Alginate beads can encapsulate a sufficient number of bacteria (Prasad and Kadokawa, 2009). Therefore, the microbial count was estimated to determine the number of bacteria entrapped in the beads with individual isolates each and in the combination of all the four selected isolates (consortium #11). Single encapsulated MAPB-2, MAPB-6, MAPB-9, and MAPB-27 indicated  $2.9 \times 10^6$ ,  $2.4 \times 10^6$ ,  $1.8 \times 10^6$ , and  $2.1 \times 10^6$  CFU/mL microbial count, respectively. The total microbial count for consortium #11(1:1:1:1 and 1:1:2:2) was found to be  $2.2 \times 10^6$  and  $2.4 \times 10^6$  CFU/mL, respectively. The bacterial count of the isolates varied as per their growth rate. In consortium #11, *P. aeruginosa* MAPB-2 and *P. Pleccoglossicida* MAPB-6 are fast-growing bacterial isolates with the property to outgrow in number, while the best PCB degrader *B. anthropi* MAPB-9 has a slow growth rate. Therefore, consortium #11 was prepared in two ratios. First, bioformulation with all the isolates in equal ratios, i.e., 1:1:1:1. In the second, two *Pseudomonas* isolates MAPB-2, MAPB-6 were half the ratio of *B. anthropi* MAPB-9 and *P. megaterium* MAPB-27, i.e., 1:1:2:2. Microbial count was found to be  $2.2 \times 10^6$  and  $2.4 \times 10^6$  for consortium #11 with 1:1:1:1 and consortium #11 with 1:1:2:2, respectively. Thus, all the encapsulated beads showed a sufficient bacterial count for PCB congener biodegradation in the pot study.

#### **5.3.2.1. Encapsulation of bacterial consortium #11 and its isolates in Ca-alginate beads**

After evaluating the successful entrapment of bacterial isolates in Ca-alginate beads, we examined them for their uniform size and surface characteristics employing FESEM. The FESEM images showed selected bacteria encapsulated in a criss-cross matrix of alginate with a smooth and uniform surface (Fig. 5.2). After confirmation of the uniform bead formation, beads were analyzed for entrapped bacteria inside beads. *P. aeruginosa* MAPB-2, *P. pleccoglossicida* MAPB-6, *B. anthropi* MAPB-9, and *P. megaterium* MAPB-27 were found to be entrapped in their respective beads (Fig 5.3. A-D). There was no cross-contamination of the bacteria found in the beads. Similar type of bacterial cell arrangement was observed in formed alginate beads to the

bacteria grown in LB. *P. aeruginosa* MAPB-2 (Fig. 5.4A), and *P. plecoglossicida* MAPB-6 (Fig. 5.4B), were in diplobacillus arrangement, confirming the cell division inside the beads. The bacterial cells of *B. anthropi* MAPB-9 were arranged in layer one above the other (Fig 5.4C), while *P. megaterium* cells (Fig. 5.4D) were found to be connected with a tube-like structure, as was observed in Chapter 3. Alginate beads maintain high bacterial cell density with maximum survival (Young et al., 2006). To degrade PCB efficiently in soil, entrapped bacteria should be in an active state. FESEM images indicate that all the entrapped bacteria are physiologically and metabolically competent.

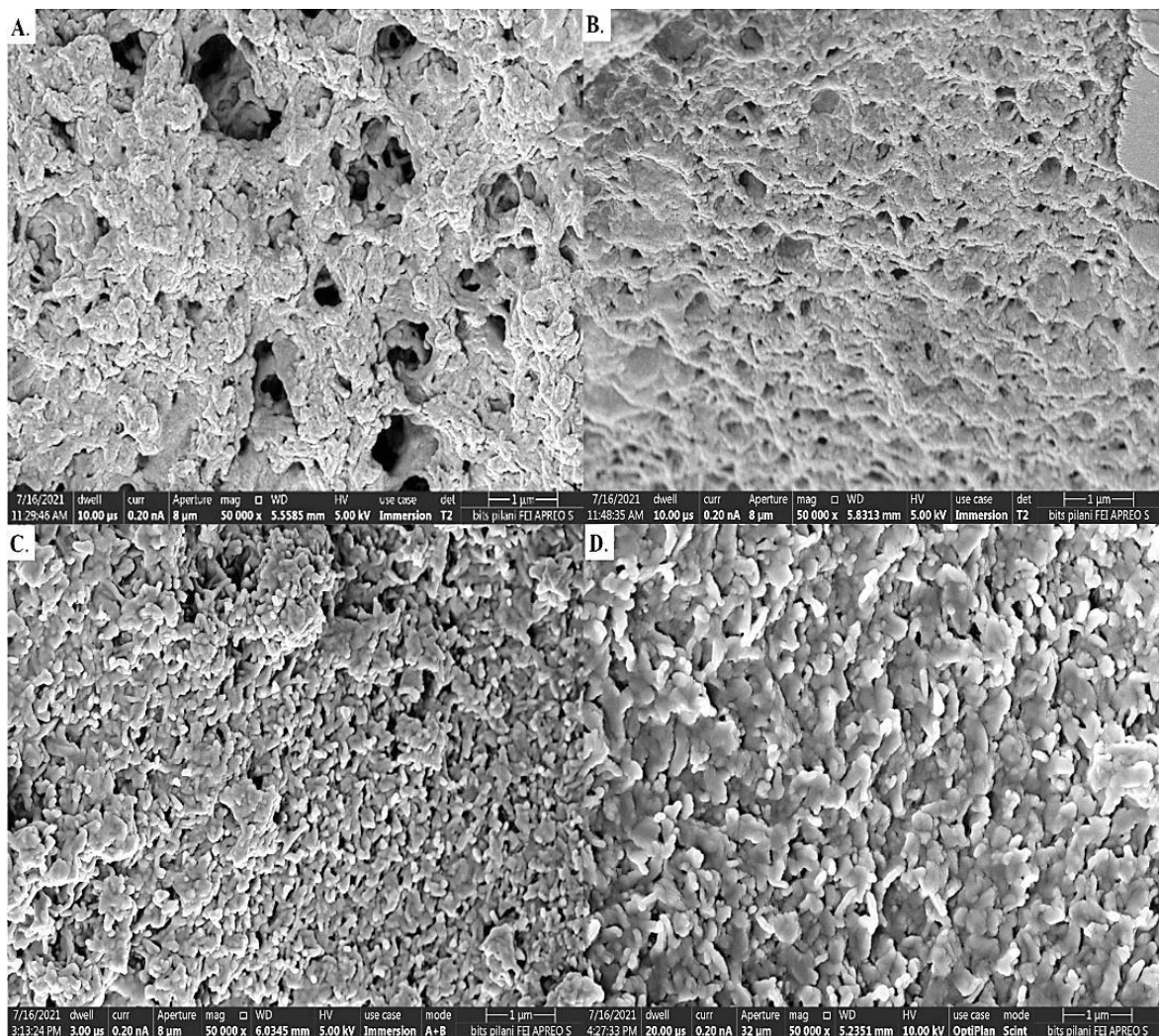


**Fig. 5.2.** FESEM analysis of encapsulated alginate bead surface of the selected bacterial isolates at a magnification of 50 000 X (A) MAPB-2 (B) MAPB-6 (C)MAPB-9 and (D) MAPB-27. Selected bacteria encapsulated in a criss-cross alginate matrix with a smooth and uniform surface. No bacteria were present on the surface of the beads.



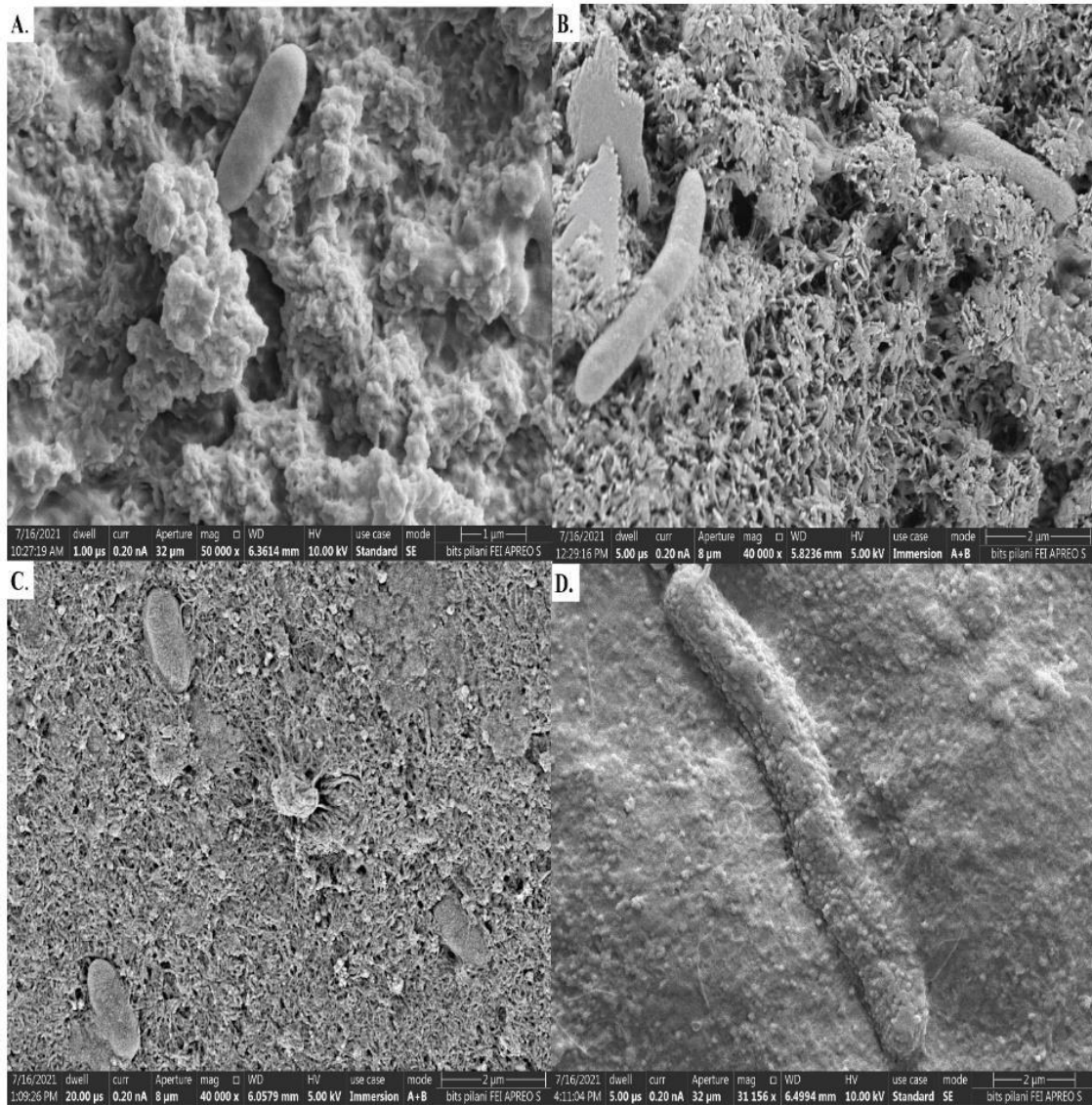


**Fig. 5.3.** FESEM analysis depicting encapsulated bacteria isolates(A) MAPB-2 at magnification 50 000X (B) MAPB-6 at magnification 40 000X (C) MAPB-9 at magnification 40 000X (D) MAPB-27 at magnification 31 156X.

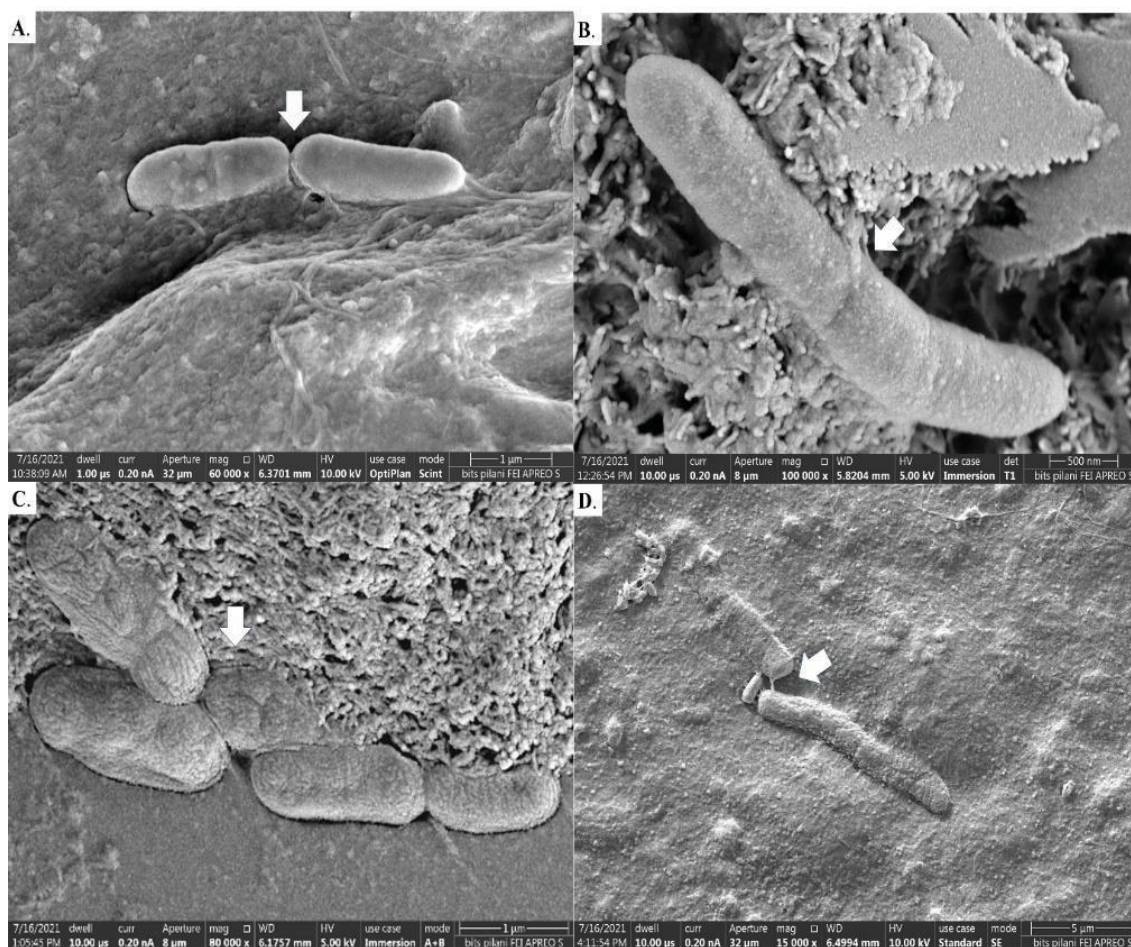


**Fig. 5.4.** FESEM analysis depicting an arrangement of encapsulated bacteria isolates(A) MAPB-2 diplobacillus arrangement observed at magnification 60 000X (B) MAPB-6 diplobacillus arrangement observed at magnification 100 000X (C) MAPB-9 side to side arrangement observed at magnification 80 000X (D) MAPB-27 cell contact through tube-like structure at magnification 15 000X.

### 5.3.3. Effect of encapsulated bioformulation on plant growth in PCB-spiked soil

Since the root exudate of the plant provides various nutrients and metabolites to associated microbiota, the efficiency of bacteria-mediated bioremediation improves in the rhizosphere. Moreover, some metabolites with similar structures to xenobiotics, like PCBs, can induce and enhance bacteria-mediated remediation of pollutants. In turn, PCB-degrading bacteria having plant growth-promoting properties can improve plant growth (Vergani et al., 2019). Therefore, we evaluated the plant-assisted degradation of PCB congener by consortium #11 (1:1:1:1) using *B. nigra* as a host plant. We also tested the effect of bacterial consortia on plant growth in PCB congener-spiked soil. An additional consortium containing a 1:1:2:2 ratio of the four isolates was prepared and evaluated. In this consortium, to match the rapidly growing ability of the two



*Pseudomonas* spp. (MAPB 2 & 6), a double ratio of comparatively slow-growing *Brucella* and *Priestia* spp. (MAPB 9 & 27) were taken. Plants belonging to the genera *Brassica* have been reported as a model plant (Ficko et al. 2010). Thus, the plant *B. nigra* was selected according to previous reports suggesting its use for the phytoremediation of PCBs.

The growth of *B. nigra* treated with individual isolates and the consortia was estimated by measuring the root and shoot length, the number of leaves, and the number of buds (Fig. 5.5. & Fig. 5.6). The experimental group T2 treated with bioformulation #11 containing the bacterial isolates in the ratio (1:1:2:2) showed the highest growth in terms of shoot and root length as compared to all the other treatment and control plants. Root/ shoot ratios of the *B. nigra* under investigation changed due to PCB-spiked soil (Fig 5.5). There was a slight increase in the root and shoot length of most treatments (T1-T8) than the control (C2 and C3) used in these experiments. T2 plant showed increased growth with an equal increase in shoot and root length, formation of a bud, and flower. In case of individual isolates T5 (MAPB-2), T6 (MAPB-6), T7 (MAPB-9) and T8 (MAPB-27) also showed increase in length compared to controls C2 and C3. From these data, it can be concluded that *B. nigra* was able to grow on PCB-spiked soil and also showed increased growth in the presence of bioformulation.

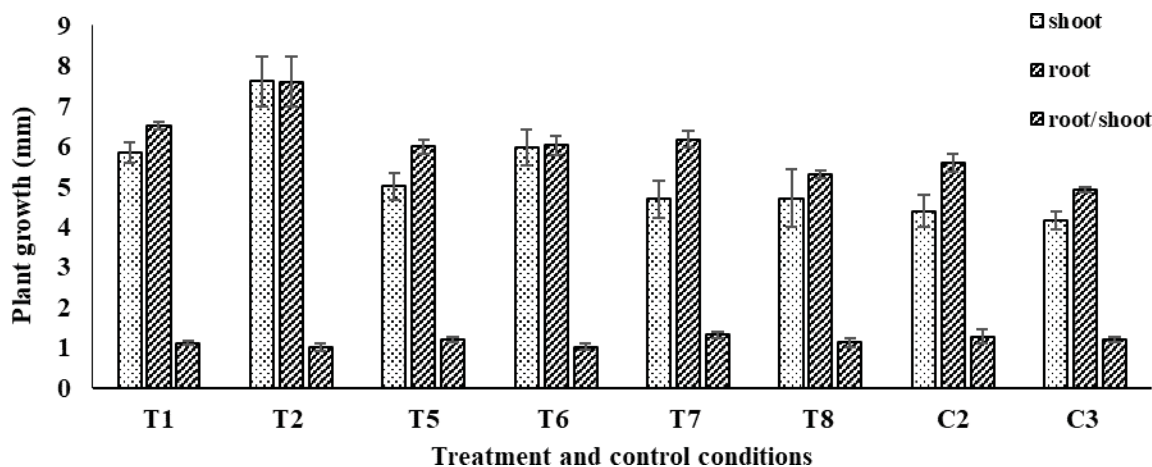


**Fig. 5.5.** Effect of encapsulated bacterial bioformulation on the growth of *B. nigra* and respective control. T1 and T2 represent plants in PCB congener spiked soil, bioformulation with consortium #11 in 1:1:1:1 and 1:1:2:2, respectively. T5 to T8 are bioformulation with individual entrapped isolates MAPB-2, MAPB-6, MAPB-9, and MAPB-27, respectively. C2 represents plants grown in sterile soil without bioformulation, while C3 represents the control group with plants grown in PCB congener spiked soil (refer to Table 5.2).



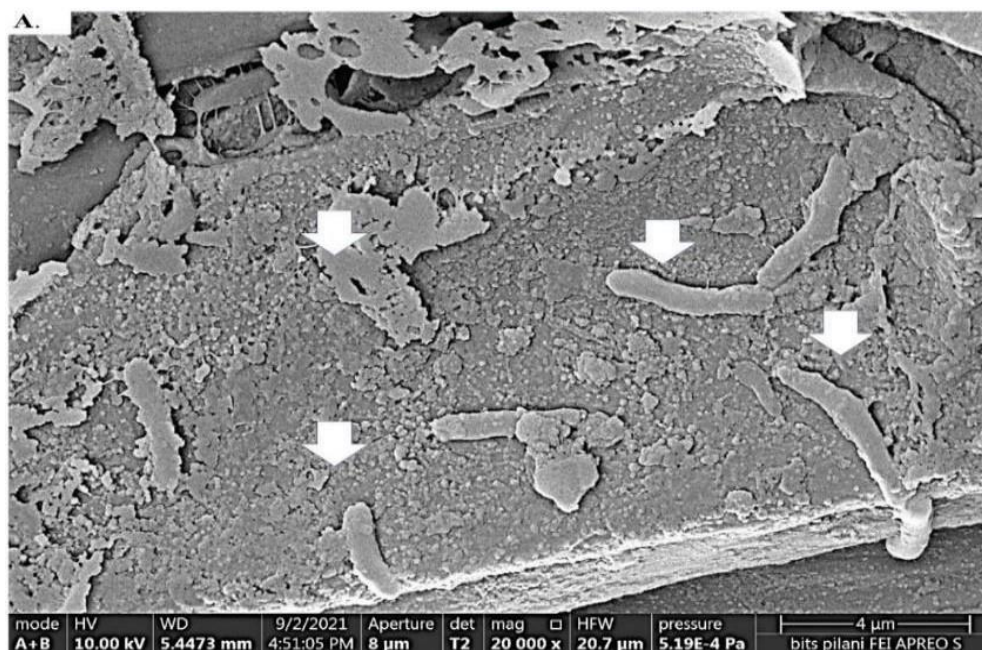
**Fig. 5.6.** Pot study of *B. nigra* growth in various bioformulation treatment and control groups. (A) T1: bioformulation with consortium #11 in ratio 1:1:1:1; (B) T2: bioformulation with consortium #11 in ratio 1:1:2:2; (C) C1 Control with PCB congener spiked soil; (D) C2 control having sterile soil with the plant (E) C3 control with PCB congener spiked soil and plant (F) T5 encapsulated MAPB-2 with spiked soil and plant; (G) T6 encapsulated MAPB-6 with spiked soil and plant; (H) T7 encapsulated MAPB-9 with spiked soil and plant (I) T8 encapsulated MAPB-27 with spiked soil and plant. The pot study was conducted for 45 days.



Plant present in the treatments T1 and T2 showed healthy growth with five leaves per plant. In addition, T2 showed bud and flower formation. The plant survival was equivalent to the control C2 with normal soil. However, in C3, there was stunted plant growth with fewer plants and leaves. Treatment T2 showed the best growth of *B. nigra*. Along with PGPR property, bioformulation T2 with the highest degradation potential, must have made soil conditions less toxic for plant growth than the other treatments.

#### 5.3.4. FESEM analysis of plant roots treated with different bioformulations

The rhizosphere is the most critical soil section that has maximum microbial activity. FESEM analysis was performed for the rhizosphere soil and root samples of the plants treated with bioformulation. FESEM analysis of the rhizospheric region of the spiked soil with encapsulated *P. aeruginosa* MAPB-2 isolate confirmed its presence along with the remains of beads (Fig. 5.7 A). The higher magnification image (60 000X) of the same area indicated the presence of tube-like appendages of the MAPB-2 with the *B. nigra* plant root (Fig 5.7B). Further magnification at 100 000X, MAPB-2 showed it between the bacterial cells and the roots of *B. nigra* (Fig. 5.7C). *Pseudomonas* spp. are well known for attachment to the roots. Flagella and pili are filamentous proteinaceous appendages that extend from the bacterial cell surface. In addition to a role in motility, flagella and pili can also function for adhesion (Pratt and Kolter, 1998; Zheng et al., 2015; Wheatley and Poole, 2018).



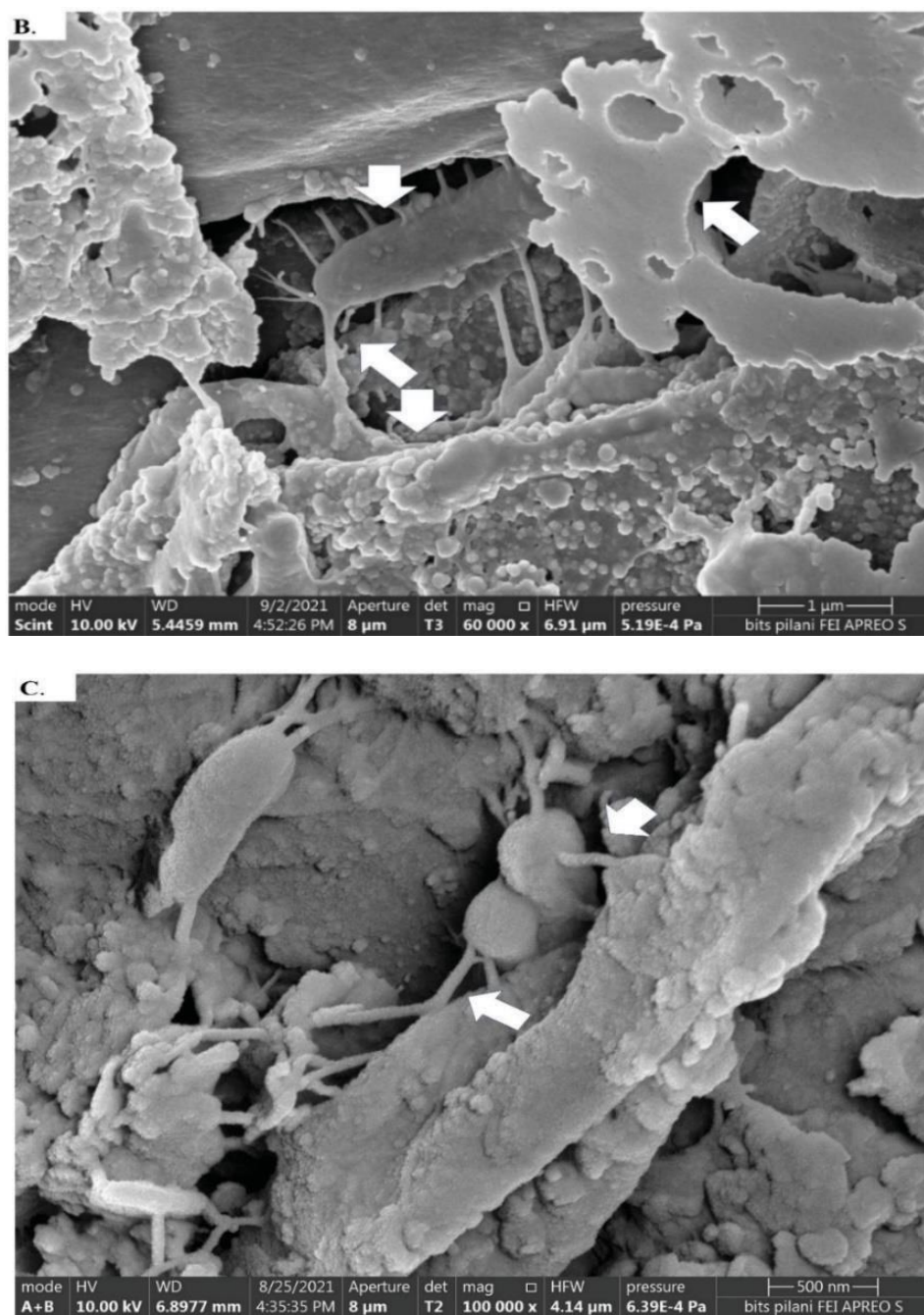


**Fig. 5.7.** FESEM analysis of the rhizospheric region of the spiked soil with encapsulated *P. aeruginosa* MAPB-2 isolates (A) MAPB-2 in the rhizospheric region and the remains of beads [20 000X] (B) MAPB-2 tube-like attachments with the *B. nigra* plant root observed [60 000X] (C) MAPB-2 attached to another and with the roots [100 000X].

A similar observation was noted for *P. plecoglossicida* MAPB-6 (Fig. 5.8B), *B. anthropi* MAPB-9 isolate (Fig. 5.9A & 5.9B), and *P. megaterium* MAPB-27 (Fig. 5.10B). In addition, *P. megaterium* MAPB-27 also showed secretion of EPS in the rhizospheric region of the *B. nigra* (Fig. 5.10 A-B). Encapsulated consortium #11 with four bacterial isolates was observed (Fig. 5.11)



under 30 000X magnification. Thus, FESEM analysis supported the release of bacterial isolates from the alginate beads in the rhizospheric region and roots of *B. nigra* indicating that they were viable and could proliferate for bioremediation.

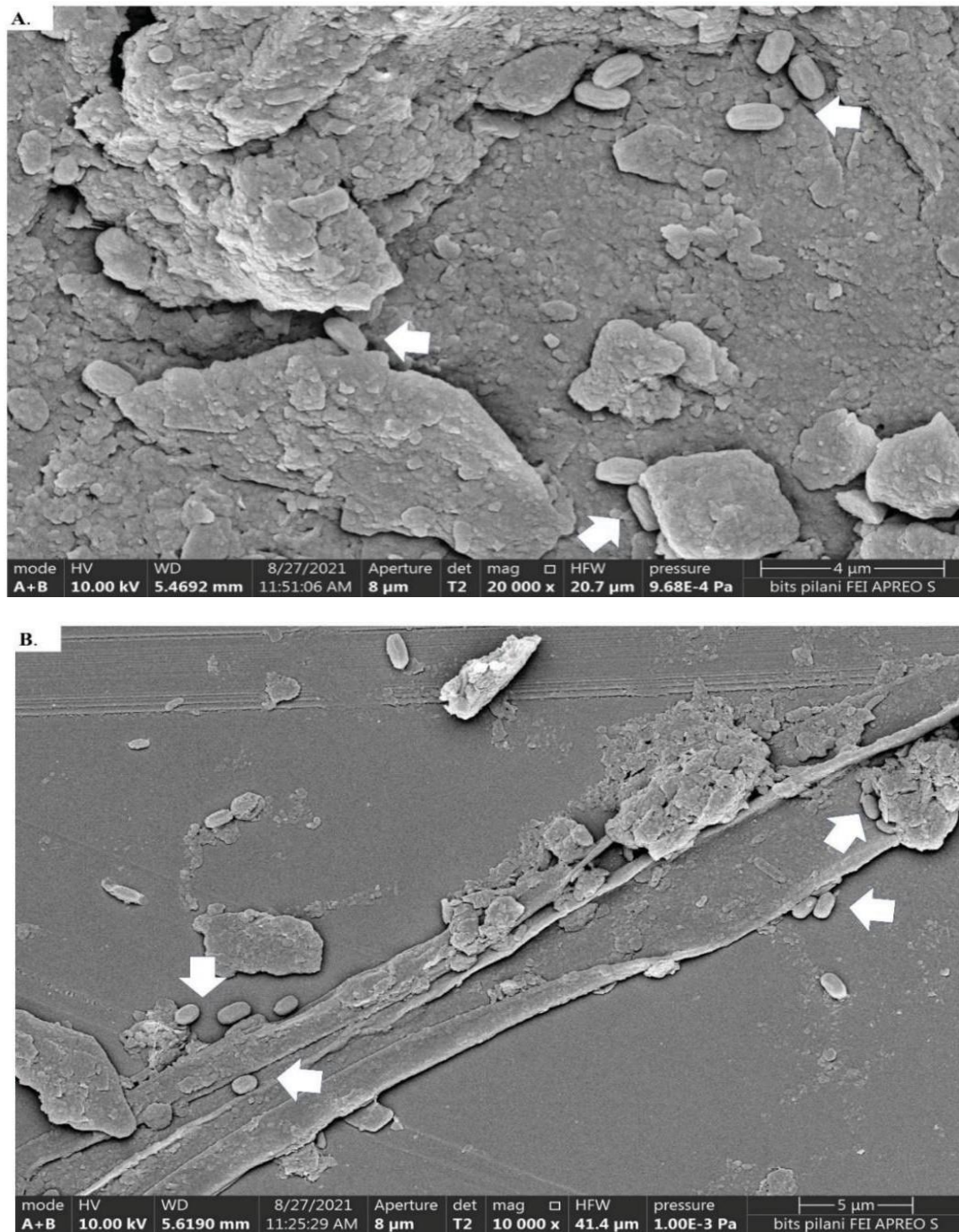


**Fig. 5.8.** FESEM analysis of the rhizospheric region of the spiked soil with encapsulated *P. plecoglossicida* MAPB-6 isolates (A) MAPB-6 in the rhizospheric region [20 000 X] (B) MAPB-6 attached with the *B. nigra* plant root [10 000 X].

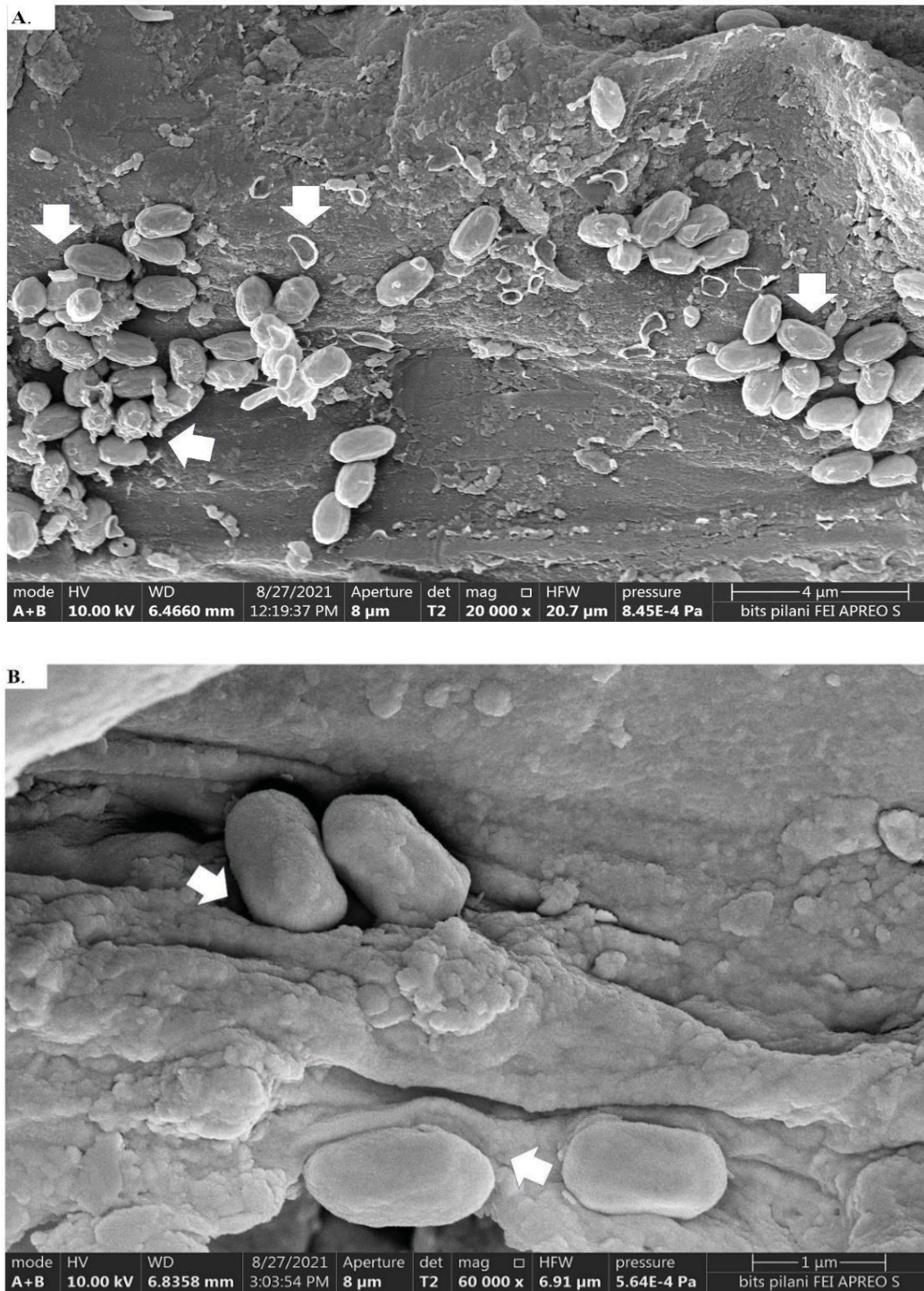


**Fig. 5.9.** FESEM analysis of the rhizospheric region of the spiked soil with encapsulated *B. anthropi* MAPB-9 isolates (A) MAPB-9 in the rhizospheric region and the remains of beads (B) MAPB-9 attached with the *B. nigra* plant root.



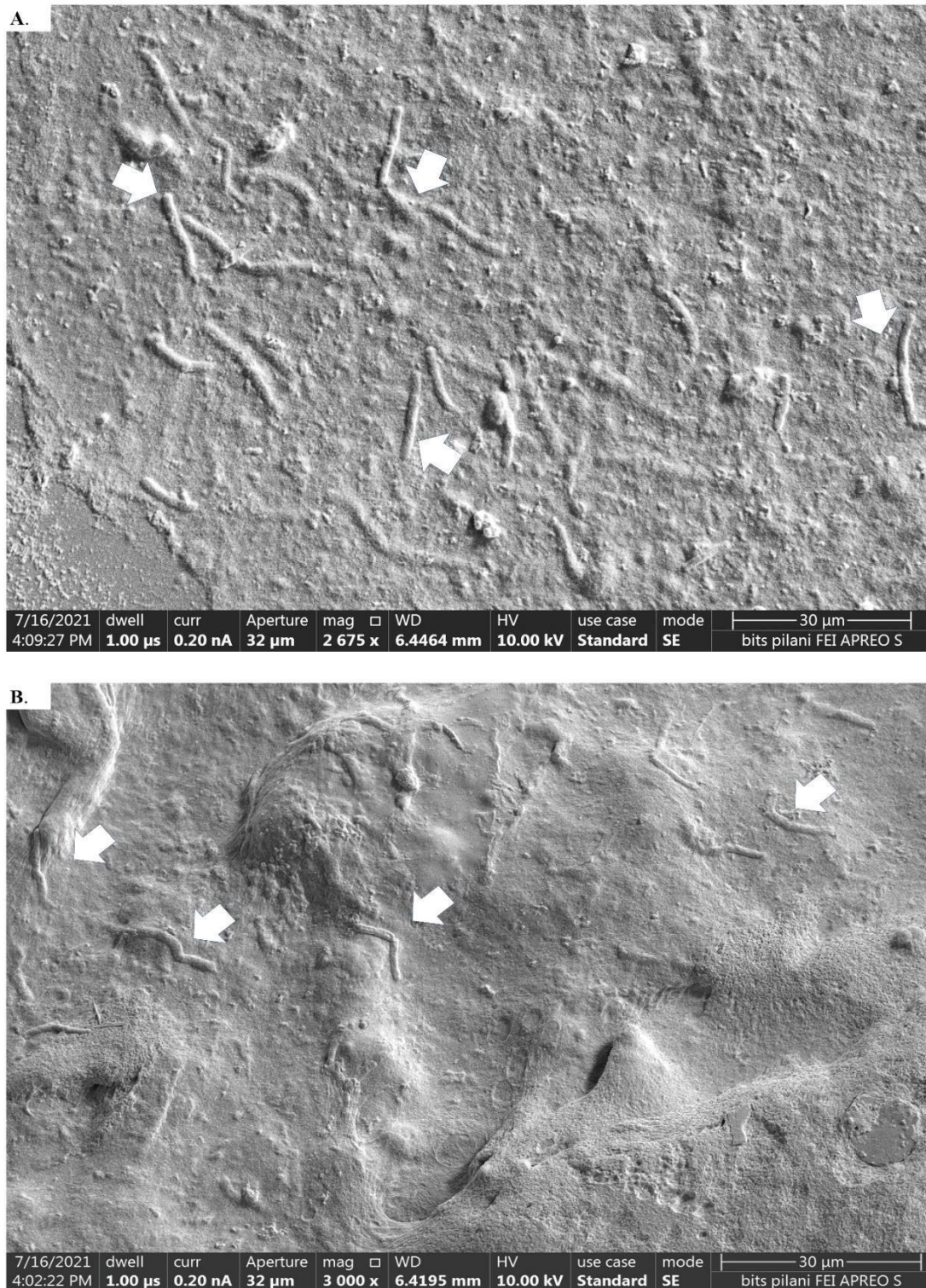


**Fig. 5.10.** FESEM analysis of the rhizospheric region of the spiked soil with encapsulated *P. megaterium* MAPB-27 isolates (A) MAPB-27 EPS secretion in the rhizospheric region observed (B) MAPB-27 attached with the *B. nigra* plant root is not observed.

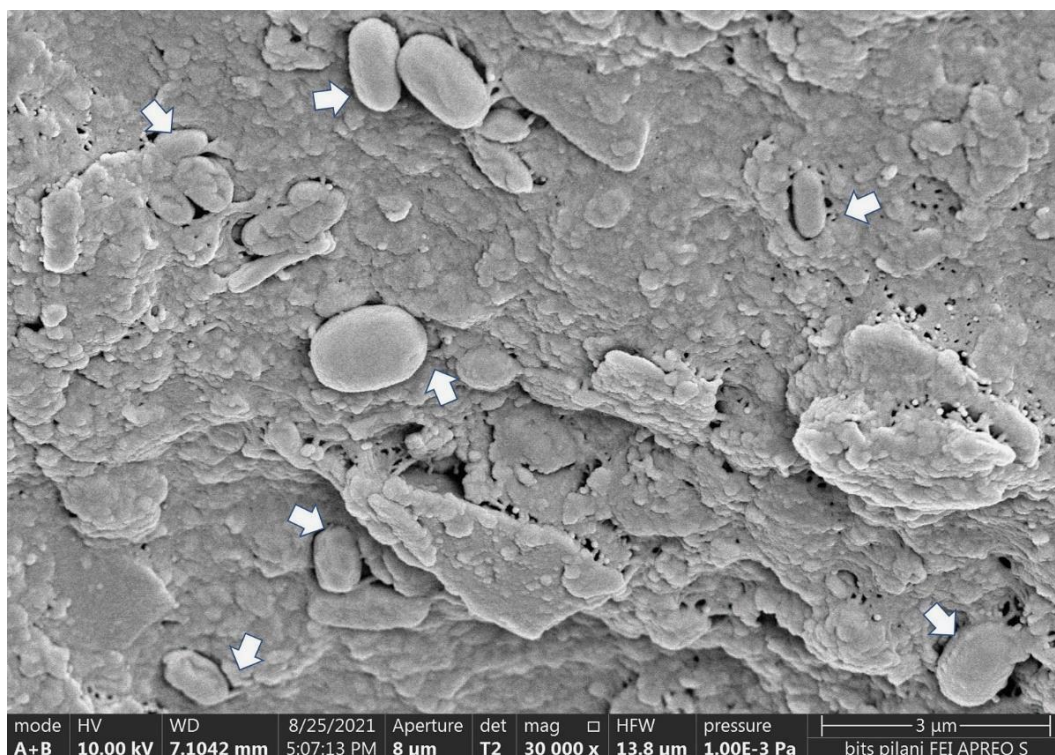


**Fig. 5.11.** FESEM analysis of the rhizospheric region of the spiked soil with encapsulated consortium #11. MAPB-2, MAPB-6, MAPB-9, and MAPB-27 isolates in the rhizospheric region are observed.

### Microbial enumeration

The survival of the bacterial inoculum in the pollutant-contaminated soil is one of the most important factors determining biodegradation efficiency. Therefore, we enumerated bacterial count in rhizospheric soil treated with encapsulated bacterial bioformulations. There was a decrease from the initial microbial count to  $2.2 \times 10^2$  CFU/g of soil for treatment T1 and  $2.8 \times 10^2$  CFU/g of soil for treatment T2 in the consortium. The bacterial population was observed to be higher than unplanted inoculated soil treatment T3 and T4, suggesting the role of *B. nigra* in promoting the growth of bacteria. Further, the microbial count for individual bacterium-based bioformulations (T5-T8) was higher than the consortium (T1-T4) with  $4.2 \times 10^4$ ,  $2.6 \times 10^4$ ,  $2.7 \times 10^4$ , and  $1.9 \times 10^5$  CFU/g of soil microbial count. The decrease in microbial count could be due to competition amongst the consortium members and adaptation to survive in a stressful environment (Liang et al., 2014). There were a good number of bacterial counts in the treatments that provided evidence that the bioformulation is capable of catering to the growth and release of bacteria into the soil.



### 5.2.4. Evaluation of PCB congener mix degradation by bioformulations in the pot experiment

Based on the result of the biodegradation study of PCB congener (section 5.3.1.), bioformulation consortium #11 showed the highest degradation potential. Therefore, this bioformulation was selected for its PCB degrading capability in the pot study. A pot experiment was performed to understand how the developed consortia bioformulation would perform PCB degradation in the simulated soil condition. PCB degradation potential of the bioformulations (based on consortium #11) in sterile soil spiked with PCB congeners mix was assessed by GC-MS/MS (Fig. 5.12A-B).

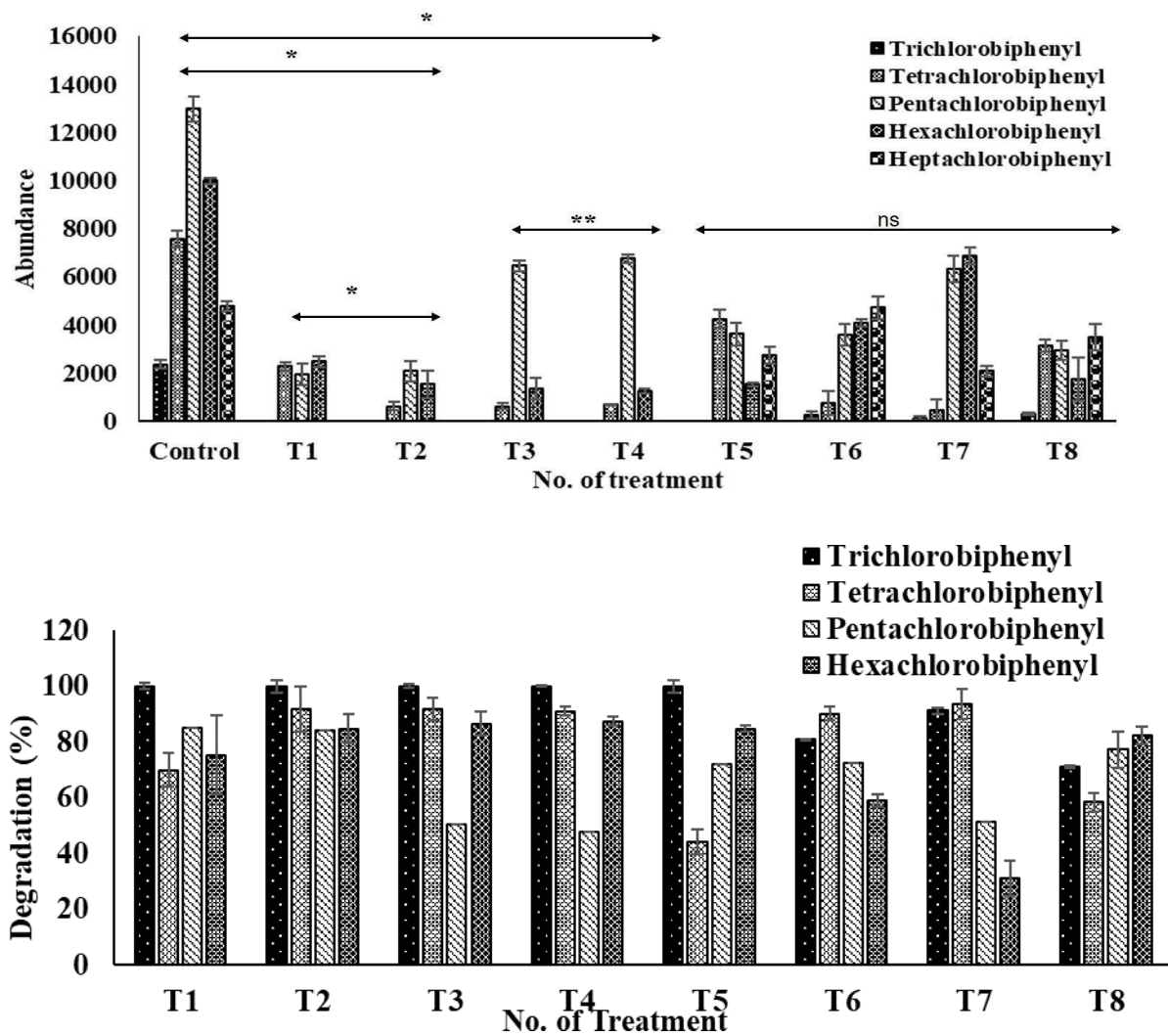


**Fig. 5.12.** GC-MS/MS analysis of PCB congener mix degradation by different treatments. The number on the X-axis refers to the no. of treatments. (A) Y-axis refers to the abundance of PCB congener (B) Y-axis refers to the percent degradation of PCB congener. PCB congeners consist of tri-, tetra-, penta-, hexa-, and hepta-chlorinated biphenyls. Treatment includes bioformulation,

with consortium #11 having four bacteria (T1-T4) and a single bacterial isolate (T5-T8). The result was presented as the mean values of triplicate experiments (\*\* $P < 0.01$ , \* $P < 0.05$ ).

The complete degradation of PCBs requires various bacterial strains with specific congener preferences. In addition, the position and the number of chlorine on the biphenyl molecule influence the rate of the first oxygenase attack. The results were also compared with individual isolates used in consortium #11. In our study, bioformulations T1 and T2 with all four selected bacterial isolates in the ratio (1:1:1:1) and (1:1:2:2) showed enhanced PCB congeners degradation. Bioformulations T1 and T2 showed 100 % degradation for tri- and hexachlorobiphenyl, whereas more than 70% and 80% for tetra and penta-chlorobiphenyl in T1 and T2, respectively (Fig. 5.12A-B). In bioformulations T5 to T8, 100% trichlorobiphenyl was degraded, while tetrachloro- and pentachloro- showed more than 50% degradation by all the encapsulated bacteria. It can be concluded that the encapsulated consortia #11 could biodegrade the PCB congener mix more effectively in the presence of *B. nigra* (T1 and T2) compared to encapsulated consortia #11 alone. This observation was more evident, especially in the case of the penta homolog of PCB, which was least degraded in the absence of *B. nigra* (T3 and T4). Thus, the study showed enhanced PCB bioremediation from the spiked soil with the help of bioformulation-mediated phytoremediation.

#### **Metabolite and product identified in degradation of PCB congeners of the treated and controlled samples**

The scheme for PCB degradation outlined in the previous chapters, in which PCBs are co-metabolized by a pathway analogous to the upper pathway for biphenyl degradation, is very much a simplified overview. There are a large number of different chlorinated metabolites produced using this approach. In addition to the chlorinated intermediates from the upper chlorobiphenyl pathway, several other products accumulate from PCB co-metabolism (Table 5.3). Various reports describe the potential of aerobic bacteria to degrade higher chlorinated congeners (Commandeur et al., 1995; Dercova et al., 1996; Lizet et al., 2009). The ability to degrade highly chlorinated PCB congeners is attributed to 2,3-dioxygenase, which can oxidize the carbon bound to a chlorine atom (Komancova et al., 2003). Similar mechanisms are also described for chlorobenzoates (Fava et al., 1993).

The types of products that can accumulate are largely independent of the bacterial strain used. They are determined primarily by the reacting ring's chlorine substitution pattern via either

2,3 dioxygenase or 3,4 dioxygenase attack (Bedard and Haberl, 1990). It has been reported that 2,4,4'-trichlorobiphenyl (PCB-28), 2,2,5,5'-tetrachlorobiphenyl (PCB-52), 2,2', 4,5' tetrachlorobiphenyl, 2,2',5,6' tetrachlorobiphenyl undergoes cleavage at 2,3 position of the less chlorinated ring by 2,3 dioxygenase enzyme (Komancova et al., 2003). It results in the formation of 2,4-dichloro benzoate as a final product. *P. aeruginosa* is capable of degrading chlorobenzoates, and thereby complete mineralization of the PCBs occurs. 1,1'-biphenyl 3,3'-diol 4,4' chloro metabolite identified in the extract of T2 could be the result of degradation of 3,3',4,4' tetrachlorobiphenyl (PCB-77). The accumulation of the corresponding diol results from 3, 4 dioxygenation of PCBs.

2,2',5,6' tetrachlorobiphenyl undergoing 3,4 dioxygenase attack results in the formation of monochloroacetophenone, while degradation *via* 2,3 dioxygenase produces 4-(2,5-dichlorophenyl)-4-oxobutanoic acid. 2'-chloroacetophenone and 4-(2,5-dichlorophenyl)-4-oxobutanoic acid was identified in extracts of both T1 and T2, thereby confirming the degradation of 2,2',5,6' tetrachlorobiphenyl. 4 chlorobiphenyl (the product of tetrachlorinated biphenyl) was also identified in the extract of T2. Barton and Crawford (1988) reported the accumulation of 4-chloroacetophenone by *Pseudomonas* sp. MB86 when grown with 4-chlorobiphenyl. Mass fragmentation patterns of some of the identified metabolites in T2 during biodegradation of PCB congener mix in spiked soil are provided in Fig. 5.13.

2,4',5-trichloro acetophenone is a metabolite formed by the degradation of 2, 2',4, 4', 5, 5'-hexachlorobiphenyl (PCB-153) that was identified in the extract of T1. This is in accordance with the formation of 2,4',5-trichloro acetophenone by *Alcaligenes* sp. JB1 degrading 2,2',4,4',5,5'-hexachlorobiphenyl with no adjacent unsubstituted carbons. The presence of acetophenone indicated 3,4-dioxygenase-mediated degradation pathway instead of a more known 2,3-dioxygenase pathway (Bedard, 1990) or from the attack on a 2,5- or 2,4'5 trichlorophenyl ring of a PCB (Bedard et al., 1987). It is reported that dechlorination of hepta- and hexa- chlorobiphenyl results in tetra and pentachlorobiphenyl containing mostly *ortho* or *para* substituted chlorines (Borja et al., 2005). Thus, the high abundance of pentachlorobiphenyl congener in T2 extracts could be due to the release of chlorine functional group from hepta- and hexa-chlorinated biphenyl congener.

**Table 5.3.** List of metabolites identified during the degradation of PCB congeners by bioformulation of consortia in pot experiment.

Metabolite identified	T1	T2	T3	T4	T5	T6	T7	T8
Dichloro acetophenone	✓	X	X	X	X	X	X	X
4-Chlorobenzoate	✓	✓	X	X	X	X	X	X
2,4',5 Trichloro acetophenone	✓	X	X	X	X	X	X	X
2/4 Chlorobiphenyl	X	✓	X	X	X	X	X	X
1,1' Biphenyl 3,3'-diol 4,4' Chloro	X	✓	X	X	X	X	X	X
2'Chloroacetophenone	✓	✓	X	X	X	X	X	X
4-(2,5-dichlorophenyl)-4-oxobutanoic acid	✓	✓	X	X	X	X	X	X
Acetophenone	X	✓	X	X	X	✓	X	X
2,4' dihydroxy acetophenone	X	✓	X	X	X	X	X	X
Benzoate	X	✓	✓	✓	✓	✓	✓	✓
1,2 Benzenediol (Catechol)	X	✓	X	X	X	X	X	X
4-hydroxybenzoate	X	X	✓	✓	✓	✓	✓	✓
2 ketoglutaric acid	X	X	X	✓	X	X	X	X

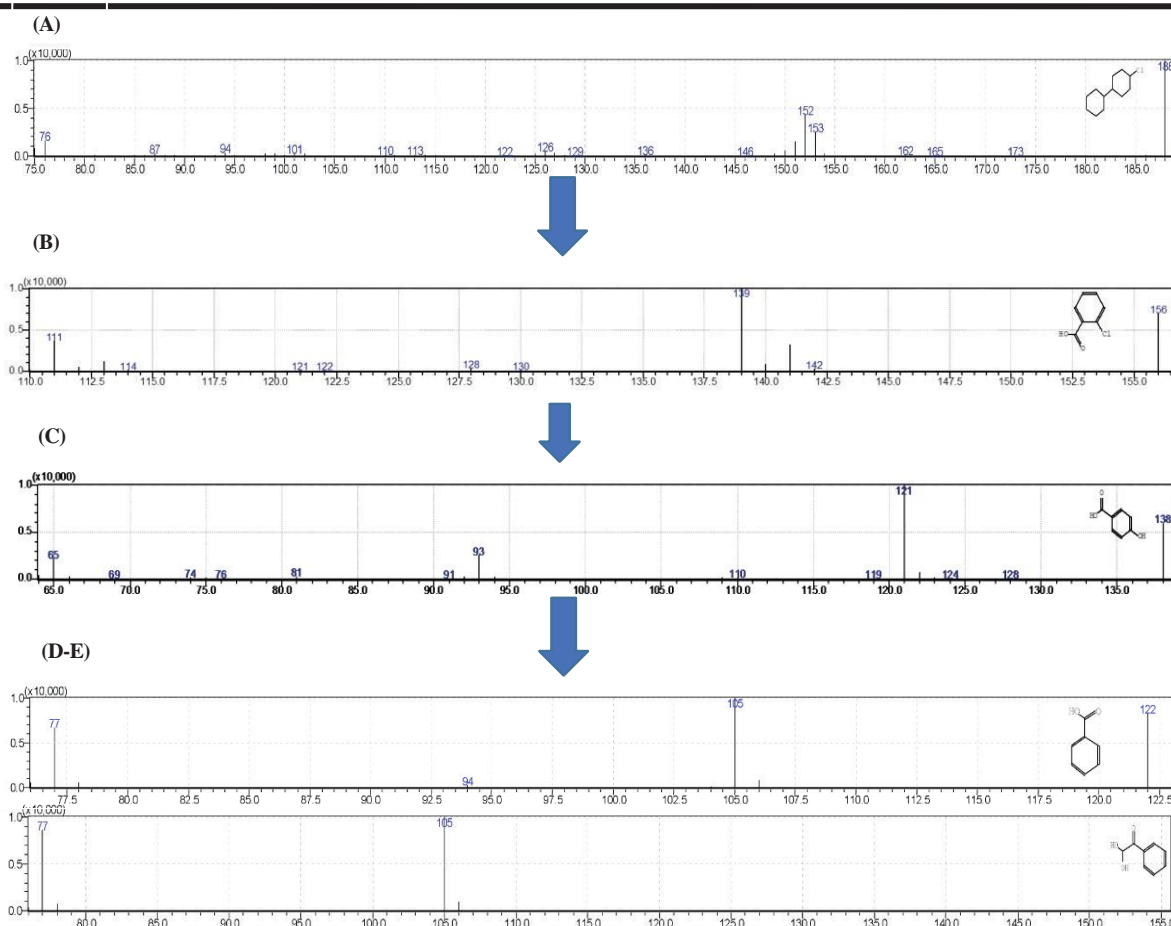


**Fig. 5.13.** Mass fragmentation pattern of some of the identified metabolites in T2 during biodegradation of PCB congener mix in spiked soil. 4-chloro 1,1'-Biphenyl with base peak  $m/z$ 188 (B) 4-chloro benzoate; base peak and molecular ion peak at  $m/z$ 139, 156 respectively (C) 4-hydroxybenzoate base peak and molecular ion peak at 121,138 respectively (D) Benzoate base peak and molecular ion peak at  $m/z$ 122, 105 respectively. (E) Dihydroxyacetophenone base peak and molecular ion peak at  $m/z$ 105. X-axis represents  $m/z$  ratio, while Y axis represents the abundance.

The usual product from the degradation of PCBs is chlorobenzoates. Tetrachlorobiphenyl is reported to form mono and di chlorobenzoate. These compounds are believed to be dead-end metabolites, and the organism's growth is said to be inhibited by the build-up of these metabolites. Chlorobenzoate degradation has been proposed as one of the rate-limiting steps in the overall PCB degradation process (Stratford et al., 1996). It has been shown that the removal of the CBAs produced is an important step for the efficient degradation of PCBs. Both chloroacetophenones and chlorobenzoates are produced during the oxidation of PCB congeners. Further, bacteria can degrade chlorobenzoate to hydroxybenzoate and catechol. Thus, complete mineralization of the PCB congener is possible by the bacterial consortium.

**Chapter VI**  
**Whole Genome Sequencing of**  
***Brucella anthropi* MAPB-9**



## 6.1. Introduction

Based on PCB biodegradation potential, *B. anthropi* MAPB-9 emerged as the most promising among the four selected bacterial isolates. It degraded 100%, 38.2%, 34.3%, and 47.2 % of tri-, tetra-, penta-, and hexa-chlorinated biphenyls, respectively. In addition, MAPB-9 was also found to produce biosurfactants and exhibit PGPR properties. Based on 16S rDNA identification, MAPB-9 showed the closest match with type strain *O. anthropi* ATCC 49188. The *Ochrobactrum* genus has been reclassified to *Brucella*. Thus, MAPB-9 was identified as a gram-negative, aerobe, rod-shaped *alpha-Proteobacteria*, belonging to the family Brucellaceae. The taxonomy of *B. anthropi* MAPB-9 is described in Table 6.1.

**Table 6.1.** Taxonomy of *B. anthropi* MAPB-9

Cellular organism	Bacteria
Phylum	Proteobacteria
Class	Alpha-proteobacteria
Order	Hyphomicrobiales
Family	Brucellaceae
Group	Brucella/Ochrobactrum group
Genus	<i>Brucella</i>
Species	<i>anthropi</i>

This species has been isolated from various environmental sources and is considered an opportunistic pathogen of low virulence in humans. *B. anthropi* spp. has been considered attractive for biotechnological applications with various degradation abilities such as polychlorinated biphenyls (PCBs), PAH biodegradation, and chlorobenzene degradation. *O. anthropi* (referred to as *B. anthropi* hereafter) has been reported to degrade penta-, hexa-, and hepta-chlorinated PCB congeners (Murínová and Dercová, 2014a). Other than PCB, *B. anthropi* can degrade PAH (e.g pyrene and naphthalene) (Aziz et al., 2018), PAH by *B.anthropi* W13P3 (Wang et al., 2015), *B.anthropi*IITR07 (Tripathi et al., 2020), and naphthalene by *B.anthropi* BPyF3 (Ortega-Gonzalez et al., 2015). Also, *Brucella* sp. DDT-2 was found to degrade and utilize DDT as a sole source of carbon (Pan et al., 2017). In addition, *Brucella* sp. JAS2 (Abraham and Silambarasan, 2016) was also reported for the degradation of organochloro pesticides such as chlorpyrifos, while *B. anthropi* NC-1 (Pujar et al., 2019) was able to degrade the herbicide phenmedipham.

Whole-genome sequencing (WGS) is considered the ideal tool to study genomic variations of organisms in detail. With the advancement and development of next-generation sequencing technologies, complete bacterial genome sequencing has become easy, economical, and highly accessible. Whole-genome sequences provide identification and characterization of the gene in the microbes. Bioinformatic pipelines with optimized resolution aid in understanding the genome sequencing of several biodegraders. It also offers complete genome insights into the genetic background of the organisms' metabolic capability and biodegradation versatility. Whole genome sequencing techniques have unveiled several enzymes participating in pollutant degradation in different environments. genome analysis of pollutant- degrading bacterial strains, pollutant degradation/uptake mechanism, and their genetic adaptation for growing in pollutant -stressed environments might prove useful (Das et al., 2015; Elusfisan et al., 2020). In the past two years, the genome of several bacteria relevant to biodegradation processes have been sequenced and their complete, or nearly complete, sequences have become available.

A thorough understanding of the different properties of *B. anthropi* MAPB-9 will be helpful in its extensive exploitation for PCB bioremediation. The major objective of whole genome sequencing was to analyse the overall genome analysis of PCB degrading *B. anthropi* MAPB-9 for detailed exploration of genes related to xenobiotics degradation, metabolism, biosurfactant, chemotaxis, PGPR, and metal tolerance.

## **6.2. Material and Methods**

### **6.2.1. Bacterial, growth conditions, and chemicals**

*B. anthropi* MAPB-9 was cultured overnight in an LB culture medium at 30 °C for 48 h. Bacterial cells were collected by centrifugation and subjected to genomic DNA extraction using a commercial kit (Qiagen DNA isolation kit). The genomic DNA was monitored by 0.8% agarose gel electrophoresis and quantified using nanodrop (Simplinano). Whole genome sequencing was outsourced by AgriGenomePvt. Ltd. Kochi, India.

### **6.2.2. Genome sequencing, assembly, and annotation of *B. anthropi* MAPB-9**

High-quality 100 ng DNA was used for sequencing. Sequencing was performed using an Illumina NovaSeq 600HiSeq PE150 second-generation sequencer for de novo whole genome sequencing, followed by its processing and assembly. The raw reads obtained from Illumina paired-end sequencing were quality-checked using FastQC, which included analysis of base quality score

---

distribution, the average base content per read, and GC distribution in the reads. AdapterRemoval-V2v2.3 software was used to obtain high-quality clean reads to cast aside adapter sequences, low-quality bases, and ambiguous reads (Schubert et al., 2016). High-quality reads were used for de novo assembly using the Unicycler v0.4.8 genome assembler (Wick et al., 2017). Unicycler is an open-source GPL v3 used to assemble a bacterial genome from the data combining long and short reads. A Fastq quality check was performed to check the base quality score distributions, Fastq quality and filtering, average base content per read, and GC distribution in the read.

The initial assembly graph was generated from the short reads using the SPAdes assembler. The statistical analysis of the assembled data was performed using QUAST v4.6 (Gurevich et al., 2013), and BUSCO v4.1.4 software (Simao et al., 2015) was used for the generation of conserved gene levels. The whole Genome Shotgun sequence of MAPB-9 is deposited in the DDBJ/ENA/GenBank database under accession JAFNPK000000000 with submission ID SUB11804935, BioProject PRJNA859370, and BioSample SAMN29782699 and in Joint genome institute JGI genome portal with Gold project ID: Gp0690493 under Integrated Microbial Genomes (IMG) system with IMG Annotation Pipeline v.5.1.11 and gene calling program GeneMark.hmm-2 v1.25\_lic.

### 6.2.3. Gene Prediction and genome annotation

The prediction of coding sequences (CDS) from the Unicycler assembled contigs of *B. anthropi* MAPB-9 genome was predicted using Prokaryotic Dynamic Programming Gene finding Algorithm, Prodigal v2.6.3 software (Hyatt et al., 2010). The annotation of the predicted genes included matched gene sequences with the UniProt database using BLASTX v 2.6.0. organism annotation and gene ontology (GO) annotation (Ashburner et al., 2000). The predicted genes were compared with the UniProt database using the BLASTX program, considering the E-Value cutoff to be  $10^{-3}$ . It was followed by filtering out the best BLASTX hit based on the query coverage, similarity score, identity, and gene description. The organism's name was extracted from the top BLASTX hit for the organism annotation. After the organism annotation, GO for the genes was mapped, which included three categories: biological process (BP), molecular function (MF), and cellular component (CC). The other tools, such as PATRIC v3.6.9 (PATHosystems Resource Integration Centre) (Davis et al., 2020) that uses RASTtk (Rapid Annotation using Subsystems Technology) (Bertin et al., 2015) server for the annotation of the genome has also been used for

the annotation, circular map generation, and phylogenetic analysis. JGI online portal was used for analysis and annotation of the genome in a comprehensive comparative context.

#### 6.2.4. Alignment of the genome and phylogenetic analysis

The phylogenetic analysis of the *B. anthropi* MAPB-9 genome with the other reference and representative genome was performed using PATRIC v3.6.9. The identification of the closest reference and representative genome was performed by Mash/MinHash (Ondov et al., 2016). The phylogenetic placement of the genome was done by the selection of PATRIC global protein families (PGFams) (Davis et al., 2016) from the genome, which was followed by the alignment of protein sequence from the families using MUSCLE (Edgar, 2004) and nucleotide mapping of each sequence to the protein alignment. The amino acid and nucleotide alignments were joined into a data matrix that was analyzed using RaxML (Stamatakis, 2014) with fast bootstrapping (Stamatakis et al., 2008) that has been represented as the support value in the tree. The evolutionary history was inferred by using the Maximum Likelihood method and the Kimura 2- parameter model (Kimura, 1980). The bootstrap consensus tree inferred from 1000 replicates is taken to represent the evolutionary history of the taxa analyzed. Initial tree(s) for the heuristic search were obtained automatically by applying Neighbor-Join and BioNJ algorithms to a matrix of pairwise distances estimated using the Maximum Composite Likelihood (MCL) approach and then selecting the topology with superior log likelihood value. Evolutionary analyses for the ARHD gene were conducted in MEGA11 (Tamura et al., 2021).

### 6.3. Results and Discussion

#### 6.3.1. Whole genome sequencing, *de novo* assembly, and genome characterization of MAPB-9

##### 6.3.1.1. Bioinformatics analysis pipeline

The Bioinformatics analysis pipeline for the De novo genome assembly of *B. anthropi* MAPB-9 having R1 and R2 paired-end reads with mean reads length 151 bp (Table 6.2).

**Table 6.2.** Raw read summary of *B. anthropi* MAPB-9

Sample	Read orientation*	Number of reads	Number of bases (MB)	% GC	Mean read length (bp)
MAPB-9	R1	15,120,879	2283.25	56.57	151.0
	R2	15,120,879	2283.25	56.46	151.0

\*R1 and R2 represents the paired end reads for forward and reverse strands

The top BLASTX hit of each gene was studied, and the organism's name was extracted. The top 10 organisms are shown in Fig. 6.1. Majority of the top BLASTX hit belong to *O. anthropi* ATCC 49188/ DSM 68882/ JCM 21032/ NBRC 15819/ NCTC 12168. The *Ochrobactrum* genus has been reclassified to *Brucella* (Hordt et al., 2020). Therefore, the analyzed genome sequence belongs to *Brucella anthropi*. The details of genome sequencing of ten species of *B. anthropi* have been described in Table 6.3.

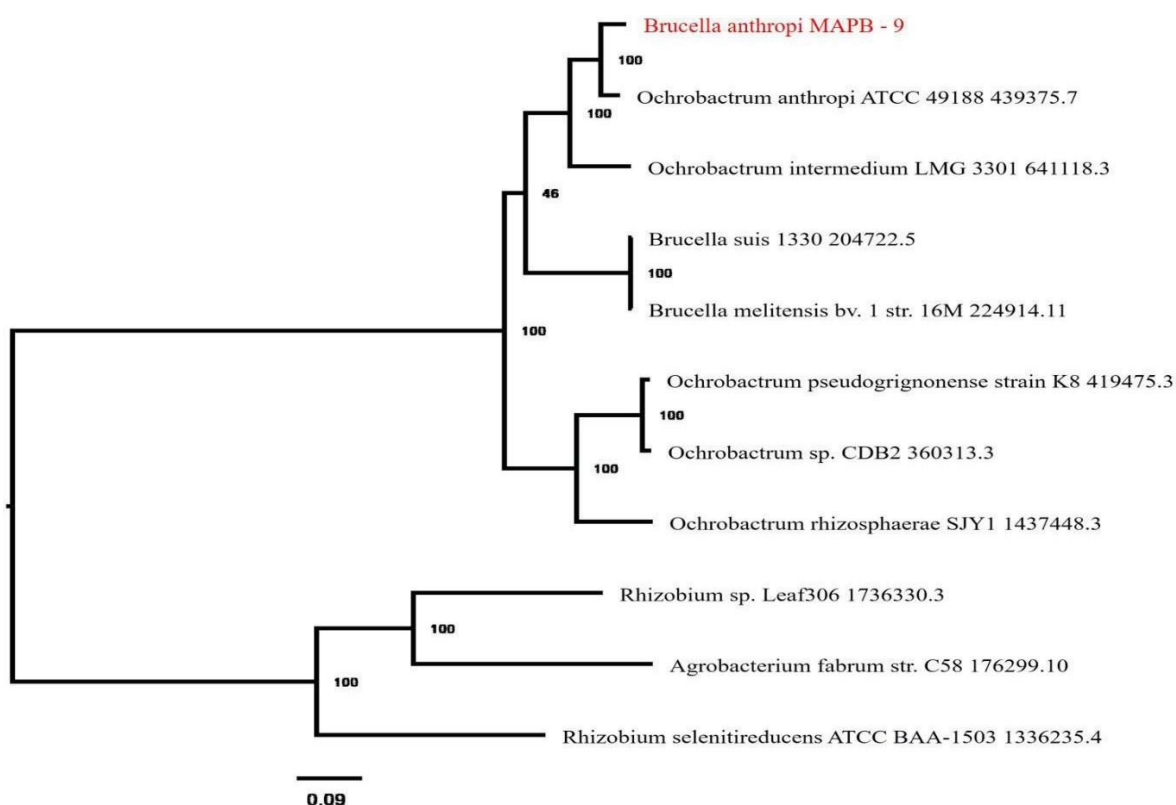


**Fig. 6.1.** Organism annotation based on the top BLASTX hits.

The hierarchical clustering of *B. anthropi* MAPB-9 based on the functional profiles showed closest match with *Ochrobactrum* sp. DDT2 as shown in Fig. 6.2.

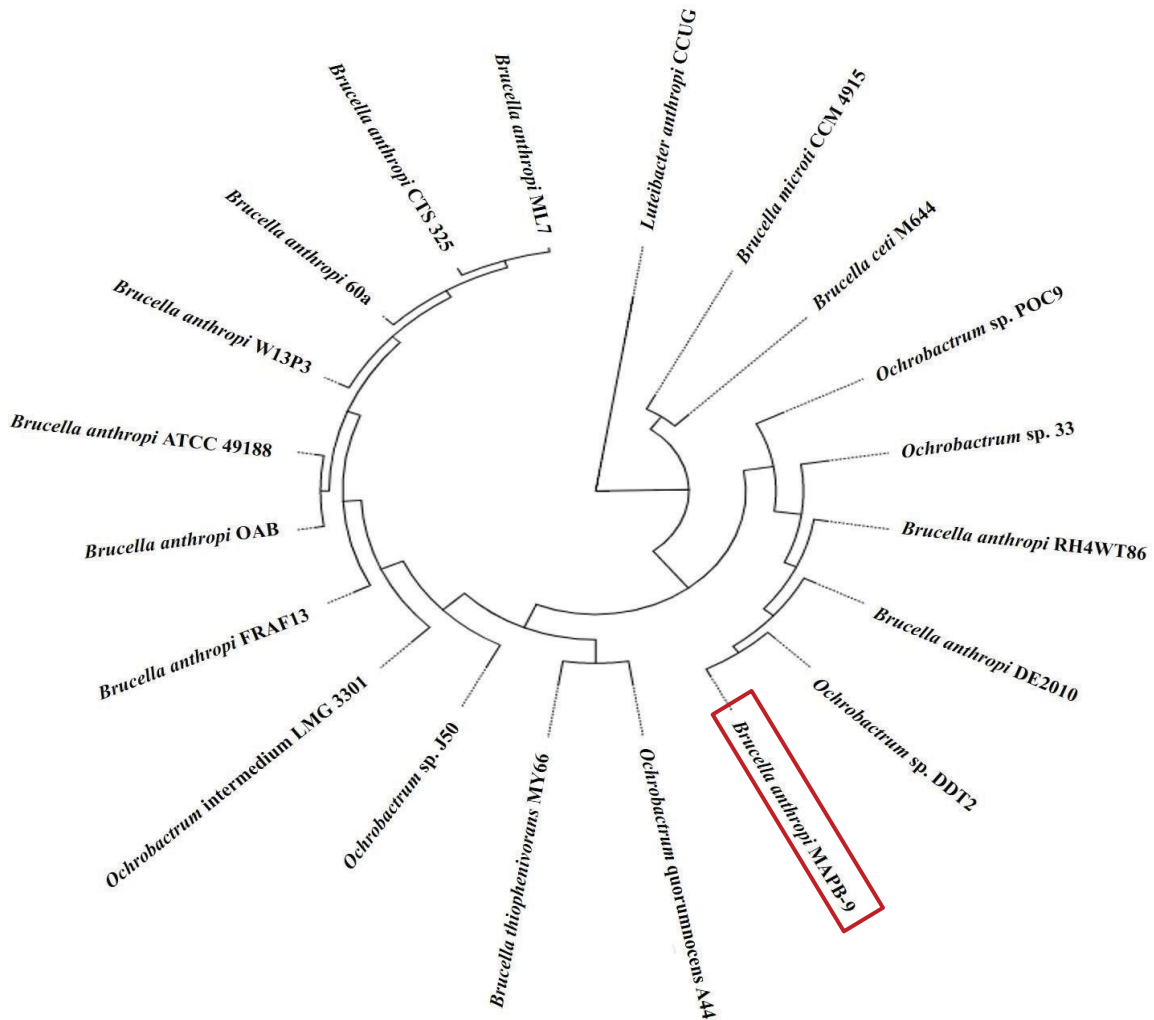


**Fig. 6.2.** Hierarchical Clustering of *B. anthropi* MAPB-9 based on the functional profiles with the 20 selected genomes belonging to *B. anthropi* and *O. spp.* The proximity of grouping indicates the relative degree of similarity of samples.



**Table 6.3.** Details of the status of genome sequencing of *B. anthropi* species.

Genome Name	Total gene count	No. of CDS genes	CDS genes (%)	RNA genes	No. of rRNA genes	No. of 5S rRNA	No. of 16S rRNA	No. of tRNA	GC (%)	Total no. of bases
<i>B. anthropi</i> MAPB-9	4749	4644	97.79	60	3	1	1	52	56	4824454
<i>B. anthropi</i> 60a	4883	4820	98.71	63	3	1	1	47	56.07	4590021
<i>B. anthropi</i> ATCC 49188	4952	4856	98.06	96	12	4	4	58	56.13	5205777
<i>B. anthropi</i> CTS-325	4532	4460	98.41	72	5	1	1	49	56.02	4712978
<i>B. anthropi</i> DE2010	4725	4620	97.78	58	3	1	1	50	56.52	4904693
<i>B. anthropi</i> FRAF13	4289	4218	98.34	71				50	55.98	4538068
<i>B. anthropi</i> ML7	4842	4770	98.51	72	3	1	1	50	56.01	4904177
<i>B. anthropi</i> OAB	4705	4608	97.94	97	12	4	4	59	56.08	4901165
<i>B. anthropi</i> RH4WT86	4695	4587	97.7	86	3	1	1	52	55.9	4808005
<i>B. anthropi</i> W13P3	5022	4965	98.86	57	3	1	1	53	56.34	5277767

Details of the assembled genome assembly of *B. anthropi* MAPB-9 are given in Table 6.3. *B. anthropi* MAPB-9 consisted of a circular genome having a total size of 4,82,4,454bp. *B. anthropi* MAPB-9 genome comprised 4,749 CDSs in which 4,644 genes represented significant BlastX match characterized using UniProt. The assembled genome was arranged in 57 contigs/scaffolds, and the total GC content was 55.87%. The isolate contains a total of 4,644 protein-coding sequences (CDS) covering 52 transfer RNA (tRNA) genes, 3 ribosomal RNA (rRNA) genes and five other RNAs (Table 6.4).

The annotation included 1,212 hypothetical proteins and 3,872 proteins with functional assignments (Table 6.5). The proteins with functional assignments included 1,267 proteins with Enzyme Commission (EC) numbers (Schomburg et al., 2004), 2,626 with KEGG Ontology (KO) assignments, and 1593 proteins that were mapped to KEGG pathways (Kanehisa et al., 2016). Protein coding genes with COGs include 3911 proteins.

**Table 6.4.** Details of assembled genome of *B. anthropi* MAPB-9

Features	Number	% of Total
<b>DNA, total number of bases</b>	4824454	100.00%
DNA coding number of bases	4269640	88.50%
DNA G+C number of bases	2695350	55.87%
<b>DNA scaffolds</b>	57	100.00%
<b>Genes total number</b>	4749	100.00%
Protein coding genes	4644	97.79%
Regulatory and miscellaneous features	45	0.95%
RNA genes	60	1.26%
Protein coding genes with function prediction	3872	81.53%
Protein coding genes with enzymes	1267	26.68%
Protein coding genes connected to KEGG pathways	1593	33.54%
Protein coding genes connected to KEGG Orthology (KO)	2626	55.30%
Protein coding genes connected to MetaCyc pathways	1124	23.67%
Protein coding genes with COGs	3911	82.35%
with Pfam	3960	83.39%
with TIGRfam	1334	28.09%
with SMART	976	20.55%

**Table 6.5.** Genome annotation of *B. anthropi* MAPB-9 providing protein features using UniProt

Protein features	No. of Feature
Hypothetical proteins	1212
Proteins with functional assignments	3,652
Proteins with EC number assignments	1,084
Proteins with GO number assignments	929
Proteins with pathway assignments	826
Proteins with genus-specific family (PLFams) assignment	25,41
Proteins with cross genus-specific family (PGFams) assignment	4,664

### 6.3.1.2. Characteristics of genome

The annotation of *B. anthropi* MAPB-9 performed by RASTtk generated complete genome annotation in the form of circular map representation (Fig. 6.3).

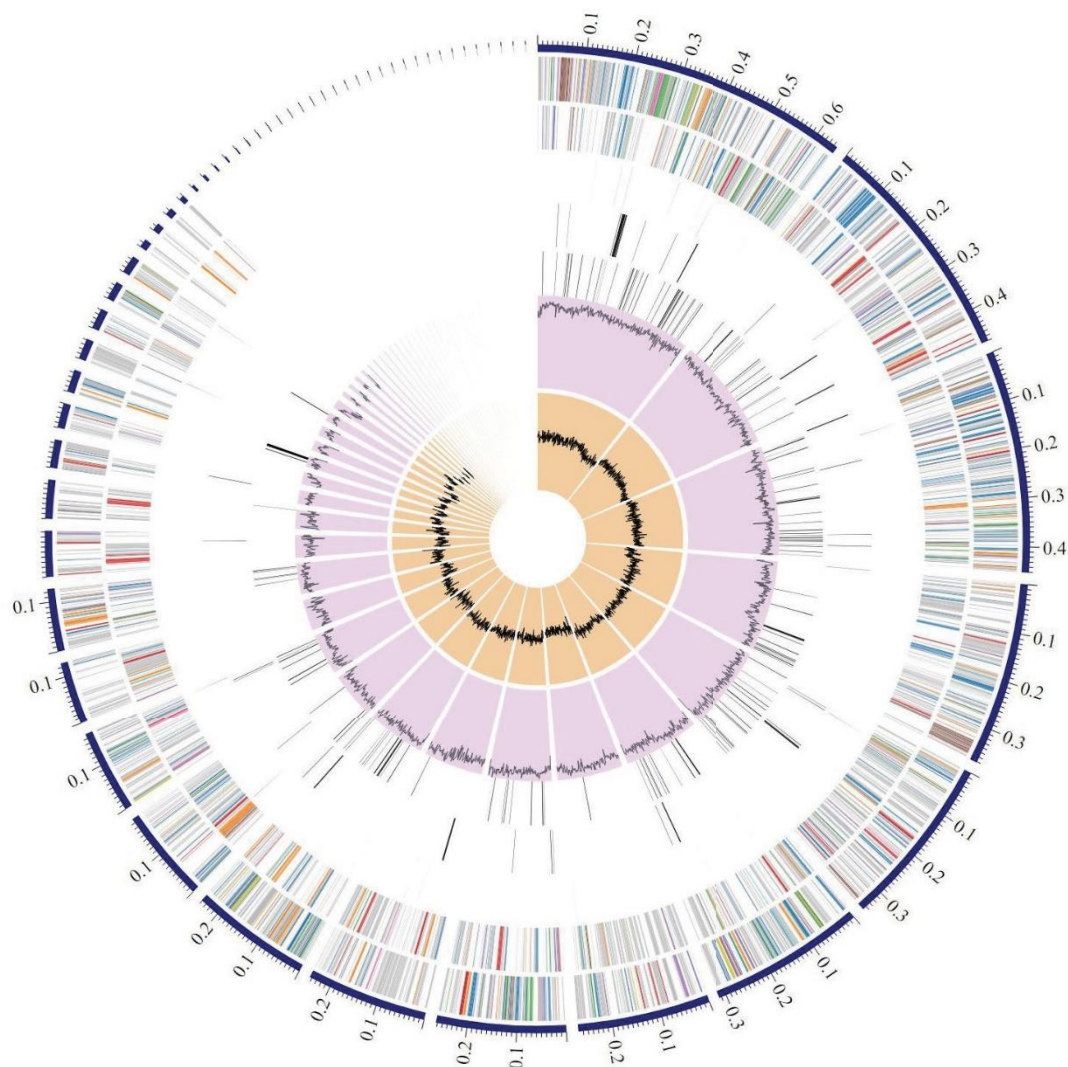


**Fig. 6.3.** A circular graphical display of the distribution of the genome *B. anthropi* MAPB-9 annotations. This includes, from outer to inner rings, the contigs, CDS on the forward strand, CDS on the reverse strand, RNA genes, CDS with homology to known antimicrobial resistance genes, CDS with homology to known virulence factors, GC content, and GC skew. The circular genome map representation was constructed using PATRIC v3.6.9.

#### Gene annotation

The annotation of the predicted genes was performed by comparing it with the BLASTX program and mapping the GO terms for the genes in three categories: BP, MM, and CC. The GO annotation based on the BP category revealed the maximum number (>100) of genes to be

involved in the transmembrane transport, followed by regulation of transcription (DNA template) (>80), Translation (=60), methylation (>40), peptidoglycan biosynthetic process (>35), amino acid transport (>35), carbohydrate metabolic process (>35), protein transport (>30), cell division (>30), and phosphor relay signal transduction system (>30) (Fig. 6.4A).

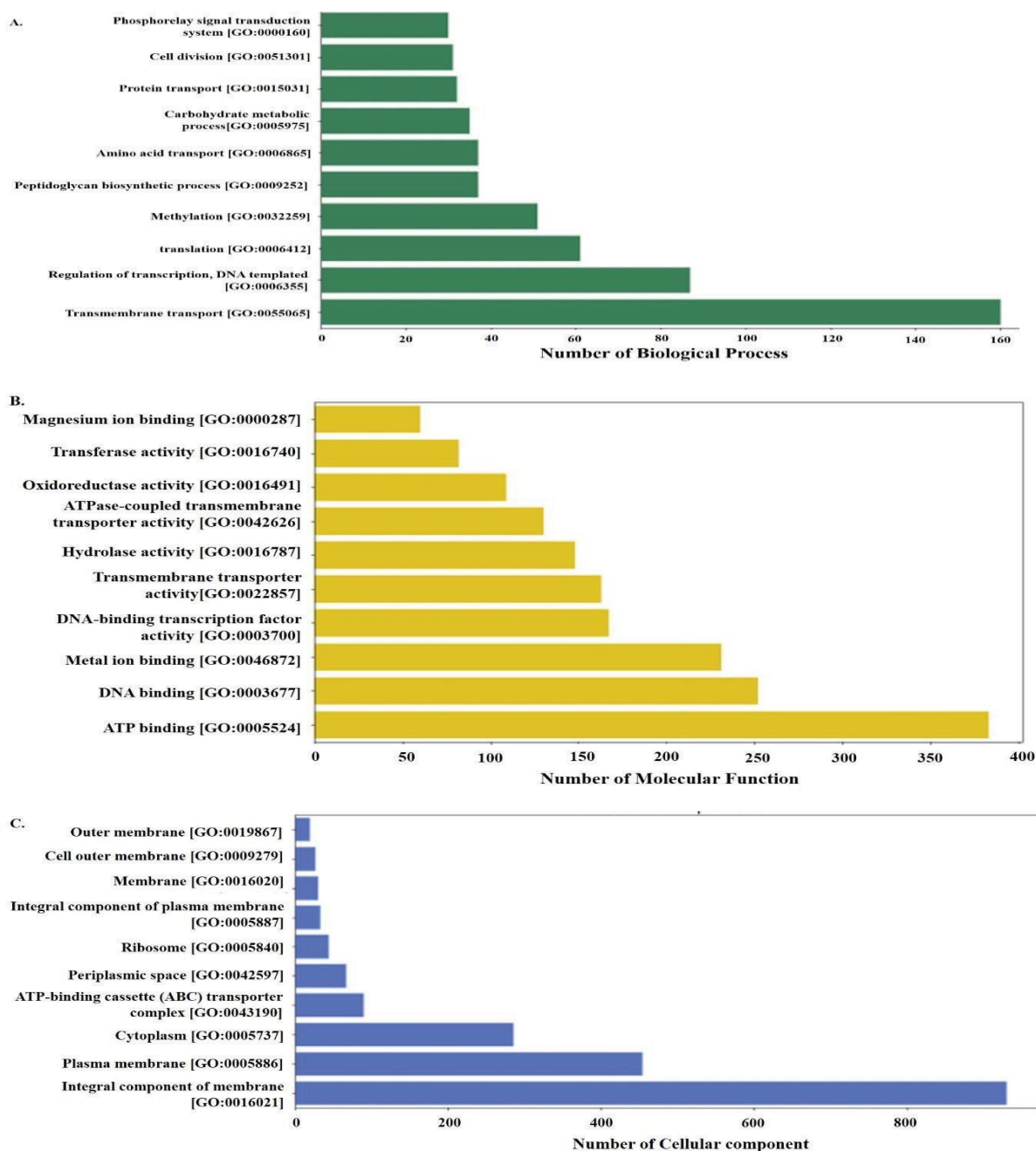


**Fig. 6.4.** Annotation of genes based on their (A) biological process, (B) molecular function, (C) cellular component.

Under the MF category, the highest number of genes belonged to ATP binding (>350), DNA binding (=250), metal ion binding (>200), DNA binding transcription factor (>150), transmembrane transporter activity (>150), hydrolase activity (~150), ATPase coupled transmembrane transporter (>100), oxidoreductase activity (>100), transferase activity (>50), and magnesium ion binding (>50) (Fig. 6.4B). The annotation based on the CC category revealed the maximum number of the genes for the integral component of the membrane (>800), followed by genes related to the plasma membrane (>400), cytoplasm (>200), ATP binding cassette transporter complex (<200), periplasmic space (<200), ribosome (<200), integral component of the plasma membrane (<200), membrane (<200), cell outer membrane (<200), and outer membrane (<200) (Fig. 6.4C).

The RASTtk annotation of *B. anthropi* MAPB-9 genome assigned subsystems to each identified gene product or protein, which is a protein group that together executes a specific biological process. The colours of the CDS on the forward and reverse strands indicate the subsystem that these genes belong to Subsystems depicted in the pie chart (Fig. 6.6).

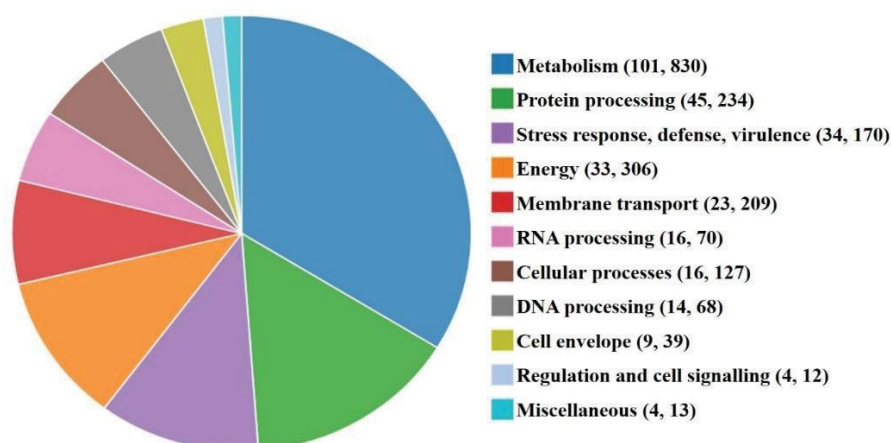


**Fig. 6.5.** Subsystem distribution statistic of *B. anthropi* MAPB-9 based on genome annotation by PATRIC software. The pie chart denotes the abundance of subsystem categories, and each subsystem feature with protein coding genes is listed in parentheses separated by comma in the legend chart.

The RASTtk annotation of *B. anthropi* MAPB-9 genome assigned subsystems to each identified gene product or protein which is protein group that together execute a specific biological process or form a structural complex. An overview of the subsystem has been depicted in the form of a pie chart Fig. 6.6. Among different types of subsystems found in the bacterial genome, the most abundant subsystem categories were related to metabolic processes with



101 subsystems and 830 protein-coding genes followed by protein processing with 45 subsystems and 234 protein-coding genes. Stress response, defense, and virulence consists of 34 subsystem categories and 170 protein-coding features. The other subsystems consist of energy (33), membrane transport (23), RNA processing (16), cellular processes (16), DNA processing (14), cell envelop (9), regulation and cell signaling (4), and Miscellaneous (4) with 306, 209, 70, 127, 68, 39, 12 and 13 protein-coding genes, respectively

### Gene distribution

The whole genome of *B. anthropi* MAPB-9 describes the annotation of subsystem distribution based on the RAST server (Fig. 6.6). Genes annotated for amino acid and derivatives (373), carbohydrate metabolism (251 ORFs), protein metabolism (200), cofactor, vitamins, prosthetic and pigment (169), respiration (117) and membrane transport (99), DNA metabolism (93), nucleosides and nucleotides (82), stress response (64), fatty acid, lipid and isoprenoids (57), chemotaxis (51), and nitrogen metabolism (50) were abundant amongst the subsystem categories.

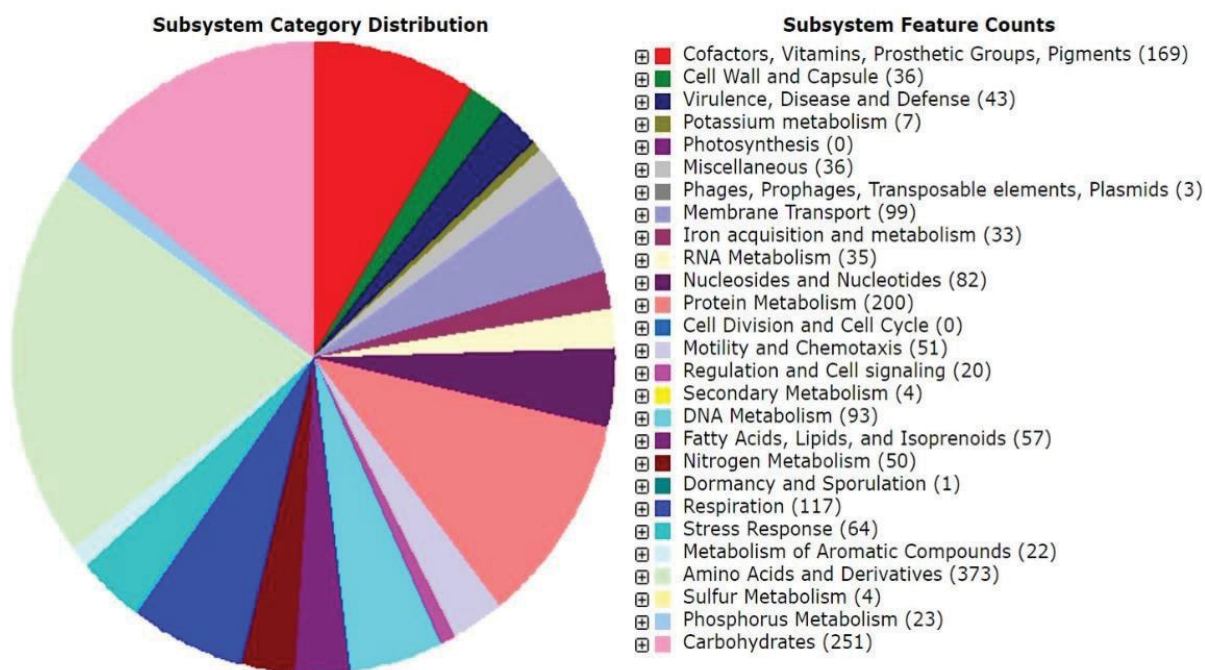


**Fig. 6.6.** RAST server based on genome annotation revealed the subsystem distribution of *B. anthropi* MAPB-9. The pie chart represents the abundance, and the count of each subsystem category is listed in parenthesis in the chart legend.



### 6.3.2. Genomic potential of *B. anthropi* MAPB-9 for xenobiotic degradation and metabolism

The genes in a subset of the KEGG xenobiotic biodegradation pathways with peripheral aromatic degradation pathways involve benzoate, chloroalkane and chloroalkene, chlorocyclohexane and chlorobenzene, toluene, xylene, nitrotoluene, ethylbenzene, styrene, dioxin, naphthalene, polycyclic aromatic hydrocarbons, and metabolism of xenobiotics by cytochrome P450). Degradation of aromatic compounds *B. anthropi* is known for its ability to degrade many organic aromatic compounds, usually by using ring hydroxylating dioxygenases in the first step of their catabolism. JGI genome online portal was used to identify genes accounting for the ability of the *B. anthropi* MAPB-9 for xenobiotic degradation, esp. dioxin, PCB, biphenyl, naphthalene, and benzoate. These genetic clusters putatively involved in the degradation of aromatic compounds are summarized as follows:

#### Chloroalkane and chloroalkene biodegradation and metabolism

Some of the gene KEGG number and gene name involved in chloroalkane and chloroalkene biodegradation and metabolism includes aldehyde dehydrogenase (NAD<sup>+</sup>) [EC:1.2.1.3] K01560 E3.8.1.2; 2-haloacid dehalogenase [EC:3.8.1.2] K00121 *frmA*, *ADH5*, *adhC*; S-(hydroxymethyl) glutathione dehydrogenase/alcohol dehydrogenase [EC:1.1.1.284 1.1.1.1] K00001 E1.1.1.1, *adh*; alcohol dehydrogenase [EC:1.1.1.1] K13953 *adhP*; alcohol dehydrogenase [EC:1.1.1.1] K00148 *fdhA*; alcohol dehydrogenase [EC:1.2.1.10 1.1.1.1].

#### Chlorocyclohexane and Chlorobenzene biodegradation and metabolism

List of the gene KEGG number and gene name involved in Chlorocyclohexane and Chlorobenzene biodegradation and metabolism include K00462 *bphC*; biphenyl-2,3-diol 1,2- dioxygenase [EC:1.13.11.39] carboxymethylene butenolidase [EC:3.1.1.45], K15237 *linC*; hydroquinone 1,2-dioxygenase [EC:1.13.11.66] K15246 *tftD*; muconate cycloisomerase [EC:5.5.1.1] K00446 *dmpB*, *xyIE*; catechol 2,3-dioxygenase [EC:1.13.11.2] K07104 *catE*; catechol 2,3-dioxygenase [EC:1.13.11.2] K15253 *tcbC*, *tfdC*; 2-haloacid dehalogenase [EC:3.8.1.2] K01561 *dehH*; haloacetate dehalogenase [EC:3.8.1.3].

#### Dioxin biodegradation and metabolism

List of the gene KEGG number and gene name involved in dioxin biodegradation and metabolism includes K00480 E1.14.13.1; salicylate hydroxylase [EC:1.14.13.1] K02554 *mhpD*;

K18088 *bphAd*, *bphA4*, *bphG*; biphenyl 2,3-dioxygenase ferredoxin reductase component [EC:1.18.1.3].

### **Naphthalene biodegradation and metabolism**

List of the gene KEGG number and gene name includes in naphthalene biodegradation and metabolism: K00121 *adhC*; alcohol dehydrogenase [EC:1.1.1.284 1.1.1.1] K00001 E1.1.1.1, *adh*; alcohol dehydrogenase [EC:1.1.1.1] K13953 *adhP*; alcohol dehydrogenase, propanol-preferring [EC:1.1.1.1] K00480 E1.14.13.1; salicylate hydroxylase [EC:1.14.13.1] K14578 *nahAb*, *nagAb*, *ndoA*, *nbzAb*, *dntAb*; naphthalene 1,2-dioxygenase ferredoxin component K18243 *nagH*; salicylate 5-hydroxylase small subunit [EC:1.14.13.172] K18242 *nagG*; alcohol dehydrogenase [EC:1.1.1.1] K14581 *nahAa*, *nagAa*, *ndoR*, *nbzAa*, *dntAa*; naphthalene 1,2-dioxygenase ferredoxin reductase component [EC:1.18.1.7] K04072 *adhE*; acetaldehyde dehydrogenase/ alcohol dehydrogenase [EC:1.2.1.10 1.1.1.1] naphthyl-2-oxomethyl-succinyl-CoA thiolase subunit [EC:2.3.1.-] K00152 *nahF*; salicylaldehyde dehydrogenase [EC:1.2.1.65] K14584 *nahD*; K14579 *nahAc*, *ndoB*, *nbzAc*, *dntAc*; naphthalene 1,2-dioxygenase subunit alpha [EC:1.14.12.12 1.14.12.23 1.14.12.24] K14580 *nahAd*, *ndoC*, *nbzAd*, *dntAd*.

### **Polycyclic aromatic hydrocarbon biodegradation and metabolism**

List of the gene KEGG number and gene name involves in Polycyclic Aromatic Hydrocarbon (PAH) biodegradation and metabolism: K14579 *nahAc*, *ndoB*, *nbzAc*, *dntAc*; naphthalene 1,2-dioxygenase subunit alpha [EC:1.14.12.12 1.14.12.23 1.14.12.24] K14580 *nahAd*, *ndoC*, *nbzAd*, *dntAd*; naphthalene 1,2-dioxygenase subunit beta [EC:1.14.12.12 1.14.12.23 1.14.12.24] K14578 *nahAb*, *nagAb*, *ndoA*, *nbzAb*, *dntAb*; naphthalene 1,2-dioxygenase ferredoxin component K14581 *nahAa*, *nagAa*, *ndoR*, *nbzAa*, *dntAa*; naphthalene 1,2-dioxygenase ferredoxin reductase component [EC:1.18.1.7] K00480 E1.14.13.1; salicylate hydroxylase [EC:1.14.13.1] K11943 *nidA*; K11945 *phdF*; extradiol dioxygenase [EC:1.13.11.-] K11947 *nidD*; aldehyde dehydrogenase [EC:1.2.1.-] phthalate 3,4-dioxygenase ferredoxin reductase component [EC:1.18.1.3] 3-hydroxybenzoate 4-monooxygenase [EC:1.14.13.23] K00448 *pcaG*; protocatechuate 3,4-dioxygenase, alpha subunit [EC:1.13.11.3] K00449 *pcaH*; protocatechuate 3,4-dioxygenase, beta subunit [EC:1.13.11.3]

## Benzoate biodegradation and metabolism

List of the gene KEGG number and gene name involves in benzoate biodegradation and metabolism: K01055 *pcaD*; 3-oxoadipate enol-lactonase [EC:3.1.1.24] K14727 *pcaC*; 4-carboxymuconolactone decarboxylase [EC:4.1.1.44] K01031 *pcaI*; 3-oxoadipate CoA-transferase, alpha subunit [EC:2.8.3.6] K01032 *pcaJ*; 3-oxoadipate CoA-transferase, beta subunit [EC:2.8.3.6] K00632 *fadA*, *fadI*; acetyl-CoA acyltransferase [EC:2.3.1.16] K07823 *pcaF*; 3-oxoadipyl-CoA thiolase [EC:2.3.1.174] K00446 *dmpB*, *xylE*; catechol 2,3-dioxygenase [EC:1.13.11.2] K07104 *catE*; catechol 2,3-dioxygenase [EC:1.13.11.2] K00217 E1.3.1.32; maleylacetate reductase [EC:1.3.1.32] K00448 *pcaG*; protocatechuate 3,4-dioxygenase, alpha subunit [EC:1.13.11.3] K00449 *pcaH*; protocatechuate 3,4-dioxygenase, beta subunit [EC:1.13.11.3] K01857 *pcaB*; 3-carboxy-cis,cis-muconate cycloisomerase [EC:5.5.1.2] K01607 *pcaC*; 4-carboxymuconolactone decarboxylase [EC:4.1.1.44] K10218 *ligK*, *galC*; 4-hydroxy-4-methyl-2-oxoglutarate aldolase [EC:4.1.3.17] K00481 *pobA*; p-hydroxybenzoate 3-monooxygenase [EC:1.14.13.2] K19065 *mobA*; 3-hydroxybenzoate 4-monooxygenase [EC:1.14.13.23] K01782 *fadJ*; 3-hydroxyacyl-CoA dehydrogenase / enoyl-CoA hydratase / [EC:10.1.1.35 4.2.1.17] K01825 *fadB*; 3-hydroxyacyl-CoA dehydrogenase / enoyl-CoA hydratase / [EC:1.1.1.35 4.2.1.17] K07516 *fadN*; 3-hydroxyacyl-CoA dehydrogenase [EC:1.1.1.35] K00252 GCDH, *gcdH*; glutaryl-CoA dehydrogenase [EC:1.3.8.6] K01692 *paaF*, *echA*; enoyl-CoA hydratase [EC:4.2.1.17] K13767 *fadB*; enoyl-CoA hydratase [EC:4.2.1.17] K00074 *paaH*, *hbd*, *fadB*, *mmgB*; 3-hydroxybutyryl-CoA dehydrogenase [EC:1.1.1.157] K00626 ACAT, *atoB*; acetyl-CoA C-acetyltransferase [EC:2.3.1.9].

Regarding central aromatic metabolism, genes for  $\beta$ -keto adipate (*pcaGHBCDIJ*) metabolism was found predominantly in the MAPB-9 chromosome. Two copies of the catechol 2,3-dioxygenase-encoding genes (*catE*) involved in catechol meta-cleavage are probably related to specific catabolic pathways of aromatic compounds. Interestingly, genes involved in protocatechuate degradation suggest specialized metabolism of aromatic compounds.

## Dehalogenases and dioxygenases

Halogenase and dioxygenase are the most important genes for the removal of chlorine and cleavage of the aromatic ring of organic compounds such as PCB. Thus, dehalogenase, ARHD,

naphthalene dioxygenase, bleomycin resistance protein, glyoxalase I, and type I ring-cleaving dioxygenases were explored and were found to be present in *B. anthropi* MAPB-9.

### Haloacid dehalogenases

Chlorinated aromatic compounds such as chlorobenzoates, chlorobenzenes, chlorophenols, polychlorinated biphenyl, hexachlorobenzene, chloronitrophenols, atrazine, and chloroaminophenols comprise major environmental pollutants. Due to the presence of carbon-chlorine bonds, they are difficult to degrade. Therefore, the cleavage of carbon-chlorine bonds is the most crucial step in their degradation. Bacterial haloacid dehalogenases (HADs) belong to a large superfamily of hydrolases with diverse substrate specificity. The genes encoding HAD superfamily hydrolase (TIGR01509 family), 2-haloacid dehalogenase, putative hydrolase of the HAD superfamily, and 4-hydroxybenzoate polyprenyl transferase were found to be present in different contigs. The presence of dehalogenase in *B. anthropi* MAPB-9 suggests its potential to remove chlorine molecules from the PCB, dioxin, and other chlorinated pollutants like chloroalkane and chloroalkene chlorocyclohexane, and chlorobenzene. Duplication of genes leading to the existence of families with related functions is common in bacteria (Rai et al., 2012).

**Table 6.6.** Details of Haloacid dehalogenases identified in *B. anthropi* MAPB-9.

Contig	HAD	Locus tag	Nucleotide	Protein(size)	Strand	COG
#03	HAD superfamily hydrolase (TIGR01509 family)	433867-434553	687bp;	228aa	-	COG0637
#03	2-haloacid dehalogenase	438039-438653	615bp;	204aa	-	COG1011
#05	Putative hydrolase of the HAD superfamily	70831- 71535	705bp;	234aa	-	COG1011
#05	HAD superfamily hydrolase (TIGR01509 family)	102231-102902	672bp;	223aa	+	COG0637
# 06	4-hydroxybenzoate polyprenyl transferase	183146-184627	1482bp;	493aa	-	
# 06	HAD superfamily hydrolase (TIGR01509 family)	251141-251989	849bp;	282 aa	+	COG0647
# 12	2-haloacid dehalogenase	21766-22419	654bp;	217aa	+	COG1011
# 15	HAD superfamily hydrolase (TIGR01509 family)	65428-66135	708bp;	235aa	-	COG0637

These events are postulated to permit adaptation to different environments. Gene duplication of HAD relates to the adapted utilization of chlorinated contaminants such as chloroalkanes and chlorobenzoate, and PCB identified in the collected soil sample (discussed in Chapter 3). Table 6.6. details of HAD superfamily present in *B. anthropi* MAPB-9. The dioxin degradation pathway includes Polychlorinated dibenzofurans (PCDFs), Polychlorinated dibenzodioxins (PCDD), and PCB compounds. The dioxin degradation pathway is the same as PCBs (discussed in Chapter 2). The initial step includes dioxygenases consisting of a terminal aromatic-ring hydroxylating dioxygenase (ARHD) and two-electron carrier encoding proteins. Electrons from NAD(P)H are transferred to the dioxygenase *via* the electron supply system NAD(P)H-ferredoxin reductase and ferredoxin to catalyse the oxidation of PCDDs and PCDFs like PCB (Nam et al., 2001; Nojiri and Omori, 2001). In MAPB-9, contig #1 included ferroxedin-NADP reductase (gene#690) and Rieske 2Fe-2S family protein of aromatic ring-hydroxylating dioxygenase, large terminal subunit (gene #691) at locus 20663-21781, and 21815-23062 in (-) strand, respectively (Fig. 6.7). The alpha-subunits of dioxygenase gene were recognized by COG4638 (large subunits of phenylpropionate dioxygenase and ring-hydroxylating dioxygenases). Gene Neighborhoods of ARHD, a large terminal subunit of *B. anthropi* MAPB-9 (JGI submission Gold ID Ga0590102), was performed. Gene neighborhood relates to gene pairs having a conserved topological neighbourhood in many bacterial genomes and is considered to encode interacting or functionally related proteins, mainly COG.

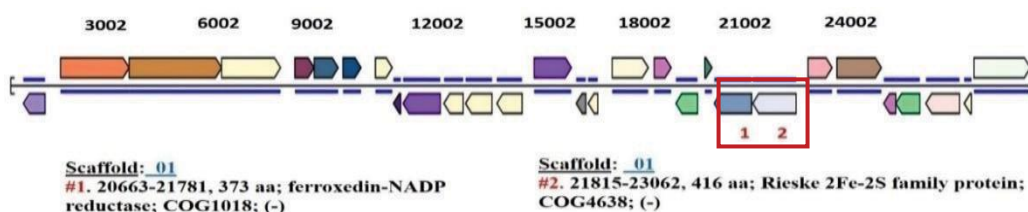


**Fig. 6.7.** Region of Contig #1 consists of ferroxedin-NADP reductase COG 1018 and Rieske 2Fe-2S ARHD alpha large unit of COG4638 in (-) strand at locus 20663-21781 and 21815-23062, respectively.

Neighborhoods of these genes in other genomes, namely *Ochrobactrum sp.* 370MF3.1, *Ochrobactrum sp.* POC9, *O. anthropi* RH4WT86, *O. anthropi* ML7, *Ochrobactrum sp.* DDT2, *Ochrobactrum sp.*, *O. lupini* LUP21, *O. cytisi* IPA7.2, and *O. anthropi* OAB with the same top Clusters of Orthologous Genes (COG) hit and with roughly the same matching length is shown in Fig. 6.8.



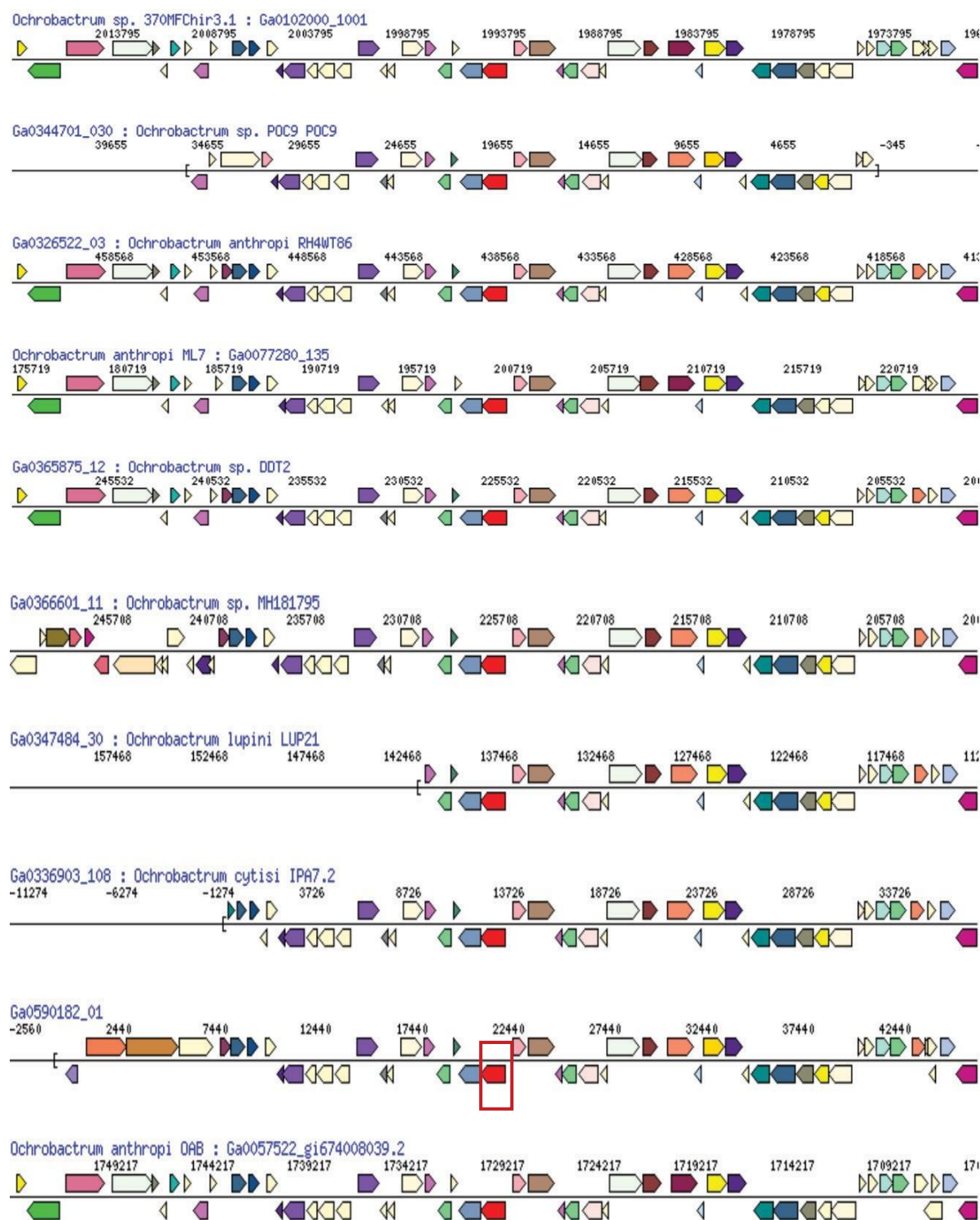


**Fig. 6.8.** Gene Neighborhoods of aromatic ring-hydroxylating dioxygenase, large terminal subunit in *B. anthropi* MAPB-9 (enclosed in red box) and 10 other isolates. Gene of the same color (except light yellow) is from the same orthologous group (top COG hit). Light yellow = no COG assignment, white = pseudo gene, Red = marker gene i.e. ARHD.



These genes are embedded in segments of the chromosome that have synteny with other PCB-degrading *Brucella/Ochrobactrum* isolates. A phylogenetic tree of the ARHD gene of *B. anthropi* MAPB-9 and other closely related bacteria was constructed (Fig. 6.9). It was observed that the gene was grouped with the sequence of *B. anthropi* RH4WT86 and *Ochrobactrum* sp. DDT2. *Ochrobactrum* sp. DDT2 was isolated from DDT-contaminated soil and was found to be capable of degrading DDT as the sole carbon and energy source (Pan et al., 2017). The nucleic acid sequence was converted to a protein sequence for bioinformatic analysis of ARHD.

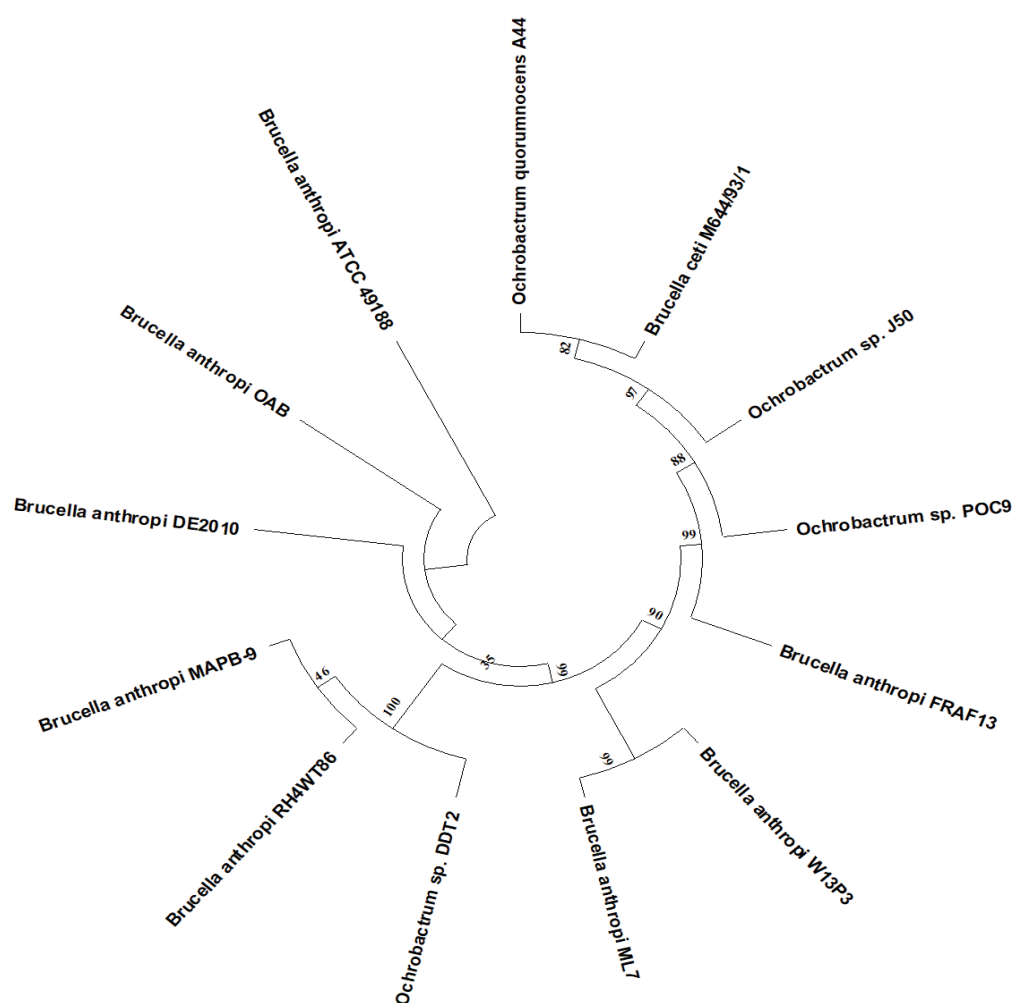


**Fig. 6.9.** A phylogenetic tree of ARHD gene of *B. anthropi* MAPB-2 and other closely related bacteria. The evolutionary history was inferred by using the Maximum Likelihood method and the Kimura 2-parameter model. The bootstrap consensus tree inferred from 1000 replicates is taken to represent the evolutionary history of the taxa analyzed. Initial tree(s) for the heuristic search were obtained automatically by applying Neighbor-Join and BioNJ algorithms to a matrix of pairwise distances estimated using the Maximum Composite Likelihood (MCL). Evolutionary analyses were conducted in MEGA5.

Contig #2 consists of the Protocatechuate *pca* operon gene and was found to be arranged in the order 3-carboxy-cis, cis-muconate cycloisomerase *pcaB* (gene#1510), protocatechuate 3,4-dioxygenase, alpha subunit *pcaG* (gene#1511), protocatechuate 3,4-dioxygenase, beta subunit *pcaH* (gene#1512), 4-carboxymuconolactone decarboxylase *pcaC* (gene#1513), 3-oxoadipate enol-lactonase *pcaD* (gene#1514) in (-) strand, LysR family *pca* operon transcriptional activator *pcaQ* (gene#1515) in (+) strand, p-hydroxy benzoate 3- monooxygenase *pobA* (gene#1516) in (-) strand, AraC family transcriptional activator of *pobA*, *pobR* (gene#1517) in (+) strand, IclR family *pca* regulon transcriptional regulator *pcaR* (gene#1518) in (-) strand, 3-oxoadipate CoA- transferase alpha subunit *pcaI* (gene#1519), 3-oxoadipate CoA-transferase beta subunit *pcaJ* (gene#1520), 3-oxoadipyl-CoA thiolase *hcaD* (gene#1521) in (+) strand (Fig. 6.10).

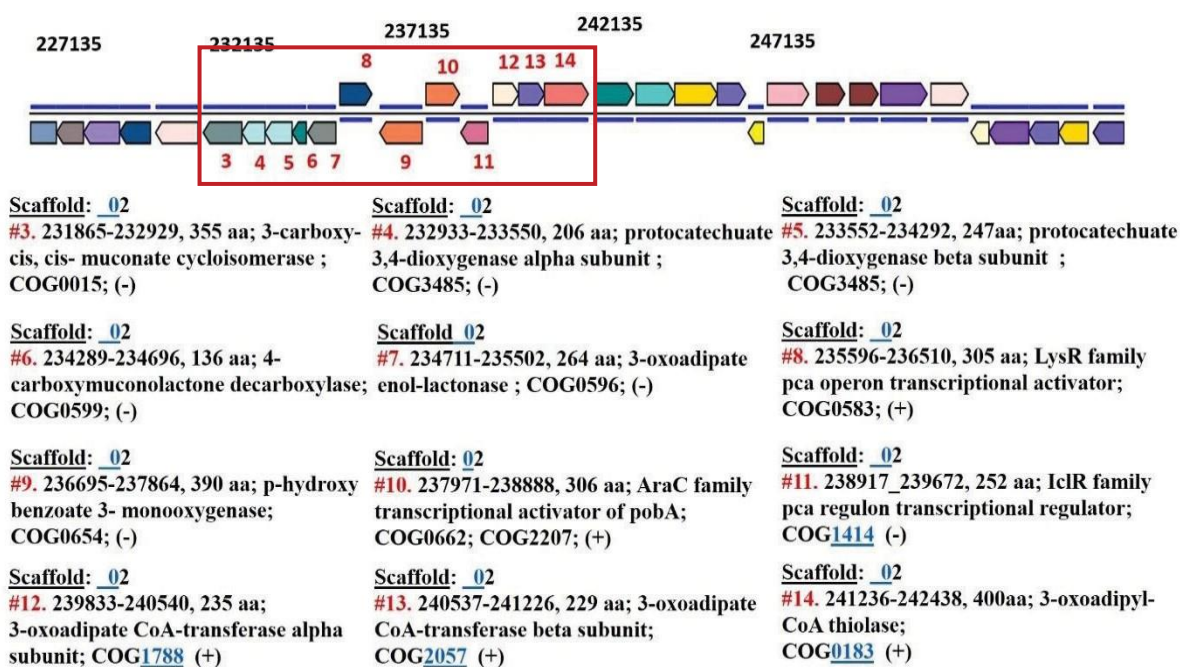


**Fig. 6.10.** Benzoate-degrading gene clusters of *B. anthropi* MAPB-9 with 14 COG in contig #2

Several regulators of the IclR family are involved in controlling catabolic pathways for the degradation of aromatic compounds (McFall, 1998). PcaR and PcaU are found to be involved in the regulation of protocatechuate degradation in *P. putida* and *Acinetobacter* sp., respectively (Romero-Steiner, 1994). PobR in *Acinetobacter* sp. strain ADP1 is the key regulator of *p* -hydroxybenzoate hydroxylase (Reyes-Ramirez, 2002). PcaU, PobR, and PcaR share a common physiological function in growth with *p* -hydroxybenzoate through the  $\beta$ -keto adipate pathway (Ornston, 1966; Harwood & Parales, 1996; McFall, 1998; Parke, 2000).



**Fig. 6.11.** Gene Neighborhoods of Protocatechuate 3,4 dioxygenase alpha subunit (*pcaG*) in *B. anthropi* MAPB-9 (enclosed in red box) and 20 other isolates. The gene of the same color (except light yellow) is from the same orthologous group (top COG hit). Light yellow = no COG assignment, white = pseudo gene, Red = marker gene, i.e., *pcaG*.

The IclR family of *pca* regulon transcriptional regulator *pcaR* is found in *B. anthropi* MAPB-9 (gene #1518) in the (-) strand. A large number of these regulators have been implicated in the regulation of aromatic degradation pathways. The IclR family of transcriptional regulators has a helix-turn-helix motif in the N-terminal domain through which they bind to the target promoters as dimers or as a dimer of dimers. For IclR regulators that act as repressors, transcription is prevented by destabilizing the activated open complex or occluding the RNA polymerase binding site. Gene Neighborhoods of *B. anthropi* MAPB-9 of Protocatechaute *pca* operon with Protocatechaute 3,4 dioxygenase, large terminal subunit, and small subunit were performed. Neighborhoods of these genes in other genomes, namely *Ochrobactrum* sp. 370 MF3.1, *Ochrobactrum* sp. POC9, *O. anthropi* RH4WT86, *O. anthropi* ML7, *Ochrobactrum* sp. DDT2, *Ochrobactrum* sp., *O. lupini* LUP21, *O. cytisi* IPA7.2, and *O. anthropi* OAB with the same top COG hit and with roughly the same matching length are shown in Fig. 6.11. These genes are embedded in segments of the chromosome that have synteny with other *Brucella/Ochrobactrum* isolates. The summary of dioxygenase genes involved in various pathways is given in Table 6.7. Naphthalene degradation is a common pollutant used as a model compound for the degradation of PAHs. Among the Gram-negative PAH-degrading bacteria, the classical NahAc- and NagAc- like amino acid sequences, coding for  $\alpha$  subunits of naphthalene dioxygenase, cluster together. Some of the related bacteria, such as *Ochrobactrum* sp. VA1 and *O. anthropi* BPyF3 were able to degrade naphthalene (Arulazhagan and Vasudevan, 2011; Ortega-Gonzalez et al., 2018). The naphthalene 1,2-dioxygenase ferredoxin reductase component (*nahAa*, *nagAa*, *ndoR*, *nbzAa*, *dntAa*) was found to be present in contig #9 (Fig. 6.12), while salicylate hydroxylase (*nahG*) was present in contig #11 in (+) strand (Fig. 6.13).

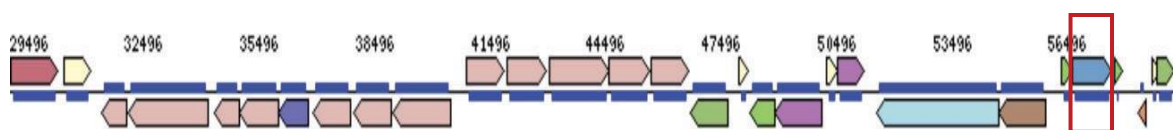


**Fig.6.12.** Region of Contig #9 consists of naphthalene 1,2-dioxygenase ferredoxin reductase component COG 0633 in (+) strand at locus 57102-58130.

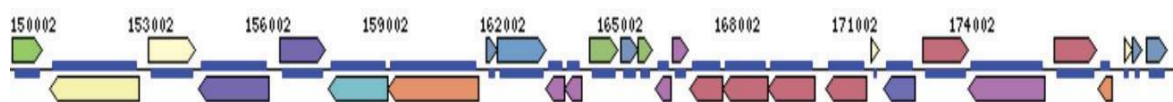


**Fig. 6.13.** Region of Contig #11 consists of salicylate hydroxylase COG 0654 in (+) strand at locus 162476-163702.

**Table 6.7.** Distribution and location of genes encoding dioxygenase *alpha*- and *beta*-subunits in the genome of MAPB-9.

Scaffold / Contig #	Strand	Locus tag	Amino acid	Function	COG	Xenobiotic degradation
01	(-)	20663-21781	373	ferredoxin-NADP reductase	COG 018	Biphenyl
01	(-)	21815-23062	416	Rieske 2Fe-2S ARHD	COG4638	PCB, Phenylpropionate
02	(-)	236695-237864	389	p-hydroxybenzoate 3-monooxygenase	COG0654	Benzoate
02	(-)	231865-232929	355	3-carboxy-cis, cis-muconate cycloisomerase	COG0015	Benzoate via Protocatechuate
02	(-)	232933-233550	206	protocatechuate 3,4-dioxygenase alpha subunit	COG3485	Protocatechuate
02	(-)	233552-234292	247	protocatechuate 3,4-dioxygenase beta subunit	COG3485	Protocatechuate
02	(+)	239833-240540	235	3-oxoadipate CoA-transferase alpha subunit	COG1788	Protocatechuate
03	(+)	141049-141894	846	2-keto-4-pentenoate hydratase/2-oxohepta-3-ene-1,7-dioic acid hydratase	COG0179	Catechol
09	(+)	57102-58130	342	ferredoxin-NAD(P)+ reductase naphthalene 1,2-dioxygenase	COG0633	Naphthalene
11	(-)	8203-9159	318	catechol 2,3-dioxygenase	COG2514	Catechol
11	(+)	162476-163702	408	salicylate hydroxylase	COG0654	Dioxin, PAH, Naphthalene

Gene Neighborhoods of *B. anthropi* MAPB-9 of naphthalene 1,2-dioxygenase ferredoxin reductase component was performed. Neighborhoods of these genes in other genomes, namely *Ochrobactrum* sp. P20RRXII, *O. anthropi* ML7, *O. anthropi* CTS-325, *Ochrobactrum* sp. MYb49, *Ochrobactrum* sp., *O. anthropi* RH4WT86, *Ochrobactrum* sp. DDT2, *O. anthropi*



W13P3, with the same top COG hit and roughly the same matching length, are shown in Fig. 6.14. These genes are embedded in segments of the chromosome that have synteny with other *Brucella/Ochrobactrum* isolates.

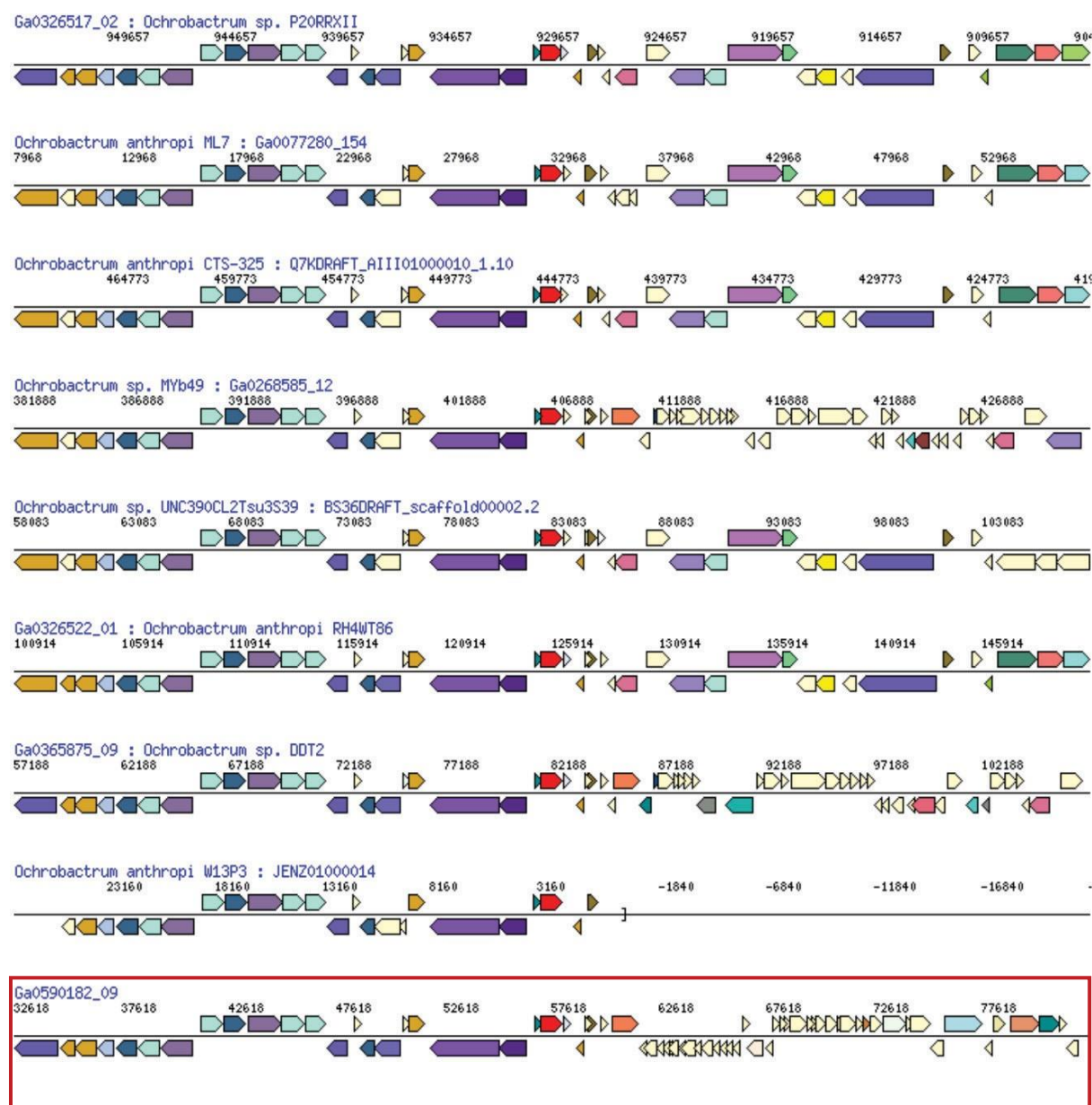


**Fig. 6.14.** Gene Neighborhoods of naphthalene 1,2-dioxygenase ferredoxin reductase (*nahAa*, *nagAa*, *ndoR*, *nbzAa*, *dntAa*) in *B. anthropi* MAPB-9 (enclosed in red box) and other isolates. Gene of the same color (except light yellow) is from the same orthologous group (top COG hit). Light yellow = no COG assignment, white = pseudo gene, Red = marker gene, i.e. (*nahAa*, *nagAa*, *ndoR*, *nbzAa*, *dntAa*).



The vicinal oxygen chelate (VOC) superfamily contains many extradiol dioxygenases, most of which are found as part of catabolic pathways degrading various aromatic pollutants. Type I extradiol dioxygenases catalyze the incorporation of both atoms of molecular oxygen into aromatic substrates, resulting in the cleavage of the aromatic rings. 2,3-dihydroxybiphenyl 1,2- dioxygenase (BphC) characterized in *Burkholderia* sp. LB400 (Vaillancourt et al., 2002) belongs to the vicinal oxygen chelate (VOC) superfamily (Cho et al., 2010). The vicinal oxygen chelate (VOC) superfamily comprises structurally related metalloproteins, including the bleomycin resistance protein, glyoxalase I, and type I ring-cleaving dioxygenases. A bound metal ion such as Fe (II), Mn(II), Zn(II), Ni(II), and Mg(II) is required for protein activities for the members of this superfamily. Various metal ions have been found in the catalytic centres of these proteins. The proteins of this family share three conserved metal-binding amino acids with the type I extradiol dioxygenases (Fig. 6.15).



**Fig. 6.15.** Region of Contig #3 consists of vicinal oxygen chelate (VOC) superfamily, including the bleomycin resistance protein, glyoxalase I, and type I ring-cleaving dioxygenases in *B. anthropi* MAPB-9 shown in red.

Glyoxalase/Catechol 2,3-dioxygenase/superfam54593/dihydroxybiphenyl dioxygenase was found in contig #3 (gene # 1530), 8 (#3491), 11 (gene # 4208, 4335, 4336, 4341), 12 (gene#4591, 4729), benzoate membrane transport protein BenE contig #8 (gene #3464), #21 (gene#5201, 5229), 2-keto-4-pentenoate hydratase/2-oxohepta-3-ene-1,7-dioic acid hydratase (contig #8, gene#3631), catechol 2,3-dioxygenase (contig #11, gene#4178). In this superfamily, gene duplication has been observed. Other xenobiotic degradation genes such as 3-hydroxybutyryl-CoA dehydrogenase5 *paaH*, *hbd*, *fadB*, *mmgB* were also observed in contig #22 with gene #5237.

The analysis of genome characteristics and comparative genome revealed that *B. anthropi* MAPB-9 contained xenobiotic degradation genes relevant to PCB, PAH chlorocyclohexane and chlorobenzene, naphthalene, and benzoate degradation pathways. In the near future, the molecular mechanism of xenobiotic biodegradation by *B. anthropi* MAPB-9 can be explored.

### 6.3.3. Genes involved in Motility, chemotaxis, and adhesion

Motility, chemotaxis, and adherence abilities help bacteria sense and locate the substrate, thus enabling PCB-degrading bacteria to utilize PCB in the contaminated area actively. Whole genome sequencing of MAPB-9 revealed the genes required for motility, chemotaxis, and adhesion gene in contig #4 (Fig. 6.16). For motility, the genes involved in the flagellar biosynthesis protein (FlhA, FlhB, FliP, FliQ, FliR), flagellar motor switch protein (FliG, FliM, FliN/FliY), flagellar basal-body rod protein (*FlgB*, *FlgC*, *FlgF*, *FlgG*), flagellar hook-basal body complex protein (FliE), flagella basal body P-ring formation protein (FlgA), flagellar P-ring protein precursor (FlgI), flagellar motility protein (MotE, *MotC* chaperone), flagellar L-ring protein precursor (FlgH), flagellar M-ring protein (FliF), flagellar hook protein (FlgE, FliR), flagellar hook-associated protein 1 (FlgK), flagellar hook-associated protein 3 (FlgL), flagellar protein (FlaF, FlgJ, FlbT), and flagellar basal-body rod modification protein (FlgD) were found to be present in the MAPB-9 genome.

Chemotaxis is a movement under the influence of a chemical gradient. Bacteria either show positive or negative chemotaxis from the chemical gradient. It helps bacteria to locate the most favourable growth and survival environment.

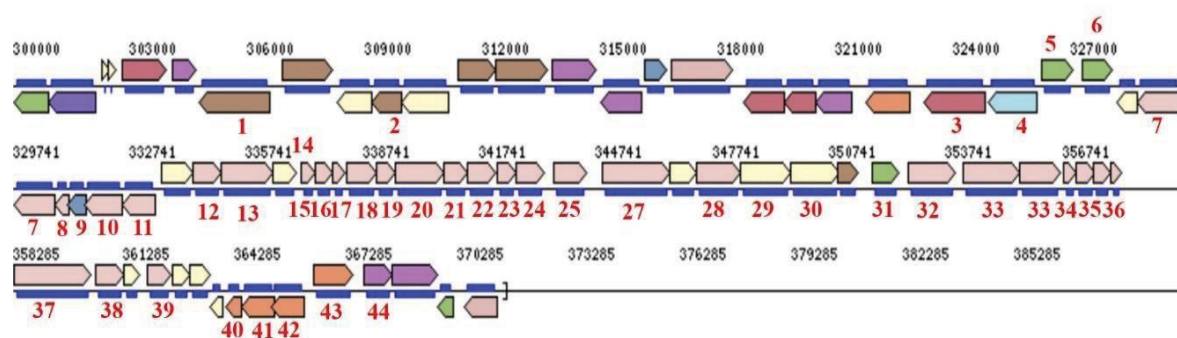


**Fig.6.16.** Contig #4 consists of exopolysaccharide, flagella, chemotaxis, and zinc transport genes in *B. anthropi* MAPB-9. #1-2 EPS biosynthesis *WeeE*, *TagA*, *CpsF*; #3-4 Multidrug efflux system *DHA2*; #5-6 *AcrR* Family transcriptional regulator; #7-8 Flagellar *FlhB*, *FlhG*, *FlhN/FlhY* #9 peptidoglycan hydrolase *CwlO*; #10 Flagellar motor switch protein *FlhM*; #11 Chemotaxis motor protein *MotA*, #12-19 Flagellar basal protein *FlhF*, *FliC*, *FlhB*, *FlhC*, *FlhE*, *FlhG*, *FlhA*, *FlhI*; #20 Chemotaxis protein *MotC*; #21-25 Flagellar basal protein *FlhE*, *FlhH*, *FliL*, *FliP*, Flagellin, *FliF*; #26-28 Chemotaxis protein *MotB*, *MotC*, *MotD*; #29 DNA response regulator *OmpR*; #30-39 Flagellar protein *FlgE*, *FlgK*, *FlgL*, *FlgF*, *FlbT*, *FlgD*, *FliQ*, *FliH*, *FliR*, *FlgJ*; #42-43 Zinc protein *Zur*, *ZnuB*, *ZnuC*, *ZnuA*.

In the last few decades, reports on bacteria with chemotactic abilities toward PCB provide a selective advantage to sense and locate PCB in the contaminated environment. *P. putida* P106 and *R. erythropolis* NY05 showed significant positive chemotactic responses toward biphenyl (Wu et al., 2003). In some cases, it also serves as a carbon and energy source. Chemotaxis protein (MotA, MotB, MotC, MotD, CheY) and methyl-accepting chemotaxis protein (MCP) were also identified in the genome.

#### 6.3.4. Characterization of genes involved in exopolysaccharide and biosurfactant

Rhamnolipids are glycolipids containing a hydrophilic group consisting of either one or two (L)-rhamnose molecules, with a glycosidic linkage to the hydrophobic group made up of one or two  $\beta$ -hydroxy fatty acids. The precursors for rhamnolipid synthesis are the sugar (dTDP-L-rhamnose) and hydrophobic moieties. Most bacteria contain the required enzymes for synthesizing the precursors in rhamnolipid biosynthesis. Synthesis of rhamnolipids and their precursors only occurs upon induction of the related gene products to express the key enzymes for the rhamnolipid biosynthesis pathway. *rmlBDAC* operon is essential for producing dTDP-L-rhamnose from D-glucose-1-phosphate (Olvera et al., 1999). In the genome analysis of *B. anthropi* MAPB-9, contig #12 contains series of enzymes such as glucose-1-phosphate thymidyl transferase (*rfbA*, *rmlA*, *rffH*, *rmlA*), dTDP-4-dehydrorhamnose 3,5-epimerase (*rfbC*, *rmlC*), dTDP-glucose 4,6-dehydratase (*rfbB*, *rmlB*, *rffG*) dTDP-4-dehydrorhamnose reductase (*rfbD*, *rmlD*), L-rhamnose mutarotase (*rhaM*), rhamnose utilization aldolase and dehydrogenase *rhaD* (predicted bifunctional)/NAD(P)-dependent dehydrogenase involved in the production of biosurfactant rhamnolipid is found to be present (Fig. 6.17). The rhamnolipid gene in the MAPB-9 genome supports isolate MAPB-9 having biosurfactant-producing properties, as described in chapter 3.

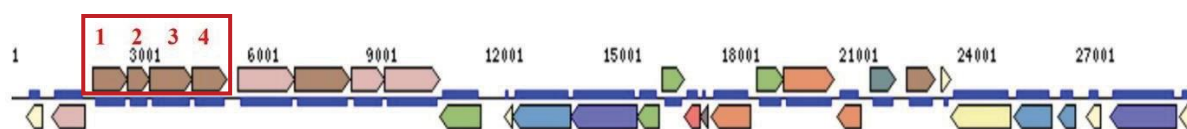


**Fig. 6.17.** Contig #12 consists of rhamnolipid synthesis genes in *B. anthropi* MAPB-9; #1 *rfbA*, *rmlA*, *rffH*; #2 *rfbC*, *rmlC*; #3 *rfbB*, *rmlB*, *rffG*; #4 *rfbD*, *rmlD* in (+) strand.

Biosurfactant, chemotaxis, and motility are the most critical characteristic that bacteria must possess in the environmental biodegradation of organic pollutants. *B. anthropi* MAPB-9 isolates genes for chemotaxis-mediated bacterial motility that is a major driver in pollutant accessibility. Also, it has the genes for exopolysaccharides secretion and rhamnolipid (RhII/RhIR) biosurfactant

production. These properties aid in the degradation process; bacteria move towards the pollutant and produce biosurfactants that solubilize the pollutants attached to the soil. It is now available for the bacteria to utilize it. Thus, the genome of *B. anthropi* MAPB-9 revealed it as a promising candidate to be used in the biodegradation of xenobiotics than the other non-motile and non-biosurfactant-producing bacteria.

### **6.3.5. Genes involved in siderophore production, metal transport, and multi-drug efflux system**

#### **Siderophore producing**

In addition to genes encoding for xenobiotic degradation and metabolism, *B. anthropi* MAPB-9 genome also possesses genes for siderophore production. These compounds primarily chelate the ferric iron ( $\text{Fe}^{3+}$ ) from different sources, making it available for bacterial cells. It facilitates the supply of iron for diverse cellular functions, including bioremediation and plant growth promotion (Gaonkar and Borkar, 2013). Siderophore biosynthetic pathways and transport identified were ferric hydroxamate transport system permease protein (*fhuB*), ferric hydroxamate transport system substrate-binding protein (*fhuD*), and transmembrane sensor (*fecR*) present in contig #4 (Fig.6.18).

#### **Metal transport**

The genome sequencing analysis revealed the presence of different genes related to the transport of different biomolecules across the cell. The presence of genes of different ABC transporter- related proteins such as iron complex outer membrane receptor protein (TC.FEV.OM), iron complex transport system ATP-binding protein (ABC.FEV.A), iron complex transport system permease protein (ABC.FEV.P), iron complex transport system substrate-binding protein (ABC.FEV.S), iron complex outer membrane receptor protein (TC.FEV.OM), iron(III) transport system permease protein (*afuB*, *fbpB*), iron(III) transport system substrate-binding protein (*afuA*, *fbpA*), iron(III) transport system ATP-binding protein (*afuC*, *fbpC*), Fur family transcriptional regulator, iron response regulator (*irr*), ferric uptake regulator (*fur*, *zur*, *furB*) were found to present in *B. anthropi* MAPB-9 genome. Peptide/nickel transport system substrate-binding protein (ABC.PE.S), permease protein (ABC.PE.P, ABC.PE.P1), and ATP-binding protein (*ddpD*, *ddpF*), were also observed in contig #4 (Fig6.18).

### Arsenic resistance gene

Arsenate family transcriptional regulator, arsenate/arsenite/antimonite-responsive transcriptional repressor (*ArsR*), arsenate reductase (thioredoxin) (*ArsC*), arsenite transporter (*ArsB*), arsenate reductase (glutaredoxin, *ArsC*), and arsenical resistance protein (*ArsH*) were found to be present in contig #4 (Fig. 6.16). All the gene products are known to provide arsenic resistance in several bacteria (Liu et al., 2013; Yan et al., 2019).

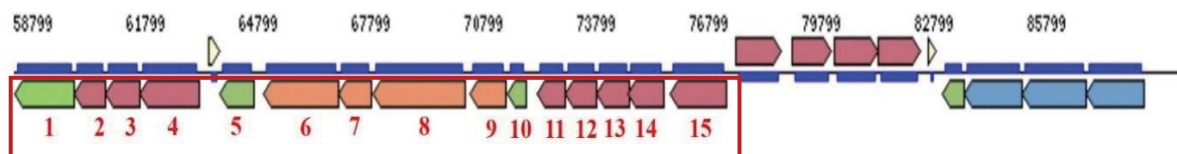


**Fig. 6.18.** Contig #4 consists of a siderophore and peptide/nickel transport system and genes in *B. anthropi* MAPB-9. #1 peptide/nickel transport system *ddpF*, #2 ABC.PE.P1, #3 ABC.PE.P, #4 ABC.PE.S, #5 LysR family transcriptional regulator; siderophore and ferric hydroxamate transport system #6 *fhuB*, #7 *fhuD*, #8 TC.FEV.OM, #9 *fecR*, #10 RNA polymerase sigma factor; #11 peptide/nickel transport system *ddpF*, #12 *ddpD*, #13 ABC.PE.P1, #14 ABC.PE.P, #15 ABC.PE.Sin (-) strand.

### Multidrug efflux system

Contig #3 consists of an osmoprotectant transport system having permease protein (*opuBD*), ATP-binding protein (*opuA*), substrate-binding protein (*opuC*), multidrug resistance efflux transporter (*EmrE*), MerR family transcriptional regulator (*cueR*), copper efflux regulator in (-) strand. In contrast, contig #2 has outer membrane efflux proteins D-aminopeptidase (*dmpA*), outer membrane protein, multidrug efflux system (*nodT*, *ameC*), membrane fusion protein, macrolide-specific efflux system (*macA*), and macrolide transport system ATP-binding/permease protein (*macB*) in (+) strand.

### Stress-related genes

Nucleotide-binding universal stress protein (*UspA*), environmental stresses-induced protein (*HutD*), large subunit ribosomal protein L25 (*rplY*), GTP-binding protein (*typA*, *bipA*) were also found to be present in *B. anthropi* MAPB-9.

Overall, the whole genome analysis confirmed *B. anthropi* MAPB-9 as a potent candidate for the biodegradation of PCB and other chlorinated organic compounds. It also opens up a futuristic scope to gain insight into the biodegradation potential of chlorinated organic compounds.

**Chapter VII**  
**Summary, Conclusions**  
**and Future Perspectives**



### Summary and Conclusions

PCBs are POPs that are omnipresent and have become a global issue for decades as a result of industrialization. They are mainly found in transformer oil, shipyard waste, industrial waste, paints, ink, municipal incinerators etc. Various human diseases such as cancer, diabetes, cardiovascular disease, hypertension, Parkinson and thyroid dysfunction are caused because of contamination due to different PCBs. Remediation of PCBs has been attempted using various strategies, including chemical/physical methods. These strategies suffer from various disadvantages for e.g., chemical/physical strategies lead to problems in operational aspects, high cost, and partial degradation resulting in the addition of harmful end products. Bioremediation is the most promising approach for removing PCB from contaminated soil. The combination of bacteria and plant bioremediation can further enhance the process of PCB removal. There are many gaps in the existing research work that attempts to bioremediate PCBs. There are very few reports on metagenomic data related to PCB degradation by bacterial population and analysis of their PCB degrading potential. There are several reports of PCB contamination in industrial sites in India, but no reports on the metagenomic analysis of PCB-contaminated sites have been conducted so far. Also, there is very scarce information about the aerobic PCB degradation activity of the bacteria isolated, especially from the steel industry. The knowledge of both synergistic and antagonistic relations between bacteria and the mechanisms of this cooperation among them in PCB degradation studies is still not fully understood. Due to the complexity of commercial PCB mixtures with varying degrees of chlorination, a single bacterium cannot degrade all or even most of the PCB congeners present in contaminated environments. A particular strain of microorganisms may degrade one or more compounds. Sometimes, for the degradation of a single compound, the synergetic action of a few microorganisms (i.e., a consortium of microbes) may be more efficient. Based on the information on the PCB degradation potential of individual microbes and the metabolites produced, the bioformulation of bacterial consortia would be a more practical approach for the biodegradation of PCB in soil. Very few attempts by various research groups have been made to deliver the PCB-degrading bacteria through bioformulation.

Considering the above potential gaps in the existing research, the present thesis aims at “Molecular and Functional Characterization of Polychlorinated Biphenyl (PCB) Degrading Bacteria”. It would involve a wide array of studies that include metagenomics, molecular biology techniques, and bioformulation preparation.

Initially, three soil samples namely MGB-1, MGB-2 and MGB-3 were collected from areas nearby Bhilai steel plant in Chhattisgarh (India). GC-MS/MS-based analysis confirmed them to be contaminated with PCBs. MGB-2 contained PCBs such as biphenyl, 1,1'-biphenyl, 4,4'-dichloro (PCB-15) in MGB-2 and biphenyl, 1,1'-biphenyl 2,2',3,5',6 pentachloro (PCB-95), and 1,1'-biphenyl 2,2',3,3',6,6' hexachloro (PCB-136) were found to be present in MGB-3. PAHs were also found to be present in the sample. Further metagenome sequencing and analysis were done to get insight into the diversity of the bacterial community and metabolic potential of the dominant bacterial community in the contaminated soil. The standard alpha diversity indices, namely Chao, Simpson, and Shannon, indices depicted equivalent overall diversity in both samples. Beta diversity among MGB-2 and MGB-3 based on Bray-Curtis dissimilarity depicted similar distribution patterns of bacterial communities in these samples. ONT and MG-RAST database search provided detailed microbial taxonomy of MGB-2 and MGB-3. The differences were noticeable at the domain level, where MG-RAST derived reads accounted majorly for bacteria (97.4%; 97.5%) followed by eukaryote (1.4%; 1.5%), archaea (1.2%; 0.9%), and virus (0.02%; 0.04%) in MGB-2 and MGB-3, respectively. Among bacteria, phylum *Proteobacteria* (45.0%; 50.0%) was the most predominant, followed by *Actinobacteria* (22.1%; 19.5%) and *Firmicutes* (6.3%; 5.4%) in both MGB-2 and MGB-3 samples. RefSeq annotations at the genus level, possessed a significant abundance level with  $p < 1e^{-5}$  for *Streptomyces*, *Candidatus*, *Koribacter*, *Gemmata*, *Conexibacter*, *Anaeromyxobacter* and *Nocardioides* in MGB-2, while *Hypomicrobium*, *Pseudomonas*, *Mycobacterium*, *Roseomonas*, and *Methylobacterium* with in MGB-3.

Further, we isolated and characterized PCB-degrading potential bacteria using biphenyl, and PCB-77 as substrates and with the help of a combination of morphological, biochemical, and analytical methods. *P. aeruginosa* MAPB-2, *P. plecoglossicida* MAPB-6, *B. anthropi* MAPB-9, and *P. megaterium* MAPB-27 were identified using 16S rRNA sequencing. In addition to the characterization of PCB-degradation potential, plant growth-promoting and biosurfactant-producing properties of the selected isolates were evaluated. Isolates MAPB-2, MAPB-6, MAPB-9, and MAPB-27 could tolerate up to 500 mg L<sup>-1</sup> biphenyl. Thus, the four selected isolates possessed high biphenyl tolerances and degradation efficiency. Optimized growth conditions led to 100% improved biphenyl biodegradation by MAPB-9 with 200 mg L<sup>-1</sup> biphenyl, while 97.1 for MAPB-6 within 48 h, respectively. The study is the first report of effective PCB-77 degradation with 59.89%, 30.49%, 27.19%, and 4.43% degradation by MAPB-6, MAPB-9, MAPB-2, and MAPB-27 respectively, using biphenyl as inducers. The biosurfactant-producing property of these

isolates can be attributed to good PCB degradation. Since the results suggested that these selected isolates have the potential to be used for bioremediation of PCBs, metabolomic profiles of these selected isolates grown in biphenyl-supplemented MM were analyzed and compared using GC-MS/MS-based metabolomics. Further, metabolite enrichment analysis was performed to confirm the active metabolism in the selected bacterial isolates. The metabolomic profiling results and the metabolism's enrichment analysis indicate that the selected bacteria show an adaptative mechanism to survive under biphenyl-induced stress conditions.

Finally, the development of bioformulation by optimization of consortia from the selected bacteria namely MAPB-2, MAPB-6, MAPB-9, and MAPB-27 was done. For this, initially, degradation of the PCB congeners by the above isolates and their consortia was evaluated. The individual isolates, namely MAPB-2, MAPB-6, and MAPB-9, completely degraded tri chlorobiphenyl, whereas MAPB-27 degraded the same to 92%. Consortia (1-11) developed were able to hydrolyse the lower chlorinated PCBs (Cl<sub>1-4</sub>) compared to the higher chlorinated PCBs (Cl<sub>≥5</sub>).

Consortium #11 (containing 4 best isolates MAPB-2, MAPB-6, MAPB-9, and MAPB-27; 1:1:1:1) was found to possess the most potential biodegradation ability wherein it caused 100%, 60.5%, 6.9%, 100% degradation of trichlorobiphenyl, tetrachlorobiphenyl, pentachlorobiphenyl, and hexachlorobiphenyl, respectively. The best consortium #11, was selected and encapsulated in sodium alginate beads, followed by a pot study using the *B. nigra* plant. The selected consortium #11 and its isolates were encapsulated with Ca-alginate to get uniform-sized beads with smooth surfaces. Two bioformulation subtypes (T1 and T2) were prepared to contain MAPB-2, MAPB-6, MAPB-9, and MAPB-27 in ratios (1:1:1:1 & 1:1:2:2). The bacterial isolates were found to be entrapped in their respective beads as understood from SEM analysis.

Bioformulations T1 and T2 showed 100 % degradation for tri and hexachlorobiphenyl. At the same time, the percentage degradation for tetra and penta chlorobiphenyl was more than 70% and 80% in T1 and T2, respectively. In bioformulations (T5-T8), trichlorobiphenyl was degraded 100%, while tetrachloro and pentachloro showed more than 50% degradation in all the encapsulated bacteria. Based on the metabolites identified by GC-MS/MS studies indicate the involvement of 2,3 dioxygenase and 3,4 dioxygenase pathways.

### **Future Perspectives**

In the present work, we have established proof of concept for a bioformulation containing consortia that were developed using bacterial isolates from contaminated sites of the Bhilai steel plant. The developed bioformulation could effectively degrade PCBs in simulated conditions in the pot experiments. Although the prototype bioformulation has been developed, several aspects could be studied in the future, which are as follows

1. Field trial of the developed bioformulation can be evaluated using an appropriate model and contaminated site such as a Steel plant
2. The consortia can be optimized using mathematical models for ratio optimization to result in more potent biodegradation of PCBs. Similar studies can be used for the identification of newer bacteria and their consortia.
3. Various other polymer-based microencapsulation can be attempted further to enhance the biodegradation efficiency of the developed consortium
4. Scaleup of the bacterial isolates using fermentation technology can be attempted to ensure the continuous source of the isolates
5. Genome sequencing of MABP-9 was done. MABP-2, 6, and 27 also can be sequenced for their whole genome
6. Strain improvement through bioengineering can be attempted to achieve degradation of the higher chlorinated PCBs

## Bibliography

---

- Abraham, J., and Silambarasan, S. (2016). Biodegradation of chlorpyrifos and its hydrolysis product 3,5,6-trichloro-2-pyridinol using a novel bacterium *Ochrobactrum* sp. JAS2: A proposal of its metabolic pathway. *Pestic. Biochem. Physiol.* 126, 13-21.
- Abraham, W.R., Nogales, B., Golyshin, P.N., Pieper, D.H., and Timmis, K.N. (2002). Polychlorinated biphenyl-degrading microbial communities in soils and sediments. *Curr. Opin. Microbiol.* 5(3), 246-253.
- Abramowicz, D.A. (1990). Aerobic and anaerobic biodegradation of PCBs: A review. *Crit. Rev. Biotechnol.* 10(3), 241-251.
- Adebusoye, S.A., Picardal, F.W., Ilori, M.O., Amund, O.O., Fuqua, C., and Grindle, N. (2007). Growth on dichlorobiphenyls with chlorine substitution on each ring by bacteria isolated from contaminated African soils. *Appl. Microbiol. Biot.* 74, 484-492.
- Adebusoye, S.A., Picardal, F.W., Ilori, M.O., and Amund, O.O. (2008). Influence of chlorobenzoic acids on the growth and degradation potentials of PCB-degrading microorganisms. *World J. Microb. Biotechnol.* 24, 1203-1208.
- Adrian, L., Dudkova, V., Demnerova, K., and Bedard, D.L. (2009). *Dehalococcoides* sp. strain CBDB1 extensively dechlorinates the commercial polychlorinated biphenyl mixture Aroclor 1260. *Appl. Environ. Microbiol.* 75, 4516-4524.
- Agency for Toxic Substances and Disease Registry (ATSDR). (2000). Toxicological Profile for Polychlorinated Biphenyls (PCBs). Atlanta, GA: U.S. Department of Health and Human Services, Public Health Service.
- Agulló, L., Cámara, B., Martínez, P., Latorre, V., and Seeger, M. (2007). Response to chlorobiphenyls of also induced by heat shock and oxidative stress. *FEMS Microbiol. Lett.* 267, 167-175.
- Agullo, L., Pieper, D.H., and Seeger, M. (2017). Genetics and biochemistry of biphenyl and PCB biodegradation. In: Fernando, R. (Ed.), *Aerobic Utilization of Hydrocarbons, Oils and Lipids*. Springer International Publishing, pp. 1-28.
- Ahmed, M., and Focht, D.D. (1973). Degradation of polychlorinated biphenyls by two species of *Achromobacter*. *Can. J. Microbiol.* 19(1), 47-52.
- Ahn, S., Jung, J., Jang, In-Ae, Madsen, E.L., and Park, W. (2016). Role of glyoxylate shunt in

## Bibliography

---

- oxidative stress response. *J. Biol. Chem.* 291 (22), 11928-11938.
- Aken, B.V., Correa, P.A., and Schnoor, J.L. (2010). Phytoremediation of polychlorinated biphenyls: New trends and promises. *Environ. Sci. Technol.* 44(8), 2767-2776.
- Al-Mailem D.M., Al-Deieg M., Eliyas M., and Radwan S.S. (2017). Biostimulation of indigenous microorganisms for bioremediation of oily hypersaline microcosms from the Arabian Gulf Kuwaiti coasts. *J. Environ. Manage.* 193, 576-583.
- Al-Mailem, D.M., Sorkhoh N.A., Al-Awadhi H., Eliyas, M., and Radwan S.S. (2010). Biodegradation of crude oil and pure hydrocarbons by extreme halophilic archaea from hypersaline coasts of the Arabian Gulf. *Extremophiles* 14(3), 321-328.
- Amaral, L., Martins, A., Spengler, G., and Molnar, J. (2014). Efflux pumps of Gram-negative bacteria: What they do, how they do it, with what and how to deal with them. *Front. Pharmacol.* 4(168), 1-11
- Aparna, A., Srinikethan, G., and Smitha, H. (2012). Production and characterization of biosurfactant produced by a novel *Pseudomonas* sp. 2B. *Colloids Surf B Biointerfaces.* 95, 23-29.
- Arai, H., Kosono, S., Taguchi, K., Maeda, M., Song, E., Fuji, F., Chung, S.Y., and Kudo, T. (1998). Two sets of biphenyl and PCB degradation genes on a linear plasmid in *Rhodococcus erythropolis* TA421. *J. Ferment. Bioeng.* 86, 595-599.
- Aranda, E. (2016). Promising approaches towards biotransformation of polycyclic aromatic hydrocarbons with Ascomycota fungi. *Curr. Opin. Biotechnol.* 38, 1-8.
- Arslan, M., Imran, A., Khan, Q.M., and Afzal, M. (2017). Plant-bacteria partnerships for the remediation of persistent organic pollutants. *Environ. Sci. Pollut. Res. Int.* 24(5), 4322-4336.
- Arulazhagan, P. and Vasudevan N. (2011). Biodegradation of polycyclic aromatic hydrocarbons by a halotolerant bacterial strain *Ochrobactrum* sp.VA1. *Mar. Poll. Bull.* 62, 388-394.
- Ashburner M., Ball C.A., Blake, J.A., Botstein, D., Butler, H., Cherry, J.M., Davis, A.P., Dolinski, K., Dwight, S.S., Eppig, J.T. (2000). Gene Ontology: Tool for the unification of biology. *Nat. Genet.* 25(1), 25-29.
- Ashitha, A., Radhakrishnan, E.K., and Jyothis, Mathew. (2020). Characterization of biosurfactant produced by the endophyte *Burkholderia* sp. WYAT7 and evaluation of its antibacterial and antibiofilm potentials. *J. Biotechnol.* 313, 1-10.



## Bibliography

---

- Atago, Y., Shimodaira, J., Araki, N., Bin Othman, N. A., Zakaria, Z., Fukuda, M., Futami, J., and Hara, H. (2016). Identification of novel extracellular protein for PCB/biphenyl metabolism in *Rhodococcus jostii* RHA1. *Biosc. Biotechnol. Biochem.* 80(5), 1012-1019.
- Aydin, Y.M., Kara, M., Dumanoglu, Y., et al. (2014). Source apportionment of Polycyclic Aromatic Hydrocarbons (PAHs) and Polychlorinated Biphenyls (PCBs) in ambient air of an industrial region in Turkey. *J. Atmos. Env.* 97, 271-285.
- Ayris, S., Currado, G.M., Smith, D., and Harrad, S. (1997). GC/MS procedures for the determination of PCBs in environmental matrices. *Chemosphere* 35 (5), 905-917.
- Aziz, A., Agamuthu, P., Alaribe, F.O., and Fauziah, S.H. (2018). Biodegradation of benzo[a]pyrene by bacterial consortium isolated from mangrove sediment. *Environ. Technol.* 39(4), 527-535.
- Baldwin, B.R., Nakatsu, C.H., and Nies, L. (2003). Detection and enumeration of aromatic oxygenase genes by multiplex and real-time PCR. *Appl Environ Microbiol.* 69(6),3350-3308.
- Bano, S., Pervez, S., Chow, J.C., Matawle, J.L., et al. (2018). Coarse particle (PM10-2.5) source profiles for emissions from domestic cooking and industrial process in Central India. *J. Sci. Tot. Env.* 627, 1137-1145.
- Barton, M. and Crawford, R.L. (1998). Novel biotransformations of 4-chlorobiphenyl by a *Pseudomonas* sp. *Appl. Environ. Microbiol.* 54, 594-595.
- Bashan, Y., and Levanony, H. (1989). Factors affecting adsorption of *Azospirillum brasilense* Cd to root hairs as compared with roof surface of wheat. *Can. J. Microbiol.* 35, 936-944.
- Bashan, Y., Hernandez, J. P., Leyva - Macario Bacilio, L. A. (2002). Alginate microbeads as inoculant carriers for plant growth-promoting bacteria. *Biol. Fertil. Soils* 35, 359-368.
- Bauer, A.W., Kirby M., Sherris, J.C., and Turck, M. (1966). Antibiotic susceptibility testing by a standardized single disk method. *Am. J. Clin. Pathol.* 45, 493-494.
- Bayat, Z., Hassanshahian, M., and Cappello, S. (2015) Immobilization of microbes for bioremediation of crude oil polluted environments: A mini review. *Open Microbiol. J.* 9, 48-54.
- Bedard, D.L., and Haberl, M. L. (1990). Influence of Chlorine substitution pattern on the degradation of polychlorinated biphenyls by eight bacterial strains. *Microb. Ecol.* 20 (2), 87-102.
- Bedard, D.L., Bailey, J.J., Reiss, B.L., and Jerzak, G.V. (2006). Development and characterization

## Bibliography

---

- of stable sediment-free anaerobic bacterial enrichment cultures that dechlorinate Aroclor 1260. *Appl. Environ. Microbiol.* 72, 2460-2470.
- Bedard, D.L., Haberl, M.L., May, R.J., and Brennan, M.J. (1987). Evidence for novel mechanism of polychlorinated biphenyl metabolism in *Alcaligenes eutrophus* H850. *Appl. Environ. Microbiol.* 53(5), 1103-1112.
- Belgacem, Z.B., Bijttebier, S., Verreth, S., Voorspoels, S., Van de Voorde, I., Aerts, G. et al. (2015). Biosurfactant production by *Pseudomonas* strains isolated from floral nectar. *J. Appl. Microbiol.* 118(6), 1370-1384.
- Bhadbhade, B.J., Sarnaik, S.S., and Kanekar, P.P. (2002). Biomineralization of an organophosphorus pesticide, Monocrotophos, by soil bacteria. *J. Appl. Microbiol.* 93 (2), 224-234. Bhat, R., Dayamani, K., Hathwar, S., Hegde, R., and Kush, A. (2015). Exploration on production of rhamnolipid biosurfactants using native *Pseudomonas aeruginosa* strains. *J. Biosci. Biotechnol.*, 4 (2), 157-166.
- Bhattacharya, A., and Khare, S.K. (2017) Biodegradation of 4-chlorobiphenyl by using induced cells and cell extract of *Burkholderia xenovorans*. *Bioremed. J.* 21, 109-118.
- Bhawsar, N.A., and Singh, M. (2016). GC-MS profile of biosurfactant producing and hydrocarbon degrading *P. aeruginosa* NGB4 in liquid culture system. *J. Pharm. Res.*, 10, 726-729.
- Bidlan R., and Manonmani, H. K. (2002). Aerobic degradation of dichlorodiphenyltrichloroethane (DDT) by *Serratia marcescens* DT-1P. *Process Biochem.* 38, 49-56.
- Bittsanszky, A., Gullner, G., Gyulai, G., and Komives, T. (2011). A case study: uptake and accumulation of persistent organic pollutants in Cucurbitaceae species. In *Organic xenobiotics and plants*, Springer Netherlands; pp. 77-85.
- Borja, J., Taleon, D.M., Auresenia, J., and Gallardo, S. (2005). Polychlorinated biphenyls and their biodegradation. *Process Biochem.* 40, 1999-2013.
- Borji, A., Farivar, G.N., Johari, P., Farivar, T.N., Senemari, S., and Karimi, G. (2014). Cleaning from the inside: Biodegradation of organophosphate pesticides by *Pseudomonas plecoglossicida*. *Biotech Health Sci.* 1(1), e19193.
- Bose, S., Aggarwal, S., Singh, D.V., and Acharya, N. (2020). Extracellular vesicles: An emerging platform in gram-positive bacteria. *Microb. Cell* 7, 12, 312 - 322.

## Bibliography

---

- Bouabidi, Z.B., El-Naas, M.H., and Zhang, Z. (2019). Immobilization of microbial cells for the biotreatment of wastewater: A review. *Environ. Chem. Lett.* 17, 241-257.
- Bouhajja, E., Agathos, S.N., and George, I.F. (2016). Metagenomics: Probing pollutant fate in natural and engineered ecosystems. *Biotechnol. Adv.* 34(8), 1413-1426.
- Brettin, T., Davis, J.J., Disz, T., Edwards, R.A., Gerdes, S., Olsen, G.J., et al. (2015). RASTtk: A modular and extensible implementation of the RAST algorithm for building custom annotation pipelines and annotating batches of genomes. *Sci. Rep.* 5, (8365)1-6
- Brown, M.B., Bush, B., Rhee, G.Y., and Shane, L. (1988). PCB dechlorination in Hudson River sediment. *Sci.* 240, 1674-1676.
- Brumfield, K.D., Huq, A., Colwell, R.R., et al. (2020). Microbial resolution of whole genome shotgun and 16S amplicon metagenomic sequencing using publicly available NEON data. *PLoS ONE* 15 (2), e0228899.
- Cai, Y., Mo, H., Wu, T., et al. (2007). Bioremediation of polycyclic aromatic hydrocarbons (PAHs)-contaminated sewage sludge by different composting processes. *J. Hazard Mater.* 142(1- 2), 535-542.
- Cajthaml, T. (2015). Biodegradation of endocrine-disrupting compounds by ligninolytic fungi: mechanisms involved in the degradation. *Environ. Microbiol.* 17, 4822-4834.
- Cammandeur, L.C.M., May, R.J., Makross, H., Bedrad, D.L., Reineke, W., Grovers, H.A.J., and Parsons, J.R. (1996). Aerobic degradation of polychlorinated biphenyls by *Alcaligenes* sp. JB1: Metabolites and enzymes. *Biodegradation* 7, 435-443.
- Cappuccino, J.C., and Sherman, N. *Microbiology: A Laboratory Manual* (3rd ed), Benjamin/cummings Pub. Co., New York (1992), pp. 125-179.
- Carpenter, D.O. (2006). Polychlorinated biphenyls (PCBs): Routes of exposure and effects on human health. *Rev. Environ. Health.* 21(1), 1-23.
- Cervantes-González, E., Guevara-García, M.A., García-Mena, J. et al. (2019). Microbial diversity assessment of polychlorinated biphenyl-contaminated soils and the biostimulation and bioaugmentation processes. *Environ. Monit. Assess.* 191 (118), 1-14.
- Chai, Y., Beauregard, P.B., Vlamakis, H., Losick, R., and Kolter, R. (2012). Galactose metabolism plays a crucial role in biofilm formation by *Bacillus subtilis*. *MBio.* 3(4), e00184-12.

## Bibliography

---

- Chakraborty, P., Zhang, G., Li, J., Xu, Y., Liu, X., Tanabe, S., and Jones, K.C. (2010). Selected organochlorine pesticides in the atmosphere of major Indian cities: Levels regional versus local variations and sources. *Environ. Sci. Technol.* 44, 8038- 8043.
- Chakraborty, J. and Das, S. (2014). Biosurfactant-based bioremediation of toxic metals. In *Microbial 2007 Biodegradation and Bioremediation*, 1st edn ed. Das, S., Rourkela Odisha, India, Elsevier, pp. 167-201.
- Chakraborty, J., and Das, S. (2016). Characterization of the metabolic pathway and catabolic gene expression in biphenyl degrading marine bacterium *Pseudomonas aeruginosa* JP-11. *Chemosphere* 144, 1706-1714.
- Chavez, F.P., Gordillo, F., and Jerez, C.A. (2006). Adaptive responses and cellular behaviour of biphenyl-degrading bacteria toward polychlorinated biphenyls. *Biotechnol. Adv.* 24, 309- 320.
- Chavez, F.P., Lunsdorf, H., and Jerez, C.A. (2004). Growth of polychlorinated-biphenyl-degrading bacteria in the presence of biphenyl and chlorobiphenyls generates oxidative stress and massive accumulation of inorganic polyphosphate. *Appl. Environ. Microbiol.* 70(5), 3064-3072.
- Chekol, T., Vough, L.R., and Chaney, R.L. (2004). Phytoremediation of polychlorinated biphenyl-contaminated soils: the rhizosphere effect. *Environ. Int.* 30(6), 799-804.
- Chen, C., Yu, C.N., Shen, C.F., Tang, X.J., Qin, Z.H., Yang, K., Hashmi, M.Z., Huang, R.L., and Shi, H.X. (2014). Paddy field - A natural sequential anaerobic-aerobic bioreactor for polychlorinated biphenyls transformation. *Environ. Pollut.* 190, 43-50.
- Cheung, P.Y., and Kinkle, B.K. (2001). *Mycobacterium* diversity and pyrene mineralization in petroleum-contaminated soils. *Appl. Environ. Microbiol.* 67(5), 2222-2229.
- Chinnaswamy, A., Coba de la Pena, T., Stoll, A., de la Peña Rojo D., Bravo, J., Rincón, A., Pueyo, J.J. (2018). A nodule endophytic *Bacillus megaterium* strain isolated from *Medicago polymorpha* enhances growth, promotes nodulation by *Ensifer medicae* and alleviates salt stress in alfalfa plants. *Ann. Appl. Biol.* 172 (3), 295-308
- Cho, H.J., Kim, K., Sohn, S.Y., Cho, H.Y., Kim, K.J., Kim, M.H. et al. (2010). Substrate binding mechanism of a type I extradiol dioxygenase. *J. Biol. Chem.* 285, 34643-34652.
- Cho, Y.C., Ostrofsky, E.B., and Rhee, G.Y. (2004). Effects of a rhamnolipid biosurfactant on the reductive dechlorination of polychlorinated biphenyls by *St. Lawrence River* (North America)

## Bibliography

---

- microorganisms. *Environ Toxicol. Chem.* 23(6),1425-1430.
- Cogliano, V.J. (1998). Assessing the cancer risk from environmental PCBs. *Environ. Health Perspect.* 106(6), 317-323.
- Commandeur, L.C.M., Van Eyseren, H.E., Opmeer, M.R., Govers, H.A., and Parsons, J.R. (1995). Biodegradation kinetics of highly chlorinated biphenyls by *Alcaligenes* sp. JB1 in an aerobic continuous culture system. *Environ. Sci. Technol.* 29, 3038-3043.
- Correa, P.A., Lin, L., Just, C.L., Hu, D., Hornbuckle, K.C., Schnoor J.L., and Aken B.V. (2010). The effects of individual PCB congeners on the soil bacterial community structure and the abundance of biphenyl dioxygenase genes. *Environ. Int.* 36 (8), 901-906.
- Couillerot, O., Prigent-Combaret, C., Caballero-Mellado, J., and Moenne-Loccoz, Y. (2009). *Pseudomonas fluorescens* and closely related fluorescent pseudomonads as biocontrol agents of soil-borne phytopathogens. *Lett Appl Microbiol.* 5, 505-512.
- Croes, S., Weyens, N., Janssen, J., Vercampt, H., Colpaert, J. V., Carleer, R., et al. (2013). Bacterial communities associated with *Brassica napus* L. grown on trace element-contaminated and non-contaminated fields: A genotypic and phenotypic comparison. *Microb. Biotechnol.* 6, 371-384.
- Cummings, P.J., Olszewicz, J., and Obom, K.M. (2017). Nanopore DNA sequencing for metagenomic soil analysis. *J. Vis. Exp.* 130, 559-579.
- Cvancarova, M., Kresinova, Z., Filipova, A., Covino, S., and Cajthaml, T. (2012). Biodegradation of PCBs by ligninolytic fungi and characterization of the degradation products. *Chemosphere* 88, 1317-1323.
- Das, D., Baruah, R., Roy, A.S., Singh, A.K., Boruah, H.P.D., Kalita, J., and Bora, T.C. (2015). Complete genome sequence analysis of *Pseudomonas aeruginosa* N002 reveals its genetic adaptation for crude oil degradation. *Genomics* 105, 182-190.
- Daâssi, D., Rodríguez-Couto, S., Nasri M., and Mechichi, T. (2014) Biodegradation of textile dyes by immobilized laccase from *Coriolopsis gallica* into Ca-alginate beads. *Int. Biodeter. Biodegr.* 90, 71-78.
- Davis, J.J., Gerdes, S., Olsen, G.J., Olson, R., Pusch, G.D., Shukla, M., et al. (2016). PATtyFams: Protein families for the microbial genomes in the PATRIC database. *Front. Microbiol.* 7(118)1-12.

## Bibliography

---

- Davis, J.J., Wattam, A.R., Aziz, R.K., Brettin, T., Butler, R., Butler, R.M., et al. (2020). The PATRIC Bioinformatics Resource Center: Expanding data and analysis capabilities. *Nucleic Acids Res.* 48(D1), D606-D612.
- Delgado-Baquerizo, M., Eldridge, D.J., Ochoa, V., et al. (2017). Soil microbial communities drive the resistance of ecosystem multifunctionality to global change in drylands across the globe. *Ecol. Lett.* 20, 1295-1305.
- Demaneche, S., Meyer, C., Micoud, J., Louwagie, M., Willison, J.C., and Jouanneau, Y. (2004). Identification and functional analysis of two aromatic ring-hydroxylating dioxygenases from a *Sphingomonas* strain that degrades various polycyclic aromatic hydrocarbons. *Appl. Environ. Microbiol.* 70, 6714-6725.
- Demirtepe, H., Kjellerup, B., Sowers, K.R., and Imamoglu, I. (2015). Evaluation of PCB dechlorination pathways in anaerobic sediment microcosms using an anaerobic dechlorination model. *J. Hazard. Mater.* 296, 120-127.
- Dercová, K., Vrana, B., Balaz, S., and Šándorová, A. (1996). Biodegradation and evaporation of polychlorinated biphenyls (PCBs) in liquid medium. *J. Ind. Microbiol.* 16, 325-329.
- Deshwal, V.K. and Kumar, P. (2004). Production of plant growth promoting substance by *Pseudomonads*. *J. Acad. Ind. Res* 2(4), 221-225.
- Devanathan, G., Subramanian, A., Someya, M., Sudaryanto, A. et al. (2009). Persistent organochlorines in human breast milk from major metropolitan cities in India. *Environ. Pollut.* 157(1), 148-154.
- Dhamecha, D., Movsas, R., Sano, U., and Menon, J.U., (2019). Applications of alginate microspheres in therapeutics delivery and cell culture: Past, present and future. *Int. J. Pharm.* 569 (118627), 1-13.
- Dudášová, H., Lucia Lukáčová, L., Murínová, S., Puškárová, A., Pangallo, D., and Dercová, K. (2014). Bacterial strains isolated from PCB-contaminated sediments and their use for bioaugmentation strategy in microcosms. *J. Basic Microbiol.* 54, 253-260.
- Duldhardt, I., Gaebel, J., Chrzanowski, L., Nijenhuis, I., Härtig, C., Schauer, F., and Heipieper, H.J. (2010). Adaptation of anaerobically grown *Thauera aromatica*, *Geobacter*, *Sulfur reducens* and *Desulfococcus multivorans* to organic solvents on the level of membrane fatty acid



## Bibliography

---

- composition. *Microbial Biotechnol.* 3(2), 201-209.
- Dworkin, M., and Foster, J.W. (1958). Experiments with some microorganisms which utilize ethane and hydrogen. *J. Bacteriol.* 75(5), 592-603.
- Dzionic, A., Wojcieszynska, D., and Guzik, U. (2016). Natural carriers in bioremediation: A review. *Electron J. Biotechnol.* 23, 28-36.
- Edgar, R.C. (2004). MUSCLE: Multiple sequence alignment with high accuracy and high throughput. *Nucleic Acids Res.* 32(5),1792-1797.
- Egland, P.G., Gibson, J., and Harwood, C.S. (1995). Benzoate-coenzyme A ligase, encoded by *bada*, is one of three ligases able to catalyze benzoyl-coenzyme A formation during anaerobic growth of *Rhodospseudomonas palustris* on benzoate. *J. Bacteriol.* 177 (22), 6545-6551.
- Eklund, T. (1985). Inhibition of microbial growth at different pH levels by benzoic and propionic acids and esters of p-hydroxybenzoic acid. *Int. J. Food Microbiol.* 2, 159-167.
- Elufisan, T.O., Rodríguez-Luna, I.C., Oyedara, O.O., Sánchez-Varela, A., Hernández-Mendoza, A., Dantán, G.E., Paz-González, A.D., Muhammad, K., Rivera, G., Villalobos-Lopez, M.A., and Guo, X. (2020). The Polycyclic Aromatic Hydrocarbon (PAH) degradation activities and genome analysis of a novel strain *Stenotrophomonas* sp. Pemsol isolated from Mexico. *PeerJ.* 8, e8102.
- Erickson, B.D., and Mondello, F.J. (1992). Nucleotide sequencing and transcriptional mapping of the genes encoding biphenyl dioxygenase, a multicomponent polychlorinated-biphenyl-degrading enzyme in *Pseudomonas* strain LB400. *J. Bacteriol.* 174, 2903-2912.
- Fang, H., Dong, B., Yan, H., Tang, F., and Yu, Y. (2010). Characterization of a bacterial strain capable of degrading DDT congeners and its use in bioremediation of contaminated soil. *J. Hazard. Mater.* 184, 281-289.
- Fava, F., Bertin, L., Fedi, S., and Zannoni, D. (2003). Methyl- $\beta$ -cyclodextrin-enhanced solubilization and aerobic biodegradation of polychlorinated biphenyls in two aged-contaminated soils. *Biotechnol. Bioeng.* 81, 381-390.
- Fava, F., Gioia, D., Marchetti, L., Quattroni, G., and Marraffa, V. (1993). Aerobic mineralization of chlorobenzoates by a natural polychlorinated biphenyl-degrading mixed bacterial culture. *Appl. Microbiol. Biotechnol.* 40, 543-548.
- Feehily, C., and Karatzas, K. A. (2013). Role of glutamate metabolism in bacterial responses

## Bibliography

---

- towards acid and other stresses. *J. Appl. Microbiol.* 114(1), 11-24.
- Fennell, D.E., Nijenhuis, I., Wilson, S.F., Zinder, S.H., and Haggblom, M.M. (2004). *Dehalococcoides ethenogenes* strain 195 reductively dechlorinates diverse chlorinated aromatic pollutants. *Environ. Sci. Technol.* 38(7), 2075-2081.
- Ficko, S.A, Rutter, A., and Zeeb, B.A. (2011). Phytoextraction and uptake patterns of weathered polychlorinated biphenyl-contaminated soils using three perennial weed species. *J. Environ. Qual.* 40, 1870-1877.
- Ficko, S.A., Rutter, A., and Zeeb, B.A. (2010). Potential for phytoextraction of PCBs from contaminated soils using weeds. *Sci. Total Environ.* 408, 3469-3476.
- Field, J. A., and Sierra-Alvarez, R. (2008). Microbial transformation and degradation of polychlorinated biphenyls. *Environ. Pollut.* 155, 1-12.
- Fira, D., Dimkic, I., Beric, T., Lozo, J., and Stankovic, S. (2018). Biological control of plant pathogens by *Bacillus* species. *J. Biotechnol.* 285, 44-55.
- Franchi, E., Agazzi, G., Rolli, E., Borin, S., Marasco, R., Chiaberge, S., et al. (2016). Exploiting hydrocarbon-degrading indigenous bacteria for bioremediation and phytoremediation of a multi-contaminated soil. *Chem. Eng. Technol.* 39, 1676-1684.
- Franzetti, A., Gandolfi, I., Bestetti, G., Smyth, T.J.P., and Banat I.M. (2010). Production and applications of trehalose lipid biosurfactants. *Eur. J. Lipid Sci. Technol.* 112, 617-627.
- Fries, G.F., and Marrow, G.S. (1981). Chlorobiphenyl movement from soil to soybean plants. *J. Agr. Food Chem.* 29(4), 757-759.
- Furukawa, K. (1994). Molecular genetics and evolutionary relationship of PCB-degrading bacteria. *Biodegradation* 5, 289-300.
- Furukawa, K., and Fujihara, H. (2008). Microbial degradation of polychlorinated biphenyls: biochemical and molecular features. *J. Biosci. Bioeng.* 105, 433-449.
- Furukawa, K., and Miyazaki, T. (1986). Cloning of a gene cluster encoding biphenyl and chlorobiphenyl degradation in *Pseudomonas pseudoalcaligenes*. *J. Bacteriol.* 166, 392-398.
- Furukawa, K., Matsumura, F., and Tonomura, K. (1978). *Alcaligenes* and *Acinetobacter* strains capable of degrading polychlorinated biphenyls. *Agri. Boil. Chem.* 42, 543-548.
- Furukawa, K., Suenaga, H., and Goto, M. (2004). Biphenyl dioxygenases: Functional versatility

and directed evolution. *J. Bacteriol.* 186(16), 5189-5196.

Gang, S., Sharma, S., Saraf, M., Buck, M., and Schumacher, J. (2019). Analysis of indole-3-acetic acid (IAA) production in *Klebsiella* by LC-MS/MS and the Salkowski method. *Bio. Protoc.* 9(9), e3230.

Gaonkar, T., and Bhosle, S.N. (2013). Effect of metals on a siderophore producing bacterial isolate and its implications on microbial assisted bioremediation of metal contaminated soils. *Chemosphere* 93 (9), 1835-1843.

Garrido-Sanz, D., Manzano, J., Martín, M., Redondo-Nieto, M., and Rivilla, R. (2018). Metagenomic analysis of a biphenyl degrading soil bacterial consortium reveals the metabolic roles of specific populations. *Front. Microbiol.* 9 (232), 1-13.

Garrido-Sanz, D., Sansegundo-Lobato, P., Redondo-Nieto, M., Suman, J., Cajthaml, T., Blanco-Romero, E., Martin, M., Uhlík, O., and Rivilla, R. (2020). Analysis of the biodegradative and adaptive potential of the novel polychlorinated biphenyl degrader *Rhodococcus* sp. WAY2 revealed by its complete genome sequence. *Microb. Genom.* 6(4), e000363.

Geng, S., Fang, J., Turner, K.B. et al. (2012). Accumulation and efflux of polychlorinated biphenyls in *Escherichia coli*. *Anal. Bioanal. Chem.* 403, 2403-2409.

Gentry, T.J., Newby, D.T., Josephson, K.L., and Pepper, I.L. (2001). Soil microbial population dynamics following bioaugmentation with a 3-chlorobenzoate-degrading bacterial culture bioaugmentation effects on soil microorganisms. *Biodegradation* 12 (5), 349-357.

Gentry, T.J., Rensing, C., and Pepper, I.L. (2004). New approaches for bioaugmentation as a remediation technology. *Crit. Rev. Environ. Sci. Technol.* 34 (5), 447-494.

Germain, J., Raveton, M., Binet, M.N., and Mouhamadou, B. (2021a). Potentiality of native ascomycete strains in bioremediation of highly polychlorinated biphenyl contaminated soils. *Microorg.* 9(3), 612-623.

Germain, J., Raveton, M., Binet, M.N., and Mouhamadou, B. (2021b). Screening and metabolic potential of fungal strains isolated from contaminated soil and sediment in the polychlorinated biphenyl degradation. *Ecotoxic. Environ. Safety.* 208, 111703.

Gibson, D.T., and Parales, R.E. (2000). Aromatic hydrocarbon dioxygenases in environmental biotechnology. *Curr. Opin. Biotechnol.* 11, 236-243.

## Bibliography

---

- Gilbert, E.S. and Crowley, D.E. (1997). Plant compounds that induce polychlorinated biphenyl biodegradation by *Arthrobacter* sp. strain B1B. *Appl. Environ. Microbiol.* 63(5), 1933-1938.
- Glick, B.R. (2010). Using soil bacteria to facilitate phytoremediation. *Biotechnol. Adv.* 28, 367- 374.
- Goldman, S., Kamel, F., Meng, C., Korell, M., Comyns, K., Umbach, D., Hoppin, J., Ross, G., Marras, C., Kasten, M., Chade, A., Blair, A., and Tanner, C. (2016). Polychlorinated Biphenyls (PCBs) and parkinson's disease (PD): Effect modification by membrane transporter variants (S32.004). *Nuerology* 86 (16 supplement)
- Gomes, H.I., Dias-Ferreira, C., and Ribeiro, A.B. (2013). Overview of in situ and ex situ remediation technologies for PCB-contaminated soils and sediments and obstacles for full-scale application. *Sci. Total Environ.* 445, 237-260.
- Gordillo F, Chávez FP, and Jerez CA. (2007). Motility and chemotaxis of *Pseudomonas* sp. B4 towards polychlorobiphenyls and chlorobenzoates. *FEMS Microbiol. Ecol.* 60(2),322-328.
- Goris, J., De Vos, P., Caballero-Mellado, J., et al. (2004). Classification of the biphenyl- and polychlorinated biphenyl-degrading strain LB400T and relatives as *Burkholderia xenovorans* sp. nov. *Int. J. Syst. Evol. Microbiol.* 54 (5), 1677-1681.
- Gudina, E.J., Fernandes E.C., Rodrigues A.I., Teixeira J.A., and Rodrigues L.R. (2015). Biosurfactant production by *Bacillus subtilis* using corn steep liquor as culture medium. *Front. Microbiol.* 6 (59),1-7.
- Gupta, R.S., Patel, S., Saini, N., and Chen, S. (2020). Robust demarcation of 17 distinct *Bacillus* species clades, proposed as novel Bacillaceae genera, by phylogenomics and comparative genomic analyses: Description of *Robertmurraya kyonggiensis* sp. nov. and proposal for an emended genus *Bacillus* limiting it only to the members of the *Subtilis* and *Cereus* clades of species. *Int. J. Syst. Evol. Microbiol.* 70, 5753-5798.
- Gurevich, A., Saveliev, V., Vyahhi, N., and Tesler, G. (2013). QUASt: quality assessment tool for genome assemblies. *Bioinformatics* 29(8), 1072-1075.
- Haas, D., Blumer, C., and Keel, C. (2000). Biocontrol ability of fluorescent pseudomonads genetically dissected: importance of positive feedback regulation. *Curr. Opin. Biotechnol.*, 11, 290-297

## Bibliography

---

- Halket, J. M., and Zaikin, V. G. (2003). Derivatization in mass spectrometry 1. Silylation. *Eur.J. of Mass Spectrom.* 9(1), 1-21.
- Harayama, S., and Kok, M. (1992). Functional and evolutionary relationship among diverse oxygenases. *Annu. Rev. Microbiol.* 46, 565-601.
- Harkness, M.R., Mcdermott, J.B., Abramowicz, D.A., Salvo, J.J., Flanagan, W.P., Stephens M.L., et al. (1993). In situ stimulation of aerobic PCB biodegradation in Hudson River sediments. *Science* 259, 503-507.
- Harwood, C.S. and Parales, R.E. (1996). The  $\beta$ -ketoacid pathway and the biology of self-identity. *Annu. Rev. Microbiol.* 50, 553- 590.
- Harwood, C.S., Parales, R.E., and Dispensa, M. (1990). Chemotaxis of *Pseudomonas putida* toward chlorinated benzoates. *Appl. Environ. Microbiol.* 56, 1501-1503.
- Hatamian-Zarmi, A., Shojaosadati, S.A., Vasheghani-Farahani, E., et al. (2009). Extensive biodegradation of highly chlorinated biphenyls and Aroclor 1242 by *Pseudomonas aeruginosa* TMU56 isolated from contaminated soils. *Int. Biodeter. Biodegr.* 63, 788-794.
- He, Z., Wang, L., Peng, Y., et al. (2015). Determination of selected polychlorinated biphenyls in soil and earthworm (*Eisenia fetida*) using a QuEChERS based method and gas chromatography with tandem MS. *J. Sep. Sci.* 38 (21), 3766-3773.
- Heider, J., Boll, M., Breese, K., et al. (1998). Differential induction of enzymes involved in anaerobic metabolism of aromatic compounds in the denitrifying bacterium *Thauera aromatica*. *Arch. Microbiol.* 170, 120-131.
- Heipieper, H.J., Diefenbach, R., and Keweloh, H. (1992). Conversion of cis unsaturated fatty acids to trans, a possible mechanism for the protection of phenol-degrading *Pseudomonas putida* P8 from substrate toxicity. *Appl. Environ. Microbiol.* 58 (6), 1847-1852.
- Heipieper, H.J., and de Bont, J.A.M. (1994). Adaptation of *Pseudomonas putida* S 12 to ethanol and toluene at the level of fatty acid composition of membranes. *Appl. Environ. Microbiol.* 60, 4440-4444.
- Hirose, J., Fujihara, H., Watanabe, T., Kimura, N., Suenaga, H., Futagami, T., Goto, M., Suyama, A., and Furukawa, K. (2019). Biphenyl/PCB degrading bph Genes of ten bacterial strains isolated from biphenyl-contaminated soil in Kitakyushu, Japan: Comparative and dynamic features as

## Bibliography

---

- integrative conjugative elements (ICEs). *Genes* 10(5), 404.
- Hofer, B., Backhaus, S., and Timmis, K.N. (1994). The biphenyl/polychlorinated biphenyl-degradation locus (bph) of *Pseudomonas* sp. LB400 encodes four additional metabolic enzymes. *Gene* 144, 9-16.
- Hong, C.Y., Gwak, K.S., Lee, S.Y., Kim, S.H., Lee, S.M., Kwon, M., and Choi, I.G. (2012). Biodegradation of PCB congeners by white rot fungus, *Ceriporiopsis* ZLY-2010, and analysis of metabolites. *J. Environ. Sci. Health Part-A*. 47, 1878-1888.
- Hong, Q., Dong, X., He, L., Jiang, X., and Li, S. (2009). Isolation of a biphenyl-degrading bacterium, *Achromobacter* sp. BP3, and cloning of the bph gene cluster. *Int. Biodeterior. Biodegrad.* 63, 365-370.
- Hördt, A., López, M.G., Meier-Kolthoff, J.P., Schleuning, M., Weinhold, L.M., and Tindall, B.J., et al. (2020). Analysis of 1,000+ type-strain genomes substantially improve taxonomic classification of alphaproteobacteria. *Front Microbiol.* 11 (468)1-112
- Horváthová, H., Lászlóvá, K, and Dercová K. (2018). Bioremediation of PCB-contaminated shallow river sediments: The efficacy of biodegradation using individual bacterial strains and their consortia. *Chemosphere* 193, 270-277.
- Horváthová, H., Lászlóvá, K., and Dercová, K. (2019). Remediation potential of bacterial mixed cultures for polychlorinated biphenyls (PCBs) biodegradation. *Acta Chim. Slov.* 12(1), 1-7,
- Hu, C., Zhang, Y., Xiaoda, T., and Luo, W. (2014). PCB Biodegradation and bphA1 gene expression induced by Salicylic acid and biphenyl with *Pseudomonas fluorescence* P2W and *Ralstonia eutropha* H850. *Pol. J. Environ. Stud.* 23(5), 1591-1598.
- Hu, J., Qian, M., Zhang, Q., Cui, J., Yu, C., Su, X., Shen, C., Hashm, M.Z., and Shi, J. (2015) *Sphingobium fuliginis* HC3: A novel and robust isolated biphenyl- and polychlorinated biphenyls-degrading bacterium without dead-end intermediates accumulation. *PLoS One* 10, e0122740.
- Hwang, H.H., Chien, P.R., Huang, F.C., Yeh, P.H., Hung, S.W., Deng, W.L., and Huang, C.C. (2022). A Plant Endophytic Bacterium *Priestia megaterium* Strain BP-R2 isolated from the halophyte *Bolboschoenus planiculmis* enhances plant growth under salt and drought stresses. *Microorganisms*, 10(10), 2047-2068.
- Hyatt, D., Chen, G.L., Locascio, P.F., Land, M.L., Larimer, F.W., and Hauser, L.J. (2010).



## Bibliography

---

- Prodigal: Prokaryotic gene recognition and translation initiation site identification. *BMC Bioinformatics* 11 (119), 1-11.
- Ibrahim, H.M.M. (2018). Characterization of biosurfactants produced by novel strains of *Ochrobactrum anthropi* HM-1 and *Citrobacter freundii* HM-2 from used engine oil-contaminated soil. *Egypt. J. Pet.* 27, 21-29.
- Ilori, M.O., Robinson, G.K., and Adebusoye, S.A. (2008). Aerobic mineralization of 4,4'-dichlorobiphenyl and 4-chlorobenzoic acid by a novel natural bacterial strain that grows poorly on benzoate and biphenyl. *World J. Microbiol. Biotechnol.* 24(8), 1259-1265.
- Isaac, P., Martinez, F.L., Bourguignon, N., et al. (2015). Improved PAHs removal performance by a defined bacterial consortium of indigenous *Pseudomonas* and *Actinobacteria* from Patagonia, Argentina. *Int. Biodeterior. Biodegrad.* 101, 23-31.
- Isaac, P., Sanchez, L.A., Bourguignon, N., et al. (2013). Indigenous PAH-degrading bacteria from oil-polluted sediments in Caleta Cordova, Patagonia Argentina. *Int. Biodeterior. Biodegrad.* 82, 207-214.
- Iwai, S., Johnson, T.A., Chai, B.L., Hashsham, S.A., and Tiedje, J.M. (2011). Comparison of the specificities and efficacies of primers for aromatic dioxygenase gene analysis of environmental samples. *Appl. Environ. Micro.* 77 (11), 3551-3557.
- Iwasaki, T., Miyauchi, K., Masai, E., and Fukuda, M. (2006). Multiple-subunit genes of the aromatic-ring-hydroxylating dioxygenase play an active role in biphenyl and polychlorinated biphenyl degradation in *Rhodococcus* sp. strain RHA1. *Appl. Environ. Microbiol.* 72(8), 5396- 5402.
- Jain, M., Olsen, H. E., Paten, B., Akeson, M. (2016). The Oxford Nanopore MinION: delivery of nanopore sequencing to the genomics community. *Genome boil.* 17(1), 239-249.
- Janßen, H.J., and Steinbuchel, A. (2014). Fatty acid synthesis in *Escherichia coli* and its applications towards the production of fatty acid-based biofuels. *Biotechnol. Biofuels* 7(1), 7-32
- Javorska, H., Tlustos, P., and Kaliszova, R. (2009). Degradation of polychlorinated biphenyls in the rhizosphere of rape, *Brassica napus* L. *Bull. Environ. Contam. Toxicol.* 82,727-731.
- Jayanna, S.K., and Gayathri, D. (2015). Degradation of 2,4 dichlorobiphenyl via meta-cleavage pathway by *Pseudomonas* spp. consortium. *Curr. Microbio.* 70, 871-876.

## Bibliography

---

- Jha, P., Panwar, J., and Jha, P.N. (2015). Secondary plant metabolites and root exudates: guiding tools for polychlorinated biphenyl biodegradation. *Int. J. Environ. Sci. Technol.* 12, 789-802.
- Jiang, L., Luo, C., Zhang, D., et al. (2018). Biphenyl-metabolizing microbial community and a functional operon revealed in E-waste-contaminated soil. *Environ. Sci. Technol.* 52(15), 8558- 8567.
- Jimoh, A.A., and Lin, J. (2019). Production and characterization of lipopeptide biosurfactant producing *Paenibacillus* sp. D9 and its biodegradation of diesel fuel. *Int. J. Environ. Sci. Technol.* 16, 4143-4158.
- Jing, R., Fusi, S., and Kjellerup, B.V. (2018). Remediation of polychlorinated biphenyls (PCBs) in contaminated soils and sediment: state of knowledge and perspectives. *Front. Environ. Sci.* 6 (79), 1-17.
- Jiun-Horng, T., Kuo-Hsiung, L., Chih-Yub, C., et al. (2007). Chemical constituents in particulate emissions from an integrated iron and steel facility. *J. Hazard. Mater.* 147, 111-119.
- Jorge, L.M., Rodrigues, C.A.K., Michael, R.A., et al. (2006). Degradation of Aroclor 1242 Dechlorination products in sediments by *Burkholderia xenovorans* LB400 (ohb) and *Rhodococcus* sp. Strain RHA1(fcb). *Appl. Environ. Microbiol.* 72(4), 2476-2482.
- Joy, S., Rahman, P.K.S.M. and Sharma, S., (2017). Biosurfactant producing bacteria from hydrocarbon contaminated environment. *Chem. Eng. J.* 317, 232-241.
- Jozefczuk, S., Klie, S., Catchpole, G., Szymanski, J., Cuadros-Inostroza, A., Steinhauser, D., Selbig, J., and Willmitzer, L. (2010). Metabolomic and transcriptomic stress response of *Escherichia coli*. *Mol. Sys. Biol.* 6, 364-379
- Kabelitz, N., Santos, P.M., and Heipieper, H.J. (2003). Effect of aliphatic alcohols on growth and degree of saturation of membrane lipids in *Acinetobacter calcoaceticus*. *FEMS Microbiol. Lett.* 220 (2), 223-227.
- Kanehisa, M., Sato, Y., Kawashima, M., Furumichi, M., and Tanabe, M. (2016). KEGG as a reference resource for gene and protein annotation. *Nucleic Acids Res.* 44, D457-462.
- Kannan, K., Tanabe, S., Ramesh, A., Subramanian, A.N., and Tatsukawa, R. (1992). Persistent organochlorine residues in foodstuffs from India and their implications on human dietary exposure. *J. Agric. Food Chem.* 40, 518-524.

## Bibliography

---

- Khan, A., Singh, P., and Srivastava, A. (2018). Synthesis, nature and utility of universal iron chelator-Siderophore: A review. *Microbiol. Res.* 212, 103-111.
- Khanpour-Alikelayeh E., Partovinia A., Talebi A., Kermanian H. (2020). Investigation of *Bacillus licheniformis* in the biodegradation of Iranian heavy crude oil: A two-stage sequential approach containing factor-screening and optimization. *Ecotoxicol. Environ. Saf.* 205, 111103.
- Khopade, A., Biao, R., Liu, X., Mahadik, K., Zhang, L., and Kokare, C. (2012). Production and stability studies of the biosurfactant isolated from marine *Nocardiopsis* sp. B4. *Desalination* 285, 198-204.
- Kikuchi, Y., Nagata, Y., Hinata, M., Kimbara, K., Fukuda, M., Yano, K., and Takagi, M. (1994). Identification of the *bphA4* gene encoding ferredoxin reductase involved in biphenyl and polychlorinated biphenyl degradation in *Pseudomonas* sp. strain KKS102. *J. Bacteriol.* 176, 1689-1694.
- Kimura, M. (1980). A simple method for estimating evolutionary rate of base substitutions through comparative studies of nucleotide sequences. *J. Mol. Evol.* 16, 111-120.
- Kimura, N., and Kamagata, Y. (2009). Impact of dibenzofuran/dibenzo-p-dioxin amendment on bacterial community from forest soil and ring-hydroxylating dioxygenase gene populations. *Appl. Microbiol. Biotechnol.*, 84, 365-373.
- Kimura, N., Kitagawa, W., Mori, T., Nakashima, N., Tamura, T., and Kamagata, Y. (2006). Genetic and biochemical characterization of the dioxygenase involved in lateral dioxygenation of dibenzofuran from *Rhodococcus opacus* strain SAO101. *Appl. Microbiol. Biotechnol.* 73, 474-484.
- Kimura, N., Watanabe, T., Suenaga, H., Fujihara, H., Futagami, T., Goto, M., Hanada, S., and Hirose, J. (2018). *Pseudomonas furukawaii* sp. nov., a polychlorinated biphenyl-degrading bacterium isolated from biphenyl-contaminated soil in Japan. *Int J. Syst. Evol. Microbiol.* 68 (5), 1429-1435.
- Klein, R., Muller, E., Kraus, B., Brunner, G., Estrine, B., Touraud, B., Heilmann, J., Kellermeier, M. and Kunz, W. (2013). Biodegradability and cytotoxicity of choline soaps on human cell lines: Effects of chain length and the cation. *R.S.C. Adv.* 3, 23347-23354.
- Kobayashi, H., Takami, H., Hirayama, H., Kobata, K., Usami, R., and Horikoshi, K. (1999). Outer

## Bibliography

---

- membrane changes in a toluene-sensitive mutant of toluene-tolerant *Pseudomonas putida* IH-2000. *J. Bacteriol.* 181(15), 4493-4498.
- Kohler, H.P., Kohler-Staub, D., and Focht, D.D. (1988). Cometabolism of polychlorinated biphenyls: enhanced transformation of Aroclor 1254 by growing bacterial cells. *Appl. Microbiol.* 54, 1940-1945.
- Komancova, M., Jurcova, I., Kochankova, L., and Burkhard, J. (2003). Metabolic pathways of polychlorinated biphenyls degradation by *Pseudomonas* sp. 2. *Chemosphere.* 50, 537-543.
- Kornberg, A., N. N. Rao, and D. Ault-Riche. (1999). Inorganic polyphosphate: A molecule of many functions. *Annu. Rev. Biochem.* 68, 89-125.
- Krzmarzick, M.J., Taylor, D.K., Fu, X., McCutchan, A.L. (2018). Diversity and niche of archaea in bioremediation. *Archaea.* 3194108, 1-17
- Kumar S., Kumar, B., Sharma, C.S., Makhijani, S.D., and Sengupta, B. (2008). Levels of polychlorinated biphenyl congeners in sea water and surface sediment of Alang ship breaking site Bhavnagar Gujrat India. *Organohalogen Comp.* 70, 19-22
- Kumar, B., Kumar, S., Gaur, R., Goel, G., Mishra, M., Singh, S.K., Dev, P., and Sharma, C.S. (2011). Persistent organochlorine pesticides and polychlorinated biphenyls in intensive agricultural soils from North India. *Soil Water Res.* 6 (4), 190-197.
- Kumar, B., Verma, V.K., Singh, S.A., Kumar, S., Sharma, C.S., and Akolkar, A.B. (2014). Polychlorinated Biphenyls in Residential Soils and their Health Risk and Hazard in an Industrial City in India. *J. Pub. Health Res.* 3, 252.
- Kumar, P., Meghvansi, M.K., Kamboj, D.V. (2021). Phenotypic characterization and whole- genome analysis of a novel bacteriophage HCF1 infecting *Citrobacter amalonaticus* and *C. freundii*. *Front. Microbiol.* 12, 1-15.
- Kurzawova, V., Stursa, P, Uhlik, O., Norkova, K., Strohalm, M., Lipov, J., Kochankova, L., and Mackova, M. (2012). Plant-microorganism interactions in bioremediation of polychlorinated biphenyl-contaminated soil. *New Biotechnol.* 30, 15-22.
- Kvasnicka, J., Burton, G.A., Semrau, J., and Jolliet, O. (2020). Dredging contaminated sediments: is it worth the risks? *Environ. Toxicol. Chem.* 39, 515-516.
- Kweon, O., Kim, S.J., Baek, S., Chae, J.C., Adjei, M.D., Baek, D.H., Kim, Y.C., Cerniglia, C.E.

## Bibliography

---

- (2008). A new classification system for bacterial Rieske non-heme iron aromatic ring- hydroxylating oxygenases. *BMC Biochem.* 9(11),1-20.
- Lambrecht, M., Okon, Y., Vande Broek, A., and Vanderley-den, J. (2000). Indole-3-acetic acid: a reciprocal signaling molecule in bacteria-plant interactions. *Trends Microbiol.* 8, 298-300.
- Langenhoff, A.A.M., Zehnder, A.J.B., and Schraa, G. (1996). Behaviour of toluene, benzene and naphthalene under anaerobic conditions in sediment columns. *Biodegrad.* 7, 267-274.
- LaRoe, S.L., Fricker, A.D., and Bedard, D.L. (2014). *Dehalococcoides mccartyi* strain JNA in pure culture extensively dechlorinates Aroclor 1260 according to polychlorinated biphenyl (PCB) dechlorination process N. *Environ. Sci Technol.* 48, 9187-9196.
- Lászlóvá, K., Dudášová, H., Olejníková, P., Horváthová, G., Velická, Z., Horváthová, H., et al. (2018). The application of biosurfactants in bioremediation of the aged sediment contaminated with polychlorinated biphenyls. *Water Air Soil Pollut.* 229, 219.
- Laue, B.E., Jiang, Y., Chhabra, S.R., Jacob, S., Stewart, G.S.A.B., Hardman, A., Downie, J.A., O'Gara, F., and Williams, P. (2000). The biocontrol strain *Pseudomonas fluorescens* F113 produces the *Rhizobium* small bacteriocin, N-(3-hydroxy-7-cis-tetradecenoyl) homoserine lactone, via HdtS, a putative novel N-acylhomoserine lactone synthase. *Microbiology*, 146, 2469-2480.
- Laver, T., Harrison, J., O'Neill, P.A., et al. (2015). Assessing the performance of the oxford nanopore technologies MinION. *Biomol. Detect. Quantif.* 3, 1-8.
- Leewis, M.C, Uhlik, O., Fraraccio, S., McFarlin, K., Kottara, A., Glover, C., Macek, T., and Leigh, M.B. (2016). Differential impacts of willow and mineral fertilizer on bacterial communities and biodegradation in diesel fuel oil-contaminated soil. *Front. Microbiol.* 7(837), 1-12.
- Leewis, M.C., Uhlik, O., and Leigh, M.B., (2016). Synergistic processing of biphenyl and benzoate: carbon flow through the bacterial community in polychlorinated-biphenyl-contaminated soil. *Sci. Rep.* 6 (22145), 1-12
- Leigh, M.B., Prouzova, P., Mackova, M., Macek, T., Nagle, D.P., and Fletcher, J.S. (2006). Polychlorinated biphenyl (PCB)-degrading bacteria associated with trees in a PCB contaminated site. *Appl. Environ. Microbiol.* 72, 2331-2342.
- Lerro, C.C., Jones, R.R., Langseth, H. et al. (2018). A nested case-control study of polychlorinated biphenyls, organochlorine pesticides, and thyroid cancer in the Janus Serum Bank cohort. *Environ.*

## Bibliography

---

Res. 165,125-132.

- Li, A., Qu, Y., Zhou, J., and Ma, F. (2009). Characterization of a newly isolated biphenyl- degrading bacterium, *Dyella ginsengisoli* LA-4. *Appl. Biochem. Biotechnol.* 159, 687-695.
- Li, X., Hou, L., Liu, M. et al. (2015). Abundance and diversity of polycyclic aromatic hydrocarbon degradation bacteria in urban roadside soils in Shanghai. *Appl. Microbiol. Biotechnol.* 99, 3639-3649.
- Liang, Y., Meggo, R., Hu, D., Schnoor, J.L., and Mattes, T.E. (2014). Enhanced polychlorinated biphenyl removal in a switchgrass rhizosphere by bioaugmentation with *Burkholderia xenovorans* LB400. *Ecol. Eng.* 71, 215-222.
- Liu, Q., Guo, H., Li, Y., and Xiang, H. (2013). Acclimation of arsenic-resistant Fe (II)- oxidizing bacteria in aqueous environment. *Int. Biodeterior. Biodegrad.* 76, 86-91.
- Livak, K.J., and Schmittgen, T.D. (2001). Analysis of relative gene expression data using real-time quantitative PCR and the 2(-Delta Delta C(T)) method. *Methods* 25, 402-408.
- Liz, J. A. Z., Jan-Roblero, J., de la Serna, J. Z., de Leon, A. V., and Hernandez-Rodriguez, C. (2009). Degradation of polychlorinated biphenyl (PCB) by a consortium obtained from a contaminated soil composed of *Brevibacterium*, *Pandora* and *Ochrobactrum*. *World J. Microbiol. Biotechnol.* 25, 165-170.
- Lorck, H. (1948). Production of hydrocyanic acid by bacteria. *Physiol. Plant.* 1,142-146
- Low, J.E., Whitfield, Aslund, M.L., Rutter, A., and Zeeb, B.A. (2010). Effect of plant age on PCB accumulation by *Cucurbita pepo* ssp. *Pepo*. *J. Environ. Qual.* 39(1), 245-250.
- Lu, C., Hong, Y., Liu, J., et al. (2019). A PAH-degrading bacterial community enriched with contaminated agricultural soil and its utility for microbial bioremediation. *J. Env. Pol.* 251, 773- 782.
- Lucy, M., Reed, E., and Glick, B.R. (2004). Application of free-living plant growth-promoting Rhizobacteria. *Anton. Leeuw. Int. J. G.* 86, 1-25.
- Ludbrook, K.A., Russell, C.M., and Greig, R.I. (1997). Exopolysaccharide production from lactic acid bacteria isolated from fermented foods. *J. Food Sci.* 62, 597-600.
- Luo, W., D'Angelo, E. M., and Coyne, M. S. (2007). Organic carbon effects on aerobic polychlorinated biphenyl removal and bacterial community composition in soils and sediments.



## Bibliography

---

Chemosphere 70, 364-373.

Luo, W., Dangelo, E.M., and Coyne, M.S. (2008). Plant secondary metabolites, biphenyl, and hydroxypropyl- $\beta$ -cyclodextrin effects on aerobic polychlorinated biphenyl removal and microbial community structure in soil. *Soil Bio. Biochem.* 39, 735-743.

Ma, Y., Prasad, M.N.V., Rajkumar, M., and Freitas, H. (2011). Plant growth promoting rhizobacteria and endophytes accelerate phytoremediation of metalliferous soils. *Biotechnol. Adv.* 29, 248-258.

Macedo, A.J., Timmis, K.N., and Abraham, W.R. (2007). Widespread capacity to metabolize polychlorinated biphenyls by diverse microbial communities in soils with no significant exposure to PCB contamination. *Environ. Microbiol.* 9(8), 1890-1897.

Madhavan, A., Sindhu, R., Parameswaran, B., Sukumaran, R.K., and Pandey, A. (2017). Metagenome analysis: A powerful tool for enzyme bioprospecting. *Appl. Biochem. Biotechnol.* 183(2), 636-651.

Maloy, S.R., Bohlander, M., and Nunn, W.D. (1980). Elevated levels of glyoxylate shunt enzymes in *Escherichia coli* strains constitutive for fatty acid degradation. *J. Bacteriol.* 143, 720-725

Mars, A.E., Kasberg, T., Kaschabek, S.R., van Agteren, M.H., Janssen, D.B., and Reineke W. (1997). Microbial degradation of chloroaromatics: use of the meta-cleavage pathway for mineralization of chlorobenzene. *J Bact.* 179, 4530-4537.

Mars, A.E., Kingma, J., Kaschabek, S.R., Reineke, W., and Janssen, D.B.(1999). Conversion of 3-chlorocatechol by various catechol 2,3-dioxygenases and sequence analysis of the chlorocatechol dioxygenase region of *Pseudomonas putida* GJ31. *J. Bact.* 181, 1309-1319.

Marx, R.B., and Aitken, M.D. (1999). Quantification of chemotaxis to naphthalene by *Pseudomonas putida* G7. *Appl. Environ. Microbiol.* 65(7), 2847-2852.

Masai, E., Yamada, A., Healy, J.M., Hatta, T., Kimbara, K., Fukuda M., and Yano, K. (1995). Characterization of biphenyl catabolic genes of gram-positive polychlorinated biphenyl degrader *Rhodococcus* sp. strain RHA1. *Appl. Environ. Microbiol.* 61, 2079-2085.

Master, E.R, Lai, V.W.M., Kuipers, B., Cullen, W.R., Mohn, W. (2002). Sequential anaerobic-aerobic treatment of soil contaminated with weathered Aroclor 1260. *Environ. Sci. Technol.* 36, 100-103.

## Bibliography

---

- Master, E.R., and Mohn, W.W. (1998). Psychrotolerant bacteria isolated from arctic soil that degrade polychlorinated biphenyls at low temperatures. *Appl. Environ. Microbiol.* 64(12), 4823- 4829.
- McFall, S.M., Chugani, S.A. and Chakrabarty, A.M. (1998). Transcriptional activation of the catechol operons: Variations on a theme. *Gene* 223, 257-267.
- McSwain, B.S., Irvine, R.L., Hausner, M., and Wilderer, P.A. (2005). Composition and distribution of extracellular polymeric substances in aerobic flocs and granular sludge. *Appl. Environ. Microbiol.* 71(2), 1051-1057.
- Meggo R.E., Schnoor J.L., Hu D. (2013). Dechlorination of PCBs in the rhizosphere of switchgrass and poplar. *Environ. Pollut.* 178, 312 - 321.
- Merlin, C.D., Springael, M., Mergeay, and Toussaint, A. (1997). Organisation of the *bph* gene cluster of transposon Tn4371, encoding enzymes for the degradation of biphenyl and 4- chlorobiphenyl compounds. *Mol. Gen. Genet.* 253, 499-506.
- Meyer-Cifuentes, I., Martinez-Lavanchy, P.M., Marin-Cevada, V., et al. (2017). Isolation and characterization of *Magnetospirillum* sp. strain 15-1 as a representative anaerobic toluene-degrader from a constructed wetland model. *PLoS One.*12(4) e0174750.
- Mishra, A. K., and Baek, K. H. (2021). Salicylic acid biosynthesis and metabolism: A divergent pathway for plants and bacteria. *Biomolecules*, 11(5), 705-720
- Mondello, F.J. (1989). Cloning and expression in *Escherichia coli* of *Pseudomonas* strain LB400 genes encoding polychlorinated biphenyl degradation. *J. Bacteriol.* 171, 1725-1732.
- Monirith, I., Ueno, D., Takahashi, S., Nakata, H., Sudaryanto, A., Subramanian, A., Karupiah, S., et al (2003). Asia-Pacific mussel watch: monitoring contamination of persistent organochlorine compounds in coastal waters of Asian countries. *Mar.Pollut. Bull.* 46(3), 281-300.
- Moody, J.D., Doerge, D.R., Freeman, J.P., and Cerniglia, C.E. (2002). Degradation of biphenyl by *Mycobacterium* sp. strain PYR-1. *Appl. Microbiol. Biotechnol.* 58(3), 364-369.
- Moran, A.C, Olivera, N., Commendatore, M., Esteves, and J.L., Sineriz, F. (2000). Enhancement of hydrocarbon waste biodegradation by addition of a biosurfactant from *Bacillus subtilis* O9. *Biodegradation* 11, 65-71.
- Mouz, S., Merlin, C., Springael, D., and Toussaint, A. (1999). A GntR-like negative regulator of

## Bibliography

---

- the biphenyl degradation genes of the transposon Tn4371. *Mol. Gen. Genet.* 262, 790-799.
- Mulligan, C.N. (2005). Environmental applications for biosurfactants. *Environ. Pollut.* 133, 183-198.
- Murinova, S. and Dercov, K. (2014a). Potential use of newly isolated bacterial strain *Ochrobactrum anthropi* in bioremediation of polychlorinated biphenyls. *Water Air Soil Pollut.* 225 (1980), 1-16.
- Murinova, S., and Dercova, K. (2014b). Response mechanisms of bacterial degraders to environmental contaminants on the level of cell walls and cytoplasmic membrane. *Int. J. Microbiol.* 873081, 1-16.
- Nam, J.W., Nojiri, H., Yoshida, T., Habe, H., Yamane, H., and Omori, T. (2001). New classification system for oxygenase components involved in ring-hydroxylating oxygenations. *Biosci. Biotechnol. Biochem.*, 65, 254-263.
- Nascimento, F.X., Tavares, M.J., Franck, J., Ali, S., Glick, B.R., and Rossi, M.J. (2019). ACC deaminase plays a major role in *Pseudomonas fluorescens* YsS6 ability to promote the nodulation of Alpha- and Betaproteobacteria rhizobial strains. *Arch. Microbiol.* 201(6), 817-822.
- Nayak, Y., Sahu, Y. K., Patel, K. S., Sharma, S., Hung, C.-C., Martín-Ramos, P., and Yurdakul, S. (2021). Distribution and Sources of Polychlorinated Biphenyls in Air, Dust, and Sediment from India. *J. Hazard. Toxic. Radioact.* 25(1), 05020001-13.
- Nicolitch, O., Feucherolles, M., Churin, J.L., et al. (2019). A microcosm approach highlights the response of soil mineral weathering bacterial communities to an increase of K and Mg availability. *Sci. Rep.* 9 (14403) 1-13
- Nojiri, H., Habe, H., and Omori, T. (2001). Bacterial degradation of aromatic compounds via angular dioxygenation. *J. Gen. Appl. Microbiol.* 47(6), 279-305.
- Ohtsubo, Y., Nagata, Y., Kimbara, K., Takagi, M., and Ohta, A. (2000). Expression of the *bph* genes involved in biphenyl/PCB degradation in *Pseudomonas* sp. KKS102 induced by the biphenyl degradation intermediate, 2-hydroxy-6-oxo-6-phenylhexa-2,4-dienoic acid. *Gene* 256(1- 2), 223-228.
- Olvera, C., Goldberg, J.B., Sánchez, R., and Soberón-Chávez, G. (1999). The *Pseudomonas aeruginosa algC* gene product participates in rhamnolipids biosynthesis. *FEMS Microbiol. Lett.*

## Bibliography

---

179, 85-90.

Omidvari, M. (2010). Role of fluorescent *Pseudomonas* siderophore to increase bean growth factors. *J. Agri. Sci.* 2(3), 242-247.

Onbasli, D., and Aslim, B. (2009). Biosurfactant production in sugar beet molasses by some *Pseudomonas* spp. *J. Environ. Biol.* 30(1), 161-163

Ondov, B.D., Treangen, T.J., Melsted, P., Mallonee, A.B., Bergman, N.H., Koren, S., Phillippy, A.M. (2016). Mash: Fast genome and metagenome distance estimation using MinHash. *Genome Biol.* 17(1), 132-145

Ontiveros-Cuadras, J.F., Ruiz-Fernandez, A.C., Sanchez-Cabeza, J.A., et al. (2019). Recent history of persistent organic pollutants (PAHs, PCBs, PBDEs) in sediments from a large tropical lake. *J. Hazard. Mater.* 368, 264-273.

Ornston, L.N. (1966). The conversion of catechol and protocatechuate to  $\beta$ -ketoadipate by *Pseudomonas putida*. IV. Regulation. *J. Biol. Chem.* 241, 3800- 3810.

Ortega-González, D.K., Cancino-Diaz, J.C., Zaragoza, D., Flores-Ortiz, C.M., Cruz-Maya, J.A., and Jan-Roblero, J.J. (2018). *Ochrobactrum anthropi* BPyF3: Naphthalene biodegradation and the involvement of dioxygenase. *Rom. Biotechnol. Lett.* 23(1), 13310- 13316.

Ortega-Gonzalez, D.K., Cristiani-Urbina E., Flores-Ortiz C.M., Cruz-Maya, J.A., Cancino-Diaz, J.C., and Jan-Roblero, J. (2015). Evaluation of the removal of pyrene and fluoranthene by *Ochrobactrum anthropi*, *Fusarium* sp. and their coculture. *Appl. Biochem. Biotechnol.* 175,1123- 1138.

Pagnout, C., Frache, G., Poupin, P., et al. (2007). Isolation and characterization of a gene cluster involved in PAH degradation in *Mycobacterium* sp. strain SNP11: expression in *Mycobacterium smegmatis* mc (2) 155. *Res. Microbiol.*158, 175-186.

Pan, X., Xu, T., Xu, H., Fang, H., and Yu, Y. (2017). Characterization and genome functional analysis of the DDT-degrading bacterium *Ochrobactrum* sp. DDT-2. *Sci. Total Environ.* 592, 593- 599.

Pandey, G., and Jain, R.K. (2002). Bacterial chemotaxis toward environmental pollutants: Role in bioremediation. *Appl. Environ. Microbiol.* 68 (12), 5789-5795.

Parales, R.E., and Harwood, C.S. (2002). Bacterial chemotaxis to pollutants and plant-derived

## Bibliography

---

- aromatic molecules. *Curr. Opin. Microbiol.* 5(3), 266-273.
- Parales, R.E., Luu, R.A., Hughes, J.G., and Ditty, J.L. (2015). Bacterial chemotaxis to xenobiotic chemicals and naturally-occurring analogs. *Curr. Opin. Biotechnol.* 33, 318-326.
- Parke, D., D'Argenio, D.A. and Ornston, L.N. (2000). Bacteria are not what they eat: That is why they are so diverse. *J. Bacteriol.* 182, 257-263.
- Parks, D.H., and Beiko, R.G. (2010). Identifying biologically relevant differences between metagenomic communities. *Bioinformatics* 26 (6), 715-721.
- Parnell, J. J., Deneff, V. J., Park, J., Tsoi, T., and Tiedje, J. M. (2010). Environmentally relevant parameters affecting PCB degradation: carbon source- and growth phase-mitigated effects of the expression of the biphenyl pathway and associated genes in *Burkholderia xenovorans* LB400. *Biodegradation* 21, 147-156.
- Parnell, J.J., Park, J., Deneff, V., Tsoi, T., Hashsham, S., Quensen, J., and Tiedje, J.A. (2006). Coping with polychlorinated biphenyl (PCB) toxicity: Physiological and genome-wide responses of *Burkholderia xenovorans* LB400 to PCB-mediated stress. *Appl. Environ. Microbiol.* 72, 6607- 6614.
- Pascual, F. (2020). Polychlorinated biphenyls as a cardiovascular health risk: A new threat from an old enemy? *Environ. Health Perspect.* 128(11), 114003-114004.
- Passatore, L., Rossetti, S., Juwarkar, A.A., and Massacci, A. (2014). Phytoremediation and bioremediation of polychlorinated biphenyls (PCBs): State of knowledge and research perspectives. *J. Hazard. Mater.* 278, 189-202.
- Patel, K.S., Ramteke, S., Sahu, B.L., et al. (2015). Polychlorinated biphenyls contamination of sludge in India. *Am. J. Analyt. Chem.* 6, 867-877.
- Pathiraja, G., Egodawatta, P., Goonetilleke, A., and Te'o, V.S.J. (2019). Effective degradation of polychlorinated biphenyls by a facultative anaerobic bacterial consortium using alternating anaerobic aerobic treatments. *Sci. Total Environ.* 659, 507-514.
- Pavuk, M., Serio, T.C., Cusack, C., Cave, M., Rosenbaum, P.F., Birnbaum, L.S. (2019). Hypertension in relation to dioxins and polychlorinated biphenyls from the Anniston community health survey follow-up. *Environ. Health Perspect.* 127 (12), 1-11.
- Penrose, D.M., and Glick, B. R. (2003). Methods for isolating and characterizing ACC deaminase-

## Bibliography

---

- containing plant growth-promoting rhizobacteria. *Physiol. Plant.* 118(1),10-15.
- Perfumo, A., Banat, I.M., Canganella, F. et al. (2006). Rhamnolipid production by a novel thermophilic hydrocarbon-degrading *Pseudomonas aeruginosa* AP02-1. *Appl. Microbiol. Biotechnol.* 72, 132-138.
- Petric I., Bru, D., Udikovic-Kolica, N., Hršak, D., Philippot, L., and Martin-Laurent, F. (2011). Evidence for shifts in the structure and abundance of the microbial community in a long-term PCB-contaminated soil under bioremediation. *J. Hazard. Mater.* 195, 254-260.
- Petric, I., Hrsak, D., Fingler, S., Voncina, E., Cetkovic, H., Begonja Kolar, A., and UdikovicKolic, N. (2007). Enrichment and characterization of PCB-degrading bacteria as potential seed cultures for bioremediation of contaminated soil. *Food Technol. Biotechnol.* 45(1), 11-20.
- Pieper, D.H. (2005). Aerobic degradation of polychlorinated biphenyls. *Appl. Microbiol. Biotechnol.* 67, 170-191.
- Pieper, D.H., and Seeger, M. (2008). Bacterial metabolism of polychlorinated biphenyls. *J. Mol. Microbiol. Biotechnol.* 15, 121-138.
- Pino, N.J., Munera, L.M., and Penuela, G.A. (2019). Phytoremediation of soil contaminated with PCBs using different plants and their associated microbial communities. *Int. J. Phytoremed.* 21(4), 316-324.
- Plotnikova, E. G., Solyanikova, I. P., Egorova, D. O., Shumkova, E. S., and Golovleva, L. A. (2012). Degradation of 4-chlorobiphenyl and 4-chlorobenzoic acid by the strain *Rhodococcus ruber* P25. *Microbiology* 81, 143-153.
- Potrawfke, T., Timmis, K.N., and Wittich, R.M. (1998). Degradation of 1,2,3,4-tetrachlorobenzene by *Pseudomonas chlororaphis* RW71. *Appl Environ. Microbiol.* 64 (10), 3798-3806.
- Prasad, K. and Kadokawa, J.I., (2009). Alginate-based blends and nano/microbeads. In *Alginates: Biology and Applications* Springer, Berlin, Heidelberg, 175-210.
- Pratt, L.A., and Kolter, R. (1998). Genetic analysis of *Escherichia coli* biofilm formation: Roles of flagella, motility, chemotaxis and type I pili. *Mol. Microbiol.* 30, 285-293.
- Pujar, N.K., Laad, S., Premakshi, H.G., Pattar, S.V., Mirjankar, M., and Kamanavalli, C.M. (2019). Biodegradation of phenmedipham by novel *Ochrobactrum anthropi* NC-1. *3Biotech.* 9(2), 52-61.



## Bibliography

---

- Qin, H., Brookes, P.C., Xu, J., and Feng, Y. (2014). Bacterial degradation of Aroclor 1242 in the mycorrhizosphere soils of zucchini (*Cucurbita pepo* L.) inoculated with arbuscular mycorrhizal fungi. *Environ. Sci. Pollut. Res.* 21, 12790-12799.
- Raffetti, E., Donato, F., De Palma, G. et al. (2020a). Polychlorinated biphenyls (PCBs) and risk of hypertension: A population-based cohort study in a North Italian highly polluted area. *Sci. Total Environ.* 714 (136660), 1-7.
- Raffetti, E., Donato, F., De Palma, G. et al. (2020b). Polychlorinated biphenyls (PCBs) and risk of dementia and Parkinson disease: A population-based cohort study in a North Italian highly polluted area. *Chemosphere* 261 (127522), 1-7.
- Rahman, K.S.M, Thahira-Rahman, J., Lakshmanaperumalsamy, P., and Banat, I.M. (2002). Towards efficient crude oil degradation by mixed bacterial consortium. *Bioresour. Technol.* 85, 257-261.
- Rahmoune, B., Morsli, A., Khelifi-Slaoui, M. et al (2017). Isolation and characterization of three new PGPR and their effects on the growth of *Arabidopsis* and *Datura* plants. *J. Plant. Interact.* 12, 1-6.
- Rai, A.R., Singh, R.P., Srivastava, A.K., and Dubey, R.C. (2012). Structure prediction and evolution of a halo-acid dehalogenase of *Burkholderia mallei*. *Bioinformatics* 28(22), 1111-1113.
- Rajendran, R.B., Imagawa, T., Tao, H., and Ramesh, R. (2005). Distribution of PCBs, HCHs and DDTs, and their ecotoxicological implications in Bay of Bengal, India. *Environ. Int.* 31(4), 503-512.
- Ramos-González, M.I., Godoy, P., Alaminos, M., Ben-Bassat, A., and Ramos, J.L. (2001) Physiological characterization of *Pseudomonas putida* DOT-T1E tolerance to p-hydroxybenzoate. *Appl. Environ. Microbiol.* 67 (9), 4338-4341.
- Ramu, K., Kajiwara, N., Mochizuki, H., et al. (2006). Occurrence of organochlorine pesticides, polychlorinated biphenyls and polybrominated diphenyl ethers in deep-sea fishes from the Sulu Sea. *Mar. Pollut. Bull.* 52(12), 1827-1832.
- Randle-Boggis, R.J., Helgason, T., Sapp, M., and Ashton, P.D. (2016). Evaluating techniques for metagenome annotation using simulated sequence data. *FEMS Microbiol. Ecol.* 92 (7), 1-15
- Rawat, P., Das, S., Shankhdhar, D. et al. (2021). Phosphate-Solubilizing Microorganisms:

## Bibliography

---

- mechanism and their role in phosphate solubilization and uptake. *J. Soil Sci. Plant Nutr.* 21, 49-68.
- Reyes-Ramírez, F., Little, R. and Dixon, R. (2002). Mutant forms of the *Azotobacter vinelandii* transcriptional activator NifA resistant to inhibition by the NifL regulatory protein. *J. Bacteriol.* 184, 6777- 6785.
- Rio, D.C., Ares, M. Jr., Hannon, G.J., Nilsen, T.W. (2010). Purification of RNA using TRIzol (TRI reagent). *Cold Spring Harb Protoc.* 6, 1-4.
- Romero-Steiner, S., Parales, R.E., Harwood, C.S. and Houghton, J.E. (1994). Characterization of the *pcaR* regulatory gene from *Pseudomonas putida*, which is required for the complete degradation of p-hydroxybenzoate. *J. Bacteriol.* 176, 5771-5779.
- Ron, E.Z., and Rosenberg, E. (2001). Natural roles of biosurfactants. *Environ. Microbiol.* 3, 229- 236.
- Royan, S., Parulekar, C., and Mavinkurve, S. (1999). Exopolysaccharides of *Pseudomonas mendocina* P2d. *Lett. Appl. Microbiol.* 29, 342-346.
- Safe, S. (1990). Polychlorinated biphenyls (PCBs), dibenzo-p-dioxins (PCDDs), diebenzofurans (PCDFs) and related compounds: environmental and mechanistic considerations which support the development of toxic equivalency factors (TEFs). *Crit. Rev. Toxicol.* 21,51-88.
- Safe, S.H. (1994). Polychlorinated Biphenyls (PCBs): Environmental impact, biochemical and toxic responses, and implications for risk assessment. *Crit. Rev. Toxicol.* 24(2), 87-149.
- Sajbidor, J. (1997). Effect of some environmental factors on the content and composition of microbial membrane lipids. *Crit. Rev. Biotechnol.* 17 (2), 87-103.
- Sakai, M., Ezaki, S., Suzuki, N., and Kurane, R. (2005). Isolation and characterization of a novel polychlorinated biphenyl-degrading bacterium, *Paenibacillus* sp. KBC101. *Appl. Microbiol. Biotechnol.* 68, 111-116.
- Sakthipriya, N., Doble, M., Sangwai, J.S. (2015). Biosurfactant from *Pseudomonas* species with waxes as carbon source - Their production, modeling and properties. *J. Ind. Eng. Chem.* 31, 100- 111.
- Samanta, S.K., Bhushan, B., Chauhan, A., and Jain, R.K. (2000). Chemotaxis of a *Ralstonia* sp. SJ98 toward different nitroaromatic compounds and their degradation. *Biochem. Biophys. Res. Commun.* 269, 117-123

## Bibliography

---

- Samson, R., Shah, M., Yadav, R., Sarode, P., et al. (2019). Metagenomic insights to understand transient influence of Yamuna River on taxonomic and functional aspects of bacterial and archaeal communities of River Ganges. *J. Sci. Tot. Env.* 674, 288-299.
- Sandhu, M., Jha, P., Paul, A.T., and Jha, P.N. (2022). Metagenomic analysis for taxonomic and functional potential of Polyaromatic hydrocarbons (PAHs) and Polychlorinated biphenyl (PCB) degrading bacterial communities in steel industrial soil. *PLoS ONE* 17(4), 1-22: e0266808.
- Sandhu, M., Jha, P., Paul, A.T., Singh, R.P., and Jha, P.N. (2020). Evaluation of biphenyl- and polychlorinated-biphenyl (PCB) degrading *Rhodococcus* sp. MAPN-1 on growth of *Morus alba* by pot study. *Int. J. Phytoremed.* 22(14), 1487-1496.
- Schalk, I.J., Rigouin, C., and Godet, J. (2020). An overview of siderophore biosynthesis among fluorescent Pseudomonads and new insights into their complex cellular organization. *Environ. Microbiol.* 22, 1447-1466.
- Schoebitz, M., López, M.D., and Roldán, A. (2013). Bioencapsulation of microbial inoculants for better soil-plant fertilization: A review. *Agron. Sustain. Dev.* 33, 751-765.
- Schomburg, I., Chang, A., Ebeling, C., Gremse, M., Heldt, C., Huhn, G., and Schomburg, D. 2004. BRENDA, the enzyme database: updates and major new developments. *Nucleic Acids Res.* 32, D431-D433.
- Schubert, M., Lindgreen, S. and Orlando, L. (2016). AdapterRemoval v2: Rapid adapter trimming, identification, and read merging. *BMC Res. Notes* 9, 88-95.
- Schwyn, B., and Neilands, J.B. (1987). Universal chemical assay for the detection and determination of siderophores. *Anal. Biochem.* 160 (1), 47-56.
- Secher, C., Lollier, S., Jezequel, K., Cornu, J.Y., Amalric, L., and Lebeau, T. (2013). Decontamination of a polychlorinated biphenyls contaminated soil by phytoremediation-assisted bioaugmentation. *Biodegradation* 24, 549-562.
- Seo, J.S., Keum, Y.S., and Li, Q.X. (2009). Bacterial degradation of aromatic compounds. *Int. J. Environ. Res. Public Health* (1), 278-309.
- Seto, M., Kimbara, K., Shimura, M., Hatta, T., Fukuda, M., and Yano, K. A. (1995). Novel Transformation of polychlorinated biphenyls by *Rhodococcus* sp. Strain RHA1. *Appl. Environ. Microbiol.* 61(9), 3353-3358.

## Bibliography

---

- Sharma, J.K., Gautam, R.K., Nanekar, S.V., Weber R., Singh, B.K., Singh, S.K., and Juwarkar, A. (2018). Advances and perspective in bioremediation of polychlorinated biphenyl-contaminated soils. *Environ. Sci. Pollut. Res.* 25(17), 16355-16375.
- Shimura, M., Mukerjee-Dhar, G., Kimbara, K., Nagato, H., Kiyohara, H., and Hatta, T. (1999). Isolation and characterization of a thermophilic *Bacillus* sp. JF8 capable of degrading polychlorinated biphenyls and naphthalene. *FEMS Microbiol. Lett.* 178, 87-93.
- Sifour, M., Al-Jilawi, M. H., and Aziz, G. H. (2007). Emulsification properties of biosurfactant produced from *Pseudomonas aeruginosa* RB 28. *Pak. J. Biol. Sci.* 10, 1331-1335.
- Silverstone, A.E., Rosenbaum, P.F., Weinstock, R.S., Bartell, S.M., Foushee, H.R., Shelton, C., and Pavuk, M. (2012). Polychlorinated biphenyl (PCB) exposure and diabetes: Results from the Anniston Community Health Survey. *Environ. Health Perspect.* 120 (5), 727-732.
- Simão, F.A., Waterhouse, R.M., Ioannidis, P., Kriventseva, E.V., and Zdobnov, E.M. (2015). BUSCO: assessing genome assembly and annotation completeness with single-copy orthologs. *Bioinformatics* 31(19), 3210-3212.
- Singer, A.C., Smith, D., Jury, W.A., Hathuc, K., and Crowley, D.E. (2003). Impact of the plant rhizosphere and augmentation on remediation of polychlorinated biphenyl contaminated soil. *Environ. Toxicol. Chem.* 22, 1998-2004.
- Singh, R., Lemire, J., Mailloux, R.J., and Appanna V.D. (2008). A novel strategy involved anti-oxidative defense: The conversion of NADH into NADPH by a metabolic network. *PLoS ONE* 3, e2682.
- Siragusa, S., De Angelis, M., Di Cagno, R., Rizzello, C.G., Coda, R. and Gobbetti, M. (2007). Synthesis of  $\gamma$ -aminobutyric acid by lactic acid bacteria isolated from a variety of Italian cheeses. *Appl. Environ. Microbiol.* 73, 7283-7290.
- Sowndhararajan, K., Marimuthu, S., and Manian, S. (2013). Biocontrol potential of phylloplane bacterium *Ochrobactrum anthropi* BMO-111 against blister blight disease of tea. *J. Appl. Microbiol.* 114 (1), 209-218.
- Sritharan, M. (2016). Iron homeostasis in *Mycobacterium tuberculosis*: Mechanistic insights into siderophore-mediated iron uptake. *J. Bacteriol.* 198, 2399-2409.
- Stamatakis, A. (2014). RAxML version 8: A tool for phylogenetic analysis and post-analysis of

## Bibliography

---

- large phylogenies. *Bioinformatics* 30(9), 1312-1313.
- Stamatakis, A., Hoover, P., and Rougemont, J. (2008). A rapid bootstrap algorithm for the RAxML Web servers. *Syst. Biol.* 57(5), 758-771.
- Stanford, R.A., Cole, J.R., and Tiedje, J.M. (2002). Characterization and description of *Anaeromyxobacter dehalogenans* gen. nov., sp. nov., an Aryl-halo-respiring facultative anaerobic *Myxobacterium*. *Appl. Environ. Microbiol.* 68 (2), 893-900.
- Steiger, M.G., Punt, J.P., Ram, A.F.J., Mattanovich, D., and Sauer, M. (2016). Characterizing *MttA* as a mitochondrial cis-aconitic acid transporter by metabolic engineering. *Metab. Eng.* 35, 95-104.
- Storz, G.T., and Hengge-Aronis, R. (2000). *Bacterial stress responses*. 2nd edn, ASM Press, Washington, p. 1-502.
- Stratford, J., Wright, M.A., Reineke, W., Mokross, H., Havel, J., Knowles, C.J., and Robinson, G.K. (1996). Influence of chlorobenzoates on the utilization of chlorobiphenyls and chlorobenzoates mixtures by chlorobiphenyl/chlorobenzoate-mineralizing hybrid bacterial strains. *Arch. Microbiol.* 165, 213-218.
- Subramanian, A., Ohtake, M., Kunisue, T., and Tanabe, S. (2007). High levels of organochlorines in mother's milk from Chennai (Madras) city, India. *Chemosphere* 68 (5), 928-939.
- Sulochana, M. B., Jayachandra, S. Y., Kumar, S. A., Parameshwar, A. B., Reddy, K. M., and Dayanand, A. (2014). Siderophore as a potential plant growth-promoting agent produced by *Pseudomonas aeruginosa* JAS-25. *Appl. Biochem. Biotechnol.* 174(1), 297-308.
- Sylvester-Bradley, R., Asakawa, N., Torraca, S.L., Latorraca, S., Magalhães, F.M.M., Oliveira, L.A., and Pereira, R.M. (1982). Quantitative survey of phosphate solubilizing microorganisms in the rhizosphere of forage grasses and legumes in the Amazon. *Acta Amaz.* 12,15-22.
- Taguchi, K., Motoyama, M., Iida, T., and Kudo, T. (2007). Polychlorinated biphenyl / biphenyl degrading gene clusters in *Rhodococcus* sp. K37, HA99, and TA431 are different from well-known *bph* gene clusters of *Rhodococci*. *Biosci. Biotechnol. Biochem.* 71,1136-1144.
- Takagi, S., Shirota, C., Sakaguchi, K., Suzuki, J., Sue, T., Nagasaka, H., Hisamatsu, S., Sonoki, S. (2007). Exoenzymes of *Trametes versicolor* can metabolize coplanar PCB congeners and hydroxy PCB. *Chemosphere* 67, 54-57.

## Bibliography

---

- Takeda, H., Yamada, A., Miyauchi, K., Masai, E. and Fukuda, M. (2004). Characterization of transcriptional regulatory genes for biphenyl degradation in *Rhodococcus* sp. strain RHA1. *J. Bacteriol.* 186, 2134-2146.
- Tamura, K., Stecher, G., and Kumar, S. (2021). MEGA11: Molecular Evolutionary Genetics Analysis Version 11. *Mol. Biol. Evol.* 38 (7), 3022-3027.
- Tanabe, S., Kannan, N., Subramanian, An., Watanabe, S., and Tatsukawa, R. (1987). Highly toxic coplanar PCBs: Occurrence, source, persistency and toxic implications to wildlife and humans. *Environ. Pollut.* 47(2), 147-163.
- Tanabe, S., Kumar, S.K., Kannan, K., and Subramanian, A.N. (1998). Accumulation features of polychlorinated biphenyls and organochlorine pesticides in resident and migratory birds from south India. *Arch. Environ. Contam. Toxicol.* 34, 387-397.
- Tandlich, R., Vrana, B., Payne, S., Dercova, K. and Balaz, S. (2011). Biodegradation mechanism of biphenyl by a strain of *Pseudomonas stutzeri*. *J. Environ. Sci. Health Part A*, 46(4), 337-344.
- Teng, Y., Li, X., Chen, T., Zhang, M., Wang, X., Li, Z., and Luo, Y. (2016). Isolation of the PCB-degrading bacteria *Mesorhizobium* sp. ZY1 and its combined remediation with *Astragalus sinicus* L. for contaminated soil. *Int. J. Phytoremediation.* 18, 141-149.
- Thijs, S., Sillen, W., Rineau, F., et al. (2016). Towards an enhanced understanding of plant-microbiome interactions to improve phytoremediation: Engineering the metaorganism. *Front. Microbiol.*, 7, 1-15.
- Thorat, V., Kirdat, K., Tiwarekar, B., DaCosta, E., Debbarma, P., Shouche, Y., Sathe, S., Goel, R., Lodha, T., and Yadav, A. (2020) *Pseudomonas lalkuanensis* sp. nov., isolated from a bacterial consortium of contaminated soil enriched for the remediation of e-waste. *Int. J. Syst. Evol. Microbiol.* 70(12), 6468-6475.
- Tigini, V., Prigione, V., Di Toro, S. et al. (2009). Isolation and characterisation of polychlorinated biphenyl (PCB) degrading fungi from a historically contaminated soil. *Microb. Cell Fact.* 8 (5), 1- 14
- Tomza-Marciniak, A., Pilarczyk, B., Witczak, A., Rząd, I., and Pilarczyk, R. (2019). PCB residues in the tissues of sea ducks wintering on the south coast of the Baltic Sea, Poland. *Environ. Sci. Pollut. Res. Int.* 26(11), 11300-11313.



## Bibliography

---

- Totevova, S., Prouza, M., Burkhard, J. et al. (2002). Characterization of polychlorinated biphenyl-degrading bacteria isolated from contaminated sites in Czechia. *Folia Microbiol.* 47, 247-254.
- Toussaint, J.P., Pham, T.M.M., Barriault, D., and Sylvestre, M. (2012). Plant exudates promote PCB degradation by a rhodococcal rhizobacteria. *Appl. Microbiol. Biotechnol.* 95, 1589-1603.
- Tremaroli, V., Suzzi, C.V., Fedi, S., Ceri, H., Zannoni, D., and Turner, R.J. (2010). Tolerance of *Pseudomonas pseudoalcaligenes* KF707 to metals, polychlorobiphenyls and chlorobenzoates: effects on chemotaxis-, biofilm- and planktonic-grown cells. *FEMS Microbiol. Ecol.* 74, 291-301.
- Trinh, M.M., Kuo, C.H., and Chang, M.B. (2019). Characterization of PCDD/Fs and dl-PCBs emission from combustion of PCB-containing oil in a fluidized-bed incinerator. *Chemosphere* 225, 35-42.
- Tripathi, V., Gaur, V.K., Dhiman, N., Gautam, K., and Manickam, N. (2020). Characterization and properties of the biosurfactant produced by PAH-degrading bacteria isolated from contaminated oily sludge environment. *Environ. Sci. Pollut. Res.* 27(22), 27268-27278.
- Tu, C., Teng, Y., Luo, Y., Sun, X., Deng, S., Li, Z., Liu, W., and Xu, Z. (2011). PCB removal, soil enzyme activities, and microbial community structures during the phytoremediation by *alfalfa* in field soils. *J. Soils Sediments* 11, 649-656.
- Uhlik, O., Jecna, K., Mackova, M., Vlcek, C., Hroudova, M., Demnerova, K., et al. (2009). Biphenyl-metabolizing bacteria in the rhizosphere of horseradish and bulk soil contaminated by polychlorinated biphenyls as revealed by stable isotope probing. *Appl. Environ. Microbiol.* 75, 6471-6477.
- UNEP (2004). Inventory of World-Wide PCB Destruction Capacity. United Nations Environment Programme, UNEPChemicals, Geneva. [http://www.chem.unep.ch/POPs/pcb\\_activities/pcb\\_dest/PCB\\_Dest\\_Cap\\_SHORT.pdf](http://www.chem.unep.ch/POPs/pcb_activities/pcb_dest/PCB_Dest_Cap_SHORT.pdf)
- Vaillancourt, F.H., Labbé, G., Drouin, N.M., Fortin, P.D., and Eltis, L.D. (2002). The mechanism-based inactivation of 2,3-dihydroxybiphenyl 1,2-dioxygenase by catecholic substrates. *J. Biol. Chem.* 277, 2019-2027.
- Valderrama, J.A., Durante-Rodriguez, G., Blazquez, B., Garcia, J.L., Carmona, M., and Diaz, E. (2012). Bacterial degradation of benzoate cross-regulation between aerobic and anaerobic pathways. *J. Biol. Chem.* 287 (13), 10494 -10508.

## Bibliography

---

- Venkatachalam, K., Arzuaga, Chopra, X.N., Gavalas, V.G., Xu, J., Bhattacharyya, D., Hennig, B., and Bachas, L.G. (2008). Reductive dechlorination of 3,3',4,4'-tetrachlorobiphenyl (PCB 77) using palladium or palladium/iron nanoparticles and assessment of the reduction in toxic potency in vascular endothelial cells. *J. Hazard. Mater.* 159, 483-491.
- Vergani, L., Mapelli, F., Suman, J., Cajthaml, T., Uhlik, O., and Borin, S. (2019). Novel PCB-degrading *Rhodococcus* strains able to promote plant growth for assisted rhizoremediation of historically polluted soils. *PLoS One*. 14(8), e0221253.
- Vergani, L., Mapelli, F., Zanardini, E., Terzaghi, E., Di Guardo, A., Morosini, C., Raspa, G., and Borin, S. (2017). Phyto-rhizoremediation of polychlorinated biphenyl contaminated soils: An outlook on plant-microbe beneficial interactions. *Sci. Total Environ.* 575, 1395-1406.
- Vrana, B., Dercova, K., Balaz, S., and Sevcikova, A. (1996). Effect of chlorobenzoates on the degradation of polychlorinated biphenyls (PCB) by *Pseudomonas stutzeri*. *World J. Microbiol. Biotechnol.* 12, 323-326.
- Wagi, S., and Ahmed, A. (2019). *Bacillus* spp.: Potent microfactories of bacterial IAA. *PeerJ*. 7, e7258.
- Walker, M.C., van der Donk, and W.A. (2016). The many roles of glutamate in metabolism. *J. Ind. Microbiol. Biotechnol.* 43(2-3), 419-430.
- Wang, H., Hu, J., Xu, K., Tang, X., Xu, X., and Shen, C. (2018). Biodegradation and chemotaxis of polychlorinated biphenyls, biphenyls, and their metabolites by *Rhodococcus* spp. *Biodegradation* 29, 1-10.
- Wang, S., and He, J. (2013). Dechlorination of commercial PCBs and other multiple halogenated compounds by a sediment-free culture containing *Dehalococcoides* and *Dehalobacter*. *Environ. Sci. Technol.* 47(18), 10526-10534.
- Wang, X., Jin, D., Zhou, L., and Zhang, Z. (2015). Draft Genome Sequence of *Ochrobactrum anthropi* Strain W13P3, a halotolerant polycyclic aromatic hydrocarbon-degrading bacterium. *Genome Announc.* 30, 3(4), e00867-15.
- Wang, X., Teng, Y., Luo, Y., and Dick, R.P. (2016). Biodegradation of 3,3',4,4'- tetrachlorobiphenyl by *Sinorhizobium meliloti* NM. *Bioresour. Technol.* 201, 261-268.
- Wang, Y., Garnon, J., Labbe, D., Bergeron, H., and Lau, P.C. (1995). Sequence and expression of

## Bibliography

---

- the bpdC1C2BADE genes involved in the initial steps of biphenyl/chlorobiphenyl degradation by *Rhodococcus* sp. M5. *Gene* 164, 117-122.
- Watanabe, T., Fujihara, H. and Furukawa, K. (2003). Characterization of the second LysR-type regulator in the biphenyl-catabolic gene cluster of *Pseudomonas pseudoalcaligenes* KF707. *J. Bacteriol.* 185, 3575-3582.
- Weiland-Brauer, N., Fischer, M.A., Schramm, K.W., et al. (2017). Polychlorinated biphenyl (PCB)-degrading potential of microbes present in a cryoconite of Jamtalferner Glacier. *Front. Microbiol.* 8 (1105), 1-17.
- Westbrock-Wadman, S., Sherman, D.R., Hickey, M.J., et al. (2004). Characterization of a *Pseudomonas aeruginosa* efflux pump contributing to aminoglycoside impermeability. *Antimicrob. Agents Chemother.* 43, 2975-2983.
- Wheatley, R.M., and Poole, P.S. (2018). Mechanisms of bacterial attachment to roots. *FEMS Microbiol. Rev.* 42 (4), 448-461.
- Wick, R.R., Judd, L.M., Gorrie, C.L., and Holt, K.E. (2017). Unicycler: Resolving bacterial genome assemblies from short and long sequence reads. *PLoS Comput. Biol.* 13 (6), e1005595.
- Willdigg, J.R., and Helmann, J.D. (2021). Mini Review: Bacterial membrane composition and its modulation in response to stress. *Front. Mol. Biosci.* 8 (634438), 1-11.
- Wittich, R.M., Strompl, C., Moore, E.R.B. et al. (1999). Interactions of *Sphingomonas* and *Pseudomonas* strains in the degradation of chlorinated dibenzofurans. *J. Ind. Microbiol. Biotechnol.* 23, 353-358.
- Wu, G., Feng, Y., and Boyd, S.A. (2003). Characterization of bacteria capable of degrading soil-sorbed biphenyl. *Bull. Environ. Contam. Toxicol.* 71(4), 768-775.
- Xiang, Y., Xing, Z., Liu, J., Qin, W., and Huang, X. (2020). Recent advances in the biodegradation of polychlorinated biphenyls. *World J. Microbiol. Biotechnol.* 36, 1-10.
- Xiao, Z., and Xu, Ping. (2007). Acetoin metabolism in bacteria. *Crit. Rev. Microbiol.* 33 (2), 127-140.
- Xing, Z., Hu, T., Xiang, Y., Qi, P., and Huang, X. (2020). Degradation mechanism of 4-chlorobiphenyl by consortium of *Pseudomonas* sp. strain CB-3 and *Comamonas* sp. strain CD-2. *Curr. Microbiol.* 77, 15-23.

## Bibliography

---

- Xu, L., Teng, Y., Li, Z.G., Norton, J.M., and Luo, Y.M. (2010). Enhanced removal of polychlorinated biphenyls from alfalfa rhizosphere soil in a field study: The impact of a rhizobial inoculum. *Sci. Total Environ.* 408(5), 1007-1013.
- Yadav, A., Rajhans, K.P., Ramteke S., Sahu, B.L., Patel, K.S., and Blazhev, B. (2016). Contamination of industrial waste water in central India. *J. Environ. Prot.* 7(1), 72-81.
- Yadav, J.S., Quensen, J.F., Tiedje, J.M., and Reddy, C.A. (1995). Degradation of polychlorinated biphenyl mixtures (Aroclors 1242, 1254, and 1260) by the white rot fungus *Phanerochaete chrysosporium* as evidenced by congener-specific analysis. *Appl. Environ. Microbiol.* 61(7), 2560-2565.
- Yan, G., Chen, X., Du S., Deng, Z., Wang, L., and Chen, S. (2019). Genetic mechanisms of arsenic detoxification and metabolism in bacteria. *Curr. Genet.* 65(5), 329-338.
- Yang, C., Kong, A.P.S., Cai, Z., and Chung, A.C.K. (2017). Persistent organic pollutants as risk factors for obesity and diabetes. *Curr. Diab. Rep.* 17, 1-11.
- Yang, H.H., Lai, S.O., Hsieh, L.T., et al. (2002). Profiles of PAH emission from steel and iron industries. *Chemosphere* 48, 1061-1074.
- Yang, X., Liu, X., Song, L., Xie, F., Zhang, G., and Qian, S. (2007). Characterization and functional analysis of a novel gene cluster involved in biphenyl degradation in *Rhodococcus* sp. strain R04. *J. Appl. Microbiol.* 103 (6), 2214-2224.
- Yao, X., Tao, F., Tang, H., Hu, H., Wang, W., and Xu, P. (2021). Unique regulator SrpR mediates crosstalk between efflux pumps TtgABC and SrpABC in *Pseudomonas putida* B6-2 (DSM 28064). *Mol. Microbiol.* 115 (1), 131-141.
- Yao, X., Tao, F., Zhang, K., Tang, H., and Xu, P. (2017). Multiple roles for two efflux pumps in the polycyclic aromatic hydrocarbon-degrading *Pseudomonas putida* strain B6-2 (DSM 28064). *Appl. Environ. Microbiol.* 83 (24), 1-12
- Young, C.C., Rekha, P.D., Lai, W.A., Arun, A.B. (2006). Encapsulation of plant growth-promoting bacteria in alginate beads enriched with humic acid. *Biotechnol. Bioeng.* 95(1), 76-83.
- Yrjala, K., Keskinen, A.K., Akerman, M.L., Fortelius, C., and Sipila, T.P. (2010). The rhizosphere and PAH amendment mediate impacts on functional and structural bacterial diversity in sandy peat soil. *Environ. Pollut.* 158, 1680-1688.

## Bibliography

---

- Yun, Q., Lin, Z., and Xin, T. (2009). Cometabolism and immobilized degradation of monochlorobenzoate by *Rhodococcus erythropolis*. *Afr. J Microbiol. Res.* 3,482-486.
- Zanaroli, G., Balloi, A., Negroni, A., Borruso, L., Daffonchio, D., Fava, F. (2012). A *Chloroflexi* bacterium dechlorinates polychlorinated biphenyls in marine sediments under in situ-like biogeochemical conditions. *J. Hazard. Mater.* 209- 210, 449- 457.
- Zhang, De-C., Mortelmaier, C, and Margesin, R. (2012). Characterization of the bacterial archaeal diversity in hydrocarbon-contaminated soil. *Sci. Tot. Environ.* 421-422, 184-196.
- Zhang, S., Hu, Z., Wang, H. (2019). Metagenomic analysis exhibited the co-metabolism of polycyclic aromatic hydrocarbons by bacterial community from estuarine sediment. *Environ. Int.* 29, 308-319.
- Zhang, Y.M., and Rock, C.O. (2008). Membrane lipid homeostasis in bacteria. *Nat. Rev. Microbiol.* 6(3), 222-233.
- Zheng, H., Mao, Y., Teng, J. et al. (2015). Flagellar-dependent motility in *Mesorhizobium tianshanense* is involved in the early stage of plant host interaction: Study of an flgE mutant. *Curr. Microbiol.*70, 219-227.
- Zhou, Z., Tran, P.Q., Kieft, K., et al. (2020). Genome diversification of globally distributed novel marine proteobacteria is linked to environmental adaptation. *ISME J* 14, 2060-2077.
- Zhu, M., Yuan, Y., Yin, H., Guo, Z., Wei, X., Qi, X., Liu, H., Dang, Z. (2022). Environmental contamination and human exposure of polychlorinated biphenyls (PCBs) in China: A review. *Sci Total Environ.* 805 (150270) 1-17
- Zorádová, S., Dudášová, H., Lukáčová, L., Dercová, K., and Certík M. (2011). The effect of polychlorinated biphenyls (PCBs) on the membrane lipids of *Pseudomonas stutzeri*. *Int. Biodeter. Biodegr.* 65, 1019-1023.
- Zoradova-Murinova, S., Dudasova, H., Lukacova, L., Certik, M., Silharova, K., Vrana, B., et al. (2012). Adaptation mechanisms of bacteria during the degradation of polychlorinated biphenyls in the presence of natural and synthetic terpenes as potential degradation inducers. *Appl. Microbiol. Biotechnol.* 94, 1375-1385.

### List of publications

---

- Sandhu M, Paul AT, Proćków J, de la Lastra JMP, and Jha PN (2022). PCB-77 biodegradation potential of biosurfactant producing bacterial isolates recovered from contaminated soil. *Front. Microbiol.* 13:952374.
- Sandhu M, Paul AT, and Jha PN (2022). Metagenomic analysis for taxonomic and functional potential of Polyaromatic hydrocarbons (PAHs) and Polychlorinated biphenyl (PCB) degrading bacterial communities in steel industrial soil. *PLoS One.* 17(4): e0266808.
- Sandhu M, Jha P, Paul AT, Singh RP. and Jha PN (2020). Evaluation of biphenyl- and polychlorinated-biphenyl (PCB) degrading *Rhodococcus* sp. MAPN-1 on growth of *Morus alba* by pot study. *Int. J. Phytoremediation.* 22:1487-1496.
- Sandhu M, Paul AT, and Jha PN. Comparative whole genome analysis of Polychlorinated biphenyl (PCB) degrading bacterial communities in steel industrial soil [Ready for communication]

### Patents

---

- Patent entitled “PCB degrading bacterial consortia and its bio-formulation (TETRABAC MAPB)” filed [Application no. 202311035865]

### Awards and Achievements

---

- **DST- Women Scientist-B (WOS B)** [Internship mode (2016-2017) and Project mode (2017-2021)]
- **Best poster award:** Sandhu M, Jha P, Paul AT, Singh RP, Jha PN (2016). Characterization of biphenyl metabolizing Gram-positive bacterium *Rhodococcus* sp. MAPN-1 isolated from the rhizosphere of *Morus alba* (Mulberry plant)” In: Mini-symposium on Environmental Biotechnology, Biorefinery and Solid Waste Management organized jointly by School of Environmental Sciences, Jawaharlal Nehru University and The Biotech Research Society, India (BRSI) at JNU Convention Centre from 11<sup>th</sup> -13<sup>th</sup>, pp EB 11-12.



---

**List of conferences attended**

---

- Poster presentation on “*Evaluation of soil isolates from polychlorinated biphenyl contaminated soil for PCB degradation potential*” at 60<sup>th</sup> Annual Conference of Association of Microbiologist of India and International Symposium on Microbial Technologies in Sustainable Development of Energy, Environment, Agriculture and Health, Central University of Haryana, Mahendergarh (2019)
  - Attended Regional Young Investigator's meet held at IIT Jodhpur (2019)
  - Poster presentation on “*Characterization of polychlorinated biphenyl degrading bacteria isolated from the contaminated soil*” at Life Science Research & its Interface with Engineering and Allied Sciences, BITS Pilani, Pilani (2018)
  - Poster presentation on “*Characterization of biphenyl metabolizing Gram-positive bacterium Rhodococcus sp. MAPN-1 isolated from the rhizosphere of Morus alba (Mulberry plant)*” at In: Mini-symposium on Environmental Biotechnology, Biorefinery and Solid Waste Management organized jointly by School of Environmental Sciences, Jawaharlal Nehru University and The Biotech Research Society, India (BRSI) at JNU, New Delhi (2016)
- 

**List of Workshops attended**

---

- Participated in 2-day Training workshop on **GC-MS/MS** organized by Sophisticated Instrumentation Facility, BITS Pilani and Spinco Biotech Pvt. Ltd
- Participated in online workshop on **Metagenomics** organized by ArrayGen Pvt Ltd

**Biography of Prof. Prabhat N. Jha**

Dr. Prabhat N. Jha, is working as a Professor in Department of Biological Sciences, Birla Institute of Technology and Science Pilani, Pilani campus, Rajasthan. He obtained his master's degree in Biotechnology from Lalit Narayan Mithila University, Darbhanga (Bihar). He completed his PhD in the area of Microbial Biotechnology from Banaras Hindu University, Varanasi (U.P.). He did his post-doctoral research at National Botanical Research Institute, Lucknow in the area of plant molecular biology and at Michigan State University, USA in microbial ecology. He has been engaged in teaching and research since 2007. His broad area of research interests is: Host-Microbe interaction, Plant Microbiology, and Applied Microbiology. Dr. Jha has completed two research projects funded by DST and DBT as principal investigator and one as Co-PI. Currently he is having one research project each as PI and Co-PI funded by ICAR and DST-NSM respectively. He has published 55 research articles in journal of international repute, seven chapters in edited books and, edited two books. He also has filed one patent jointly. He has successfully guided three students for PhD and guided more than thirty undergraduate and post-graduate students for their research studies. He is currently guiding four students for Ph.D.

He is a recipient of Raman post-doctoral fellowship under India-US knowledge initiative 2013 programme (University Grant Commission, New Delhi), DST travel grant to attend international conference at Czeck-Republic, DBT- Postdoctoral fellowship, CSIR-SRF and K.C. Bose Young Scientist award (Gold medal). He was a Visiting Fellow in Department of Botany and Zoology, Institute of Life Sciences, Rajiv Gandhi University, Rono Hills, Doimukh, Itanagar, Arunachal Pradesh, India to teach Molecular Biology and Plant Biotechnology to post-graduate student. He has delivered motivational talk to students of Navodaya Vidhyalaya, and NTSE scholars and scientific talks at research and academic institutes. In addition to academics, Dr. Jha has also served as Head, Department of Biological Sciences, BITS Pilani (2016-2020), Member of library committee, Member of Departmental Research Committee, Member of Human Ethics Committee, and nucleus member of research and consultancy division. Currently he is serving as Member Secretary, Institute Biosafety Committee, BITS Pilani (2017-till date); Co-coordinator, sophisticated instrument facility, BITS Pilani; DBT nominee, IBSC, IIT-Jodhpur; Member of

National Steering committee of NetSCoFAN (Biological group), FSSAI, India; Member of Board of Studies, Choudhary Banshi Lal University, Bhiwani, Haryana.

### **Biography of Monika Sandhu**

Monika Sandhu was born in Mandi district of Himachal Pradesh. She has done her B.Sc. from Himachal Pradesh University and M.Sc. (Microbiology) from Dr. Y.S. Parmar University of Horticulture and Forestry, Nauni, Solan (HP). She has successfully completed an internship project (DST/Disha/SoRF-IM/009/2015/01a **Amt: 3.52 Lakhs**) titled “Screening and characterization of polychlorinated biphenyl degrading bacterial isolates from the rhizosphere of *Morus alba* (Mulberry plant)” under the DST Women Scientist (WOS-B) scheme. After the successful completion of the previous grant, she was awarded a 3-year project grant (SR/WoS-B/570/2016 **Amt: 20.8 Lakhs**) under the same scheme titled “Development of bio-inoculant based formulation for enhanced phytoremediation of polychlorinated biphenyl (PCB) contaminated soil”. She has published 3 research papers on bioremediation and metagenomics in Journals of International repute. She has attended 05 conferences and received best poster presentation award at the International Conference on Strategies for Environmental Protection and Management (ICSEPM - 2016) conducted by BRSI India in JNU, New Delhi. She has undergone hands on training workshop on GC-MS/MS conducted by Sophisticated Instrumentation Facility, BITS Pilani and Metagenome analysis conducted by ArrayGen Pvt Ltd, respectively.